Role of miR-140-3p and miR-140-5p in lung cancer invasion

By

Valentina Flamini

Cardiff China Medical Research Collaborative

Cardiff School of Medicine

September 2017

Thesis submitted to Cardiff University for the degree of Doctor of Philosophy

Dedicated to Adriana,

Who inspired my life

Acknowledgements

I want to express my gratitude to my supervisors, Professor Wen Jiang and Doctor Yuxin Cui, for their support and guidance in these three years.

A very special thanks to all my previous supervisors, Dr Addolorata Pisconti, Dr Armando Magrelli and Dr Marco Salvatore for passing down to me the love for the research. Without them, I would not be here today.

I am also very grateful to all the Cardiff China Medical Research Collaborative members for making me feel welcome. In particular, I want to thank Ms. Fiona Ruge for her remarkable support in my everyday life as a PhD student. Thanks to Dr. Nicola Jordan and Dr. Sioned Owen for their teaching and suggestions. A special thanks also to Dr Alwyn Dart for his support and guidance through the RNA-sequencing experiments.

Thanks to Prof. Cheng and her team in for giving me the chance to work in Beijing. I really enjoyed the time I spent in China.

Thanks to all my "travel buddies" Sarah, Emily, Ross, Robyn, Beth, David, Jeyna, Bruno, Nelly, Matina and Ben. Thanks for all the suggestions and the time we spent together.

I want to thank my wonderful husband Davide, who encouraged and sustained me all the time. My parents have been the pillars of my life and taught me all the practical and intellectual skills in life, especially perseverance, sacrifice, and courage. I will be grateful to them forever. Last, but not the least, I want to thanks my siblings Marco and Eva because they have always believed in me.

Summary

The precursor of miR-140 is located on chromosome 16q22.1 and produces two mature single strands named miR-140-3p and miR-140-5p, which have been associated with several cancers including non-small cell lung cancer (NSCLC). I aim to investigate the differential expression of these two miR-140 strands in NSCLC and their roles in the invasion of lung cancer cells. My hypothesis is that these two miR-140 strands suppress the progression of the NSCLC by targeting specific gene transcripts.

MiR-140-3p and miR-140-5p were downregulated in tissues from NSCLC patients and lung cancer cell lines (A549 and SK-MES-1). The sequencing of the miR-140 precursor indicated two DNA variants in SK-MES-1 cells but not in A549 cells. This might affect the biogenesis of its mature strands because the expression levels of both miR-140-3p and miR-140-5p were lower in SK-MES-1 than in A549 cells.

Mimics of miR-140-3p and miR-140-5p reduced the invasive properties of A549 cells and enhanced their adhesion to laminin and collagen, two of the main components of the extracellular matrix. In SK-MES-1 cells, both miR-140-3p and miR-140-5p mimics reduced invasion but only miR-140-5p decreased the migration of the cells. The conditioned media from lung cancer cells treated with the miR-140-3p mimics impaired the tubule formation of primary endothelial cells, suggesting its role as an angiogenesis inhibitor.

By using bioinformatic tools, the integrin β 3 (ITGB3) was predicted as a novel target of miR-140-3p, which was validated by Dual-Luciferase miRNA Target Expression Vectors and western blotting. By combining the global data from Kinex™ Antibody Microarray (with 878 antibodies) and RNA-Sequencing, I speculate that miR-140-3p inhibits lung cancer invasion and limits the angiogenic potential of the endothelial cells through the epidermal growth factor receptor (EGFR) signalling pathway. In contrast, miR-130-5p may target cyclin-dependent kinase 3 (CDK3) and sulfatase 2 (SULF2) in NSCLC.

Relevant publications

Flamini V, Jiang WG, and Cui Y (2015). "The two forms of miRNA 140 in lung cancer-associated angiogenesis". *Anticancer research* (conference abstract).

Flamini V, Jiang WG, Lane J and Cui Y (2016). "Significance and therapeutic implications of endothelial progenitor cells in angiogenic-mediated tumour metastasis." *Critical Reviews Oncology and Haematology.* (doi: 10.1016/j.critrevonc.2016.02.010).

Flamini V, Jiang WG, and Cui Y (2017). "Therapeutic Role of MiR-140-5p for the Treatment of Non-Small Cell Lung Cancer". *Anticancer Research.* (37(8):4319-4327).

Flamini V, Ed Dudley, Jiang WG, and Cui Y. "Distinct mechanisms by which two forms of miR-140 suppress the metastatic properties of lung cancer cells" (in preparation).

Other publications

Salvatore M, Magrelli A, Flamini V, Brunati A, Basso E, Romagnoli R, David E, and Taruscio D. Hepatoblastoma and microRNA-483 Two Forms and One Outcome. *Journal of Genetic Syndromes & Gene Therapy*. (doi:10.4172/2157-7412.1000278).

Cui Y, Bradbury R, Flamini V, Bo W, Jordan N and Jiang WG (2017). MicroRNA-7 suppresses the homing and migration potential of human endothelial cells to highly metastatic human breast cancer cells. *British Journal of Cancer* (doi: 0.1038/bjc.2017.156).

Zheng F, Flamini V, Bradbury R, Zhang Z, Jiang, WG, Cui Y. "CXCR4 promotes adhesion capacity and activates the AKT signalling pathway in colorectal cancer cells" (2017). *European Journal of cancer* (doi: 10.1016/S0959-8049(17)30302-7).

Flamini V, Ghadiali RS, Antczak P, Rothwell A, Turnbull JE, and Pisconti A. "The satellite cell niche regulates the balance between myoblast differentiation and self-renewal via p53". *Stem Cell Reports* (accepted).

Contents

Chapter 2. Materials and Methods

List of figures

List of Tables

Abbreviations

2-DG: 2-deoxy-glucose

ACTB: β-Actin

ADP: adenosine diphosphate

AGO: Argonaute

AIDS: acquired immune deficiency syndrome

AKT1: v-akt murine thymoma viral oncogene homolog 1

ALK: Anaplastic lymphoma kinase

AP: alkaline phosphatase

APS: Ammonium Persulphate

ARAF: serine/threonine-protein kinase A-Raf

ARID1A: adenine-thymine-rich (AT-rich) interactive domain-containing protein 1A

ATP: adenosine triphosphate

BCL-2: B-cell lymphoma 2

BSA: bovine serum albumin

CCDC144B: coiled-Coil domain containing 144B

CD302: C-type lectin domain family 13 member A

CDC25C: cell division cycle 25C

CDK: Cyclin-dependent kinases

cDNA: complementary DNA

CDS: Cell Dissociation Solution

CHIC 2: cysteine rich hydrophobic domain 2

CLL: chronic lymphocytic leukemia

COA6: cytochrome C oxidase assembly factor 6

COPD: chronic obstructive pulmonary disease

CSRNP2: cysteine and serine rich nuclear protein 2

CT: Computed tomography

CXR: Chest radiography

DCLRE1A: DNA cross-link repair 1A

DDR2: Discoidin domain-containing receptor 2

DEPC: Diethylpyroncarbonate

DFFB: DNA fragmentation factor subunit beta

DGCR8: Di George syndrome Critical Region 8

DMSO: dymethylsulphoxide

DNA: deoxyribonucleic acid

DNMT: DNA methyltransferases

dNTP: triphosphate deoxyribonucleotides

dsRBD: double-stranded RNA binding domain

dsRBP: dsRNA-binding proteins

ECAR: extracellular acidification rate

ECM: extracellular matrix

EDTA: Ethylenediaminetetraacetic acid

EGFR: endothelial growth factor receptor

EHS: Engelbreth-Holm-Swarm

ELISA: Enzyme Linked Immunosorbent Assay

EMT: epithelial-mesenchymal transition

ERK1: extracellular signal-regulated kinase 1

ETC: electron transport chain

EXP5: exportin-5

FBS: foetal bovine serum

FBXO46: F-box protein 46

FCCP: Carbonyl cyanide-4 (trifluoromethoxy) phenylhydrazone

FCS: forward scatter light

FDG: 18 fluorodeoxyglucose

FGF: Fibroblast Growth

FGFR: Fibroblast growth factor receptor

FITC: fluorescein isothiocyanate

FOXO: Forkhead box O

GAPDH: Glyceraldehyde-3-phosphate-dehydrogenase

GDP: guanosine diphosphate

GSK3: Glycogen synthase kinase 3

GTP: guanosine triphosphate

GTPase: Guanosine-5'-triphosphatase

GW182: Glycine-Tryptophan Protein 182

H3K27: histone3lysine27

HDACs: histone-deacetilases

HELQ: helicase, POLQ-like

HER2: Human Epidermal Growth Factor Receptor 2

HIF: Hypoxia-Inducible Factor

HIV: Human Immunodeficiency Virus

hnRNA: heterogeneous nuclear RNA

HOTAIR: HOX Transcript Antisense Intergenic RNA

HOX: homeobox

HRP: horseradish peroxidase-

IGFR: Insulin-Like Growth Factor 1 receptor

IgG: Immunoglobulin G

iRNA: interfering RNA

ITGB3: integrin-β3

KSHV: Kaposi's sarcoma-associated herpesvirus

lincRNA: large intergenic non-coding RNA

LNA: Lock Nucleic Acid

lncRNA: long non coding RNAs

Luc: luciferase reporter gene

M7: 5' 7-methylguanosine

MAGI1: membrane associated guanylate kinase

MALAT1: RNA Metastasis Associated Lung Adenocarcinoma Transcript 1

MCS: Multiple cloning site

MEK1: mitogen-activated kinase/ERK kinase 1

MET (or HGF): hepatocyte growth factor

microRNA (miRNA): small non-coding RNA

miRISC: miRNA-containing RNA-Induced Silencing Complex

mlncRNA: mRNA-like noncoding RNA

M-MuLV: Moloney Murine Leukemia Virus

MRE: miRNA recognition element

mRNA: messenger RNA

mTOR: mammalian target of rapamycin

NADH: nicotinamide adenine dinucleotide

ncRNA: non-coding RNA

ncRNA: non-coding RNA

NEAT1: RNA Nuclear Enriched Abundant Transcript 1

NPC: nuclear pore complex

NSCLC: Non-Small Cell Lung cancer

OCR: oxygen consumption rate

OTC: ornithine transcarbamylase

PABP: poly(A) binding protein

PAZ: Piwi Argonaut and Zwille

PBS: Phosphate-buffered saline

PCOLCE: procollagen C-endopeptidase enhancer

PCR: polymerase chain reaction

PDGF-A: platelet-derived growth factor-A

PDGFR-A: Platelet Derived Growth Factor Receptor A

PDK1: Phosphoinositide-dependent kinase-1

PE: phycoerythrin

PET: Positron emission tomography

PGK: phosphoglycerate kinase

PI: propidium iodide

PI3K: Phosphoinositide-3-kinase

PIK3CA: Phosphatidylinositol-4,5-Bisphosphate 3-Kinase Catalytic Subunit Alpha

PIP3: phosphatidylinositol 3,4,5-trisphosphate

piRNA: PIWI-interacting RNA

PIWI: P-element Induced WImpy testis

Pol: polymerase

PRC2: Polycomb Repressive Complex 2

pre-miRNA: precursor miRNA

pri-miRNA: primary miRNA transcript

PTEN: Phosphatase and TENsin homolog

qRT-PCR : Real Time Quantitative Reverse Transcription Polymerase Chain Reaction

rasiRNA: repeat associated RNA

RET: REarranged during Transfection

RISC: RNA induced silencing complex

RNA: ribonucleic acid

ROS1: c-ros oncogene 1

rRNA: ribosomal RNA

RT: reverse transcription

SCLC: Small-cell lung cancer

scnRNA: small-scan RNA

SDS-PAGE: Sodium Dodecyl Sulphate Polyacrylamide Gel Electrophoresis

SEER: surveillance, epidemiology and end results

SEM: standard error of the mean

SETD2: SET domain containing 2

siRNA: small interfering RNAs

SNORA70F: small nucleolar RNA, H/ACA box 70F

snoRNA: small nucleolar RNA

snoRNP: small nucleolar ribonucleoprotein

SNP: Single Nucleotide Polymorphism

SNX16: sorting nexin 16

SSBP3: single stranded DNA binding protein 3

SSC: side scatter light

SULF2: sulfatase 2

T2DM: type 2 diabetes mellitus

tasiRNA: trans-acting RNA

TBE: Tris-Boric-Acid-EDTA

TBS: Tris Buffered Saline

TBS-T: Tris Buffered Saline/Tween 20

TEKT4P2: tektin 4 pseudogene 2

TEMED: Tetramethylethylenediamine

TGF-β: Transforming growth factor-β

TNM: Tumour Node Metastasis

tRNA: transfer RNA

TSC1/2: Tuberous sclerosis ½

TU: transcription unit

TUBA1: α-Tubulin TUBA1

T-UCR: non-coding RNAs from ultra-conserved regions

U2AF1: U2 Small Nuclear RNA Auxiliary Factor 1

UCR: ultra-conserved region

UTR: untranslated region

VEGF: Vascular Endothelial Growth Factor

VEGFR: vascular endothelial growth factor receptor

WC: Watson-Crick

WT: wild-type

WWP2: E3 ubiquitin protein ligase 2

XIST: X-Inactivation Specific Transcript

ZNF101: zinc finger protein 101

ZXDA: zinc finger, X-linked, duplicated A

CHAPTER 1

GENERAL INTRODUCTION

1.1 Main features and hallmarks of cancer

Cancer is a disease involving dynamic changes in the genome and epigenome and, nowadays, it is the first leading cause of death in the world (Ferlay et al., 2015b). In 2012, there were an estimated 14.1 million new cases of cancer in the world: 7.4 million (53%) in males and 6.7 million (47%) in females, giving a male:female ratio of 10:9 (Ferlay J, 2013).

We can define tumourigenesis as a multi-step process which reflects the genetic alterations that drive the progressive transformation of normal human cells into highly malignant derivatives (Hanahan and Weinberg, 2000).

The earliest knowledge of what now we identify as "cancer" was identified by Egyptians in 1600 BC in the Edwin Smith papyrus, which contains discussion of "cancer" cases. However, the origin of the words related to cancer comes from the Hippocratic physicians in 400 BC, who used the terms *karkinos* and *karkinoma* to describe tumours. *Karkinos* (crab) was referred to any non-healing swelling or ulcerous formation, even haemorrhoids and *karkinoma* was reserved for non-healing cancer (Weiss, 2000). Also the term *oncos* (swelling) is credited to ancient Greek medicine. The first scientific basis for cancer by correlating clinical outcomes with microscopic findings, was proposed in the 19th century that Rudolph Virchow, the father of the modern cellular pathology (Lobo et al., 2007). Comparing hyperplasia with differentiating cells in developing epithelium he theorised that cancer derives from immature cells that grow without any control. Since then new observations have served to clarify the origins and progression of this complex disease.

Table 1.1: Hippocratic terms related to cancer. Modified from (FS, 1986).

Primary terms	Secondary terms
Cancer	Growth; tumor
Carcinoma	Grows
Carcinia	Small growth
Becoming cancerous	Ulcer
	Indurated; Hard
	Hidden
	Superficial
	Deep-seated

Despite remaining mostly unclear, the scientific community agrees on the fact that cancer includes many heterogeneous diseases and can be considered a complex disease, determined by genetic, epigenetic and environmental factors. In addition, some infectious agents could play an important role in human malignancies, such as hepatitis-C virus in hepatocellular carcinoma and papilloma viruses in cervical cancers (Organization, 2014, Walboomers et al., 1999). In the malignant transformation, a single cell acquires a sequence of characteristics which cause out of control growth and make it able to invade other distant tissues through blood circulation or lymph vessels (metastasis). Specifically, the abnormal new growth of cells is called "neoplasia".

From the clinical point of view, malignant progression of a neoplasm means the increasing probability of local spread through a direct invasion of the malignant cells of neighbouring tissues, perifocal spread through migration of a single malignant cell into the interstitial space, regional spread through metastasis to the lymph nodes and distant spread through metastasis into distant sites. Malignant progression is also associated with increasing resistance toward therapies (Hockel and Vaupel, 2001).

From the molecular point of view, normal cells evolve progressively to a neoplastic state and acquire a succession of characteristics, which are common for all type of cancers. Hanahan and Weinberg defined "hallmarks of cancer" the distinctive and complementary capabilities that enable tumour growth and metastatic dissemination (Hanahan and Weinberg, 2011) (Figure 1.1).

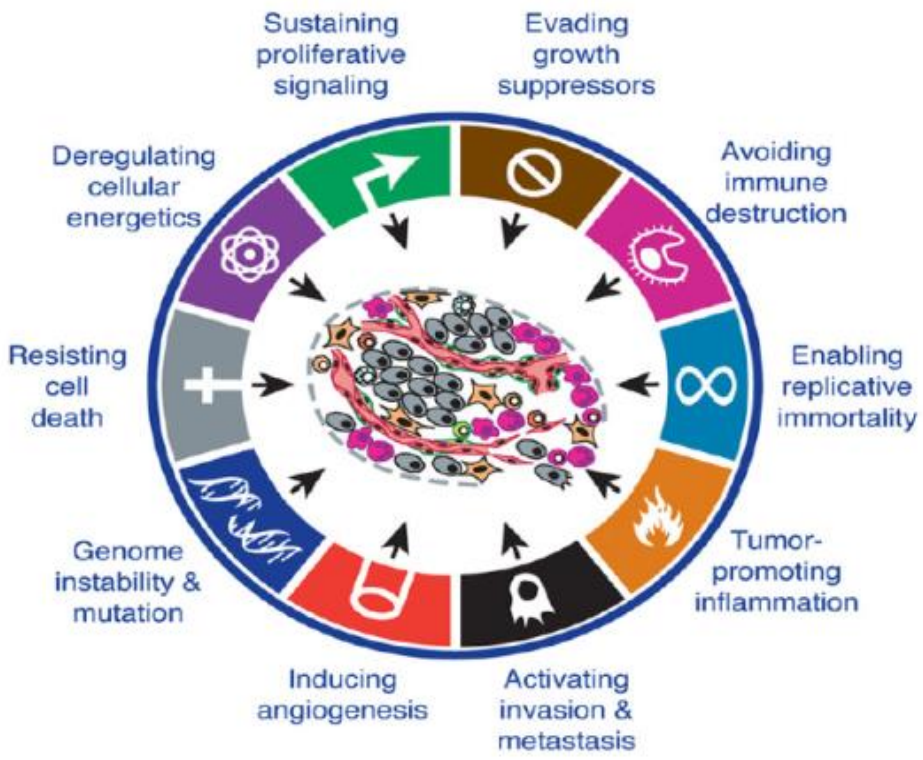

Figure1.1: Features acquired by cells during tumour onset and progression (Hanahan and Weinberg, 2011).

The hallmarks identified by Hanahan and Weinberg allow us to rationalise the complexities of the neoplastic disease. They are defined by the authors as "distinctive and complementary capabilities that enable tumour growth and metastatic dissemination" and include:

- Capacity to proliferate without any limits thanks to their ability to sustain a proliferative signal;
- Capacity to evade the growth suppressors in order to promote the neoplastic transformation;
- Activation of invasion and metastasis;
- Enabling replicative immortality thanks to the acquisition of the ability to escape to all mechanisms of controls;
- Induction of angiogenesis, the development of new vessels for the supply of nutrients and oxygen from the blood;
- Resistance to cell death in particular by avoiding apoptosis, the mechanism that causes the death of the abnormal cells without releasing harmful substances which can activate an immune response. Consequently, the immune response is constitutively active, producing a chronic inflammation status;
- Acquisition of genome mutations that lead the loss of function of genes that encode for proteins able to suppress or promote the tumour progression, named oncosuppressors and oncogenes, respectively;
- De-regulation of cellular metabolism in a condition defined "Warburg effect" that creates the optimal environment for the survival of the cancerous cells promoting glycolysis instead of anaerobic respiration. The consequent acid environment promotes angiogenesis and tumour spread.

In addition to aberrations in cancer cells, tumours have one more step of complexity: the "microenvironment", a combination of various stromal cell types recruited from the adjacent normal tissues, mainly coming from the bone

marrow (Hanahan and Weinberg, 2011). Soluble factors and signalling molecules that can promote neoplastic transformation, support tumour growth and invasion, protect the tumour from host immunity, therapeutic treatments and provide the ideal niches for the development of metastases (Swartz et al., 2012). The concept that the microenvironment is a crucial regulator of carcinogenesis was hypothesised for the first time in 1889 by the French surgeon Stephen Paget in his "seed and soil" theory (Albini and Sporn, 2007) and it was the second evidence-based theory on tumours after Virchow in 1858. He observed the metastatic preference of cancer cells for specific organs, identifying the cancer cells as the "seed" and the specific organ microenvironment as "soil". Despite the metastatic process having been incompletely understood and unknown to Paget, his theory has been later confirmed by numerous publications.

1.2 Lung cancer

1.2.1 General aspects and risk factors

Lung cancer is the most frequent cause of cancer worldwide, with 46,403 new cases (13.0% of the total) diagnosed in the UK in 2014 . The other two most common types of cancers in the UK and worldwide are breast cancer and colorectal cancer (Ferlay et al., 2015a). Lung cancer is the second most common cancer in both men and women. In contrast, prostate and breast cancer are more common in males and females, respectively . Patients- deaths from lung cancer are the most numerous (1.6 million, 19.4% of the total), followed by people affected by liver and stomach cancers, 0.8 million (9.1%) and 0.7 million (8.8%) respectively (Ferlay J, 2013).

The prognosis of lung cancer is poor, with 5-years survival rates of approximately 18.1% in most countries (https://seer.cancer.gov/statfacts/html/lungb.html).

We can consider lung cancer as a disease typical of elderly people. In fact, the Surveillance, Epidemiology and End Results (SEER) data from 2004 to 2008 reported the median age at diagnosis for cancer of the lung and bronchus was 71 years and no cases were diagnosed in patients younger than 20 years. Lung cancer incidence and mortality rates in both sexes are higher in less developed countries than in the more developed world (Ferlay et al., 2015a). However, the World Health Organization estimates that lung cancer deaths worldwide will continue to rise, as a result of an increase in global tobacco use, especially in Asia. In general, the incidence and mortality of lung cancer varies mainly according to gender and geographical distribution (Figure 1.2).

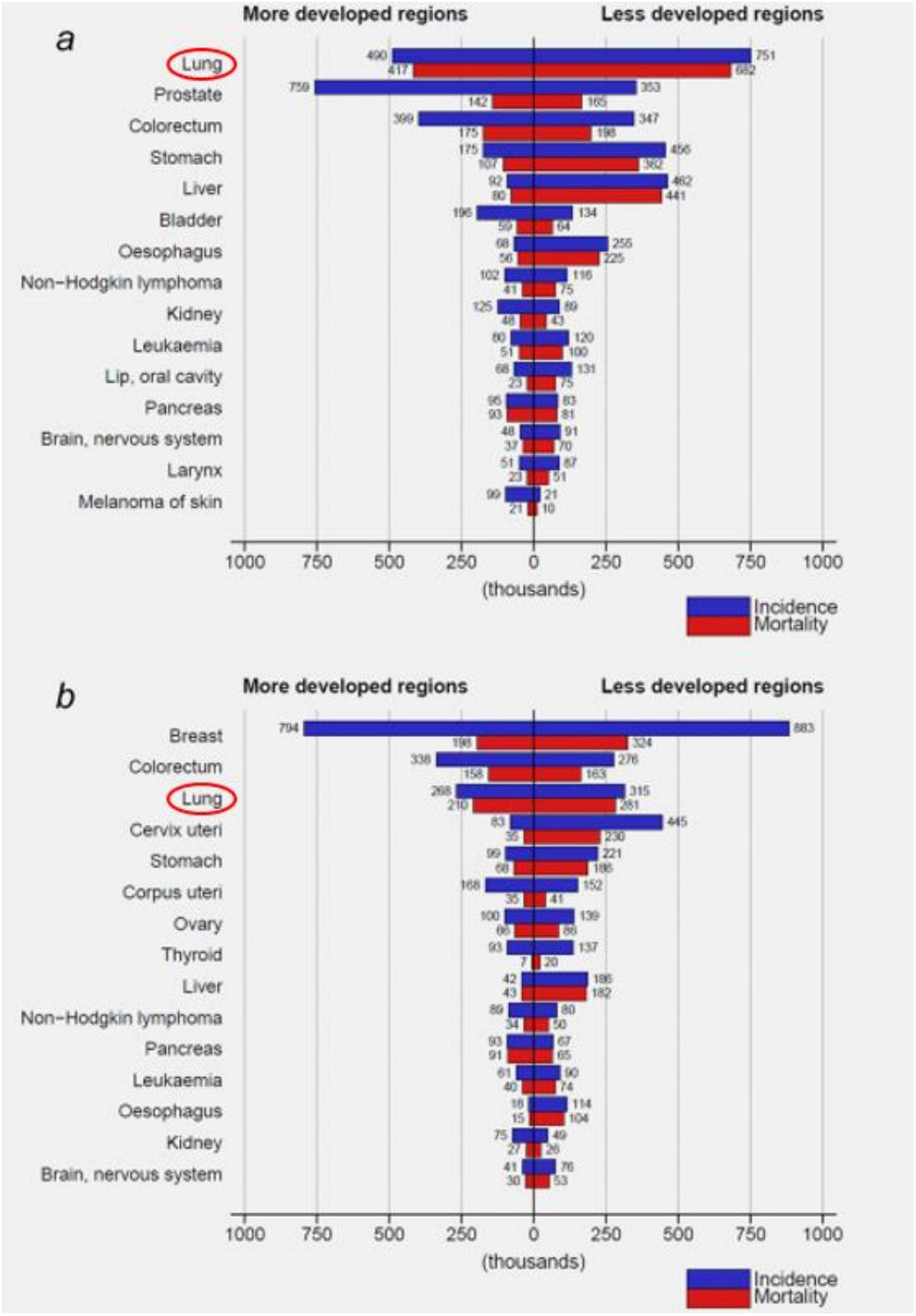

Figure 1.2. Lung cancer incidence according to gender and geographic areas. Estimated numbers (thousands) of cancers incidence and mortality in men (a) and women (b) in more (on the left) and less (on the right) developed countries. Modified from (Ferlay et al., 2015a).

Tobacco smoking is a powerful determinant of risk, so trends in lung cancer incidence and mortality reflect population-level changes in smoking behaviour, including dose, duration and type of tobacco used. So, it has been estimated that over 90% of cases are due to smoking among men and over 80% among women, although there is considerable variation by world region. In fact, in men, the areas with the highest incidence and mortality are Europe (Eastern Europe in particular), North America, Australia/New Zealand, and South America. The rates in China, Japan and South-East Asia are moderately high and the lowest rates are found in southern Asia (India, Pakistan), and sub- Saharan Africa. In women, the geographic pattern mainly reflects the differences in historical exposure of tobacco smoking and secondly in nicotine metabolism and metabolic activation or detoxification of lung carcinogens. Thus, the highest incidence rates in women are observed in North America and North-West Europe (U.K., Iceland, Denmark) and moderate incidence rates in Australia, New Zealand and China. Moreover, several studies have demonstrated the causal association between involuntary tobacco smoking and lung cancer risk in non-smokers (Lortet-Tieulent et al., 2014). Lifetime non-smokers are included in the category of *never smokers*, which refers to people who have smoked fewer than 100 cigarettes in their lifetime. There are copious differences in terms of lung cancer incidence and mortality between smokers, ex-smokers and non-smokers. The first study on the negative effects of tobacco smoking on longevity was published in Science in 1938 by Raymon Pearl. He developed a "life tables" for heavy smokers, moderate smokers and non-smokers, using data from 6813 white men. He concluded that the smoking of tobacco was statistically associated with a shorter duration of life. Specifically, after 30 years, life span was reduced by about 10 years in heavy smokers compared with non-smokers and nearly 4

years in moderate smokers compared to non-smokers (Pearl, 1938). Ex-smokers, that is people who quit for more than 15 years, have an 80% to 90% reduction of their risk for lung cancer compared with persons who continue to smoke. Moreover, stopping smoking before middle age reduces the risk attributable to tobacco by more than 90%.

Cigarette smoke is a complex aerosol composed of gaseous and particulate compounds. In particular, smoke consists of two components: the mainstream (that is inhaled directly into the lungs) and the side stream (the smoke that is emitted from the burning end of a cigarette, cigar or pipe). The primary determinant of tobacco addiction is nicotine, and tar is the total particulate matter of cigarette smoke after nicotine. Other potential carcinogens are the polycyclic aromatic hydrocarbons (PAHs), aromatic amines, N-nitrosamines, and other organic and inorganic compounds, such as benzene, vinyl chloride, arsenic and chromium.

Other types of smoking, such as marijuana and cocaine, have been studied but a clear association with lung cancer has not yet been established (http://www.iarc.fr/). People with chronic obstructive pulmonary disease (COPD) are at a high risk to develop lung cancer (Leary, 2012) and even if the COPD is a consequence of smoking, it is now considered as a risk factor itself.

Exposure to asbestos is a critical environmental factor associated with lung cancer (Leary, 2012). Asbestos is a natural fibrous rock, used for electrical and building insulation and 20-25% of asbestos-exposed workers have been estimated to develop lung cancer.

Other risk factors associated with lung tumours are diet (for instance, low serum concentrations of antioxidants, such as vitamins A, C, and E), infections (risk is almost three times higher in people with the Human Immunodeficiency Virus HIV or acquired immune deficiency syndrome AIDS), environmental air pollution, workplace substances (such as radon, asbestos and silica), previous lung diseases (pneumonia, for example) and family history (especially in non-smokers).

In addition to the environmental factors, genetic and epigenetic alterations also play a crucial role in the development of lung cancer. The most common mutated genes are p53, KRAS, Endothelial Growth Factor Receptor (EGFR), BRAF, Phosphatidylinositol-4,5-Bisphosphate 3-Kinase Catalytic Subunit A (PIK3CA), Hepatocyte growth factor receptor (MET) and the small Guanosine-5'-triphosphatase (GTPase) genes RIT1. Mutations in chromatin modifying genes SET domain containing 2 (SETD2), Adenine-Thymine-rich (A-T rich) interactive domain-containing protein 1A (ARID1A), SMARCA4 and the RNA splicing genes RBM10 and U2 Small Nuclear RNA Auxiliary Factor 1 (U2AF1) have been also associated with lung cancer. These aberrations affect multiple key pathways, such as receptor tyrosine kinase (RTK)/RAS/RAF, phosphoinositide-3-kinase (PI3K)- mechanistic target of mammalian target of rapamycin (mTOR), p53, alteration of cell cycle regulators , changes in oxidative stress pathways and mutation of various chromatin and RNA splicing factors, thus leading to the development of the disease (Risch and Plass, 2008, The Cancer Genome Atlas Research, 2014). The most common genetic alterations in Non-Small Cell Lung Cancer (NSCLC) patients are listed in the table below

(https://www.mycancergenome.org/content/disease/lung-cancer/) and will be further discussed in Section 1.2.6.

Table 1.2. The most common genetic alterations found in NSCLC patients.

Gene	Alterations	Frequency in NSCLC	References
EGFR	Mutation	12-35%	(Pao and Chmielecki, 2010, Gridelli et al., 2015)
KRAS	Mutation	15-25%	(Wan et al., 2004)
FGFR1	Amplification	20%	(Pao and Chmielecki, 2010)
PTEN	Mutation	4-8%	(Yuan and Cantley, 2008)
ALK	Rearrangements	3-7%	(Meyerson, 2007)
DDR2	Mutation	4%	(Shtivelman et al., 2014)

MET	Amplification	2-4%	(Pao and Chmielecki, 2010)
HER2	Mutation	2-4%	(Gridelli et al., 2015)
BRAF	Mutation	1-3%	(Wan et al., 2004)
PIK3CA	Mutation	1-3%	(Yuan and Cantley, 2008)
AKT1	Mutation	1%	(Altomare and Testa, 2005)
NRAS	Mutation	1%	(Wan et al., 2004)
MEK1	Mutation	1%	(Wan et al., 2004)
RET	Rearrangement	1%	(Shtivelman et al., 2014)
ROS1	Rearrangement	1%	(Shtivelman et al., 2014)

1.2.2 Symptoms and diagnosis

Patients with lung cancer have symptoms not easily distinguishable because they are common with other diseases. The most common symptoms are (Leary, 2012) persistent cough, coughing up blood (haemoptysis), chest pain, persistent breathlessness and tracheal obstruction.

Once one or more of the symptoms above appears, blood and breath tests are usually done by the general practitioner and, if the condition needs to be explored in more depth, the patient is referred to a specialist for further investigation. The diagnosis of lung cancer is obtained through one of the following techniques (Leary, 2012):

- Chest radiography (CXR) is the first test used to diagnose lung cancer. However, a definitive diagnosis of lung cancer cannot rely just on CXR because it is not able to discriminate lung cancer from other conditions, such as non-malignant pulmonary nodules.
- Computed tomography (CT) scan provides cross-sectional imaging and enables images from other parts of the body thanks to the injection of a contrast solution. In this way it is possible to check whether a tumour invaded other tissues, such lymph nodes, brain, bones, liver and adrenal glands (http://about-cancer.cancerresearchuk.org/about-cancer/lung-cancer/advanced/about).
- Ultrasonography is used for the analysis of the neck of lung cancer patients suspected to have mediastinal metastases.
- Positron emission tomography (PET) scan is performed after the patients are administrated the isotope 18 fluorodeoxyglucose (FDG), a

glucose analogue. This allows the detection of malignant cells, as they have a higher metabolism than the normal ones, and take up more glucose (or its analogue). Although this test is very helpful for the diagnosis of lung cancer, false negative results occur, for example because of other inflammatory conditions, including infections. PET is however recommended in some specific cases, such as detecting metastases in the bones.

Other common investigations used for lung cancer diagnosis include the analysis of sputum, bronchoscopy, transthoracic needle aspiration and mediastinoscopy. The analysis of sputum is a non-invasive method to detect malignant cells, however, a distinction between the different types of lung cancer is not always possible and the abnormal cells may come from other parts of the aero-digestive tract. Nevertheless, it is suitable for patients who do not tolerate bronchoscopy or transthoracic biopsy. Bronchoscopy is a standard procedure to detect central lesions, whereas transthoracic needle aspiration is for patients with peripheral lung lesions and mediastinoscopy may be required for central tumours inaccessible by standard bronchoscopy.

1.2.3 Histology, grading and staging

Historically, lung cancers occurring in the cells of the respiratory epithelium have been broadly classified into two types, according to their microscopic appearance: small lung cancers (SCLC) and non-small cell lung cancers (NSCLC). SCLC comprises about 10-15% of lung cancer and it is the most aggressive one. Moreover, it is strongly related to cigarette smoking with only 1% of these tumours occurring in non-smokers. On the other hand, NSCLC is the most common type, accounting about 85-90% of all cases and has a high tendency to spread to the lymph nodes and distant sites. In this study, just NSCLC will be considered, as it is the most common. Generally, NSCLC is further divided into three main subtypes: adenocarcinoma, squamous cell carcinoma and large cell carcinoma. Adenocarcinoma is the most common type of NSCL in the USA and East Asia and although it is prevalent in smokers, it is also seen in non-smokers (especially women) (Stahel, 2007). Most adenocarcinomas arise in the peripheral areas of the lungs and these tend to spread to the lymph nodes and beyond. Squamous cell carcinomas accounts for about 25% of NSCLC cases and arise most frequently in the central chest area in the bronchi. This type of lung cancer does not very often spread to lymph nodes, but grows quite large, forming a cavity. Finally, large cell carcinomas is the less common type of NSCLC and has a high tendency to spread to lymph nodes and distant sites (Herbst et al., 2008).

Once a diagnosis of lung cancer has been made, it is important to define the stage of the disease, in order to make the best treatment decision, in terms of safety and efficacy. The stage of the disease is defined as "a particular step, phase,

or position in a developmental process" (Dictionary.com, 2014) and it is important for prognosis and treatment planning.

The staging for NSCLC is based on the international Tumour Node Metastasis (TNM) system which evaluates the overall anatomical spread of cancer by considering the tumour size and invasion, extent of lymphatic spread and the presence of metastatic disease. "T" indicates a primary tumour, "N" the absence/presence of metastasis in lymph nodes and "M" indicates that distant metastasis is present (Table 1.3). The surgical resection of a tumour is normally performed on patients graded up to N2. Otherwise, patients affected by NSLC are treated with chemotherapy, radiotherapy or a combination of these. The therapy depends on the stage when the cancer is diagnosed. Patients at the earlier stages have a better prognosis with 5-year survival for stage I disease at over 55%, whereas most of the patients with a metastatic disease at stage IV the survival is only 1% (Leary, 2012).

Table 1.3. Tumour Node Metastasis classification in Non-Small Cell Lung Cancer. Modified from (Detterbeck et al., 2009). This classification was used by the clinicians whose patients gave samples.

Descriptor	Definition	Subgroups
Primary Tumour (T)		
TX	Tumour not assessed	-
T0	No primary tumour	-
Tis	Carcinoma in situ	-

T1	Tumour<3cm, surrounded by lung or visceral pleura, no evidence of invasion more proximal than the lobar bronchus	T1a, T1b
T2	Tumour>3cm but <7cm with one of the following: invades visceral pleura, involved the main bronchus>2cm distal to the carina, associated with atelectasis/obstructive pneumonitis extending to hilar region but not involving the entire lung	T2a, T2b
T3	Tumour>7cm with one of the following: invasion of chest wall, diaphragm, phrenic nerve, mediastinal pleura or parietal pericardium	-
T4	Tumour of any size that invades any of the following: mediastinum, hearth, great vessels, trachea, recurrent laryngeal nerve, oesophagus, vertebral body or carina; or separate tumour nodule(s) in a different ipsilateral lobe	-
Regional Lymph nodes		

NX	Regional lymph nodes not assessed	-
N0	No regional node metastasis	-
N1	Metastasis in ipsilateral peribronchial and/or ipsilateral hilar lymph nodes and intrapulmonary nodes, including involvement by direct extension	-
N2	Metastasis in the ipsilateral mediastinal and/or sub carinal lymph node(s)	-
N3		
Distant metastasis (M)		
MX	Metastasis not assessed	-
M0	No distant metastasis	-
M1a	Separate tumour nodule(s) in a contralateral lobe; tumour with pleural nodules or malignant pleural (or pericardial) effusion	-
M1b	Distant metastasis	-

Table 1.4. **NSCLC staging** (Detterbeck et al., 2009).

Stage	TNM
0	Carcinoma in situ
IA	T1N0M0
IIA	T2N0M0
IB	T1N1M0
IIB	T2N1M0 T3N0M0
IIIA	T3N1M0 T3N1M0 T2N2M0 T3N2M0
IIIB	T4N0M0 T4N1M0 T4N2M0 T1N3M0 T2N3M0 T3N3M0 T4N3M0
IV	Any T, any N, M1

The TNM classification is not normally used for SCLC, because it is not accurate for the evaluation of the survival. Considering this, SCLC is generally classified as:

- Limited disease: restricted to one hemi-thorax with regional lymph node metastasis;
- Extensive disease: spread to distant sites (the equivalent of the M1 stage in TNM).

SCLC can be treated with surgery when there is no sign that cancer has spread to the lymph glands in the centre of the chest. However, the malignancy is usually spread at the time of diagnosis and chemotherapy remains the main treatment.

This study focuses on NSCLC only.

1.2.4 NSCLC treatments

Surgery is the standard treatment for the early stage of lung cancer (stages I and II), even if a systemic relapse accounts for more than 70% of all recurrences (Reck et al., 2013) and chemotherapy still remains the standard of care in locally advanced, unresectable NSCLC or for elderly patients with multiple co-morbidities (Leary, 2012). The high rate of recurrences reported above may be due to the presence of micro metastases at the time of diagnosis and for this reason, an additional therapy with adjuvants (in addition to the surgery) or neo-adjuvants (before the surgery) is highly recommended (http://pathways.nice.org.uk/pathways/lung-cancer#path=view%3A/pathways/lung-cancer/treating-non-small-cell-lung-cancer.xml&content=view-index, 2017). However, in some cases, such as elderly

patients with multiple co-morbidities, chemotherapy is the only possible therapy. Chemotherapy significantly improves the survival and quality of life of the patients and should be given in combination with a single third-generation drug (eg. Gemcitabine) plus a platinum drug, either carboplatin or cisplatin by taking into account their toxicity (Leary, 2012).

Recently, new biological drugs are emerging for the treatment of many diseases, including cancer, with the aim to better develop a so-called: "personalised medicine". Personalised medicine is an emerging field that takes into account not only the disease itself but also the individual characteristics of each patient. In the case of NSCLC, some genetic aspects that drive the malignancy have been elucidated and now new biological drugs for the treatment of specific patients have been designed. The Epidermal Growth Factor Receptor (EGFR) and Anaplastic Lymphoma Receptor Tyrosine Kinase (ALK) are the most common mutated genes in NSCLC patients and play a crucial role, with the result of constitutive activation of their relative proteins and, therefore the progression of the malignancy. The effect of these mutations can be antagonised using specific drugs, such as Erlotinib, that inhibits the EGFR tyrosine kinase domain, thus switching off the receptor or Crizotinib, that compete within the ATP-binding pocket of ALK, thus making it inactive. The formation of new blood vessels from pre-existing ones is a common feature in all cancers, including lung. Considering this, drugs able to inhibit the formation of new vessels have been developed, with the aim to deprive the tumour of oxygen and nutrients needed for its growth. In NSCLC, the use of Avastin, a Vascular Endothelial Growth Factor (VEGF) inhibitor, is widely used in patients. A list of the approved biological drugs for the treatment of NSCLC is reported in Table 1.5. The

negative aspect of the use of the biological drugs, as well as the chemotherapeutics, is the acquired resistance of the patients after the treatment. The resistance may be due to a second mutation in the target gene or the activation of other oncogenic pathways (Reck et al., 2013). For this reason, the efficacy of a miRNA based treatment is now becoming popular and has been further investigated in this study. A single miRNA can target up to 2,000 transcripts, therefore may potentially act on many oncogenic pathways, rather than on only one. Targeting multiple molecules by using a single agent may be a good strategy for the cancer treatment. For this reason, in this study, the effects of a single miRNA on many aspects of cancer progression have been investigated.

Table 1.5. Approved biological drugs for the management of Non-Small Cell Lung Cancer.

Target	Drugs	Most common side effects
Epithelial Growth Factor Receptor (EGFR)	Erlotinib Gefinitib	Skin problems, diarrhoea, mouth sores, loss of appetite
Anaplastic Lymphoma Receptor Tyrosine Kinase (ALK)	Crizotinib	Nausea and vomiting, diarrhoea, constipation, fatigue
Vascular Endothelial Growth Factor (VEGF)	Bevacizumab (Avastin)	High blood pressure, fatigue, bleeding, low white blood cell, loss of appetite, diarrhoea

1.2.5 Molecular and biological features of lung cancer

The progression of lung cancer involves multiple environmental, genetic and epigenetic factors. The genetic alterations include the deletion, amplification, point mutation or translocation of specific genes, as listed in Table 1.2. Mutations in growth factor receptors lead to their constitutive activation and the result is the activation of some downstream pathways involved in the acquisition and maintenance of the malignant characteristics, such as an uncontrolled proliferation and growth and the suppression of apoptotic signals (Figure 1.3). Genetic mutations also occur also in some key molecules involved in these pathways, thus making the management of lung cancer more difficult.

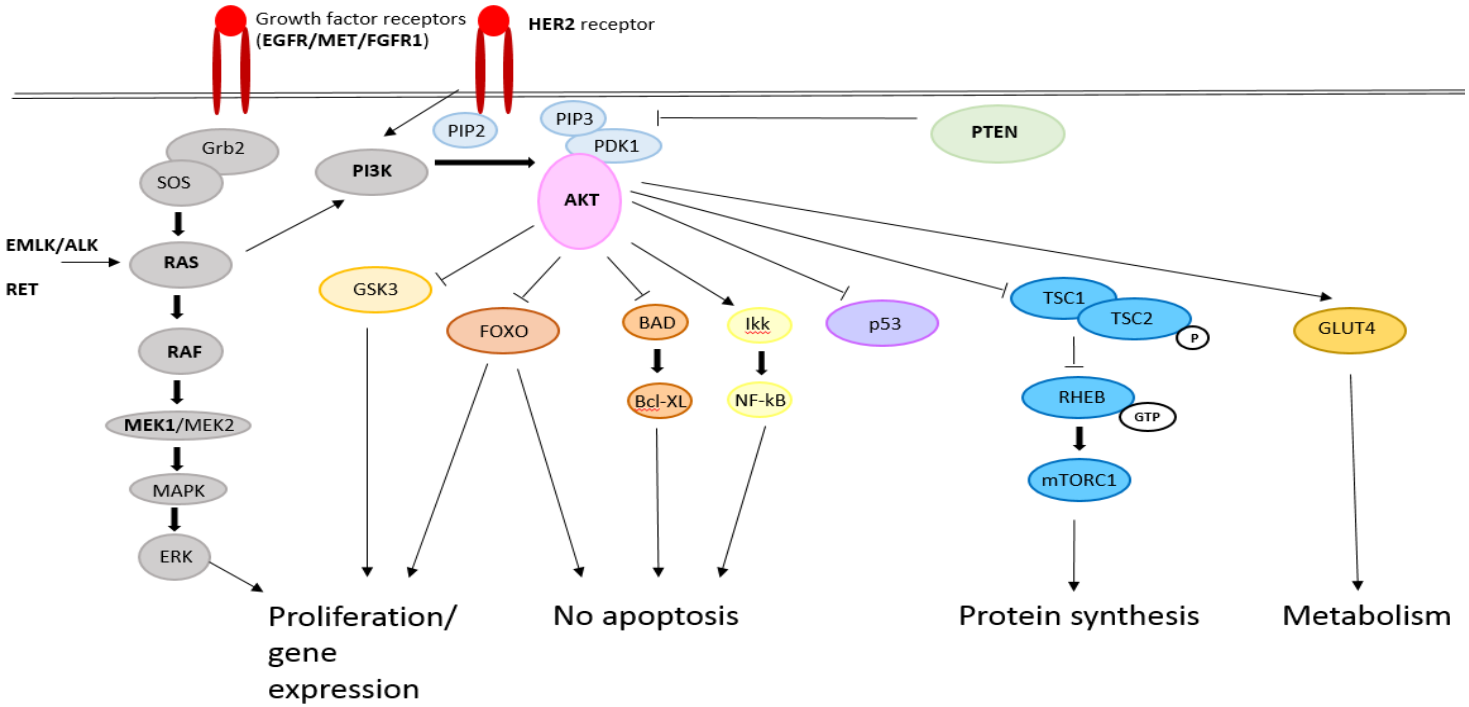

Figure 1.3. Main pathways involved in lung cancer progression. The mutated proteins shown in bold are found more often in patients affected by lung cancer (Wan et al., 2004, Shtivelman et al., 2014, Yuan and Cantley, 2008).

Most of lung cancer patients are diagnosed with mutations in the Epidermal Growth Factor Receptor (EGFR) gene, with deletions in 85% of all cases (Shtivelman et al., 2014). EGFR is a transmembrane tyrosine kinase receptor, activated by the binding of its ligand, the epidermal growth factor (EGF), which triggers its homo- or hetero-dimerization. The activated phosphorylated receptor recruits other proteins, such as Grb2 and Sos, which activate downstream pathways, including PI3K and RAS oncogenes. RAS proteins are GTP-binding proteins, usually divided into different families (KRAS, NRAS, HRAS), according to the conservation of their sequence. Once activated, RAS binds one of the members of the RAF serine/threonine kinase family, thus leading to the activation of the mitogen-activated protein kinase kinases MEK1/2, MAPK and, finally, the signal-regulated kinase (ERK), that translocates into the nucleus and causes the transcription of genes involved in the proliferation of cells (Figure 1.3). The same pathway may be triggered by other transmembrane tyrosine receptors, such as the hepatocyte growth factor receptor c-MET and the Fibroblast Growth Factor Receptor 1 (FGFR1) (Pao and Chmielecki, 2010).

Lung cancer patients are also found with mutations in other genes within the pathway triggered by EGFR (Table 1.2, Figure 1.3), such as RAS, RAF and MEK1 (Wan et al., 2004, Shtivelman et al., 2014). RAS signalling may also be amplified by the mutated form of the Anaplastic lymphoma kinase (ALK) or the Rearranged during Transfection (RET) proteins (Shtivelman et al., 2014).

PI3K/AKT is another important pathway that may be activated constitutively by mutations in the genes encoding the two proteins, or by mutated RAS or HER2, another receptor of the EGFR family that has no ligands. PI3K

phosphorylates a protein named Phosphoinositide-dependent kinase-1 (PDK1), a serine/threonine kinase which leads to the production of phosphatidylinositol 3,4,5-trisphosphate (PIP3), a messenger that recruits AKT, thus leading to the activation of many downstream signalling pathways, such as protein synthesis which is involved in the survival of malignant cells (Figure 1.3). Mutations in the Phosphatase and TENsin homolog (PTEN), an upstream effector of AKT1, may also trigger the progression of the malignancy (Shtivelman et al., 2014), as PTEN acts as a repressor of PIP3 (Figure 1.3).

Over the past few years, epigenetics has been widely studied and it has been discovered that many epigenetic changes may be involved in lung cancer onset and progression. These variations are heritable and are reversible. This means that the epigenetic changes may be influenced by the environment, such as cigarette smoking in lung cancer. DNA methylations, histone modifications and microRNA (miRNA) regulations are the main epigenetic factors involved in the malignancies related to the lungs. Some epigenetic therapies have been approved for the treatment of some tumours, but none of them for lung cancer (Ansari et al., 2016). DNA methylation is crucial during embryonic development and cell differentiation. This process also plays an important role during post-natal life, as it contributes to the repression of gene activity through specific enzymes named DNA methyltransferases (DNMTs). DNMTs transfer a methyl group from S-adenosyl-L-methionine to the CpG islands 5'-cytosine carbon, thus maintaining a gene in a silenced state. In lung cancer, the overexpression of DNMTs has been observed (Ansari et al., 2016). In NSCLC, CpG island hyper methylation results in silencing of tumour suppressor and DNA repair genes, which are involved in the cell cycle and as negative regulators of the epithelial-

mesenchymal transition (EMT), the process that leads to metastasis (Mehta et al., 2015).

The histone-deacetylases (HDACs) are a class of enzymes that repress transcription by removing acetyl groups from the histones, thus allowing the histones to condense the DNA. They are divided into four groups (I, II, III, IV), according to their homology with yeast. They are involved in many processes in the body and in tumours they repress the transcription of proto-oncogenes. In lung cancer, many histone aberrations have been observed and it has been demonstrated that HDAC inhibitors are able to reduce the progression of lung cancer by acting on many steps of the tumour progression, including apoptosis, autophagy, cellular necrosis, ROS, cell cycle arrest, angiogenesis and inflammation (Ansari et al., 2016).

The role of microRNAs in lung cancer will be discussed in the further section.

1.3 MicroRNAs

1.3.1 Non-coding RNAs and their general characteristics

The non-protein-coding portion of the genome plays an important role during development and maintenance of physiological functions.

Coding DNA represents about just 2% of the genome, whereas the remaining part is composed of non-coding regions. Since the sequencing of the human genome, it has been clear that higher eukaryotes have increased their complexity not increasing the number of genes but through a sophisticated regulation which also involves non-coding RNAs (ncRNAs). So, the differences between the

organisms reside in the non-coding genome, which was mistakenly labelled as "junk DNA" for many years.

Non-coding RNAs are broadly classified into five categories: small non coding RNAs (microRNA), non-coding RNAs from ultra-conserved regions (T-UCRs), small nucleolar RNAs (snoRNAs), P-element Induced WImpy testis (PIWI)-interacting RNAs (piRNAs), large intergenic non-coding RNAs (lincRNAs) and the group of long non coding RNAs (lncRNAs) (Esteller, 2011).

Many types of disorders, such as neurological, cardiovascular, imprinting disorders and tumours are correlated with disruptions of non-coding regions.

MiRNAs are small ncRNAs of 19-22 nucleotide, expressed in metazoan animals and plants. Their role is to mediate post-transcriptional gene silencing by controlling translation of proteins. The biogenesis and activities of these elements will be discussed in the following paragraphs.

PiRNAs are Dicer-independent ncRNAs of 24-30 nucleotides (nt). They are involved mainly in germline activities in association with some proteins of the Argonaute family (PIWI) (Thomson and Lin, 2009). PiRNAs are transcribed as precursors in the nucleus from the region containing repetitive and transposable elements. When exported to the cytoplasm, they are converted to the mature form by the slicer action of PIWI proteins. Mature piRNAs are very important in epigenetic regulation, suppressing the transposable element expression and mobilization and playing a crucial role in DNA methylation and heterochromatin-mediated silencing (Watanabe et al., 2011). The overexpression or ectopic expression of PIWI genes is correlated with tumours, both in Vertebrates and Invertebrates. For instance, in Drosophila melanogaster ectopic

expression of the genes encoding PIWI proteins drives malignant brain tumour growth (Janic et al., 2010) and in humans, the same situation is associated with several cancer types (Thomson and Lin, 2009).

SnoRNAs are ncRNAs of 300-600 nt in length. In association with a group of ribonucleoproteins called small nucleolar ribonucleoproteins (snoRNPs), they regulate the 2'-O-methylation (Kiss-László et al., 1996) and pseudouridylation (Ni et al., 1997) of ribosomal RNA (rRNA), facilitating the rRNA folding and stability in the nucleolus. SnoRNAs are located in the human genomic locus 15q11-q13 and play a crucial role in some imprinting disorders, such as Prader-Willy and Angelman syndromes. In Prader-Willy syndrome the loss of the snoRNA HBII-52 produces an alternative splicing which results in a change of the sequence of the pre-mRNA that encodes for serotonin receptor HTR2C (Kishore and Stamm, 2006). Interestingly, the misregulation of snoRNA sequence has been observed also in other diseases, including tumours (Su et al., 2014, Mannoor et al., 2012).

LncRNAs are a heterogeneous group of non-coding transcripts more than 200 nt in length, including RNA transcribed from intergenic regions (lincRNAs) and RNAs transcribed from ultra-conserved regions (UCRs). They are involved in several epigenetic modifications of DNA, mainly by recruiting chromatin remodelling complexes to specific loci. Several ncRNAs are located in human homeobox (HOX) loci. One of the best known is HOTAIR (HOX Transcript Antisense Intergenic RNA) which is transcribed from the HOX C locus (12q.13). HOTAIR is able to silence the domains of chromatin binding Polycomb Repressive Complex 2 (PRC2) of Polycomb complex, that is required for histone3lysine27 (H3K27) trimethylation and transcriptional silencing of the

HOX D locus (Rinn et al., 2007). It has been observed that in epithelial cancer cells, high levels of HOTAIR increase the capacity of these cells to metastasize (Gupta et al., 2010). LcnRNAs are also important in physiological processes, such as X-chromosome inactivation in mammals: the X-Inactivation Specific Transcript (XIST) recruits the Polycomb complex to silence the X-chromosome; the lncRNA TSIX is transcribed in the opposite direction of XIST and represses XIST RNA accumulation acting in cis (Navarro et al., 2006).

LincRNAs transcribed from intergenic regions are associated with the transcription. In particular, they are engaged in several biological activities, such as the response to DNA damage mediated by p53 (Huarte et al., 2010). LincRNA p-21, located near p21 gene, binds p53 promoter and represses the expression of downstream genes in the pathway of p53.

The last class of lncRNAs is represented by transcripts from ultra-conserved regions (UCRs), some of which overlap with encoding exons and do not encode any protein (T-URCs) (Calin, 2007). T-URCs are expressed in several tissues and although their function is unknown, it seems that some of them are able to bind miRNAs.

1.3.2 General characteristics of miRNAs

The first studies on small RNAs were carried out by Charlie et al. in 1981 and by Ambros and Horvitz in 1984 using the nematode *Caenorhabditis elegans* as a model organism. They focused on lin-14, lin-28 or lin-29 genes, which are involved in the first steps of the larval development. Their studies revealed that these genes cause heterochronic developmental defects: the timing of specific developmental events in several tissues is altered relative to the timing of events

in other tissues. These abnormalities are due to a temporal mutation that causes a delayed or early development. The transcription of lin-4 starts at the first stage (L1) and its expression level remains constant for the following larval stages (L2, L3, L4) (Ambros and Horvitz, 1984). A loss-of-function mutation of lin-4 results in an aberrant adult phenotype, such as the absence of the adult cuticle and vulva. On the other hand, a loss of function mutation in lin-14 produces a precocious expression of cell fates that normally occur at later larval stages and a gain-of-function mutation that results in retarded larval phenotypes (Ambros and Horvitz, 1987).

In 1993, Lee and Ambros used this information to investigate the mechanism that regulates the correct development in *C. elegans* in detail. They first observed that at the end of the first larval stage (L1) a decrease in lin14 transcript did not correspond to a decrease of LIN4 protein level. Starting from this experimental evidence they found that LIN14 expression was negatively regulated by lin4 at a post-transcriptional level. The Lin-4 gene, in fact, located within an intronic region and does not encode a protein but a small RNA of 22 nucleotides partially complementary to the untranslated region at the 3' end of lin-14 (3'UTR). This was the first evidence that the protein translation can be inhibited at a post-transcriptional level by small RNAs which are called miRNAs (Lee et al., 1993).

In the same time period it was discovered that in rare cases the post-transcriptional regulation of some proteins does not involve the 3'UTR but the opposite end, the 5'UTR , as in the case of ferritin biosynthesis (Aziz and Munro, 1987).

A few years later, in 1998, Fire and his colleagues described the phenomenon of genetic interference using once again *C. elegans* as an animal model. They were

able to disrupt the function of endogenous genes by the injection into gonads of RNA that hybridized with the gene considered (Fire et al., 1998). They observed that the injection of a single-stranded RNA (ss-RNA) in adult animals caused a modest effect on the endogenous messenger RNA transcript. On the other hand, the double-stranded RNA (dsRNA) was able to interfere in a very potent manner with the expression of the gene, with the same effects of a loss-of-function mutation. The stable and specific interference has been observed not only in the adult animals but also in their progeny when the double-stranded fragments were injected into the cavity of the tail or into the head of the animals.

Contrary to the discovery of Lee and Ambros, Fire and colleagues observed that the interfering effect occurs when the region of homology of the double-stranded RNA is within the target (Fire et al., 1998). There was no interference if the region of homology was located in non-coding region, such as 5' or 3' UTR. Moreover, the effect of the interference was not the inhibition of the translation but the translation of the corresponding endogenous mRNA transcript. This mechanism of interference was named "interfering RNA" (iRNA).

Some years later, using Drosophila melanogaster as an animal model, Dicer was identified as an important enzyme. Dicer is expressed in embryos and in adult animals and plays a key role in a complex called RISC (RNA induced silencing complex) (Bernstein et al., 2001).

Dicer belongs to the members of RNase III, a family of endoribonucleases specific for dsRNAs. This family of enzymes is able to cleave dsRNA molecules into small fragments about 19-22 in length with 2-nt 3' overhangs and a 5'

terminal phosphate group. The characterization of RISC represented a milestone in the discovery of biogenesis of small RNAs, including miRNAs.

After the discovery of the mechanisms responsible for the production of small RNAs (which will be discussed in a following paragraph) the definition of interference RNA has been revised as follow: iRNA is a post-transcriptional gene silencing mechanism which can be triggered by small non-coding RNA molecules similar in size and processed by Dicer, such as miRNAs and small interfering RNAs (siRNAs). The main difference between miRNAs and siRNAs is represented by the binding to the target. In particular, miRNAs inhibit the translation of a mRNAs by a non-perfect base pairing to the 3'UTR of the target, whereas siRNAs recognize targets by the precise complementarity of sequence and mediates the degradation of the target (Ambros et al., 2003, Filipowicz et al., 2005).

Both miRNAs and siRNAs act in the cytoplasm. However siRNAs are also involved in another process in the nucleus in association with a complex called RITS (RNA-induced Initiation of Transcriptional gene Silencing) and induce the epigenetic gene silencing at specific chromosomal loci (Verdel et al., 2004).

MiRNAs have been found in almost all eukaryotes, including yeast (*Schizosaccharomyces pombe*), plants (*Arabidopsis thaliana*), nematodes (*Caenorhabditis elegans*), flies (*Drosophila melanogaster*), mice and human (Ying and Lin, 2005). In contrast, natural siRNAs are abundant in plants and in simple animals but are very rare in mammals.

1.3.3 Regions encoding miRNAs

In humans, the genes encoding for miRNAs are located in all chromosomes, except the Y. Almost 50% of the known miRNAs are found in clusters and are transcribed as polycistronic primary transcripts. Probably they derive from events of duplication that occur during the evolution.

The majority of mammalian miRNAs are located in defined transcription units (TUs) which are defined as follows: sequences of nucleotides in DNA that code for a single RNA molecule, along with the sequences necessary for its transcription. They normally contain a promoter, an RNA-coding sequence, and a terminator (http://www.nature.com/scitable/definition/transcription-unit-260). These miRNAs have their own promoters and are classified as "intergenic miRNAs". On the contrary some other miRNAs do not have their own promoters but share promoters with their host genes and are classified as "intronic miRNAs" For intronic miRNAs, the heterogeneous nuclear RNA (hnRNA) of their respective host genes are considered to be their pri-miRNAs and the steps of their biogenesis are the same as for intergenic miRNAs. However some intronic miRNAs might be transcribed from unique transcription units having their own promoters independent of their host genes. All these considerations underline the complexity of regulation of miRNA biogenesis (Rodriguez et al., 2004, Ramalingam et al., 2014).

1.3.4 Biogenesis of miRNAs

Overview

In the canonical pathway of miRNA biogenesis, miRNA maturation occurs in two main steps according to the compartment in which the precursors are processed.

In the first step, miRNAs are transcribed in the nucleus by RNA polymerase II (RNA Pol II) as long primary monocistronic, dicistronic or polycistronic miRNA precursor known as primary miRNA transcripts (pri-miRNAs). Pri-miRNAs fold into hairpins and then are converted into precursor miRNAs (pre-miRNAs) 70-100 nt in length by the cleavage of RNase III Drosha operating in complexes with dsRNA-binding proteins, such as Di George syndrome Critical Region 8 (DGCR8). In the non-canonical pathway of miRNA biogenesis, some pre-miRNAs are produced from very short introns (mirtrons) as a result of splicing and debranching, thereby bypassing the Drosha–DGCR8 step (Krol et al., 2010).

After being exported to the cytoplasm by the karyopherin Exportin-5, pre-miRNAs are processed into miRNA duplexes 19-22 nucleotides in length by Dicer, operating in complex with the dsRNA-binding proteins (dsRBPs). One strand of the duplex, representing a mature miRNA, is incorporated into a complex called miRISC (miRNA-containing RNA-Induced Silencing Complex). This induces the translational repression or the degradation of the mRNA target. through the interaction between the seed region (nucleotides 2–8) of the miRNA and the 3-UTR of the mRNA target (Krol et al., 2010, Bartel, 2009).

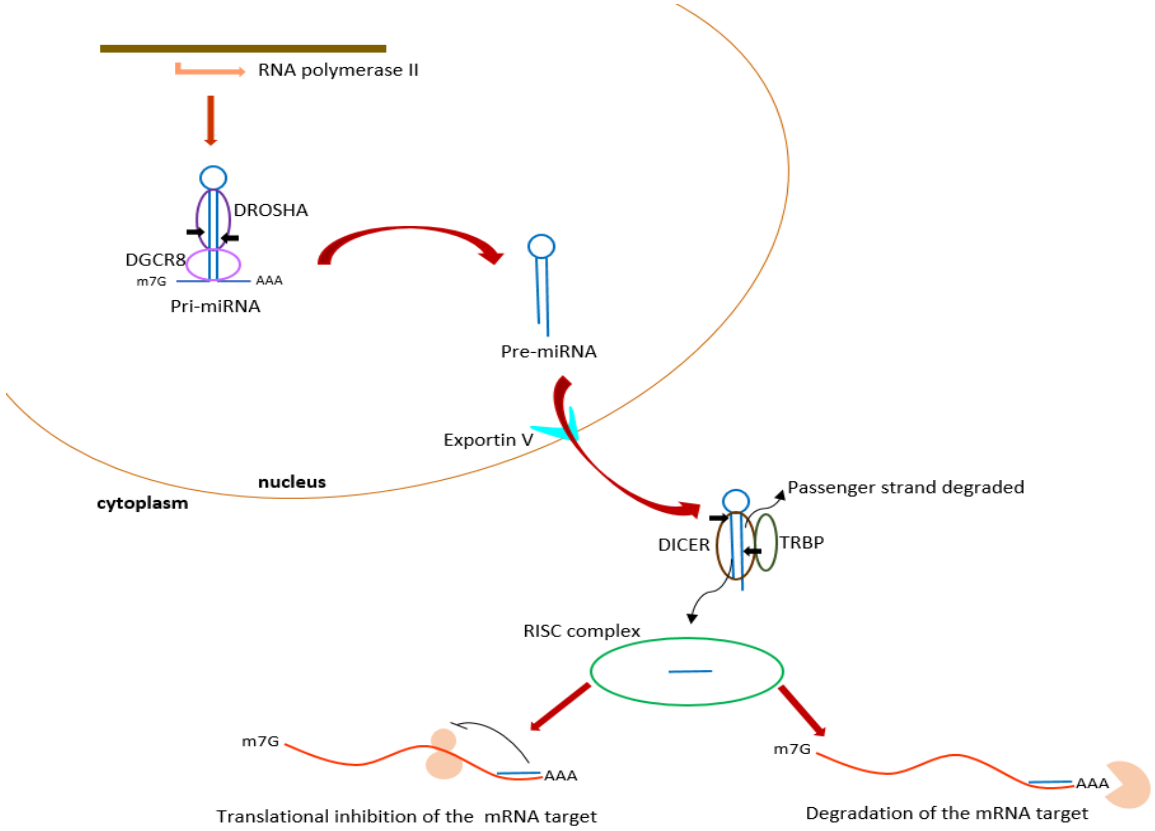

Figure 1.4. Canonical miRNA biogenesis. Transcription of miRNA genes by RNA Pol II results in the production of pri-miRNAs which have a stem and loop structure. Cleavage of the pri-miRNAs by the endoribonuclease III enzyme Drosha and its cofactor Di George syndrome chromosomal region 8 (DGCR8) results in the production of pre-miRNAs, which are exported into the cytoplasm by the Exportin V protein. Following their export from the nucleus, pre-miRNAs are processed into miRNA duplexes by the cytoplasmic ribonuclease Dicer. The Trans-Activation Response RNA Binding Protein (TRBP), together with other factors, allows the loading of one of the two miRNA strands into RISC complex, thus leading to the translational inhibition or degradation of the mRNA targets Modified from (Krol et al., 2010).

Nuclear processing

Most mammalian miRNAs are within introns of either protein-coding or noncoding TUs, whereas ~10% are encoded by exons of long non-protein-coding transcripts, also known as mRNA-like noncoding RNAs (mlncRNAs) (Rodriguez et al., 2004). Intergenic miRNAs have a dedicated promoter, whereas clustered miRNAs share one promoter and are co-regulated as a part of long pri-miRNAs (Treiber et al., 2012).

In mammalian cells three major RNA polymerases are involved in the transcription of the nuclear genome: Polymerase I (Pol I) that is specific for the ribosomal RNA (rRNA), Polymerase II (Pol II) that transcribes the mRNA coding genes and Polymerase III (Pol III) that is involved in the transcription of non-coding RNA, included tRNAs.

Although miRNAs belong to ncRNA genes, several pieces of evidence suggest that they are transcribed by Pol II, although the possibility that a small number of miRNA genes might be transcribed by other RNA polymerases cannot be excluded. In particular, it is reasonable to assume that Pol II transcribes the miRNAs involved in various regulatory processes and Pol III transcribes the miRNAs whose expression is required in all tissues (Wang et al., 2013). Similar to other genes transcripted by Pol II, miRNAs have a cap structure and a poly(A) tail and their expression profiles indicate that miRNAs are under control during development and in various tissues. Moreover, a mature miRNA can be obtained from a plasmid that contains a pri-miRNA under the control of heterologous Pol II promoter and miRNA transcription activity that is sensitive to the concentration of α-amanitin that inhibits Pol II activity but not the Pol I and Pol III (Kim, 2005a). The physical association of Pol II with the promoters

of several miRNAs has been demonstrated by immunoprecipitation analysis (Kim, 2005b).

Transcription of miRNA genes by RNA Pol II results in the production of pri-miRNAs which have a stem and loop structure with both 5' 7-methylguanosine (m7) caps and 3' poly(A) tails. Cleavage of the pri-miRNAs by the endoribonuclease III enzyme Drosha and its cofactor DGCR8 results in the production of pre-miRNAs, which are hairpins of approximately 70-100 nt in length and contain a monophosphate at the 5' terminus and a 2-nucleotide overhang with a hydroxyl group at the 3' terminus.

The complex formed by Drosha and DGCR8 is called Microprocessor and it has been demonstrated that both of these two factors are necessary for the maturation of pre-miRNA. Specifically, neither recombinant DGCR8 nor Drosha alone is able to process pri-miRNA (Yeom et al., 2006).

Drosha is a conserved protein of 160 kDa and belongs to the RNase III family of proteins, which are enzymes responsible for endonucleolytic reactions. In miRNA biogenesis two members of this family are involved: Drosha in the nucleus and Dicer in the cytoplasm. The difference between them is in the substrate specificity and mechanism of action (46): Drosha binds to pri-miRNA and introduces a cut from the terminal loop, whereas Dicer cleaves from the 3' terminus (Kim, 2005b).

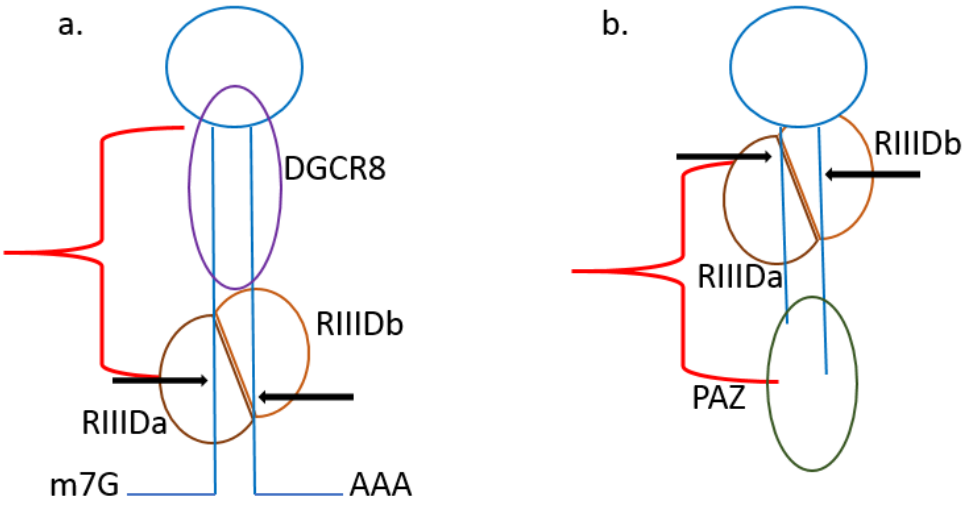

Figure 1.5. Mechanism of action for Drosha (a) and Dicer (b). Modified from (Kim, 2005b). a) DGCR8 works as a molecular anchor for Drosha. DGCR8 recognises and binds the junction between the stem and the loop of a pri-miRNA. Drosha binds DGCR8 and cuts approximately 11 bp away from the junction through its two RNase III domains, RIIIDa and RIIIDb. RIIIDa cleaves the 3' strand, whereas RIIIDb cleaves the 5'strand. b) PAZ domain recognizes and binds the 3' end of the pre-miRNA cleaved by DROSHA. Dicer cuts approximately 22 nt from the 3'end through the RIIIDa and RIIDb subunits.

Drosha is composed of two RNase III domains (RIIIDs) and a double-stranded RNA binding domain (dsRBD), both of them essential for catalysis (Han et al., 2004).

DGCR8/PASHA is a 120 kDa protein that contains two dsRBDs and a putative domain (WW). The human DGCR8 gene is located on chromosome 22q11 and is expressed ubiquitously in both the foetus and adults. Its name is linked to a group of diseases, which occur in case of a mutation in this region and that are indicated as Di George syndrome.

The mechanisms that regulate how the Microprocessor can recognize the target, are largely unknown. However, it is reasonable to assume that the complex is able to bind molecules with a stem and loop structure, avoiding the widespread similar RNA stem loop-structures that can form across the transcriptome (Han et al., 2004, Conrad et al., 2014).

Basically, the role of DGCR8 is to bind the pri-miRNA and the role of Drosha is to cleave it. Notably, Drosha seems not to have any pri-miRNA binding activity (Yeom et al., 2006).

DGCR8 recognizes the target in correspondence of the ssRNA-dsRNA junction and interacts with the whole stem region (about 33 bp) and with the loop. A small region of DGCR8 (residues 484 through 750) is sufficient to facilitate pre-miRNA processing in vitro and includes both the dsRBDs and the C-terminal Drosha-binding domain; the N-terminal region is not involved in processing but it is important for nuclear localization of DGCR8. DGCR8 also stabilize Drosha protein.

Drosha cleavage is shown in Figure 1.5: after DGCR8, the dsRBD of Drosha maytransiently interact with the substrate to place the processing centre approximately at11 bp from the point in which a double strand is formed. In particular, Drosha cleaves at 2 helical turns away from the terminal loop and 1 helical turn away from the basal segment. Pri-miRNA stem, defined by internal and flanking structural elements, guides the binding position of Drosha-DGCR8, which consequently determines the cleavage site (Burke et al., 2014).

The result of processing is a pre-miRNA stem and loop which are hairpins that contain a monophosphate at the 5' terminus and a 2-nucleotide overhang with a hydroxyl group at the 3' terminus.

There is a post-transcriptional crossregulation between Drosha and DGCR8. In fact, DGCR8 stabilizes Drosha via protein-protein interaction but if the level of both Drosha and DGCR8 are high in the cell, Microprocessor would cleave and destabilize the DGCR8-mRNA, decreasing the level of the corresponding protein. This system has been demonstrated in vitro and in vivo and suggests that it could contribute to the control of miRNA biogenesis (Han et al., 2009).

Nuclear export

The transport of pre-miRNA from the nucleus to the cytoplasm is mediated by the nuclear pore complex (NPC), a proteinaceous channel embedded in the nuclear membrane (Nakielny and Dreyfuss, 1999).

In particular, exportin-5 (Exp5), a Ran-dependent importin-β-related transport receptor, mediates nuclear export of pre-miRNA Exp5 and forms a complex cooperatively with the substrate (cargo) and the GTP-bound form of Ran (RanGTP) Upon export, hydrolysis of GTP to GDP on Ran results in release of the cargo from the export complex (Kim, 2004).

Nuclear transport receptors usually recognize specific sequences on the target but in pre-miRNAs no consensus sequence has been found. Probably Exp-5 recognizes the structural motif common in all pre-miRNAs which contain a 2 nt-3' overhangs and a loop.

Cytoplasmic processing

Following their export from the nucleus, pre-miRNAs are processed into 19-22 nucleotide miRNA duplexes by the cytoplasmic ribonuclease Dicer (Figure 1.4).

Dicer is a highly conserved protein found in almost all eukaryotes. Some organisms contain multiple Dicer homologues, such as *D. melanogaster*, which has two isotypes of the enzyme (Dicer-1 and Dicer-2).

Human Dicer, a protein of 160 kDa, belongs to the RNase III family of enzymes showing either an endonucleolytic or a helicase activity. In fact, it first cleaves the pre-miRNA and then contributes to the loading of miRNA into RISC. Dicer contains the following domains: an N-terminal ATPase/RNA helicase domain, a DUF283 domain, a Piwi Argonaut and Zwille (PAZ) domain, two RNase III domains (RIIa and RIIb) and a dsRNA binding motif domain (dsRBD). Moreover Mg2+ ions are present in each catalytic centre (Filipowicz et al., 2005, Zhang et al., 2004).

The dsRNA binding motif domain binds the pre-miRNA to close the loop. The C-terminal RIIb, proximal to the dsRBD, cleaves the 5' strand of the hairpin and RIIa cleaves the 3' strand. On the opposite site, at the terminus, PAZ domain interacts with the 3' overhang of the substrate. RNase III domains functions as a ruler measuring the distance from the 3' end of pre-miRNAs to cleavage site to allow the correct production of the mature miRNA duplex (Figure 1.5) (Filipowicz et al., 2005, Han et al., 2006, Ando et al., 2011). Notably, it has also been demonstrated that Dicer is able to cleave without the 3'overhangs, interacting directly with only the 5' strand (Zhang et al., 2002).

The products of cleavage by Dicer are 19-22 nucleotide mature miRNA duplexes, which are usually approximately 21 nucleotides in length with both sets of termini having 5' monophosphates, 3' 2-nucleotide overhangs and 3' hydroxyl groups. The miRNA guide strand, the 5' terminus of which is energetically less stable, is then selected for incorporation into miRISC (Schwarz et al., 2003, Khvorova et al., 2003).

Mature miRISC is composed of Ago proteins and binds both miRNA and mRNA targets. In mammals four different Ago proteins have been discovered (Ago1-Ago4), all characterized by the same two domains, PAZ, MID (middle) and PIWI.

PAZ-domain function is to anchor the 3'-end of the miRNA with its oligonucleotide/oligosaccharide binding (OB) fold and bind the 3'hydroxilated end (Song et al., 2004).

On the other hand, the MID domain anchors the 5' end of the miRNA, owing to its ability to discriminate between the four different bases. In particular it preferentially binds the uridine base (Frank et al., 2010).

The PIWI domain is structurally similar to RNase H, with an endonuclease activity which is Mg2+ dependent. Both of them are able to cleave the RNA but RNase H recognises the RNA-DNA interaction whereas RISC recognises the RNA-RNA interaction (Chendrimada et al., 2005).

In mammals, all the proteins of the Ago family can mediate both the translation repression of mRNA and the mRNA decay in P-bodies, but only Ago2 has an endonucleolytic activity. In addition, other factors, such as the Trans-Activation Response RNA Binding Protein (TRBP) and Protein kinase RNA activator

(PACT) are involved in strand selection and RISC assembly. In particular, the TRBP association with Dicer provides a platform for RISC and aids the recruitment of Ago2. PACT binds the N-terminal region of Dicer containing the helicase motif (Lee et al., 2006, Bartel, 2009). Neither TRBP nor PACT is required for the pre-microRNA cleavage, however, their role is crucial for the efficiency of miRNA processing. In fact, it has been demonstrated that their depletion causes a decrease in the mature miRNA level (Chendrimada et al., 2005, Lee et al., 2006).

In the canonical pathway of miRNA biogenesis, the imperfect base-pair between a miRNA and the sequence in the 3'UTR of target mRNA has an effect on inhibiting protein synthesis by either repressing translation or promoting mRNA deadenylation and decay (Krol et al., 2010). Deadenylation is the first step in mRNA decay, and is generally followed by removal of the m7G cap (the 7-methylguanosine-triphosphate structure) at the 5' end of mRNAs, which promotes their translation and protects them from degradation and exonucleolytic 5' to 3' degradation of mRNA. In the deadenylation of mRNA, Glycine-Tryptophan Protein of 182 kDa (GW182) and other proteins are involved and act in association with RISC. While the amino-terminal part of GW182 interacts with Ago through its GW repeats, the carboxy-terminal part interacts with the poly(A) binding protein (PABP) and recruits the deadenylases CCR4 and CAF1 proteins (Krol et al., 2010) (Figure 1.4).

In addition to this canonical process, another non-canonical miRNA biogenesis pathway has been discovered in flies and mammals. This alternative process involves a group of miRNAs derived from short hairpin introns (mirtrons) that undergo to splicing and directly exert the pre-miRNAs bypassing Drosha

cleavage. Following the completion of splicing, the branch point of the lariat-shaped intron is resolved and the debranched intron forms a hairpin structure that resembles premiRNA. Some precursors (mirtrons) contain tails at either the 5' or 3' end, which therefore require exonucleolytic trimming for nuclear export (Kim et al., 2009).

1.4 MiRNAs and human pathologies

MiRNAs regulate all the biological functions, including cell growth, differentiation, proliferation, apoptosis and signal transduction pathways (Giza et al., 2014). Their dysregulation may be due to mutations in their encoding genes or in the miRNA biogenesis machinery and their levels may change during either the pre-natal development or the post-natal life. As epigenetic features, they are heritable but may change spontaneously or in response to environmental factors.

The first evidence of the correlation between miRNAs and human diseases has been identified by studying the DGCR8 protein, the RNase III enzyme that, together with Drosha, is responsible for the cleavage of the pri-miRNA in the nucleus. The DGCR8 gene is located on 22q11.2 chromosome and deletions in this gene cause the so-called Di George Syndrome, a rare disease. Children affected by the DGCR8 syndrome develop severe learning disabilities, such as autism, shows congenital malformations, such as the cleft palate, and have many other problems, such as congenital heart diseases and hormone-related disorders. Moreover, microdeletions of 22q11.2 are responsible for up to 1–2% of schizophrenia cases (Karayiorgou et al., 1995). It has been demonstrated that a Dgcr8 haploinsufficiency impairs the miRNA biogenesis and contributes to the behavioral and neuronal deficits associated with the disease *in vivo* (Stark et al., 2008).

Since then, the regulatory role of miRNAs in both physiological and pathological conditions has been widely demonstrated.

Some miRNAs have also been found in viruses, such as the gamma herpesvirus Kaposi's sarcoma-associated herpesvirus (KSHV) and the simian virus 40 (SV40) (Gottwein et al., 2006, Sullivan et al., 2005). SV 40 gene encodes for a miRNA that downregulates the T-antigens by binding their mRNAs. This mechanism does not influence the infection directly but protects the infected cells from the effect of the T-cells, thus promoting the survival of the virus in the host cells.

MiRNAs regulate the immune and autoimmune response in many ways. MiR-21, for example, regulates the T-cell response, the differentiation of dendritic cells and the myeloid cell function (Wang et al., 2016b). This is possible through the ability of a single miRNA to bind and repress the activity of multiple mRNAs at the same time.

MiRNAs are also involved in the normal development of the cardiovascular system, as well as in many pathological conditions of the heart, such as the miR-208a, that is encoded by the MYH6 gene. MiR-208a has shown to be upregulated in hypertrophic mice (van Rooij and Olson, 2012) and an anti-miR-208a leads to a reduced fibrosis, hypertrophy and obesity *in vivo,* thus suggesting a possible use of this miRNA as a therapeutics agent.

MiRNAs are involved in the embryonic development at the gene level and their de-regulation may cause important congenital defects during the different stages of specific pathways. For example, miR-140, miR-17-92 cluster (miR-17, miR-18a, miR-19a, miR-20a, miR-19b-1 and miR-92a-1) and miR-200b play an

important regulatory role during all the stages of palatogenesis (Schoen et al., 2017). MiR-140-5p regulates the first step of the process of the craniofacial formation, by regulating the migration of the neural crest cells to a more ventral position in the embryo, in order to differentiate in multiple tissues, including the craniofacial cartilage. The levels of miR-140-5p may be affected by a SNP (rs7205289: C>A) located in the precursor, that impairs its maturation (Li et al., 2010) or by a mutation on one of its targets, the Platelet Derived Growth Factor Receptor A (PDGFRA) (Rattanasopha et al., 2012). The palatal growth is the second stage of the palatogenesis and is characterized by the proliferation of the cells and accumulation of the extracellular components, such as collagen. The miR-17-92 cluster sustains the proliferation of the cells by inhibiting many anti-proliferative molecules. The activation of the cluster in the post-natal life, however, may contribute to the proliferation of some tumours (Schoen et al., 2017). In the final stage of palatogenesis, the epithelium between the two palatal shelves is removed in a process named "epithelial-to-mesenchymal transition". In this step, the expression of miR-200 must gradually decrease. MiR-200, which targets many factors involved in the Transforming Growth Factor-β (TGF-β) pathway, should be active to allow the closure of the palatal shelves.

1.5 MiRNAs and cancer

MiRNAs in cancer can act either as onco-suppressors (tumour-suppressor miRs) or oncogenes (oncomiRs) and may have a direct impact on cancer phenotypes, depending on their specific targets and the pathways with which miRNAs interact. MiRNAs act as onco-suppressors by targeting oncogenic mRNAs and as oncogenes when they repress the translation of mRNAs with tumour

suppressor functions. This dual classification is complicated by the fact that miRNAs can act as onco-suppressor and oncogenes at the same time and this mainly depends on the context in which miRNAs are expressed. The levels of specific miRNAs in human tumours are like a signature that reflects and is associated with the diagnosis, staging, progression, prognosis and response to therapies (Calin and Croce, 2006).

The first evidence of the involvement of miRNAs in cancer was formulated by Croce et al (Calin et al., 2002). They found that two miRNAs, miR-15 and miR-16, were downregulated in patients affected by B cell chronic lymphocytic leukaemia (CLL) and that the two miRNAs were located at chromosome 13q14, a region frequently deleted in CLL. The target of the miR-15/16 cluster is the B-cell lymphoma 2 (BCL2), an anti-apoptotic protein. The downregulation of the two miRNAs contributes to a higher expression of BCL2, thus conferring resistance to programmed cell death to the malignant cells.

Since then, many groups have investigated the role of miRNAs in cancer and demonstrated their usefulness either as biomarkers, as they were detected in a wide range of biological fluids, or indicators of the tumour subtypes and patient response to treatments (Hayes et al., 2014).

MiRNAs are extremely plastic and their levels may change easily. As all the other epigenetic regulators, their levels may vary according to the time and the stage of the disease. Considering this, the variation of miRNA levels in cancer may be involved in the progression of the disease. This is because MiRNAs themselves are under the control of genetic and epigenetic mechanisms that contribute to their de-regulation. For example, pre-transcriptional regulators are able to affect the biogenesis of miRNAs leading a gain or loss of function of miRNA gene

copy number, mutations of the miRNA precursor, histone deacetylation and hypermethylation of miRNA promoters (Shi et al., 2008). Some miRNAs are clustered in regions of genomic instability or fragile sites and this may contribute to their level and function (Calin et al., 2004). MiRNA levels are also regulated by other transcription factors associated with RNA Polymerase II and all the other nuclear and cytoplasmic enzymes involved in their biogenesis. For instance, it has been shown that the deletion of Drosha, DGCR8 and Dicer1, the main components of the miRNA maturation machinery, enhances the tumour development in a K-Ras–induced mouse model of lung cancer (Kumar et al., 2007). The level of miRNAs may also be influenced by Single Nucleotide Polymorphisms (SNPs) within their own sequence or the sequence of their target genes, thus influencing the activity of the cancer cells (Preskill and Weidhaas, 2013). This is the case of a SNP in the 3'UTR binding region of let-7, which halts the binding of the miRNA and this leads to a higher level of KRAS levels in NSCLC patients (Preskill and Weidhaas, 2013).

The dysregulation of miRNAs may contribute to the malignant transformation in distant sites by directly modulating enzymes which take part in methylation-mediated silencing and chromatin remodelling, in a paracrine manner through exosomes, microvesicles and protein complexes able to influence the tumour microenvironment and by promoting the release of mediators which activate pro- or anti-cancer immune activity (Rusek et al.). In the tumour microenvironment, miRNAs have been found encapsulated in microvescicles, associated with protein complexes and, in some cases, free. They may derive from live, necrotic or apoptotic cells and are released into the tumour microenvironment, where they may be incorporated into the recipient cells and

contribute to the spread of a tumour in a paracrine manner (Turchinovich et al., 2014). In a multiple myeloma model *in vivo*, miR-135 is encapsulated and released into the extracellular space by the malignant cells of the bone marrow. It then penetrates into the endothelial cells and enhances the angiogenesis by targeting the inhibitor of the Hypoxia-Inducible Factor (HIF) (Umezu et al., 2014). The presence of miRNAs in all biological fluids, including saliva, breast milk and blood, has drawn attention on their role as biomarkers, as the dysregulation of specific circulating miRNAs can reflect the physiological and pathological status of patients (Weber et al., 2010). Finally, the activity of miRNAs in cancer and other diseases may be influenced by other RNA molecules named "competing endogenous RNAs" (ceRNAs) that compete with the miRNAs as they share the miRNA binding site with other RNAs (Wang et al., 2016c).

1.6 Strand selection and miRNA prediction tools

During miRNA biogenesis, one of the two strands of the double-stranded molecule is processed (guide strand or miR) and the other one (passenger strand or miR*) is degraded. This process is generally named "strand selection". The guide and passenger strands are frequently named -3p and -5p, according to the direction of the mature miRNA strand. Although the two sister strands are partially complementary and come from the same precursor, they have different targets and are involved in distinct biological pathways or may target the same mRNA but in different sites. The miRNA strand selection may vary among tissues and between normal and malignant cells. Moreover, mutations in the miRNA-precursor, or in proteins involved in miRNA biogenesis, may change

the ratio between the sister strands, resulting in a dysregulation of key biological pathways (Ha and Kim, 2014b).

In Mammals, previous models have suggested that the choice of the mature miRNA depends on the thermodynamic and structural properties of the processed duplex. The more stable strand generally starts with a 5' Uracil (U) base and is rich in purines, whereas the less stable strand starts with a 5' Cytosine (C) base and is rich in pyrimidines (Meijer et al., 2014). According to this theory, the less stable fragment is loaded into RISC because the purine residues may facilitate the strand loading through sequence-independent interactions. In fact, the PAZ domain of Ago2, which participates to the initial steps of DNA recognition and binding, contains numerous aromatic residues involved in RNA binding, and the interaction between these residues and the purine-rich duplex may contribute to strand selection (Meijer et al., 2014). However, data from sequencing studies suggest that it is not always the case, as often both of the strands are active and the choice of the active strand may vary with time and tissues (Okamura et al., 2008). In fact, the predominant form of a miRNA differs among tissues, times of development, and between species suggesting the existence of other mechanisms for controlling the selection of mature miRNAs, such as variations in the proteins that form the RISC complex (Griffiths-Jones et al., 2011, Barbato et al., 2009). The most common modifications of the pre-miRNA are located at the 3'end, probably because they have a little effect on the target selection (Li et al., 2012). MiRNAs recognise the 3'-UTR of their mRNA targets and for this reason, presumably, the modifications at the 3' end may have a smaller impact on strand selection than the changes at the 5' end. However, it is not possible to exclude that the modifications at the 3'end of the duplex may

have a functional role. The strand selection process may also vary due to mismatches in the pre-miRNA sequence (Noland and Doudna, 2013), as these variations are recognised by different proteins of the RISC. Finally, Single Nucleotide Polymorphisms in the miRNA gene sequence may affect both the miRNA processing and the binding with the mRNA targets (Sun et al., 2009).

To assess the biological role of a miRNA, the potential mRNA targets should be identified. As described previously, one single miRNA can target up to 2,000 transcripts and considering that the miRNA sequence is short and not perfectly complementary to the mRNA targets, this research may be difficult. The most common way to make this search easier is to use some bioinformatics tools. The main criteria used by these algorithms are the Watson-Crick base paring between the nt 2-8 at the 5' end of the miRNA (seed region) and the 3'UTR of the mRNA, the free energy of the binding and the conservation of the miRNA binding sites between the species. Some of these tools will be further described in Section 2.16. However, not all miRNAs can bind their targets following the base pairing, for example in the case of a SNP in the pre-miRNA or for an imperfect binding. For this reason, in this study, the classical bioinformatics tools have been integrated with an alternative approach with the use of synthetic miRNA mimics designed with a biotin stretch at the 3' end. These mimics can be transfected into cells and then purified by using streptavidin beads in to obtain just the mRNA bound to the miRNA of interest. The mRNA profile can then finally be analysed through sequencing and validated by qPCR. This method, as will be discussed later, will allow, ideally, to identify all the targets that are not predicted by the bioinformatics algorithms, especially the non-seed based interactions. Although it is a good approach to find the direct targets of a

specific miRNA, this method also shows some limitations. The main limitation is due to inability to detect some transcripts because they might be regulated and expressed differently among the cells or because other transcripts compete for the miRNA binding (Tan et al., 2014). For these reasons we decided to use an integrated approach to better address the biological role of the two forms of miR-140 in lung cancer invasion.

1.7 Potential and current applications of miRNAs in human diseases, including cancer

1.7.1 Diagnosis

Many studies have shown the possible applications of miRNAs as biomarkers, as in many cases a miRNA signature has been associated with the progression of specific diseases and/or the response to a treatment. According to the World Health organisation, a biomarker is "any substance, structure or process that can be measured in the body or its products and influence or predict the incidence of outcome or disease" (http://www.inchem.org/documents/ehc/ehc/ehc222.htm). A good biomarker should be easily detectable by using non-invasive methods and should reflect the health status of the patient, thus allowing either an early diagnosis or prognosis. MiRNAs are ubiquitously expressed in all biological fluids, including saliva, urine, breast milk and blood and correlate with many pathological conditions (Weber et al., 2010). All these characteristics, together with the powerful techniques available that allow detection of small molecules, made them particularly attractive as diagnostic and prognostic markers for many

diseases, including cancer. MiRNAs are tissue and disease specific and their variation may be an indicator of a pathological condition. An early diagnosis, together with an accurate classification of the disease, is crucial for an incisive decision on the patient treatment.

MiRNAs have been found useful for the diagnosis of many diseases, such as cancer, cardiovascular and metabolic disorders (Di Leva and Croce, 2013, Goretti et al., 2014, Wang et al., 2016a). In cancer, miRNAs can discriminate between two or more different cell subtypes because they vary according to the oncogenic pathway activated and the expression of miRNAs in blood reflects their levels in the tumour tissues (Di Leva and Croce, 2013, Salvatore et al., 2016). The miR-200 family, for example, is upregulated in an advanced state of breast cancer and this reflects the stage of the disease, as the members of miR-200 family target zeb1 and zeb2, two of the transcription factors deeply involved in the Epithelial-Mesenchymal Transition (EMT) (Di Leva and Croce, 2013). In other cases, miRNAs are predictive of cancer with specific mutations, as in the case of melanoma, where the low levels of miR-193a, miR-338 and miR-565 have been found in patients positive for BRAF mutations (Di Leva and Croce, 2013).

MiRNAs regulate many proteins involved in the physiological processes of the heart and recently many circulating miRNAs have been used for the stratification of myocardial infarction (Goretti et al., 2014). In clinical practice, multiple factors such as age, gender, systolic blood pressure and smoking habits, are usually evaluated to estimate the cardiovascular risk and it has been demonstrated that the cardiovascular risk is associated with the circulating levels of miRNAs (Goretti et al., 2014). The utility of miRNAs for the diagnosis of

cardiovascular diseases has been further strengthened by the demonstration that specific miRNAs are released into the bloodstream after an infarction (Goretti et al., 2014).

A specific miRNA signature has been recently discovered in patients affected by the type 2 diabetes mellitus (T2DM) and this may help to monitor the progression of this disease. In particular, five miRNAs, miR-661, miR-571, miR-770, miR-892b and miR-1303, have been found highly expressed in patient serum and a higher level has been shown in patients with complications (Wang et al., 2016a). These five miRNAs may be useful as predictive biomarkers for T2DM-related complications and may be involved in the progression of the disease.

Some research groups argued that many factors make the applications of miRNAs in clinical practice quite hard (Tiberio et al., 2015). In fact, the levels of miRNAs may vary amongst people because of the diet or pharmacological treatments, such as aspirin, that may reduce the plasma levels of miR-126 in patients affected by T2DM, thus making this miRNA in the blood not predictive of cardiovascular diseases (de Boer et al., 2013). However, the variability is the major concern of all the biomarkers currently used in the clinical practice and, in the case of the miRNAs, this is not always the case. Some miRNAs, in fact, are tightly associated with the genetic features of a disease and their levels are weakly influenced by other factors, such as miR-483-5p, that may be used to discriminate between the paediatric and adult liver tumours and may not be influenced by any treatment (Salvatore et al., 2016). Another issue related to the use of miRNA as biomarkers is the normalisation method used in the quantification of circulating miRNAs as, to date, a stable housekeeping gene has

not been identified. Moreover, it is still hard to establish the range within the levels of specific miRNAs may be considered physiologically. Finally, same standard operating procedures should be published and followed internationally (Goretti et al., 2014).

All these observations, however, do not weaken the validity of the miRNAs, which may be used in concert with other predictive molecules/factors and should be taken into account for comorbidities and treatments.

1.7.2 Treatment

MiRNAs in tumours can act as onco-suppressors when their expression is lower than in normal conditions, or as oncogenes when upregulated. Their low molecular weight and small size, together with their ability to target multiple molecules without toxicity, provides a new opportunity for cancer treatment compared to other methods such as the gene therapy. For instance, miR-181 regulates T-cell receptor sensitivity by targeting multiple phosphatases, an effect that was not observed by silencing a single component of the pathway by siRNA (Li et al., 2007). Oncogenic microRNAs can be targeted by repression and therefore the inhibition of the interaction between miRNA and mRNA and onco-suppressor expression can be restored in cells using molecules that "mimic" their activity.

Oncogenic miRNAs can be inhibited using oligonucleotides complementary to the mature miRNA (antagomiRs) (Krutzfeldt et al., 2005, Haftmann et al., 2015). AntagomiRs are cholesterol-conjugated single-stranded RNA analogues complementary to miRNAs. The chemical modifications at their 3'-end increase their stability *in vivo* and their efficient direct uptake via cell membrane into viable

cells. Another anti-miR-based strategy uses a stable transfection with virus-associated "miRNA sponges". They are transcripts that express 3' UTRs containing multiple miRNA binding sites from strong promoters, such as U6 or cytomegalovirus (Ebert et al., 2007).

MiRNA replacement therapy aims at the substitution of tumour suppressive miRNAs expressed at lower levels by using oligonucleotide mimics containing the same sequence as the mature endogenous miRNA. This can be achieved by vectors (plasmids or lentiviruses) expressing miRNA precursors or by delivering artificial miRNA duplexes (mimics). MiRNA precursors require transcription and processing, whereas miRNA mimics are directly incorporated into RISC. The challenges for miRNA re-establishment are the same as for miRNA suppression: the specificity and efficiency of the delivery. Despite the miRNA replacement using virus vectors having produced good results (Kota et al., 2009), the application of non-viral vectors, such as nanoparticles, has increased in the last few years. The efficiency of transfection in host cells is higher with viral vectors compared to non-viral vectors. However, the viral vectors show a high immunogenicity and cytotoxicity. The first person who died in a gene-therapy clinical trial suffered from a partial deficiency in a liver enzyme, the ornithine transcarbamylase (OTC). The patient died in 1999 of multi-organ failure, four days after the treatment with an adenovirus vector to deliver the gene for OTC to the liver. The autopsy showed that the vector circulated into the bloodstream and accumulated in the spleen, lymph nodes and bone marrow, although it had been infused directly into the liver through the hepatic artery (Thomas et al., 2003). One of the phenomena associated with the use of viral vectors is that of insertional mutagenesis, the ectopic chromosomal integration of viral DNA that

disrupt the expression of a tumour suppressor gene or activates an oncogene leading to the malignant transformation of cells. Due to their biosafety, the non-viral vectors, as the vehicles for gene therapy, have drawn significant attention.

Two non-viral methods have been developed to protect both miRNA mimics and inhibitors from the degradation by RNases in serum or in the endocytic compartment of the cell (Rupaimoole and Slack, 2017). Firstly, the miRNA mimics chemistry can be modified by methylation of the passenger strand to increase the stability and anti-miRNAs can be modified through the addition of chemical groups that "lock" the nucleic acid (Lock Nucleic Acid, LNA) (Rupaimoole and Slack, 2017).Secondly, vehicles to encapsulate and protect the small RNAs can be produced. Indeed the use of lipid-based nanoparticles is considered the best method to overcome the physical barriers *in vivo*, such as enzymatic degradation, and to access target cells with high tissue-specificity (Chen et al., 2010, Choi et al., 2014).

The use of miRNA mimics therapeutics have been successful in both *in vitro* and *in vivo* models (Chen et al., 2010, Hsu et al., 2013, Esquela-Kerscher et al., 2008) and recently a pharmaceutical company, MiRNA Therapeutics (Texas), has started a multicentre Phase 1 clinical trial of a single miRNA agent in humans and they plan to advance into Phase 2 (Rupaimoole and Slack, 2017). More than one hundred patents affected by liver cancer will be treated with MRX34, a synthetic miRNA mimic of miR-34, which is known to be a tumour suppressor. MRX34 is a double-stranded oligonucleotide delivered using a liposome-formulation called NOV40, which is able to avoid interactions with normal cells and achieve maximal accumulation of the mimic into the liver, due to the high liposomal accumulation in the liver. Other miRNA therapeutics in clinical trials

include the anti-miR-122 for the Hepatitis C, antimiR-103/107 for T2DM, antimiR-155 for cutaneous T cell lymphoma, miR-129 mimic for scleroderma and miR-16 mimic for NSCLC and miR-16 for malignant pleural mesothelioma (Rupaimoole and Slack, 2017, van Zandwijk et al., 2017).

1.7.3 Prognosis

The personalised medicine aims to treat patients with a particular condition by using specific approaches to better manage their health and address them to the best therapy. In the era of molecular medicine, parameters other than the clinical and pathologic features are included in the risk stratification of patients, such as DNA methylation, gene expression and microRNA expression (Hayes et al., 2014). The miRNA signature associated with each individual tumour is now easily possible through either qRT-PCR or Next Generation Sequencing and the data profiles generated are stable within the clinical samples and allow a better prognosis (Lu et al., 2005).

The miRNA molecular profiles correlate with patient survival in many cancers, such as lung and breast (Yanaihara et al., 2006, Kurozumi et al., 2017). In breast cancer, in particular, there is a specific miRNA signature that allows discrimination amongst the subtypes (Kurozumi et al., 2017). Because of the significant differences in prognosis and treatment, miRNAs may be particularly useful in concert with other molecular markers.

A miRNA signature helpful for a better diagnosis has been also found in other diseases, such as cardiovascular and metabolic disorders (Hoekstra et al., 2010, Dangwal et al., 2015). In atherosclerosis, which is the primary cause of cardiovascular diseases, the changes in miR-134, miR-198, and miR-370 in the

blood of patients may be useful to predict the clinical outcome of the disease (Hoekstra et al., 2010). In metabolic disorders, such as type 2 diabetes, circulating miRNAs are associated with those patients with impaired wound healing (Dangwal et al., 2015).

1.8 MiRNAs in lung cancer

The first evidence of the involvement of miRNAs in human lung cancer was reported by Takamizawa et al. (Takamizawa et al., 2004). In their work, they demonstrated that let-7 miRNA was downregulated both *in vitro* and *in vivo* and correlated with prognosis of lung cancer patients. Later on it has been shown that the let-7 reduction lead to an increase of RAS level (Johnson et al., 2005). Also a SNP on let-7 has been also shown to be significantly associated with an increased risk for NSCLC among moderate smokers by modifying the binding to 3' untranslated region of KRAS mRNA (Chin et al., 2008).

As previously stated, miRNAs can act as oncogenes or oncosuppressors, depending on the timing and the levels of expression. This is true for all the cancers, including NSCLC. For instance, miR-17–92 cluster, which includes miR-17, miR-18a, miR-19a, miR-20a, miR-19b-1 and miR-92a-1, is overexpressed in lung cancer and enhances the cancer cell growth (Hayashita et al., 2005). In contrast, miR-17~92 shows a tumour suppressive role in other cancers, such as breast cancer, squamous cell carcinoma of the larynx, retinoblastoma, hepatocellular carcinoma and nasopharyngeal carcinoma (Xiang and Wu, 2010). This paradox may be due to the ability of a single miRNA to target multiple mRNAs involved in distinct pathways.

.Modifications in the key enzymes involved in miRNA biogenesis are also found to be correlated with the prognosis of lung cancer patients, such as in NSCLC patients where a higher Dicer expression leads to a significantly better prognosis than low Dicer expression (Lonvik et al., 2014, Diaz-Garcia et al., 2013, Karube et al., 2005). Moreover, miRNA-related genetic variants are also associated with the clinical outcomes in early-stage NSCLC cancer patients (Pu et al., 2013) thus confirming the importance of miRNAs as prognostic markers.

Emerging evidence suggest the useful role of miRNAs as biomarkers for the early diagnosis of lung cancer. In lung cancer tissues, a meta-analysis study indicates a specific miRNA signature associated with lung cancer tissues, with seven miRNAs up-regulated (miR-21, miR-210, miR-182, miR-31, miR-200b, miR-205, and miR-183) and eight down-regulated (miR-126-3p, miR-30a, miR-30d, miR-486-5p, miR-451a, miR-126-5p, miR-143, and miR-145) (Inamura and Ishikawa, 2016). Used as non-invasive biomarkers, miRNAs detection in sputum and blood, was found to improve the sensitivity of detection and the diagnosis of NSCLC patients. For example, miR-21 has been found upregulated in the sputum of patients and low levels of miR-21, miR-126, miR-210, and miR-486-5p in plasma have been associated with this disease (Inamura and Ishikawa, 2016).

Two different research groups have studied the miRNA molecular profile for lung cancer diagnosis and prognosis (Yanaihara et al., 2006, Yu et al., 2008) and found a five-miRNA signature (let-7a, miR-221, miR-137, miR-372, and miR-182), that is associated with survival and cancer relapse in NSCLC patients. MiRNA-let-7 was downregulated in NSCLC and further studies demonstrated its onco-suppressor activity in a xenograft model (Kumar et al., 2008). MiR-221

levels were lower in tumour tissues than in controls and showed a tumour-suppressive activity in lung cancer together with miR-222 (Yamashita et al., 2015). The identification of a microRNA signature that can predict survival of patients with squamous cell carcinoma or adenocarcinoma is very important because it suggests that miRNAs may have an important role to enable better understanding of the progression of the disease. Other miRNAs important in NSCLC progression have been also discovered in later research, such as the miRNA cluster 17-92 mentioned above (Osada and Takahashi, 2011).

The current diagnostic methods for the diagnosis of lung cancer, such as the analysis of the sputum, the X-rays or CT scanning, are often not able to discriminate between SCLC and NSCLC or between adenocarcinoma and cell carcinoma (Wang et al., 2009). For this reason, new molecular markers, such as miRNAs, may help for the early diagnosis, prognosis and choice for the treatment for each individual patient, thus opening the new era of "personalised medicine".

Several studies have also demonstrated the association between specific miRNAs and the most frequent somatic mutations in lung cancer patients (Inamura and Ishikawa, 2016). Therapies are available for the treatment of people with specific mutations, such as EGFR, but very often the patients develop a resistance to the therapy and this is normally due to secondary mutations in the same or other genes (Garofalo et al., 2011). *In vivo* experiments have demonstrated that the treatment of the sensitive lung cancer cells with EGFR inhibitors leads to the downregulation of miR-30b-30c and miR221-222 and this causes the increase of apoptosis. However, at the same time, MET overexpression upregulates those four miRNAs, thus making the anti-EGFR

treatment useless. Researchers have proposed using MET-targeting miRNA inhibitors to improve the sensitivity to Gefinitib, an EGFR inhibitor, in a xenograft model (Garofalo et al., 2011).

In 2013, NSCLC patients were enrolled in a clinical trial with MRX34, a miR-34 mimic developed by Texas and the results of the study will be show near in the future (Rupaimoole and Slack, 2017).

1.9 The two forms of miR-140 in lung cancer

MiR-140-5p was first studied in craniofacial abnormalities and the platelet-derived growth factor-a (PDFG-A) was identified as direct target (Eberhart et al., 2008). The sequence of human pre-miR-140 is predicted based on homology to a miRNA from mouse and its expression was later verified in human (Lagos-Quintana et al., 2002, Landgraf et al., 2007). Pre-miR-140 was found to locate on chromosome 16 (16q22.1), in one intron of the WW domain containing E3 ubiquitin protein ligase 2 (WWP2) gene and was processed to produce two mature miRNAs, miR-140-3p and 140-5p, with different seed sequences (Rodriguez et al., 2004). As described in figure 1.6, miR-140-5p originates from the 5'arm of the hairpin of the precursor, while miR-140-3p from the 3' arm. Both these forms of miR-140 are downregulated in cancer tissues, including lung, suggesting their role as onco-suppressors (Zhai et al., 2015, Liu et al., 2016b, Zhang et al., 2015).

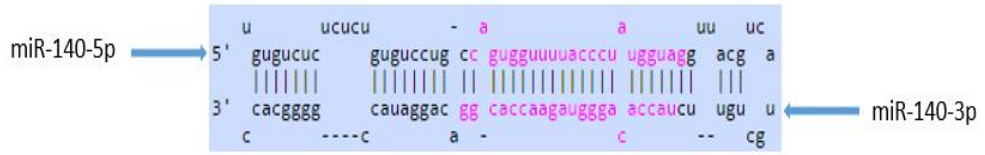

Figure 1.6. Pre-miR140 stem and loop structure. This miRNA sequence is predicted based on homology to a verified miRNA from mouse and its expression was later verified in humans (http://www.mirbase.org).

Croce et al. demonstrated that most of miRNAs downregulated in cancers are located in cancer-associated regions or fragile sites and their lower levels are due to deletions in the loci from where they are transcribed (Calin et al., 2004). Both of the two forms of miR-140 have been found downregulated in lung cancer and, presumably, their downregulation may be due to mutations in 16q22.1 locus.

MiR140-3p and 140-5p are downregulated in lung cancer cells and several studies showed that these miRNAs not only have a negative role in tumour growth and metastasis but also suppress the migration and invasion of NSCLC cells by downregulating the expression of key target genes, such as Insulin-Like Growth Factor 1 receptor (IGF1R) regulated by miR-140-5p and ATP8A1 targeted by miR-140-3p (Yuan et al., 2013, Dong et al., 2016).

These two miRNAs may also influence the expression of other non-coding RNAs. MiR-140-5p promotes the expression of the nuclear long non-coding RNA Nuclear Enriched Abundant Transcript 1 (NEAT1) that is upregulated in different malignancies, including lung cancer (Gernapudi et al., 2016, Pan et al., 2015). The long non-coding RNA Metastasis Associated Lung Adenocarcinoma Transcript 1 (MALAT1), identified for the first time in lung cancer, influences miR-140-5p levels in glioma tumours (Ma et al., 2016).

Starting from these premises, in this study both of the two forms of miR-140 were investigated.

1.10 Importance of the study of both the two forms of miR-140 in lung cancer

In the classical model of miRNA biogenesis, the miRNA duplex is produced by cutting the hairpin precursor by the endoribonuclease Dicer. Then, through some mechanisms that are largely unknown, one of the strands acts as a guide for the mature miR-mediated silencing complex (miRISC). This strand selection process is finely regulated and may vary among tissues and during development and diseases. Recent studies have demonstrated that both the sister strands may be accumulated, thus leading to the hypothesis that the strand selection might not be tissue-specific (Jazdzewski et al., 2009). Moreover, mutations in the precursors may affect the strand selection, especially if they cause a change in the seed sequence of the mature strand, because the mutated miRNA may affect different mRNAs. In the case of the pre-miR-146a, for example, a SNP leads to the maturation of three active strands, two of which generate from the passenger strand and contribute to the development of thyroid cancer (Jazdzewski et al., 2009).

MiR-140-3p and miR-140-5p were identified in congenital malformations. Together with miR-17-92 cluster and miR-200b, they both play an important regulatory role during all the stages of palatogenesis and mutations in their precursor impairs their regulatory functions, thus leading to some serious developmental defects (Schoen et al., 2017).

It is known that the dysregulation of some miRNAs contributes significantly to the loss of regulation of key pathways involved in cell homeostasis, thus allowing the growth of cancer. New studies suggest that a differential strand selection may be one of the mechanisms used by many tumours, including hepatocellular carcinoma, breast and gastric cancer, to repress the physiological regulation and to promote its survival (Tsai et al., 2016). It has been demonstrated *in vitro* and *in vivo*, that the levels of the mRNA targets may influence the abundance of their regulatory miRNAs (Chatterjee et al., 2011, Tsai et al., 2016) and this makes the arm expression preference investigation more complicated and confirms that the thermodynamic hydrogen bonding theory is not the only mechanism that influences miRNA biogenesis.

In this study, both of the two forms of miR-140 will be investigated to see whether there is a preferential strand selection and if this may affect the progression of the disease.

1.11 Aims and hypothesis

Hypothesis

The hypothesis of this study is that the two forms of miR-140 reduce the progression of NSCLC by targeting specific mRNAs.

Aims

- To verify if miR-140-3p and miR-140-5p are differentially expressed in NSCLC and normal lung cells by using tissues from patients and cell lines.
- To investigate if there is any strand selection during the biogenesis of miR-140-3p and miR-140-5p and whether this plays any role in the progression of NSCLC.
- To evaluate the effect of both miR-140-3p and miR-140-5p on cancer cell behaviour. This includes the study of proliferation, migration, invasion, adhesion to the key the extracellular matrix (ECM) proteins, cell cycle, apoptosis and metabolism of cancer cells following the treatment with specific miRNA mimics.
- To investigate the effect of the treatment with miR-140-3p and miR-140-5p mimics on the tubule formation ability of the endothelial cells (used as a model for angiogenesis) *in vitro*.
- To identify novel targets of miR-140-3p and miR-140-5p that are crucial for the changes on cancer cell behaviour following the treatment with miR-140-3p and miR-140-5p mimics.
- To dissect the molecular mechanisms in which the two forms of miR-140 are involved.

CHAPTER 2

MATERIALS AND METHODS

2.1 Cell lines

All the cell lines used for this study were purchased from American Type Culture Collection (ATTC, Rockville, Maryland, USA) and maintained at 37°C with 5% CO_2 (Table 2.1). They included two non-small cell lung cancer cell lines, A459 ATTC® CCL-185™), SK-MES-1 (ATTC® HTB-58™), the normal virus-transformed epithelial lung cell line BEAS-2B (ATCC® CRL-9609™) as control and the Human Umbilical Vein Endothelial Cells (HUVEC, ATCC® CRL-1730™). The two cancer cell lines were maintained in Dulbecco's Modified Eagle's Medium (Sigma-Aldrich, Dorset, UK), supplemented with 10% foetal bovine serum (FBS) (Sigma-Aldrich, Poole, Dorset, England, UK) and 1X penicillin/streptomycin (penicillin 100U/ml, streptomycin 100μg/ml and amphotericin B 0.25μg/ml, Sigma-Aldrich, Poole, Dorset, England, UK). BEAS-2B were maintained in BEBM supplemented with additives (BEGM Kit, Lonza, Gloucestershire, UK). HUVECs were maintained in EBM-2 containing the endothelial cell growth supplements (EGM Kit, Lonza, Gloucestershire, UK).

Table 2.1. Cell lines used in this study

Cell line	Organism	Origin	Cell morphology	Tissue type	Growth medium
BEAS-2B	Homo sapiens	Normal epithelia virus transformed	Epithelial	Lung/bronchus	Complete BEBM
A549	Homo sapiens	58 years old Caucasian male	Epithelial	Lung carcinoma	Complete DMEM
SK-MES-1	Homo sapiens	65 years old Caucasian male	Epithelial	Lung squamous cell carcinoma	Complete DMEM
HUVEC	Homo sapiens	Umbilical/vein	Endothelial	Primary cells derived from the endothelium of veins from the umbilical cord	Complete EGM

2.2 Human NSCLC tissues

Fresh lung tissue samples were collected immediately after surgery and stored at -80°C until use by Capital Medical University Hospital, Beijing, China (Tables 2.2 and 2.3). All the patients were informed and participated with a written consent. All the specimens were analysed by consultant pathologists. The unpaired normal tissues come from non-cancerous patients.

Table 2.2. Non-Small Cell Lung Cancer cohort characteristics. This table includes a total of 19 paired tissues.

	Characteristic	*Number*	*Percentage*
Gender	Female	8	42%
	Male	11	58%
TNM	T1N2M0	1	5%
	T1N2M1	1	5%
	T2N2M0	5	27%
	T2N3M0	1	5%
	T3N0M0	1	5%
	T3N2M0	1	5%
	Unknown	9	48%
Smoking history	Non-smokers	2	10%
	Smokers	13	69%
	Unknown	4	21%

Table 2.3. **Non-Small Cell Lung Cancer cohort characteristics**. This table includes a total of 21 normal and 49 NSCLC unpaired tissues.

	Characteristic	*Number*	*Percentage*
Gender	Female	20	40%
	Male	29	60%
TNM	T1N1M0	1	2%
	T2N0M0	9	18%
	T2N2M0	6	12%
	T3N2M0	2	4%
	T4N0M0	1	2%
	Unknown	30	62%
Smoking history	Non-smokers	7	14%
	Smokers	21	43%
	Unknown	21	43%

2.3 Primers

The gene and miRNA primers used in this study were designed using the Primer-BLAST online tool (https://www.ncbi.nlm.nih.gov/tools/primer-blas) and the primers for miRNA target validation were defined using TargetScan Human 7.0 (http://www.targetscan.org/vert_70/docs/help.html). All the primers were synthesised by either Invitrogen (Carlsbad, CA, USA) or Sigma-Aldrich (Poole, Dorset, England, UK). Details of the gene and miRNA primers are provided in Table 2.4. Details of the primers used for miRNA target validation are reported in table 2.5.

Table 2.4. Primers used in this study to quantify miRNA and gene expression.

Primer		Sequence
miR-specific RT-primer		CAGGTCCAGTTTTTTTTTTTTTTTTVN*
RNU6B	Forward	GTCGTGAAGCGTTCCA
	Reverse	CAGGTCCAGTTTTTTTTTTTTTTTTAAA
RNU48	Forward	ACCGCAGCGCTCT
	Reverse	TCCAGTTTTTTTTTTTTTTTGGTCA
miR140-5p	Forward	CAGCAGTGGTTTTACCCTATG
	Reverse	GGTCCAGTTTTTTTTTTTTTTTCTAC
miR140-3p	Forward	GTACCACAGGGTAGAACCA
	Reverse	GTACCACAGGGTAGAACCA
SNAIL	Forward	CACACTGGCGAGAAGC
	zReverse	ACTGAACCTGACCGTACACTTCTTGACATCTGAGTGGG
	Forward	TGGACACACATACAGTGATT

SLUG	zReverse	ACTGAACCTGACCGTACAGATCTCTGGTTGTGGTATGA
EGFR	Forward	AGAGTCTCAAAGCCATGTTAT
	zReverse	ACTGAACCTGACCGTACACCATCCTAAGCATGACTCC
ARAF	Forward	AAGTTCCACCAGCATTGTTC
	zReverse	ACTGAACCTGACCGTACAGTAGAACCTTGAGGGCTGTTG
ITGB3	Forward	CAGATTTGCCTTATTGGCAG
	zReverse	ACTGAACCTGACCGTACAAAATGTCTACAGCAGTGAGG
GAPDH	Forward	AAGGTCATCCATGACAACTT
	zReverse	ACTGAACCTGACCGTACAATCGCTCCACCAACTAAGAAC

* V = A or G or C, N = A or G or C or T.

Table 2.5. Primers used for miRNA target validation. MiRNA target regions complementary to the desired 3'UTR target region. TargetScan Human 7.0 (http://www.targetscan.org/vert_70/docs/help.html) was used to design the miRNA target region complementary to the desired 3'UTR target region. The overhangs created by oligonucleotide annealing were designed to be complementary to those generated by the restriction enzymes PmeI and XbaI. NotI internal site was added for clone digestion. ___ XbaI sequence ___ NotI internal site ___ PmeI sequence

MiR-140-3p target region	Sequence
ITGB3-miR-140-3P-F	AAACTAGCGGCCGCTGAGCCACTGCCCCCGGCTGTGGTTGT
ITGB3-miR-140-3P-R	CTAGACAACCACAGCCGGGGGCAGTGGCTCAGCGGCCGCTAGTTT
ITGB3 mutated-miR-140-3P-F	AAACTAGCGGCCGCTGAGCCACTGCCCCCGGCTAAGTTGT
ITGB3 mutated-miR-140-3P-R	CTAGACAACTTAGCCGGGGGCAGTGGCTCAGCGGCCGCTAGTTT

2.4 Antibodies

2.4.1 Primary antibodies

The primary antibodies used for Western Blot and Flow Cytometry are described in Table 2.6. All of them were supplied by Santa Cruz Biotechnology (Surrey, England, UK), except ITGB3, supplied by Abcam (Cambridge, UK).

Table 2.6. Primary antibodies used for Western Blotting

Epitope	Molecular weight (kDa)	Source	Dilution
GAPDH	37	Mouse	1:1,000
ITGB3	87	Mouse	1:200
E-cadherin	80-120	Goat	1:200
N-cadherin	130	Rabbit	1:200
Vimentin	57	Mouse	1:200
EGFR	170	Mouse	1:200
ERK1	44	Rabbit	1:200
AKT1	55	Mouse	1:200
pSRC (Tyr 530)	60	Rabbit	1:200
PTEN	55	Rabbit	1:200
B-catenin	88-94	Rabbit	1,1000

.

2.4.2 Secondary antibodies

The secondary antibodies used for Western Blot were anti-goat IgG, anti-rabbit IgG and anti-mouse IgG supplied by Sigma-Aldrich (Poole, Dorset, England, UK).

Table 2.7. Secondary antibodies used for Western Blotting

Antibody	Dilution
Anti-mouse IgG	1:1,000
Anti-goat IgG	1:1,000
Anti-Rabbit IgG	1:1,000

.

2.5 MiRNA mimics

MiRNA mimics are small, double-stranded RNA molecules that mimic the endogenous miRNA molecules in the cells. The miR-140-3p and miR-140-5p mimics were supplied by Sigma-Aldrich (Poole, Dorset, England, UK) and used at a final concentration of 20μM in each transfection. The biotinylated mimics used for the miRNA pulldown were purchased from the same company and show the same sequence as the miR-140-3p and miR-140-5p mimics. They have been modified by adding a biotinylated chain at the 3' end to allow the attachment to the streptavidin beads for pulling down. As a negative control, miR-39-3p from *C.elegans*, with the same modification at the 3'-end, was used.

2.6 Standard reagents and solutions

2.6.1 Solutions in cell culture

0.05M Ethylenediaminetetraacetic acid (EDTA)

1 g KCl (Fisons Scientific Equipment, Loughborough, UK), 5.72 g Na_2HPO_4 (BDH Chemical Ltd., Poole, England, UK), 1g KH_2PO_4 (BDH Chemical Ltd., Poole, England, UK), 40 g NaCl (Sigma-Aldrich Poole, Dorset, England, UK) and 1.4 g EDTA (Duchefa Biochemie, Haarlem, Netherlands) were dissolved in 5 l of distilled water, adjusted to pH of 7.4, autoclaved and stored until further use.

Trypsin (25mg/ml)

500 mg trypsin was dissolved in 0.05 M EDTA and then filtered through 0.2μm Minisart filters (Sartorius, Epsom, UK). This stock solution was aliquoted and stored at -20°C until further use. For the use in cell culture, 250 μl of the stock solution was diluted in 10 ml 0.05 M EDTA and used to detach the cells.

Phosphate buffered saline (PBS)

PBS tablets were purchased from Sigma Aldrich. One tablet was dissolved in 200 ml deionised water to make PBS containing 137mM NaCl, 2.7mM KCl in a 10mM phosphate buffer solution, pH 7.4. It was sterilised by autoclaving.

Antibiotics

100x antibiotics were purchased (Sigma-Aldrich) in sterile solution. 10,000 U/ml penicillin, 10mg/ml streptomycin, 25 μg/ml amphotericin. 5ml antibiotics were added to 500 ml growth medium to give a working concentration of 100 U/ml penicillin, 0.1 mg/ml streptomycin and 0.25 μg/ml amphotericin.

2.6.2 Solutions for molecular biology

Tris-Boric-Acid-EDTA (TBE)

TBE solution (5x) (1.1 M Tris, 900 mM Borate, 25 mM EDTA, pH 8.3) was made by dissolving 540 g Tris-HCl (Melford Laboratories Ltd, Suffolk, UK), 275 g Boric acid (Melford Laboratories Ltd, Suffolk, UK) and 46.5 g EDTA in 10l of distilled water and the pH was adjusted to 8.3. This stock solution was then diluted in distilled water to 1x for agarose gels.

Diethyl Pyroncarbonate (DEPC) water

500 µl Diethylpyrocarbonate (DEPC, Sigma-Aldrich Poole, Dorset, England, UK) was added to 500 ml of distilled water and autoclaved.

Loading Buffer for DNA electrophoresis

25 mg bromophenol blue (Sigma-Aldrich Poole, Dorset, England, UK) and 4 g sucrose (Fisons Scientific Equipment, Loughborough, UK) were dissolved in 10ml of distilled water and stored at +4°C.

2.6.3 Solutions for gene cloning

LB Agar

LB agar was made by dissolving 10 g tryptone (Duchefa Biochemie, Haarlem, Netherlands), 5 g yeast extract (Duchefa Biochemie, Haarlem, Netherlands), 15 g agar and 10 g NaCl in 1l of distilled water, the pH was adjusted to 7.0 and the solution was autoclaved. The solution, which was solid at room temperature, was melted by heating in a microwave and poured into 90 mm Petri Dishes.

LB Broth

10 g tryptone, 10 g NaCl and 5 g yeast extract were dissolved in 1 l of distilled water. The pH was adjusted to 7.0 and the solution was autoclaved. After cooling down, amphicillin was added.

2.6.4 Solutions for western blotting

Lysis Buffer (RIPA Buffer)

The lysis buffer was made by dissolving 880g of NaCl and 610 mg Tris base in 7 5ml of distilled water to have a final concentration of 150 mM NaCl and 50 mM Tris. After adjusting the pH to 7.6, 1 ml of Triton X100, 1ml of 10%SDS, 200 µl of 500mMEDTA and 5 ml of 10% Na-deoxycholate were added. The solution was aliquoted and stored at -20°C until further use. On the same day as the assay, a cocktail of protease and phosphatase inhibitors was added into the solution above. This cocktail included 2 mM sodium orthovanadate, 1 mM phenylmethyl sulphonyl (PMSF), 25 mM sodium fluoride, 10 µg/ml leupeptin and 8 µg/ml aprotinin. The solution was kept on ice.

10% Ammonium Persulphate (APS)

1 g APS was dissolved in 10 ml of distilled water and stored at +4°C until required (used within two weeks).

Tris Buffered Saline (TBS)

10x TBS (0.5 M Tris, 1.38 M NaCl, pH 7.4) stock solution was made by dissolving 606 g of Tris and 765 g of NaCl in 10 l of distilled water. The solution was stirred at room temperature and the pH was adjusted to 7.4.

TBS-Tween

Polyoxyethylene sorbitan monolaureate (Tween-20) (Sigma-Aldrich Poole, Dorset, England, UK) was dispersed in 1x TBS to have a final concentration of 0.01% (TBS-T).

10x Running Buffer

10x Running Buffer (0.25 M Tris, 1.92 M glycine, 1% SDS, pH 8.3) was made by dissolving 303 g of Tris, 1.44 kg of glycine and 100 g SDS in 10 L of distilled water. Diluted in distilled water ato a final 1x working solution.

10x Transfer Buffer

15.5 g Tris (25 mM) and 72g glycine (190 mM) were dissolved in 4 L distilled water. 1 L of methanol (Fisher Scientific, Leicestershire, UK) giving a 20% concentration of methanol.

Ponceau S staining solution

Ponceau S powder was purchased from Sigma-Aldrich (Poole, Dorset, England, UK) and prepared as a re-usable solution of 0.1% Ponceau S in 5% acetic acid.

Blotto/blocking buffer

Non-fat dried milk (Marvel) was dissolved in 1x TBS-T to a final concentration of 5% used for blocking membranes and for incubating antibodies.

2.6.5 Solutions for Flow cytometry

Wash buffer

The wash buffer contained 2 mM EDTA in PBS.

FACS Buffer

FACS buffer contained 5% FBS in wash buffer.

Blocking Buffer

Blocking buffer was prepared by adding 1% w/v bovine serum albumin (BSA) (Sigma-Aldrich Poole, Dorset, England, UK) to PBS-T (PBS with 0.05% Tween-20).

2.7 Cell culture, maintenance and storage

2.7.1 Cell maintenance

All the cell lines were split when confluent and maintained in 25 or 75 cm^2 culture flasks (Grenier Bio-One Ltd, Gloucestershire, UK) with a loosened cap and incubated at 37 °C, 95% humidification and 5% CO_2 and handled in a Class II Laminar Flow Cabinet using sterile equipment. Cell growth medium was changed every 2-3 days. Cell cultures were screened every 3 months for mycoplasma contamination using the EZ-PCR Mycoplasma Test Kit (Biological Industries, Israel). All cells used in this study were confirmed to be mycoplasma free.

2.7.2 Trypsinisation (detachment) of adherent cells and cell counting

Following adherent cells reaching a confluency of 80-90%, the medium was aspirated and the cells were washed with sterile PBS. Adherent cells were then detached from the flasks or wells using 1-2 ml of Trypsin/EDTA (0.51% trypsin and 0.01% EDTA in PBS), then incubated at 37°C until they rounded and detatched from the culture surface. Once detached, 4 ml and 8 ml of DMEM-containing 10%FBS, was added to each T25 or T75 flask respectively to neutralize the trypsin and all the content was transferred into a 30ml universal container. The suspension was centrifuged at 1,700 revolutions per minute (rpm) for 5 minutes in order to collect the cell pellet. The supernatant was aspirated from the universal container and the pellet resuspended in an appropriate volume of serum-free media (if being used for miRNA treatment), or in complete culture media to be reseeded into tissue culture flasks. Cells were counted using Counter II FL Automated Cell Counter (Thermo Fisher

Scientific, Waltham, MA USA) and then seeded at an appropriate concentration of cells for experimental needs. Cells were routinely passaged by typically splitting the trypsinised cells between 1:5 and 1:10 into new flasks. The cells used in this study were used between a window of passage 4 and 20.

2.7.3 Storing cells

Cell stocks of low passage number were stored in liquid nitrogen. To do this, cells were trypsinised and cell pellets were rapidly resuspended in cold growth medium containing 10% FBS and 10% Dimethyl-sulphoxide (DMSO, Sigma-Aldrich, Poole, Dorset, UK). The cell suspension, at a cell density of 10^6 cells/ml, was then divided into 1ml aliquots and added to CRYO.S tubes (Grenier Bio-One, Germany). The tubes were wrapped in protective tissue paper, stored overnight at -80˚C and then transferred to liquid nitrogen tanks for long-term storage.

2.7.4 Resuscitation of cells

In order to resuscitate cells, they were removed from liquid nitrogen and rapidly thawed in warm water, before being transferred under sterile conditions into a universal container containing 10 ml of pre-warmed medium and centrifuged at 1,700 rpm for 5 minutes to remove any excess DMSO. The supernatant was aspirated and the pellet was resuspended in 5 ml of complete growth medium. The cell suspension was then transferred into a fresh 25 cm^2 culture flask and transferred to the incubator.

2.8 Purification of total RNA

"Total RNA" indicates the total amount of RNA in a cell, including mRNAs, rRNAs, tRNAs, long and small non coding RNAs. The amount of small RNAs and microRNAs rate may vary between 12-75% and their concentration differs from one tissue to another.

In general, the extraction of both DNA and RNA consists of three stages: cell lysis combined with the inactivation of cellular nucleases, protein lysis and finally precipitation of the nucleic acid. After the cell lysis we obtained a mixture of proteins and nucleic acids. To isolate and preserve the integrity of the nucleic acids we used phenol, chloroform and ethanol. Phenol and chloroform remove proteins and ethanol causes their precipitation. It is possible to increase the efficiency of the purification and have a higher concentration of the nucleic acid using carriers, such as glycogen.

Total RNA from cells was isolated using TRIzol® LS Reagent (Invitrogen, Carlsbad, CA, USA), a monophasic solution of phenol and guanidine isothiocyanate which is able to break the protein-protein interactions and mantain the integrity of the nucleic acids.

Protocol:

- When the confluence of monolayer cells reached approximately 80-90% the medium was removed, replaced with TRIzol® LS Reagent (1ml for 5-10x10^5 cells) and everything was scraped into a 1.5 ml Eppendorf tube where the contents were pipetted vigorously.

- 0.1 ml of 1-bromo-3-choloropropane was added. Then the tube was shaken vigorously for about 15 seconds and left at room temperature for 10-15 minutes.
- The tube was centrifuged at 12,000 xg at 4 °C for 15 minutes. After that it was possible to recognise three different phases: a clear upper aqueous layer containing RNA, an interface with DNA and a red lower organic layer containing proteins.
- The upper aqueous phase was carefully transferred to a new 1.5 ml tube and isopropanol (Sigma-Aldrich, Poole, Dorset, England, UK) was added (0.5 ml per ml of TRIzol® LS Reagent). The tube with isopropanol was left at room temperature for 5-10 minutes.
- The tube with RNA and propanol was centrifuged at 12,000 xg at 4 °C for 10 minutes, the supernatant was discarded and the pellet at the bottom of the tube was washed with 1 ml 75% ethanol in DEPC water.
- The tube was centrifuged again at 7,500 xg at 4 °C for 5 minutes.
- After removed the ethanol, the tube was dried by air-drying 5-10 minutes.
- The RNA pellet was finally dissolved in 20-50µl of DEPC water to avoid the degradation of RNA by RNase enzymes.

2.8.1 Spectrophotometric quantification of RNA

The concentration and purity of the RNA were obtained by spectrophometric measurement (NanoPhotometer, Implen, Munich, Germany). The instrument is able to determine the difference of absorbance between the purified RNA (usually 1µl sample) and the DEPC-treated water (blank) in a quartz cuvette. The

software calculates a curve and assigns a concentration value in ng/µl to each sample.

The absorbance (A) is expressed as ln(I0) – ln(I1), where I1 is the intensity of the radiation (light) transmitted through the material (transmitted radiation) and I0 is the intensity of the radiation before it passes through the material (incident radiation). The absorbance measure unit is the wavelength (λ) and some typical values are reported below:

λ = 230 nm: wavelength of absorption of complex carbohydrates and phenols;

λ = 280 nm: wavelength of absorption of proteins;

λ = 260 nm: wavelength of absorption of nucleic acids;

λ = 320 nm: wavelength of absorption of other contaminants.

If these values are known, we can estimate the concentration and the purity of the RNA. So, for RNA samples the instrument detects the concentration of single strand RNA molecules (ssRNA) at a wavelength of 260 nm. The concentrations of RNA samples were automatically calculated as follows: (A260-A320) x fc x fd, where fc is the coefficient of molar extinction which depends on the acid nucleic nature (it is 50 ng/µl for ssRNA), fd is the dilution factor, A260 is the absorbance at 260 nm and A320 is the absorbance at 320 nm.

The purity of RNA with respect to contaminants is evaluated by the ratio of the readings at 260 nm and 280 nm (A260 / A280) and at 260 nm and 230 nm (A260 / A230). The A260 / A280 ratio provides an estimate of the purity of RNA with respect to contamination by protein and its value must be higher than 1.7. On the other hand, the A260 / A230 ratio provides an estimate of the purity of

RNA with respect to contamination by solvent (phenol, salts) and its value should be around 2 or slightly above. Contaminations may decrease the efficiency of the following reactions, mainly by inhibition of the enzymes.

After the purification and quantification, the RNA samples are ready to be used immediately or they can be stored at -80 °C for later use.

2.9 Real Time Quantitative Reverse Transcription Polymerase Chain Reaction (qRT-PCR)

Quantitative PCR (qPCR) is a technology used for the amplification of DNA sequences through fluorescent reagents of the Polymerase Chain Reaction (PCR). Its key feature compared to the standard PCR method is that the amplified DNA is detected in "real time". For gene expression studies or detection of RNA viruses, RNA can also be used as a template. In this case the RNA needs to be reverse transcribed into complementary DNA (cDNA) and the whole process that includes the reverse transcription and qRT-PCR reactions is called Quantitative Reverse Transcription Polymerase Chain Reaction (qRT-PCR).

2.10 Reverse Transcription (RT)

The reverse transcription is a process that retroviruses commonly use to incorporate their genome into the host cells. Specifically, a single-stranded RNA is reverse transcribed into cDNA using total cellular RNA or poly(A) RNA, a reverse transcriptase enzyme, a primer, triphosphate deoxyribonucleotides

(dNTPs) and an RNase inhibitor. Three types of primers can be used for RT reaction: oligo(dT) primers, random primers or gene specific primers. In general, the use of specific primers reduces background binding, whereas random and oligo-dT primers are particularly useful when the start amount of RNA is very low because they are able to maximise the number of molecules that can be analysed (Bustin, 2000).

Two different approaches are available to reverse transcribe miRNAs. In the first approach, miRNA specific stem-loop reverse transcription primers are used. They are designed to have a single-stranded part complementary to the 3'end of miRNA and a double-stranded part (the stem) and the loop that contains the universal-binding sequence, which is used for the amplification. In the second approach, the 3'ends of miRNAs are elongated to provide them with a tail of oligo (dT) and then universal primers are added. Alternatively, it is possible to reverse transcribe miRNAs using multiplexing stem-loop primers. In this study oligo (dT) primers were used. Oligo (dT) is a stretch of approximately 20 thymine residues that anneal to the poly(A) tail of mRNA, thereby preventing priming at internal sites in the tail. The enzyme used was the thermostable M-MuLV (Moloney Murine Leukemia Virus) reverse transcriptase isolated from *E. coli* that lacks 3'→5´ exonuclease activity and has a stretch of thymine residues that anneal to the poly(A) tail of mRNA. The reverse transcription for miRNA quantification was performed using Reverse Transcription (cDNA Synthesis) Products kit (New England BioLabs®, UK). Each reaction was set up in a 200 µl PCR tube (ABgene, Surrey, UK) and the manufacturer's protocol was adjusted as follows:

Table 2.8. Reverse Transcription reagents.

Component	Volume (µl)
10x Buffer with ATP (150µl Buffer+50µl ATP)	1
Poly(A) Polymerase 50 U/µl	0.15
4dNTP mix	1
RT primers 10µM	1
M-MLV Reverse Transcriptase 200 U/µl	0.4
RNA (20 ng/µl)	6.45
Total	10

20 ng of RNA was used, suspended in DEPC H_2O to a volume of 6.45µl. Conditions for reverse transcription were 42°C for 60 minutes and 95°C for 5 minutes using Applied Biosystems 2720 Thermal Cycler (Life Technologies, Paisley, UK). Following reverse transcription, cDNA was diluted 1:24 using DEPC water.

For gene quantification the GoScript™ Reverse Transcription System (Promega, Madison, Wisconsin, USA) was used to convert RNA into first-strand cDNA. Each reaction was set up in a 200 µl PCR tube (ABgene, Surrey, UK) and the manufacturer's protocol was adjusted as follows:

Table 2.9. Real-Time Quantitative Polymerase Reaction (qRT-PCR) reagents.

Component	Volume (µl)
GoScript™ 5X Reaction Mix	4.1
$MgCl_2$	1.2
PCR Nucleotide Mix	1
Recombinant RNasin® Ribonuclease Inhibitor	0.5
GoScript™ Reverse Transcriptase	1
DEPC H_2O	7.2
RNA+Primer Mix	5
Total	20

500 ng of RNA was used, along with DEPC H_2o to make up the solution to 4 µl, as well as 1 µl of the Primer Oligo$(dT)_{15}$. Conditions for reverse transcription were 25°C for 5 minutes, 42°C for one hour and 70°C for 15 minutes using Applied Biosystems 2720 Thermal Cycler (Life Technologies, Paisley, UK). Following reverse transcription, cDNA was diluted 1:8 using DEPC water.

2.11 Real-Time quantitative Polymerase Chain Reaction (qRT-PCR)

Real-Time qPCR is used to copy (amplify theoretically a million fold after 20 cycles) and simultaneously quantify specific sequences of a DNA or cDNA template, using sequence-specific oligonucleotides, a heat stable DNA polymerase and thermal cycling. In the traditional PCR method, the detection of the amplified sequence was performed at the end of the reaction, mainly because of the properties of the enzymes, which were not stable at high temperature for long periods. Moreover, the quantification required a post-PCR product analysis, usually by gel electrophoresis.

Specifically, the Real-Time qPCR detects the products of the reaction from the first cycle in which the amplified target becomes detectable (threshold cycle, Ct), allowing the results obtained to be much more accurate and reproducible than the traditional end-point PCR. The Ct is used to calculate the initial DNA copy number, because the Ct value is inversely related to the starting amount of target.

The qRT-PCR amplifies DNA exponentially, doubling the number of target molecules with each amplification cycle. After each cycle, the fluorescent signal increases in direct proportion to the number of molecules generated (amplicons).

Every cycle of PCR is composed of three steps:

1. Denaturation: a high temperature (~95 °C) allows the separation of the nucleic acid double chain.
2. Annealing: the two primers (forward and reverse) bind the complementary strand. The temperature used is generally between 50 and 60 °C, depending on the sequence and length of the primers. Lower

temperatures may lead to non-specific annealing of the primers, whereas higher temperatures may not enable annealing at all. The GC content of the primer should be approximately 50% and a higher level may lead to the production of stable imperfect hybrids.

3. Extension: the DNA polymerase carries on the extension of the primers at around 72 °C.

The choice of a thermostable DNA polymerase is crucial for the efficiency of the reaction. One of the most used DNA polymerases is the enzyme from the heat -esistant bacterium *Thermus aquaticus* (Taq polymerase). At the beginning of each cycle, during the denaturation phase, the Taq polymerase is partially denatured, so the enzyme maintains a high-fidelity DNA synthesis for 25-30 cycles, afterwards it may synthesize non-specific products. (Eckert and Kunkel, 1991).

When plotted on a logarithmic scale, the amplification of the PCR generates a curve which shows four different phases: a linear phase represented by a straight line parallel to the abscissa axis, a beginning of the exponential phase, the exponential phase and a plateau (Figure 2.1).

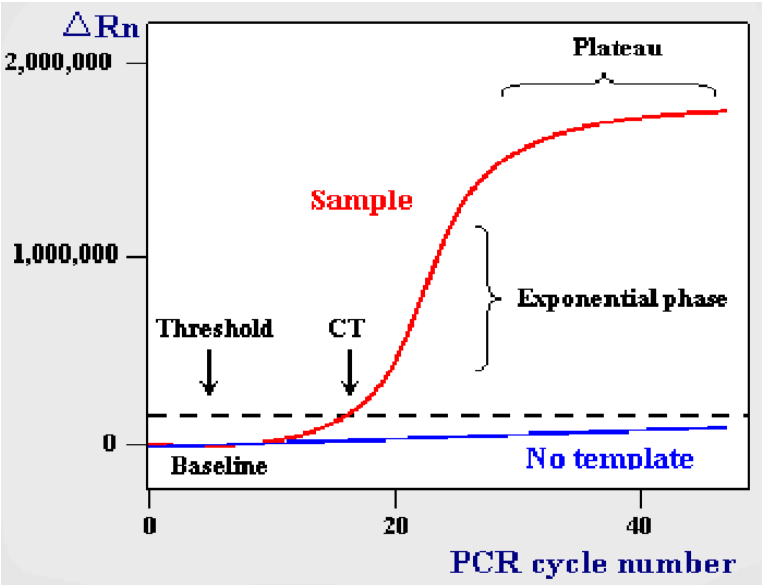

Figure 2.1. Phases of the PCR amplification curve. The PCR amplification curve charts the accumulation of fluorescent emission at each reaction cycle. The curve can be divided into four different phases: the linear ground, early exponential, log-linear, and plateau phases. Data gathered from these phases are important for calculating background signal, cycle threshold (Ct), and amplification efficiency. The baseline is defined as PCR cycles in which a reporter fluorescent signal is accumulating even if the instrument is not able to detect it. Rn is the intensity of fluorescent emission of the reporter dye divided by the intensity of fluorescent emission of the passive dye (a reference dye incorporated into the PCR master mix to control for differences in master mix volume). ΔRn is calculated as the difference in Rn values of a sample and either no template control or background, and thus represents the magnitude of the signal generated by PCR. The threshold is an arbitrary level of fluorescence chosen on the basis of the baseline variability and could be changed by the operator according to the experimental conditions. A signal above the threshold is can be used to define the Ct for a sample. Ct is defined as the fractional PCR cycle number at which the reporter fluorescence is greater than the threshold (http://www.ncbi.nlm.nih.gov/genome/probe/doc/TechQPCR.shtml).

In the first phase (10-15 cycles) the fluorescence cannot be distinguished from the baseline. Then, the fluorescence arrives at the threshold. The cycle at which the line takes the form of a curve is the Ct. From this point the exponential growth begins. This phase corresponds to the maximum efficiency of the amplification, with an exponential increase of the molecules present in the sample. Finally, the plateau phase is reached: there is no amplification and no increase in fluorescence is observed because the reagents are exhausted.

At the end of the reaction the number of DNA molecules has not risen exactly in an exponentially way. Experimental factors, such as length, secondary structures and GC content of the amplicons may influence the efficiency of the reaction. To evaluate the efficiency the following formulas are generally used:

Exponential amplification = 10^(-1/slope)

Efficiency = (Kim)-1.

A good reaction should have an efficiency between 90% and 110%, which corresponds to a slope of between -3.58 and -3.10 (Wong and Medrano, 2005).

One of the main issues in this technique depends on its powerful sensitivity: the presence of contaminants may affect the success of the analysis because non-specific amplifications may occur. Contaminants may originate from the operator (*eg* saliva droplets), by the presence of bacteria or by an incorrect purification of the template.

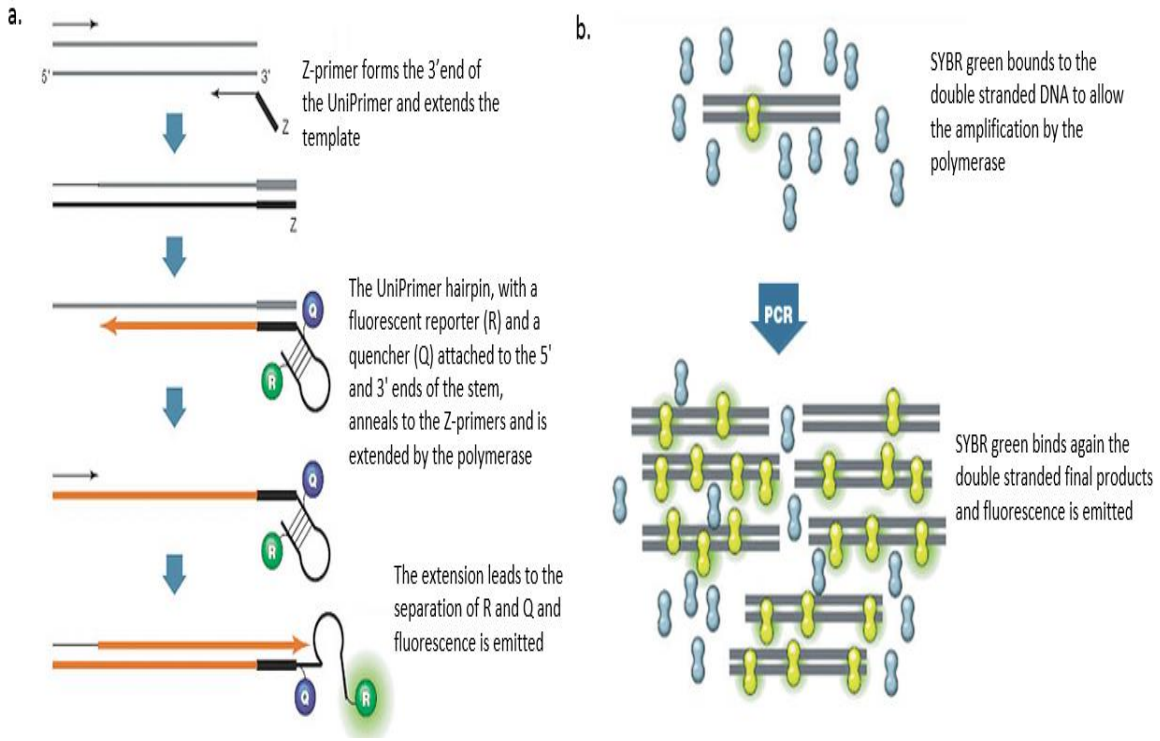

Figure 2.2. Amplifluor and SYBR green reactions. a) The AmpliFluor assay uses two target-specific DNA primers and one universal DNA primer called a UniPrimer. B) SYBR® Green is a DNA-binding dye for real-time PCR, which binds non-specifically to double-stranded DNA. Modified from (http://www.bio-rad.com/en-uk/applications-technologies/introduction-pcr-primer-probe-chemistries).

2.11.1 Gene quantification using the Amplifluor™ Assay

In this study, qPCR was performed for gene quantification using the Ampifluor™ Uniprimer™ Universal system (Intergen Company®, New York, USA). Volumes used in the reaction were shown in Table 2.10. The amplifluor probe consists of a 3'- region specific to the Z-sequence (ACTGAACCTGACCGTACA) present on the target-specific primers (this sequence is included in the design of the reverse primers and a 5' hairpin structure labelled with the fluorophore FAM.

For the current study each reaction was performed as follows:

Table 2.10. Amplifluor qPCR reaction reagents.

Component	Master Mix Volume (µl)
2X IQ Master Mix	5
F-primer (10 pmol)	0.3
zR-primer (1 pmol)	0.3
Uniprobe (10 pmol)	0.3
Diluted cDNA	4.1
Total	10

Each sample was analysed in triplicate and the cDNA was first diluted 1:8 in nuclease-free water and then loaded individually into each well of a 96 well plate (BioRad Laboratories, Hemel Hampsted, UK). The plate was then covered with optically clear Microseal® (BioRad Laboratories, California, USA) and placed in a StepOnePlus™ Real-Time PCR System (Thermo Fisher Scientific, Waltham, MA USA) at the following conditions:

Predenaturation for 10 minutes at 95 °C

(70 cycles)

Denaturation 95 °C for 10 seconds

Annealing 55 °C for 30 seconds

Elongation 72 °C for 10 seconds.

2.11.2 MiRNA quantification using the SYBR GREEN® Assay

For the SYBR-based assays, the dye emits fluorescence when it intercalates into the double-stranded (ds) DNA PCR product.

For this study each reaction was performed as follows:

Table 2.11. SYBR green qPCR reaction reagents.

Component	Master Mix Volume (µl)
SYBR Green PCR mix	7.5
Forward Primer	0.75
Reverse Primer	0.75
Diluted cDNA	6
Total	15

Each sample was analysed in triplicate and the cDNA was first diluted 1:24 in nuclease-free water and then loaded individually in each well of a 96 well plate (Bio Rad Laboratories, Hemel Hampsted, UK). The plate was then covered with optically clear Microseal® (Bio Rad Laboratories, California, USA) and placed in an iCyclerIQ thermal cycler (Bio Rad Laboratories, Humel, Hamspstead, UK) at the following conditions:

Pre-denaturation for 10 minutes at 94 °C

(40 cycles)

Denaturation 94 °C for 15 seconds

Annealing/Elongation 58 °C for 15 seconds

As mentioned above, the specificity of the amplification can be evaluated by plotting fluorescence as a function of temperature to generate a melting curve of the product.

One pure amplicon can be distinguished from other artefacts by the melting curve profile it produces. A pure product shows a typical single, sharp melting peak at the melting temperature (Tm). The artefacts products melt at lower temperatures and show broader peaks.

2.11.3 Normalization

The comparison of microRNA expression between different samples requires standardization and normalization of qPCR analysis to minimise the errors due to the variation in the quantity and quality of the starting material. One of the most accurate methods is to include in the amplification a gene that serves as an internal reference against which other amplicon values can be normalised (Karge III et al., 1998). This reference gene is also called an "endogenous control" and is crucial for the reliability, reproducibility and interpretation of miRNA experiments. An ideal endogenous control generally should have a constant level of expression and should be abundant in all tissues. Moreover, it should have the same size and it should be purified and amplified under the same conditions and with the same technology as the molecules under study (Bustin, 2000) (Chen et al., 2011b). Summarizing, the term "endogenous control" refers to a gene with a low variance in all the samples and that does not show significant changes as a result of modifications of the parameters that we consider.

Results were analysed using ΔΔCT normalisation to a housekeeping gene. To normalize qPCR data for miRNA expression analogous to Glyceraldehyde-3-

phosphate-dehydrogenase (GAPDH), β-Actin (ACTB) or α-Tubulin (TUBA1) are generally used. At present, no endogenous control miRNAs have been identified, so the selection of reference genes to normalize miRNA levels is still rather empirical and where possible one or two invariant miRNAs can be used as control (Benes and Castoldi, 2010).

The endogenous control for this study was chosen following the procedure described by Chen et al. (Chen et al., 2011a). With reference to previous data, some molecules were screened using a serial dilution of the prepared samples and the ones with the best assay linearity were selected as endogenous controls. In the current study the small nucleolar RNAs (snoRNAs) U6 was used as a housekeeping gene for miRNA quantification in cell lines, U48 for miRNA quantification in human tissues and GAPDH for gene quantification in cell lines.

2.11.4 Data analysis

There are two methods of analysing data: absolute quantification and relative quantification.

Absolute quantification determines the input copy number of the transcript of interest, usually by relating the PCR signal to a standard curve. Here a dilution series of known template concentrations are used to determining the initial starting amount of the target template in experimental samples or for assessing the reaction efficiency.

Relative quantification is also most effective when the molecules are subjected to identical conditions (purification method, storage, etc.), are physically similar (e.g., size) and are detected using a similar method (e.g., qRT-PCR with stem-loop primers). In this way, the changes in sample gene expression are measured

based on a control gene. Numerous mathematical models are available, in this study the comparative Ct (ΔΔCt) was used. This method requires the use of samples in duplicate or triplicate. In this study, triplicates were used. Finally, the data are plotted in a bar graph, in which the lengths of rectangular bars are proportional to the expression values. The x-axis shows the specific categories being compared, and the y-axis represents discrete expression values.

2.12 Methods for protein detection

Changes in the expression and/or activation of proteins in cells treated with scramble controls (negative mimics) or the two forms of miR-140 mimics were assessed using SDS-PAGE, Western Blotting, FACS and Protein Array.

2.12.1 Protein extraction and preparation of cell lysate for western blotting

Cells were seeded into T75 flasks and were treated with mimics when the confluency was around 80%. After 24 hours the transfection medium (DMEM containing 10%FBS) was replaced with normal medium and the cells incubated for further 24 hours at 37°C 5% CO_2. Following 48 hours of treatment, the cells were washed twice with ice-cold PBS and lysed in 300µl RIPA lysis buffer containing a cocktail of protease and phosphatase inhibitors.

The cellular material was collected using a cell scraper, transferred to a 1.5 ml tube and rotated on a tube rotating wheel for 30 minutes at +4°C. Cell lysates were then centrifuged at 13,000 rpm for 15 minutes at +4 °C and the supernatant stored at -20 °C.

The concentration of the total soluble proteins was determined using the Colourimetric Bio-Rad DC (detergent compatible) Protein Assay Kit (Bio-Rad Laboratories Ltd, HERTS, UK).

A standard curve was made using 50 mg/ml of bovine serum albumin (BSA) (Sigma-Aldrich Poole, Dorset, England, UK). BSA was serially diluted 1:2 in RIPA buffer and 5 µl of standard and unknown samples were dispensed in triplicate on a 96-well plate. The Bio-Rad Solutions include the Reagent A (alkaline copper tartrate solution) + Reagent S (surfactant solution) (20 µl of Reagent S for each ml of Reagent A) and Reagent B (Folin reagent). 25 µl of Reagent A+ Reagent S mix and 200 µl of Reagent B were added to the 5µl of sample or standards in each well. After 10 minutes, the plate was read at 630 nm using a spectrophotometer (Bio-Tek, Wolf Laboratories, York, UK). The sample readings were compared with those of a BSA standard curve to give the concentration of proteins in the cell lysates.

After quantification, an equal volume of 2x SDS Laemmli buffer (Sigma-Aldrich Poole, Dorset, England, UK) was added to each tube, the samples were boiled at 95 °C for 5 minutes and finally centrifuged at maximum speed for 1 minute at room temperature.

2.12.2 Sodium Dodecyl Sulphate Polyacrylamide Gel Electrophoresis (SDS-PAGE)

The Sodium Dodecyl Sulphate Polyacrylamide Gel Electrophoresis (SDS-PAGE) was performed using the Bio-Rad Mini-Protean® III apparatus powered by a Powerpac Basic™ power pack (both Bio-Rad Laboratories Ltd, HERTS, UK) following the manufacturer's instructions. The system includes a 5%

acrylamide/bis acrylamide stacking gel at pH 6.8 and an acrylamide/bis-acrylamide resolving gel at pH 8.8. The percentage of acrylamide used in the resolving gel depends on the size of the proteins being resolved. When SDS is added to proteins, they become negatively charged by their attachment to the SDS anions and, after denaturation, their migration depends only on their molecular weight.

For each gel 10 ml of stacking gel and 4 ml of resolving gel were made. The recipes for the resolving and stacking gels are reported in Table 2.12 and 2.13 respectively.

Table 2.12. Resolving gel recipes required for the preparation of 10 ml of resolving gel at 8% and 10% (w/v) acrylamide/bis-acrylamide.

Component	8% Resolving Gel (protein size > 100 kDa)	10% Resolving Gel (protein size < 100 kDa)
Distilled water	4.6 ml	4 ml
30% acrylamide mix	2.7 ml	3.3 ml
1.5M Tris (pH 8.8)	2.5 ml	2.5 ml
10% SDS	0.1 ml	0.1 ml
10% ammonium persulphate (APS)	0.1 ml	0.1 ml
Tetramethylethylenediamine (TEMED)	0.006 ml	0.004 ml

Table 2.13. Stacking gel recipes required for the preparation of 4 ml of 5% (w/v) acrylamide/bis acrylamide stacking gel.

Component	5% Stacking gel
Distilled water	2.7 ml
30% acrylamide mix	0.67 ml
1.5M Tris (pH 6.8)	0.5 ml
10% SDS	0.04 ml
10% ammonium persulphate (APS)	0.04 ml
Tetramethylethylenediamine (TEMED)	0.004 ml

Before the assay, all the components of the casting apparatus were cleaned with distilled water first and then with ethanol. The constituents of the resolving gel were mixed. TEMED was added as the last component and the solution was mixed very gently to avoid any bubbles. TEMED catalyses the polymerisation of the gel, therefore the mixture was immediately poured between the two glass plates of the apparatus up to of 1.5 cm below the top edge of the plate. To produce a smooth level surface, the gel was overlaid with water and the gel was left to polymerise at room temperature 30 minutes.

When the gel had polymerised, the overlaid water was discarded and the excess removed using a piece of filter paper. The stacking solution was poured above the resolving gel and a well comb was inserted. The gel was left to polymerise at room temperature 30 minutes.

The gel was placed in the electrophoresis apparatus and covered with cold 1x Running Buffer before removing the well comb. Using long gel loading tips, the

samples were loaded into each well of the stacking gel and 5 µl of a protein molecular weight marker was loaded in 1 well (BLUeye Prestained Protein Ladder, 10-250KDa, GeneDireX, Belgium). The gel was run at a constant current of 140 V until the protein front (visualised by the bromophenol-blue) reached the border between the stacking and resolving gels and the proteins were clearly stacked, and then the voltage was turned down to 100V and run until blue reached the end.

2.13 Protein expression using Western Blotting

Transfer procedure

Once SDS-PAGE was completed, the protein samples were transferred onto a nitrocellulose membrane by western blotting using the Bio-Rad Mini-Protean® apparatus powered by a Powerpac Basic™ power pack (both Bio-Rad Laboratories Ltd, HERTS, UK).

For each gel 6 pieces of blotting papers of the same size of as the short glass plate (7x8 cm approximately) and two sponges were soaked with ice-cold 1x Transfer Buffer. Following electrophoresis, the front glass plate was gently removed using a scalpel and then the gel was detached and transferred into a box containing ice-cold 1x Transfer Buffer. The Western Blot cassette was assembled as described in Figure 2.3 forming a sort of "sandwich". The cassette was assembled in a box containing ice-cold 1x Transfer Buffer and all the components were kept wet.

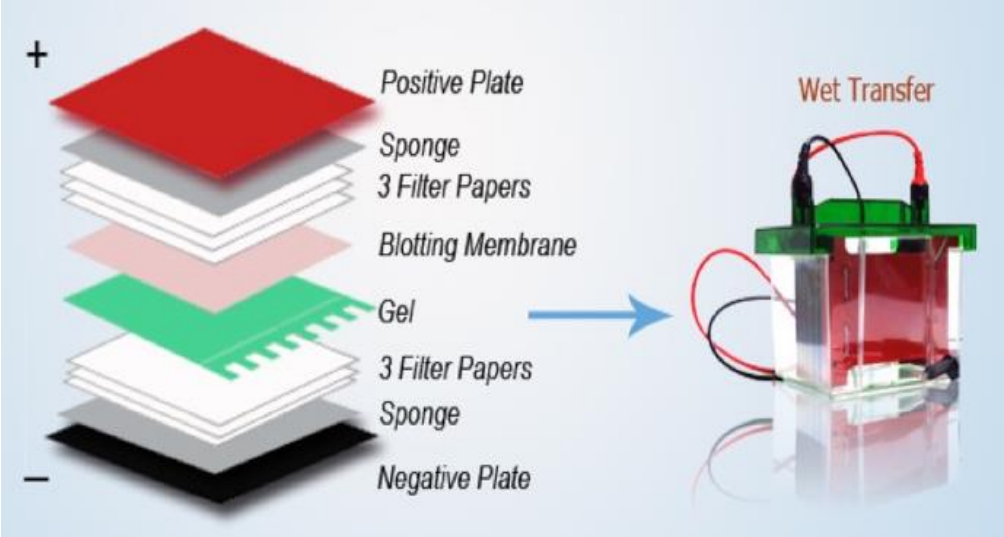

Figure 2.3. Illustration of western blotting transfer.

(https://personalwebs.coloradocollege.edu/~dkillian/Home/SDS_PAGE_and_Western_Blotting.html).

Before locking, the sandwich was rolled gently several times over the top paper to remove any bubbles that might have been introduced between the gel and membrane. The cassette was then locked and placed into the transfer apparatus with the black side (gel) facing the negative electrode (black) and the red side (membrane) facing the positive electrode (red). This ensures that the proteins, negatively charged after being mixed with SDS, migrated towards the anode, from the gel to the membrane. The transfer apparatus was placed in the cold room with an ice block to prevent the overheating of the gel and run at constant 250 mA for 1.5-2.0 hours.

Antibody staining

To confirm the successful transfer of the proteins from the gel to the membrane, the membrane was stained with the Ponceau S solution. for approximately 30 seconds, followed by de-staining in deionised water. Ponceau S has no effect on the blotted proteins and allows a rapid reversible detection of the bands. Following staining, the membrane was inserted into a transparent envelope and rapidly scanned using a Chemoilluminator.

The membrane was then washed 3 times, 10 minutes each with TBS-T (to remove all Ponceau S) and then incubated for 1 hour by gently rocking with Blotto.

The primary antibody, specific for the protein of interest, was diluted in Blotto. The dilution varies between the antibodies, as indicated in Table 2.6.

After the blocking, the membrane was incubated with the primary antibody at +4°C overnight by gently rocking.

After the primary antibody incubation, the membrane was washed three times using TBS-T. The secondary antibody used depends from the source of the primary antibody, *eg* if a primary antibody was raised in a mouse, an anti-mouse secondary antibody is required. The Horseradish Peroxidase (HRP) conjugated secondary antibody was diluted in Blotto according to the manufacturer's instructions (Table 2.7). The membrane was incubated with the secondary antibody for 1 hour at room temperature by gently rocking.

After the secondary antibody incubation, the membrane was washed 3 times, 10 minutes each with TBS-T at room temperature by gently rocking.

Chemiluminescence was performed using a luminol/peroxide based enhanced chemiluminescence (ECL) reagent (Supersignal™ West Pico, Thermo Fisher Scientific, Waltham, MA USA). The ECL reagent was used according to the manufacturer's instructions. 500 μl of ECL reagent was added to each blot and left in the dark for 5 minutes. The luminol contained in the ECL reagent works as a substrate for the HRP in the presence of peroxide. HRP is excited and then emits light when it decays to a lower state of energy. The chemiluminescent signal from the HRP-bound antibody was detected using G:Box (Syngene, Cambridge, UK), composed of an illuminator and a camera connected to a computer.

The images were captured at different exposure times, depending on the band visibility, and then analysed using the G:Box software package (Syngene, Cambridge, UK) for band quantification.

In all the experiments the Glyceraldehyde 3-phosphate dehydrogenase (GAPDH) was used as a control, due to its abundance in all the cells and conservation within the eukaryotic cells.

2.14 Protein expression using Protein array

Proteomics is the large-scale study of proteins and aims to understand the protein status under certain physiological or pathological conditions. It covers the entire content of proteins in cells, including the protein isoforms and modifications, the protein-protein interactions and the structural description of proteins. Amongst all the possible modifications, reversible phosphorylation and de-phosphorylation of proteins catalysed by protein kinases and phosphatases respectively, represent the most widespread molecular regulatory mechanism. These changes have the ability to regulate multiple processes, such as proliferation, differentiation, apoptosis and angiogenesis. Phosphorylation and de-phosphorylation at serine, threonine or tyrosine residues may induce conformational changes and may affect the activity of a protein, its cellular localisation, stability and interactions with other proteins, thus phosphorylation play a role in both normal and pathological conditions including cancer. Currently, the protein kinases represent attractive targets in the field of drug development for cancer treatment (Attoub et al., 2002, Nam et al., 2005, Saito et al., 2006). Kinexus Bioinformatic Corporation (http://www.kinexus.ca) developed a large-scale antibody microarray, the Kinex™ KAM-880 Antibody Microarray that monitors changes in the expression levels and phosphorylation states of signalling proteins which includes 518 pan-specific antibodies for protein expression and 359 phospho-site specific antibodies for phosphorylation. A complete list of the antibodies printed on the KAM-880 chip is available on the Kinexus website.

In this study, the proteins from the cell lysate were detected by using a forward phase microarray, in which one protein sample is screened against multiple

reagents. The capture reagent, normally an antibody, is immobilised on the slide surface and is used to capture antigens (Figure 2.4).

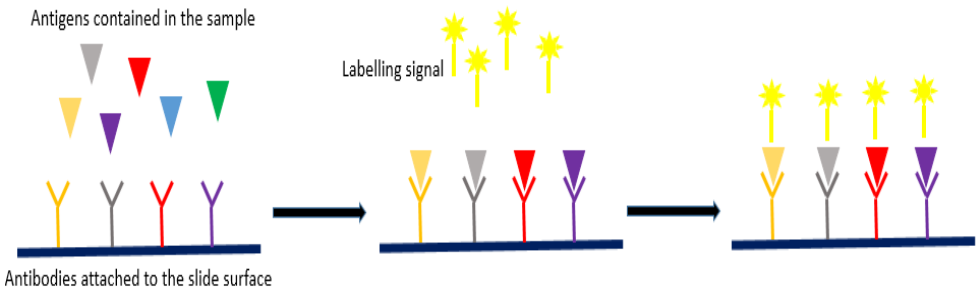

Figure 2.4. Kinexus experiment principles. Forward microarray principle. Antibodies are mobilised on the slide surface. When the sample is added onto the slide surface, the antigens are captured by their specific antibody and the interaction detected by a labelling signal.

Our protein samples from the A549 lung cancer cell line were treated with miR-140-3p and -5p mimics and sent to Kinexus for the forward reverse protein array. The major advantage of this technique is that lysate samples from control and treated cells are labelled with the same dyes and analysed together on the same chip at the same time. The major disadvantage of this technique is the number of false positive and/or false negative results due to the non-denaturating conditions used that allow the formation of protein complexes.

The amount of protein required for the Kinex™ Antibody Microarray (KABM) service is 100 µg per sample at a minimum concentration of 2 mg/ml without any SDS-PAGE sample buffer as the proteins are to remain in their native structure and non-denatured. Cells from T75 flasks were lysed in an ice-cold lysis buffer pH 7.2 as recommended by Kinexus.

Kinexus Buffer:

- 20 mM MOPS, pH 7.0;
- 2 mM EGTA (to bind calcium);
- 5 mM EDTA (to bind magnesium and manganese);
- 30 mM sodium fluoride (to inhibit protein-serine phosphatases);
- 60 mM β-glycerophosphate, pH 7.2 (to inhibit protein-serine phosphatases);
- 20 mM sodium pyrophosphate (to inhibit protein-serine phosphatases);
- 1 mM sodium orthovanadate (to inhibit protein-tyrosine phosphatases);
- 1 mM phenylmethylsulfonylfluoride (to inhibit proteases);
- 3 mM benzamidine (to inhibit proteases);
- 5 μM pepstatin A (to inhibit proteases);
- 10 μM leupeptin (to inhibit proteases);
- 1% Triton X-100.

Cells were seeded into T75 flasks and were treated with mimics when the confluency was around 80%. After 24 hours the transfection medium was replaced with normal medium and the cells incubated for a further 24 hours at 37°C 5% CO2. After 48 hours of the treatment, the cells were washed twice with PBS and the medium replaced with medium containing 2% FBS. Cells were incubated for 2 hours at 37°C 5% CO2. The samples were washed again, lysed and centrifuged at 2,000rpm for 10 minutes. The supernatant was removed and 300μl of Kinnexus Buffer was added. The samples were transferred to an Eppendorf tube and rotated on a tube rotating wheel for 1 hour at +4°C and

then centrifuged at 13,000 rpm for 10 minutes. The soluble part was transferred to a new fresh tube and quantified. The pellet was discarded

The concentration of the total soluble proteins was determined using the Fluorescamine protein assay (Thermo Fisher Scientific, Waltham, MA USA).

A fresh stock of 3 mg/ml Fluorescamine was made in DMSO in an amber tube. A standard curve was made using 50 mg/ml of BSA (Sigma-Aldrich Poole, Dorset, England, UK) serially diluted 1:5 in PBS. 45 µl of standard or unknown samples was plated in triplicate in each well of a 96 well-plate and 15 µl of fluorescamine was added. The fluorescence of the protein-dye complex which has an emission wavelength of approximately 470 nm was read with a UV 460nm emission filter in a Glomax Multi Detection System (Promega Wisconsin USA). These readings were compared with those of a BSA standard curve to give the concentration of proteins in the cell lysates.

The samples were then stored at -80°C for less than one month prior to be sent to Canada for the protein array analysis.

Kinexus™ platform recorded the intensities of dye-bound proteins on the KAM-880 chip and the software calculated the average intensities recorded for each pair of antibody spots to quantify the differences between the control (negative mimics treatment) and testing samples (miR-140-3p or miR-140-5p mimics treatment). Data were normalised according to the protein concentrations and the Z score and percent changes from control (%CFC) were calculated.

2.15 Cell cycle and apoptosis assays using Flow Cytometry

Flow cytometry is the measurement of cells in a flow system. The properties measured include a particle's relative size, relative granularity or internal complexity, and relative fluorescence intensity.

A flow cytometer is composed of three main components:

- A fluidic system that transports the cell suspension to the laser beam.
- An optical system that includes lasers to illuminate the particles and optical filters to direct the signals to specific light detectors.
- An electronics system that converts the light into electronic signals.

The value of this technique lies in the ability to measure a large number of single cells within a short period of time (ten seconds to minutes). The major disadvantage is that it requires a suspension of single cells with minimum clumps and debris. However, any suspended particle or cell from 0.2–150 micrometers in size is suitable for analysis.

The cell suspension is injected into a stream created by a surrounding sheath of a fluid (sheath fluid) that creates a laminal flow, allowing the cells to pass through. If the flow is unperturbed, the sheath fluid does not mix with the sample but constrain the cells to move through the centre of the chamber. Here a light beam, which is orthogonal to the flow, illuminates the sample creating an effect called light scattering. The fraction of light scattered is collected in the same direction as the incident light (0–10° conic angle with respect to the incidence point of the laser) is called forward scatter light (FCS) and is directly proportional to the cell size. The fraction of light scattered at approximately 90°

from the laser beam is called side scatter light (SSC) and is directly proportional to cell granularity or internal complexity. Correlated measurements of FSC and SSC can allow for differentiation of cell types in a heterogeneous cell population, such as blood cells.

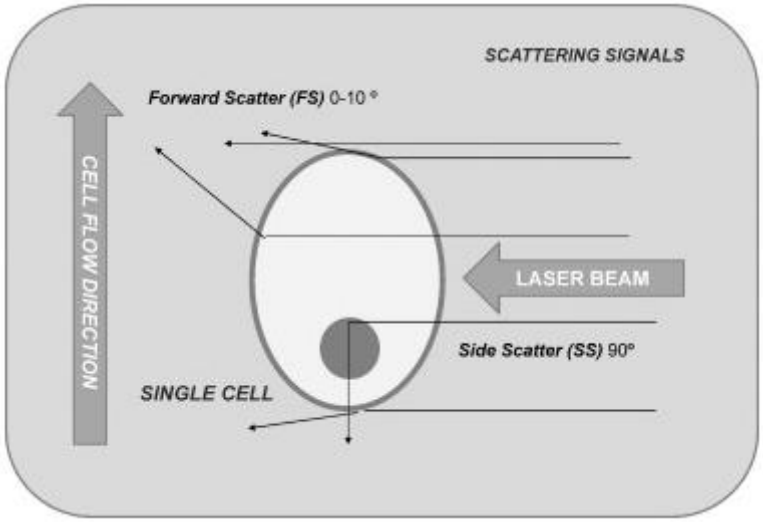

Figure 2.5: Scattering system in Flow Cytometry (Díaz et al., 2010).

Light emitted from fluorescently labelled antibodies can identify a wide array of cell surface and cytoplasmic antigens and for this reason the use of fluorochromes is very common in flow cytometry analysis. The fluorescence is a property that some molecules have to absorb light energy over a range of wavelengths that are characteristic for each compound. When a compound absorbs light, and hence energy, its electrons raise from a lower into an "excited" higher state of energy. Then the electrons release the energy in the form of light (luminescence) and return to the lower energy stage. Because the colour of the exciting and emitting light are different, they can be separated from each other by using optical filters. The range over which a fluorescent compound can be excited is termed its absorption spectrum and the range of emitted wavelengths for a particular compound is termed its emission spectrum. When a fluorescent

dye is conjugated to a monoclonal antibody, it can be used to identify a particular cell type. Different fluorochromes allow distinguishing subpopulations in a mixed population of cells. In this way the fluorescence combined with FSC and SSC data, can be used to identify which cells are present in a sample. Cells can be stained either by a direct or indirect method. In the indirect method, the antibody is labelled with a fluorochrome and incubated with the cells in a single step staining procedure. Then the cells are incubated with the primary antibody, washed and incubated again with the secondary antibody carrying the fluorochrome. With the direct method, multiple antibodies are added at the same step.

In this study two fluorochromes were used, the fluorescein isothiocyanate (FITC) and phycoerythrin (PE). In flow cytometry, more than one fluorochrome can be used simultaneously if the peak emission wavelengths are not too close to each other. The peak emission wavelength is 530 nm for FITC and 575 nm for PE. These peak emission wavelengths are far enough apart to allow the detection of each signal by a separate detector. The amount of fluorescent signal detected is proportional to the number of particles in the suspension. In figure 2.6 the emission spectra of the most common fluorochromes are shown.

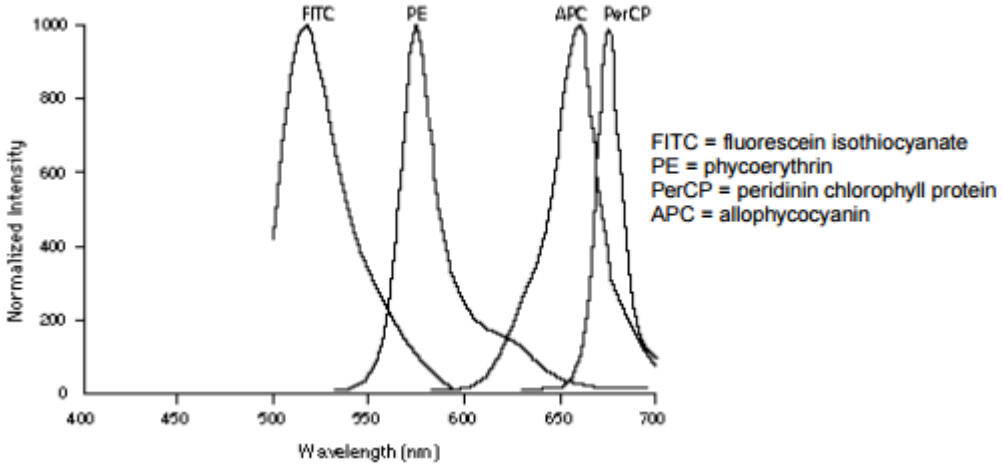

Figure 2.6. Emission spectra of the four most common fluorochromes used in flow cytometry (https://www.bdbiosciences.com/documents/BD_FACSVerse_Apoptosis_Detection_AppNote.pdf).

For the cell cycle analysis, two wells of a 6-well plate were used. Following 48 hours of transfection with negative, miR-140-3p and miR-140-5p mimics, cells were washed twice with PBS, trypsinised, re-suspended in complete medium and centrifuged at 1,700 xg for 5 minutes. The pellet was washed in ice-cold PBS and then centrifuged again at 1,700 g for 5 minutes. At this stage, the pellet was re-suspended in 1 ml of ice cold 70% v/v ethanol and left on ice for 2 hours. Following this, the cells from each treatment were centrifuged at 1,700 xg for 5 minutes and then re-suspended in PBS to a concentration of 10^6 cells in 100 µl. Each sample was divided in two, half was not stained the other half was stained by incubating with 150 µl of 2 µg/ml propidium iodide (PI; ThermoFisher) for 15 minutes at room temperature in the dark. Following this, samples were run on the BD FACSCanto™ II flow cytometer (BD) at a 575nm wavelength.

An apoptosis assay was performed to evaluate whether miR-140-3p and miR-140-5p were able to induce a programmed cell death of the cancer cells. The Annexin V Kit (Santa Cruz Biotechnology) containing fluorescent conjugated annexin V (FITC annexin V) and PI solution was used. Cells were washed twice with PBS, trypsinised, re-suspended in complete medium and centrifuged at 1,700 xg for 5 minutes. The pellet was washed in ice-cold PBS, centrifuged again at 1,700 xg for 5 minutes and each sample of $5x10^5$ cells was re-suspended in 200 µl of 1X annexin V binding buffer. Some samples were not stained. The remaining samples were stained with 3 µl of FITC annexin V (0.01 µg/ml) and 3 µl of PI (100 µg/ml) and the cells incubated at room temperature in the dark for 30 minutes. Following this, samples were run on the BD FACSCanto™ II flow cytometer (BD) using the 488nm wavelength to detect FITC and 575nm for PI.

2.16 MiRNA target prediction

At present, more than 2500 mature miRNAs have been discovered in humans (http://www.mirbase.org).

In the past, when a small RNA was discovered by cDNA cloning, four characteristics were required for its classification as miRNA. First of all its expression was confirmed by molecular methods, such as Northern Blotting, Polymerase Chain Reaction (PCR), primer extension analysis or microarray. Then its sequence should be presented in one arm of the hairpin precursor which is usually 60-80 nucleotides in length in animals. Moreover, the sequence of the mature RNA should be phylogenetically conserved. Finally, the precursor should

accumulate when there is a reduction of Dicer activity. However, it is difficult to meet all of these criteria for several reasons, such as technical difficulties, or the low expression of the candidate miRNA. For this reason, if a small RNA meets the first and the second criterion (expression and structure) or the first and the third criterion (expression and conservation), it is classified as miRNA. In contrast, small RNAs that do not meet these requirements can be classified as small interfering RNAs (Kim, 2005a) with three main categories: trans-acting RNAs (tasiRNAs), repeat-associated RNAs (rasiRNAs) and small-scan RNAs (scnRNAs). TasiRNAs have been found in plants and are encoded in intergenic regions. RasiRNAs match repetitive elements in the sense or antisense orientation in Schizosaccharomyces pombe and Arabidopsis thaliana, inducing the transcriptional gene silencing through methylation. Finally, ScnRNAs have been found in Tetrahymena thermophila (Kim and Nam, 2006).

To overcome the issues reported above, many bioinformatic approaches have been developed and are widely used by all scientists. These approaches are mainly based on the two crucial criteria of structure and conservation (Kim, 2005a).

There are four common features used in prediction tools: seed match, conservation, free energy and site accessibility. Seed matches refer to the Watson-Crick (WC) match between the seed sequence of a miRNA (the first 2-8 nucleotides starting at the 5'end and counting towards the 3'end) and its mRNA targets. The different algorithms consider the following types of seed matches, according to the number of nucleotides which show a WC match with the target:

- 6mer: a perfect WC match between the miRNA seed and mRNA for six nucleotides.

- 7mer-m8: a perfect WC match from nucleotides 2-8 of the miRNA seed.

- 7mer-A1: a perfect WC match from nucleotides 2-7 of the miRNA seed in addition to an A across from the miRNA nucleotide 1.

- 8mer: a perfect WC match from nucleotides 2-8 of the miRNA seed in addition to an A across from the miRNA nucleotide 1.

The sequence alignment of mature miRNAs from different species reveals an overall well-conserved consensus with a few variations. Conservation analysis may focus on regions in the 3'-UTR, the 5'-UTR on all miRNA sequence or on a combination of these three elements. Interestingly, there is a higher conservation in the miRNA seed region than in the non-seed region (Peterson et al., 2014). As for the genes, the conservation of miRNAs during the evolution across the species implies that that miRNA may be involved in crucial biological pathways. Free energy refers to the minimum free energy and shows the strength of the binding between a miRNA and its targets. The lower the free energy, the firmer the binding structure is and the more likely it is indicating the true binding.

Table 2.14. Main miRNA predicttion tools. Mammalian/vertebrate (m), fly (f), worm (w).

Tools	Clades	Criteria for prediction	Website	References
TargetScan	m, f, w	Stringent seed paring, conservation	http://targetscan.org/	(Peterson et al., 2014, Bartel, 2009)
PicTar	m, f, w	Stringent seed paring, conservation	http://pictar.mdc-berlin.de/	(Bartel, 2009, Krek et al., 2005)
MiRanda	m, f, w, others	Moderate seed pairing, conservation	http://www.microrna.org	(Peterson et al., 2014, Bartel, 2009)
Diana microT	m	Stringent seed pairing	http://microrna.gr/microT-CDS	(Peterson et al., 2014, Yue et al., 2009)
RNA22	m, f, w	Moderate seed pairing	http://cbcsrv.watson.ibm.com/rna22.html	(Bartel, 2009)
PITA	m, f, w	Moderate seed pairing	http://genie.weizmann.ac.il/pubs/mir07/mir07_data.html	(Bartel, 2009, Yue et al., 2009)
MiRWalk	m	Stringent seed paring, conservation	http://mirwalk.uni-hd.de/	(Dweep et al., 2011)

TargetScan predicts biological targets of miRNAs by searching for the presence of 8mer, 7mer, and 6mer sites and free energy. As an option, only conserved sites are predicted.

The input to PicTar is a fixed search set of microRNAs and multiple alignments of orthologous nucleotide sequences (3' UTRs). Output are scores that rank genes by their likelihood of being a common target of members (subsets) of the search set and probabilities for the predicted binding sites in each UTR. After checking whether perfect matches are conserved or not, PicTar further checks the binding free energy and finally calculates the probability that the probing 3'UTR is targeted by the set of coexpressed miRNAs (Yue et al., 2009, Krek et al., 2005).

MiRanda uses a three steps analysis. The algorithm aligns miRNA a 3'UTR miRNA sequences to check WC matches, calculates the free energy and finally the conservation is used as a filter. Unlike most miRNA target predictors, miRanda considers matching along the entire miRNA sequence and matches are allowed to contain limited G-U wobble pairs and insertions or deletions (Peterson et al., 2014, Bartel, 2009, Krek et al., 2005, Yue et al., 2009).

Diana microT algorithm is based on parameters that are calculated individually for each miRNA and for each miRNA recognition elements (MREs), UTR sites that have 7-, 8- or 9-nt long consecutive WC base pairing with the miRNA. Using as features the MRE binding type and the MRE conservation profile, all identified MREs are scored through comparative analysis versus a set of MREs identified based on mock miRNA sequences. The overall miTG score is calculated as the weighted sum of the scores of all identified MREs on the 3'-UTR. The algorithm uses up to 27 species to assess the MRE conservation

profile taking into account both conserved and nonconserved MREs for the estimation of the final miTG score (Maragkakis et al., 2009).

RNA22 only contains known miRNAs, permits combinations of G:U wobbles and bulges in the seed region of a heteroduplex and does not require a target's conservation across genomes. RNA22 has successfully predicted non-canonical targets as well as targets beyond the 3'-untranslated region (3'-UTR) (Loher and Rigoutsos, 2012).

PITA uses the target-site accessibility as the main feature for miRNA target prediction. Site accessibility is a measure of the ease with which a miRNA can locate and hybridize with its mRNA target. This is based on the important observation that the preferential and conserved sites of the target are located in the more accessible regions of the UTR. PITA first identifies a potential site by seed match criteria, and then considers site accessibility (Peterson et al., 2014).

MiRWalk generates possible miRNA-binding sites by "walking" the genes of three genomes (human, mouse, rat). It offers the putative miRNA-binding sites within the complete sequence (promoter,coding region, 5'-, -3'-UTR) and provides a comparative platform for the possible miRNA-binding sites within the 3'UTR mRNA regions which result from the miRWalk algorithm and the other eight predictors Diana mT, miRanda, miRDB, RNA hybrid, PICTAR, PITA, RNA22 and TargetScan (Dweep et al., 2011).

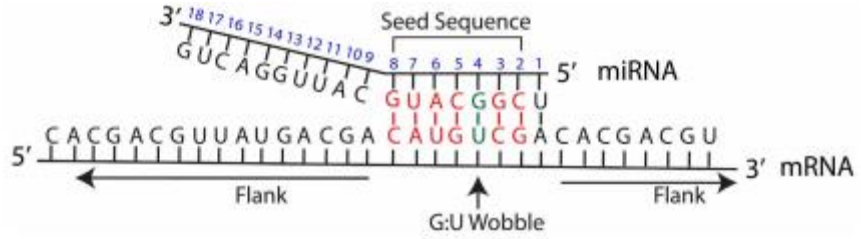

Figure 2.7: Example of miRNA-mRNA interaction. MiRNA position number is shown in blue. The nucleotides in miRNA position number 2-8 represent the seed region. Flank refers to the mRNA sequence on either side of the region corresponding to the miRNA seed sequence. WC matches in the seed sequence are shown in red, and an example of G-U wobble in the seed sequence is shown in green (Peterson et al., 2014).

2.17 Transient transfection using miRNA mimics

Cells were prepared at a concentration of 10^6 cells/ml and 100µl, 300µl and 1ml were added to the wells of 96, 24 or 6 well plates, respectively. Cells were incubated overnight at 37°C and then transfected with miRNA mimics at a concentration of 20µM in antibiotic-free medium using 2µl/ml DharmaFECT1 (Thermo Fisher Scientific, Waltham, MA USA) according to manufacturer's instructions. Cells were used harvested for experiments at different time points after transfection. To verify the efficiency of transfections, the transfected cells were incubated overnight and miRNA levels were evaluated by qPCR.

2.18 PmirGLO Dual-Luciferase miRNA Target Expression Vector cloning

MiRNAs interact with targets in the 3'UTR of transcript and result in either mRNA degradation or inhibition of translation. The pmirGLO Dual-Luciferase miRNA Target Expression Vector (Promega, Hampshire, UK) allows a quantitative evaluation of miRNA activity by inserting 3´ of the firefly luciferase gene (luc2) into miRNA target site. These target sites have been introduced by cloning the miRNA putative binding sites fused to the end of the luciferase reporter gene. If the sequence is a target of a miRNA, the reporter transcript stability will decrease and the luciferase signal will drop. Renilla luciferase (hRluc-neo) is used as a control for normalisation.

The pmirGLO Dual-Luciferase miRNA Target Expression Vector contains a 3' UTR cloned downstream of the luc2 firefly luciferase gene under the control of the weak human phosphoglycerate kinase (PGK) promoter. PGK is a weak, nonviral universal promoter and can be expressed in yeast, rat, mouse and human cells. A weak promoter is useful in this assay to better observe subtle changes in gene expression.

This vector contains the following features:

• Human phosphoglycerate kinase (PGK) promoter.

• Firefly luciferase reporter gene (luc2).

• Multiple cloning site (MCS) located at the 3´ end of luc2.

• Humanized Renilla luciferase-neomycin resistance cassette (hRluc-neo).

• Amp^r gene.

• SV40 late poly(A) signal sequence downstream of luc2.

• Synthetic poly(A) signal/transcription stop site.

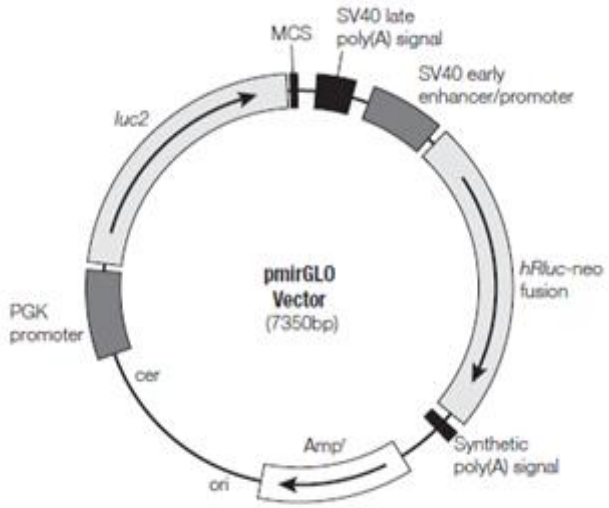

Figure 2.8. pmirGLO Vector pmiRGLO Dual-Luciferase miRNA Target Expression Vector (Promega).

The following workflow explains the procedure followed to verify the targets of miRNAs in mammalian cells.

Design oligonucleotides that contain the desired miRNA target region

↓

pmirGLO vector amplification in E.coli cells

↓

pmirGLO vector purification

↓

pmirGLO vector cloning (amplification and ligation of the desired miRNA target region)

↓

Transformation of E.coli cells with the pmirGLO vector containing the desired miRNA target region

↓

Vector purification

↓

Validation through electrophoresis and sequencing

2.18.1 Design of the oligonucleotides that contain the desired miRNA target region

TargetScan Human 7.0 (http://www.targetscan.org/vert_70/docs/help.html) was used to design the miRNA target region complementary to the desired 3'-UTR target region. The overhangs created by oligonucleotide annealing were designed to be complementary to those generated by the restriction enzymes PmeI and XbaI. NotI internal site was added for clone digestion. In Figure 2.9 all the restriction sites of the pmirGLO vector are shown.

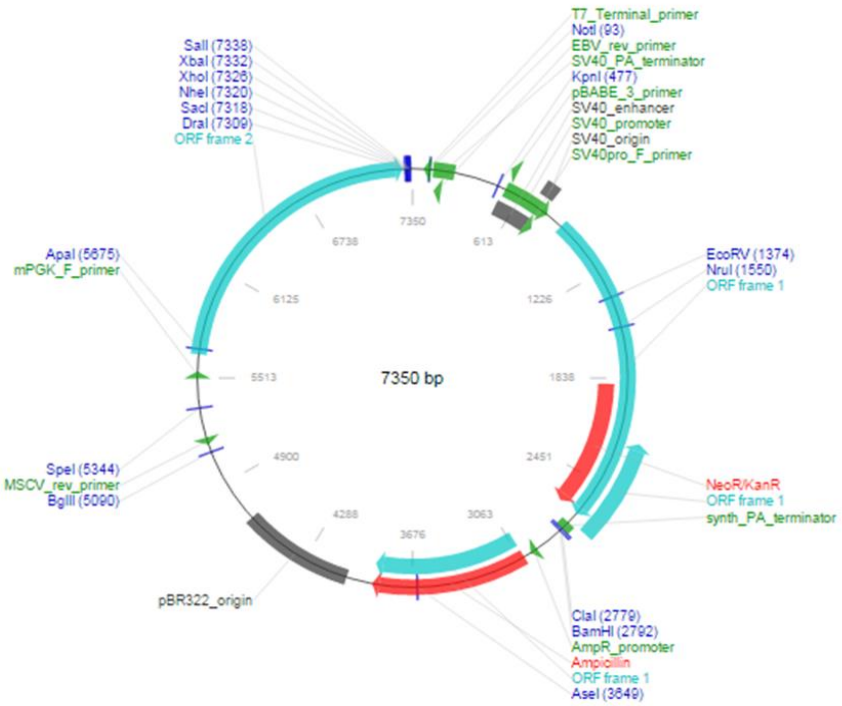

Figure 2.9. pmirGLO Vector restriction sites (https://www.addgene.org/vector-database/8236/).

2.18.2 Transformation of chemically competent E.coli cells

The following protocol was used to transform *E. coli* cells with pmirGLO vector:

- 3 µl pmirGLO vector was mixed with 25 µl chemically competent One Shot™ TOP10 *E.Coli* (Invitrogen Inc., Paisley, UK) and incubated in ice 30 minutes.
- The cells were heat-shocked at 42°C for 30 seconds in a water bath and placed on ice for 2 minutes.
- 250 µl pre-warmed S.O.C. medium (20 g/L Tryptone, 5 g/L Yeast Extract, 4.8 g/L MgSO4, 3.603 g/L dextrose, 0.5g/L NaCl, 0.186 g/L KCl) was added to the cell suspension and the vials were shaken horizontally at 225 rpm on an orbital shaker (Bibby Stuart Scientific, UK) at 37 °C for an hour.
- For pmirGLO amplification, *E.coli* cell suspension was transferred into a T25 flask containing 15ml of pre-warmed LB broth and 100 µg/ml ampicillin and incubated at 37 °C overnight. For the transformation of E.coli cells with the pmirGLO vector containing the desired miRNA target region, an E.coli cell suspension at high and low densities was spread onto pre-warmed selective LB-agar plates containing 100 µg/ml ampicillin and incubated at 37 °C overnight.

The pmirGLO vector contains a gene that confers resistance to ampicillin. The next day it was possible to perform a positive selection of the transformed cells.

2.18.3 Plasmid purification

The purification of the plasmids was performed using the GenElute Plasmid Miniprep Kit (Sigma Aldrich, Dorset, UK), according to the manufacturer's instructions:

- *E.coli* transformed cells were centrifuged at 4 °C, 10 minutes, 5000 rpm.
- The pellet was resuspended in 200 µl of Resuspension solution containing RNase A by pipetting.
- 200 µl of Lysis solution was added and the solution was gently mixed by inverting 6-8 times and left at room temperature 5 minutes.
- The solution was then transferred to a 2 ml tube and 350 µl of Neutralisation solution were added. The tube was gently inverted 4-6 times and centrifuged at maximum speed 10 minutes.
- The columns were prepared by adding 500 µl of Column preparation solution and spinning at 12,000 xg 1 minute. The flow-through was discarded.
- The cleared lysate was transferred to a new 2ml tube containing the column and centrifuged at 12,000 xg 1 minute.
- The flow-through was discarded and 750 µl of Wash solution containing ethanol was added. The tube with the column was centrifuged at 12,000 xg 1 minute and the flow-through discarded again.
- The columns were centrifuged again at 12,000 xg 1 minute to dry.
- The columns were then transferred to a new 2 ml tube and 40 µl of Elution solution were added. The tube was centrifuged at 12,000 xg 1 minute. The flow through was recovered, transfer into the same column and centrifuged again to increase the concentration of the eluate.

- The column was discarded and the DNA concentration was quantified using a spectrophotometer.

2.18.4 Vector cloning

After amplification and purification, pmirGLO vector was digested and then the desired miRNA target region was ligated. The following protocol was designed, using New England BioLabs website (http://nebcloner.neb.com/#!/):

1. Digestion

Component	*50µl Reaction*
DNA	1 µg
10x CutSmart Buffer	5 µl (1X)
PmeI	1 µl (10 units)
XbaI	1 µl (10 units)
Nuclease-free water	To 50 µl

The assembled reaction was incubated at 37 °C for 10 minutes and a 0.8% agarose gel was run to verify if the vector was digested. A non-digested vector was used as a control.

In the meantime, the oligonucleotides were diluted in nuclease-free water to a final concentration of 1 µg/µl and then annealed using the following reagents:

Component	*50µl Reaction*
Oligonucleotide A (1µg/µl)	2 µl
Oligonucleotide B (1µg/µl)	2 µl
Oligo Annealing Buffer	46 µl

The reaction was then incubated at 90 °C for 3 minutes and then transferred into a water bath at 37 °C for 15 minutes.

2. Ligation

The annealed nucleotides were diluted 1:10 for a final concentration of 4ng/µl and the following reaction was assembled:

Component	*Negative control (40µl Reaction)*	*Standard (40µl Reaction)*
10x T4 DNA Ligase Buffer	4 µl	4 µl
Vector (50ng/µl)	2 µl	2 µl
Annealed oligonucleotides (4ng/µl)	-	2 µl
Nuclease-free water	32 µl	30 µl
T4 DNA Ligase (3units/µl)	2 µl	2 µl

The reaction was then incubated at 16°C overnight and a 0.8% agarose gel was run to verify if the vector was digested. Two controls were used: one without oligonucleotides and the second one without oligonucleotides and DNA ligase.

2.18.5 Experimental validation

All the plasmids were sent to the CBS DNA Sequencing facility (Cardiff University) and specific primers (Table 2.5) were used to verify if the inserted sequence contained the desired miRNA target sequence.

2.18.6 Dual-Glo® Luciferase Assay System

A549 cells were suspended at 10^4 cells/ml in DMEM and 100 µl added to each well in a white 96-well plate. Six replicates were set up for each condition and cells were incubated overnight at 37 °C. The following day, the plasmids, which contain the putative miRNA target sites 3'-UTR (or its mutated version) fused to the end of the luciferase reporter gene, were diluted to 20 ng/µl and transfected into A549 cells using 2 µl/ml DharmaFECT Duo (Thermo Fisher Scientific, Waltham, MA USA) in a total volume of 75 µl. After twenty-four hours, the plate was removed from the incubator and equilibrated at room temperature and then the following protocol was used, according to the manufacturer's instructions:

- To each well, a volume of Dual-Glo® Reagent equal to the volume of culture medium was added.

- The plate was left at room temperature for 20 minutes to allow cell lysis to occur and then the firefly luminescence was read using Glomax Multi Detection System.
- To each well a volume of 1:100 diluted Dual-Glo® Stop & Glo® Reagent equal to the original culture medium was added.
- After 10 minutes the renilla luminescence was read using Glomax Multi Detection System (Promega, Wisconsin, USA).

The ratio of firefly/renilla luminescence for each well was calculated and normalised to the control vector (pmirGLO Dual-Luciferase miRNA Target Expression Vector).

2.19 Biotinylated miRNA mimic pulldown

The conventional approach to identifying miRNA targets relies on the bioinformatics predictions as described above, and the subsequent experimental validation. However, these tools generate false-positive and false-negative data and sometimes fail to predict some important biological miRNA targets. For example, the transcription factor E2F2, which has been demonstrated to be a direct target of miR-24, was not predicted by any computational tool because of the lack of a seed match in its 3'-UTR (Lal et al., 2009). In fact, miRNAs may interact with their targets in some non-canonical ways, thus making their identification more difficult (Tan et al., 2014). In this study the bioinformatics approach was integrated by a method based on the RNA pulldown with biotinylated miRNA mimics. Briefly, the cells were transfected with biotinylated mimics and then the complexes formed by the miRNA and the mRNAs were

pulled down using streptavidin coated magnetic beads. Afterwards the total RNA was extracted and sequenced.

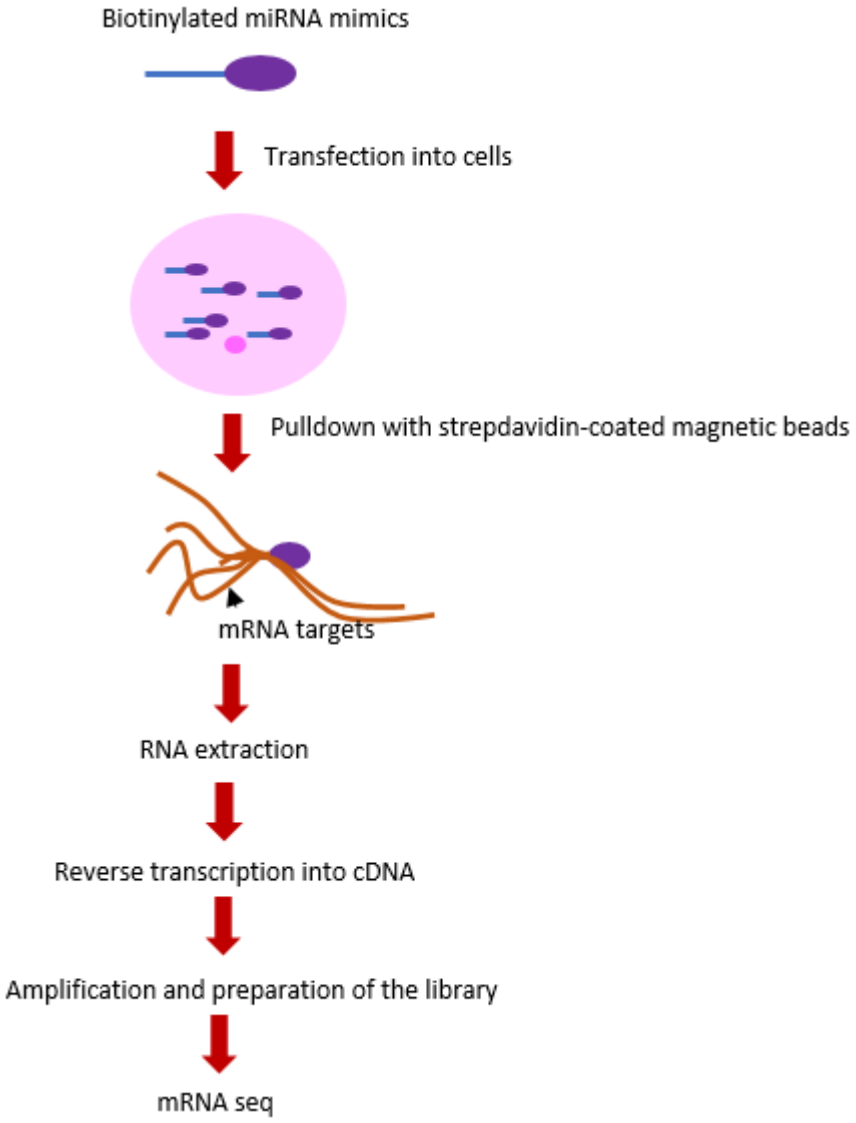

Figure 2.10. MiRNA pulldown procedure. Biotinylated mimics were transfected into cells and, following 24 hours, the complexes of miRNA-mRNA pulled down with streptavidin-coated magnetic beads. After wash steps, the captured mRNAs were purified and further analysed by RNA-sequencing or qPCR.

Cells were transfected in 6-well plates with miRNA mimics biotinylated at a concentration of 20 μM and 2 μl/ml DharmaFECT1 (Thermo Fisher Scientific,

Waltham, MA USA) in serum-free media. Following 24 hours of treatment, the following protocol was used to isolate the RNA bound to the biotinylated miRNA mimics:

- MyOne C1 Dynabeads (Life Technologies, Paisley, UK) were washed twice in hypotonic lysis buffer made with 10 mM KCl, 1.5 mM $MgCl_2$, 10 mM Tris-HCl pH 7.5, 5mM Dithiothreitol (DTT), 0.5% NP40, 60 U/ml SUPERase In (Thermo Fisher Scientific, Waltham, MA USA) and 5 μl/ml protease inhibitors.
- 25 μl/sample of MyOne C1 Dynabeads were incubated with 1 μg/μl BSA and 1 μg/μl yeast tRNA prepared in hypotonic lysis buffer to block non-specific binding sites and then rotated at 4 °C for approximately 3 hours.
- Cells were lysed with hypotonic lysis buffer, on a cold room rocker for 15 minutes and then scraped into pre-cooled tubes.
- Cells were then vortexed and kept on ice 10 minutes. This was repeated twice.
- Samples were centrifuged at 5,000 xg, 4 °C 5 minutes and the supernatant was transferred into a new tube.
- The beads were then washed twice with 300μl hypotonic solution and resuspended to 50 μl per 25μl of the original volume.
- The beads were divided between an appropriate number of tubes and mixed with the cell lysate, with NaCl added at a final concentration of 1 M.
- The cell lysate-bead mix was left rotating at 4 °C for 1 hour.

- The cell lysate-bead mix was washed four times with 200 µl hypotonic buffer and then the RNA was extracted by using Trizol, as described in Section 2.8. The samples were all resuspended in 20 µl RNase-free water.

2.20 RNA sequencing (RNA-seq)

2.20.1 RNA quantification and reverse transcription

To evaluate the complete removal of 18S and 20S ribosomal RNA, the Bio-analyser-2100 (Aligent, Santa Clara, USA) was used. Once the quality of mRNA was evaluated, the reverse transcription of RNA into cDNA was performed by using the Ion AmpliSeq™ Transcriptome Human Gene Expression Kit (Life Technologies, Paisley, UK) for each sample as follows:

Component	*Volume per reaction*
5x VILO Rt Reaction Mix	1.0 µl
10X SuperScript III Enzyme Mix	0.5 µl
DNase-treated total RNA [1]	3 .5 µl
Total	5 µl

[1] We assumed that the amount of the RNA was very low and we used as much as RNA as possible

The conditions for reverse transcription were 42 °C for 30 minutes and 85 °C for 5 minutes using Applied Biosystems 2720 Thermal Cycler (Life Technologies, Paisley, UK).

2.20.2 cDNA amplification

cDNA amplification was performed by using the Ion AmpliSeq™ Transcriptome Human Gene Expression Kit (Life Technologies, Paisley, UK) for each sample as follows:

Component	*Volume per reaction*
5x Ion AmpliSeq HiFi	4 µl
Ion AmpliSeq Transcriptome Human Gene Expression Core Panel	8 µl
PCR master mix	15 µl
Nuclease-free water	3 µl
Total	30 µl

The conditions for the amplification were:

- 99°C for 2 minutes
- 99°C for 15 seconds, 60°C for 16 minutes (16 cycles)

2.20.3 Library preparation

The samples were partially digested by adding 2 µl of FuPa Reagent supplied with the Transcriptome Human Gene Expression Kit (Life Technologies, Paisley, UK) and digested at the following conditions: 50 °C for 10 minutes, 55 °C for 10 minutes, 60 °C for 20 minutes. The amplicons are about 200 bp.

After the digestion, adaptors were assigned to each sample in order to identify each individual sample. The bar-code was enumerated and a mix of Adapters

and barcodes at a final dilution of 1:4 for each adapter have been used. All the reagents come from the Transcriptome Human Gene Expression Kit (Life Technologies, Paisley, UK) and were combined as follows:

Example barcode adapter mix for up to 4 reactions	
Component	***Volume per reaction***
Ion P1 Adapter	2 µl
Ion Xpress Barcode X	2 µl
Nuclease-free water	4 µl
Total	8 µl

At this stage, 2 µl of the diluted barcodes above were mixed with a Switch Solution (Transcriptome Human Gene Expression Kit, Life Technologies, Paisley, UK), 22 µl of the digested amplicon and 2 µl of DNA Ligase, giving a volume of 30 µl for each sample.

To purify the library, 45 µl of Agencourt AMPure XP magnetic beads (Beckman Coulter, USA) per sample were used. The library mixed to the magnetic beads were washed twice with 70% v/v ethanol and then the library quantified by using the Bionalyzer.

Figure 2.11. Ligation procedure for library preparation before RNA sequencing. Through the adaptors, the cDNA is linked to the beads and can be purified. The barcodes discriminate between the samples. 16 barcodes are included in the kit, thus potentially allowing the process of 16 samples together.

2.20.4 Amplification and quantification of the library using Agilent Bioanalyser

To amplify the purified library, 50 µl of 1xLibrary Amp Mix and 2 µl of 25x Library Amp Primers were added. All the reagents are included in the Transcriptome Human Gene Expression Kit (Life Technologies, Paisley, UK). The solution was left on a magnetic stand to separate the beads from the samples and the approximately 50 µl of supernatant was transferred into a clean tube.

The conditions for the amplification were:

- 98 °C for 2 minutes
- 98 °C for 15 seconds, 64°C for 1 minute (5 cycles).

To purify the amplified library the following protocol was used:

- Add 25 µl of Agencourt AMPure XP magnetic beads (Beckman Coulter, USA) to each sample and mix by pipetting
- Incubate at room temperature 5 minutes

- Place the samples onto a magnetic stand and wait until the solution becomes clear
- Transfer the supernatant into a new tube and add 60 μl of XP magnetic beads (Beckman Coulter, USA). Mix by pipetting.
- Place the samples onto a magnetic stand and wait until the solution becomes clear
- Discard the supernatant and wash 150 μl 70% v/v ethanol. Remove and discard the supernatant.
- Repeat the previous step
- Remove all the ethanol, then remove the sample from the magnetic stand and add 50 μl of low TE (Transcriptome Human Gene Expression Kit, Life Technologies, Paisley UK).
- Place the sample on the magnetic stand again and transfer 45 μl of the supernatant to a new tube.
- Analyse 1 μl of the amplified library on the Agilent Bioanalyser

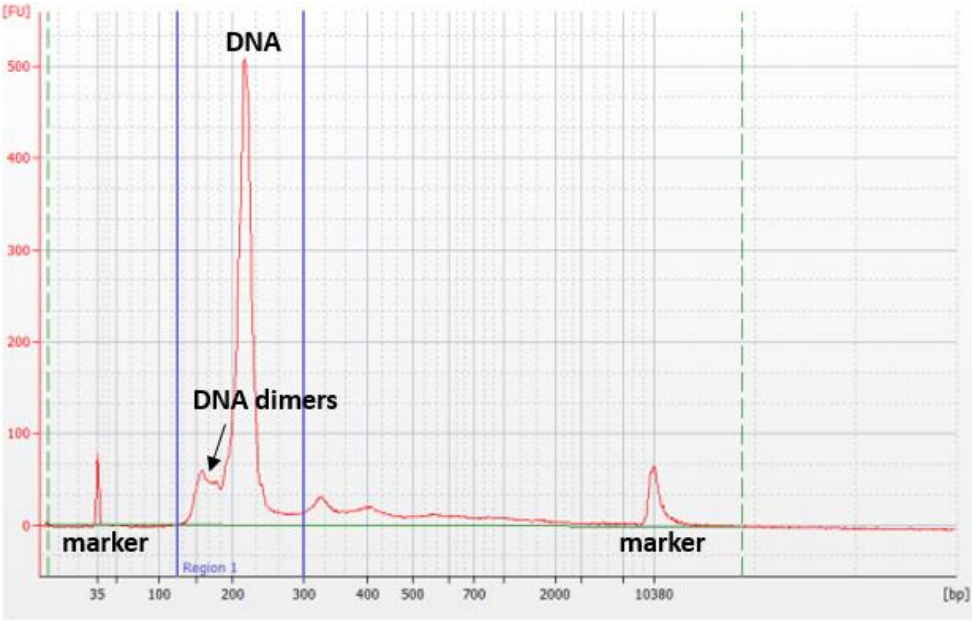

Figure 2.12. Library analysis through Bioanalyser for RNA sequencing.

Through the bioanalyser the quality of the library was evaluated. The fragments of the library should be around 200 bp, whereas the dimers, not detected by the sequencer, are between 100 and 200 bp and indicate the purity of the library. If the DNA peak is too low and the dimers too high, the RNA-sequencing could be unsuccessful.

2.20.5 RNA sequencing

The cDNA library was amplified through an emulsion PCR by using Ion Sphere Particles (IPSs). The Ion OneTouch2 system and the PI template OT2 200 kit (Life Technologies, Paisley, UK) were used and the Template positive IPS's were recovered. The template positive IPS's were processed using the Ion Proton 200 sequencing kit and loaded onto a P1 chip, that was then sequenced on an Ion Proton (Life Technologies, Paisley, UK). Samples were aligned to the human genome (version Hg19) and normalisation was carried out via the RPKM

normalisation method (Mortazavi et al., 2008) along with a 1-way ANOVA test for differential gene expression (n=2). Data were expressed in reads per million (RPM) and the differences between the control and testing samples calculated as $\log_2$ (RPM sample-RPM control) on an Excel spreadsheet.

2.21 *In vitro* cell functional assays

2.21.1 Proliferation assay

Cell proliferation assays monitor actively dividing cells, expressed either as the actual number of active cells or the ratio of proliferating to non-proliferating cells in culture. In this study cell proliferation in response to treatment with miRNA mimics was measured using 0.5% Crystal Violet (Sigma, Aldrich, Dorset, UK) which stains nuclei a deep purple colour.

Cells (5×10^3cells/well) cells were seeded into 96-well plates in triplicate in 100µl growth medium. Three identical plates were set up in total. Before transfection (time 0) and following 24 and 48 hours of incubation at 37˚C, the cells were fixed by using 100µl formalin for 15 minutes, before being stained with 100 µl 0.5% Crystal Violet for further 15 minutes. The dye was then washed off with water and the plates left to dry overnight. 200 µl of acetic acid was added into each well to solubilise the crystal violet and the absorbance at 540 nm measured using a spectrophotometer (BIO-TEK, Elx 800, UK).

2.21.2 Transwell migration and invasion assay

Cell migration and invasion occur in many physiologic processes, such as embryonic development and wound healing. However, there are also some pathological conditions, like cancer, in which malignant cells are able to translocate from their site of origin to different tissues to generate a secondary tumour, a process that is normally called "metastasis".

In experimental cell biology the terms "migration" and "invasion" are used to indicate different processes. *Migration* refers to the directed movement of cells on a substrate such as basal membranes, ECM fibres or plastic plates. Therefore, migration is occurring on 2D surfaces without any obstructive fibre network. *Invasion* is defined as cell movement through a 3D matrix, which is accompanied by a restructuring of the 3D environment. To acquire the ability to pass through the matrix, a cell must modify its shape and interact with the extracellular matrix, which provides the cell attachment substrate and at the same time represents a barrier toward the moving cell body. Thus, the term "invasion" describes the restructuring or destructive movement of cells through a 3D barrier, whereas "3D migration" is used to indicate non-destructive, non-proteolytic movement in a 3D tissues or matrix. The ability to migrate is a prerequisite to invade; a cell cannot invade without migration but can move without invasion (Kramer et al., 2013). There are two methods to detect and quantify the migrated cells. The first method is used to number directly the cells that have passed through the membrane by staining with a cytological dye such as crystal violet. In the second method, the migrated cells are stained fluorescently, removed from the membrane by dissociation using cell dissociation agents and quantified using a

fluorescent reader. In this study, the migrated cells were quantified with the second method, using a Calcein AM solution to measure the fluorescence.

The Transwell Migration Assay was originally introduced by Boyden to analyze the chemotactic responses of leukocytes (Boyden, 1962). This system was modified and improved and now plastic inserts for multi-well plates are commercially available for both the evaluation of the migration and invasion properties of many different cell types. A porous membrane chamber is placed on a well of the multi-well plates and create a two-chamber system separated by the cell-permeable membrane as shown in Figure 2.13.

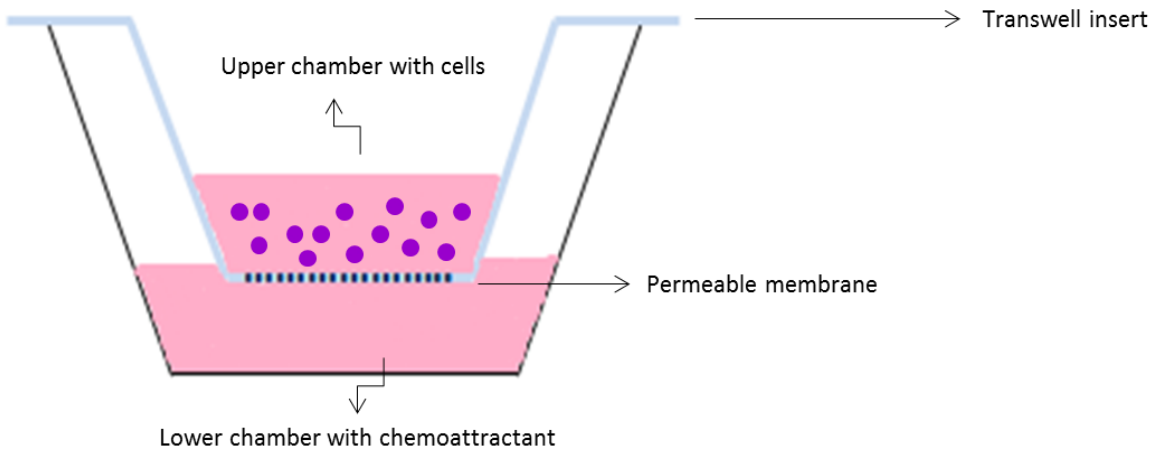

Figure 2.13. Illustration of the transwell migration assay.

The membranes commercially available have pore diameters between 3 and 12 μm. and the size of the pores depends on the cells to be analysed. Pore diameter must be much smaller than the diameter of cells in order to measure the cell that actively "squeeze" through the pores in the membrane, as opposed to just falling through the pores. In this study, the bottom membrane of upper chamber was an 8μm pore polycarbonate membrane (Costar, Corning, NY, USA). Cells were

seeded in medium in the upper chamber and could migrate in vertical direction through the pores of the membrane into the lower compartment, which contained medium alone or medium containing an attractant.

The transwell invasion assay is very similar to the transwell migration assay, however it requires that cells migrate through an extracellular matrix (ECM) or basement membrane extract (BME). In this study, the porous filter was overlaid by a thin layer of BME, before seeding the cells into the top chamber as illustrated in Figure 2.13. The commercial name of the BME used is Matrigel, a reconstituted basement membrane preparation that is extracted from the Engelbreth-Holm-Swarm (EHS) mouse sarcoma, a tumour rich in extracellular matrix proteins. This material contains approximately 60% laminin, 30% collagen IV, and 8% entactin. Entactin is a bridging molecule that interacts with laminin and collagen IV, and contributes to the structural organization of these extracellular matrix molecules. Matrigel matrix also contains heparan sulphate proteoglycan (perlecan), TGF-β, epidermal growth factor, insulin-like growth factor, fibroblast growth factor, tissue plasminogen activator, and other growth factors which occur naturally in the EHS tumor. There are also residual matrix metalloproteinases which occlude the membrane pores, blocking non-invasive cells from migrating through. By contrast, invasive cells can degrade the matrix and move through the Matrigel layer and adhere to the bottom of the filter (https://www.corning.com/media/worldwide/cls/documents/CLS-DL-CC-026%20DL.pdf).

Protocol:

- In the invasion assay, Matrigel was thawed overnight on ice in a 2°C to 6°C refrigerator. 8μm polycarbonate pore size ThinCert™ 24-well plate inserts (Grenier, Bio-One GmbH, Austria) were coated with 50μl serum-free medium containing 10% Matrigel (BD Biosciences, NJ USA) and incubated one hour at 37°C. The rest of the invasion assay was undertaken in the same way as the migration assay above.
- Cells were detached using HYQTase Cell Detachment Solution (Hyclone, Logan, UT, USA) 24 hours after being transfected with miRNA mimics and resuspended in serum-free medium, at a concentration of $1x10^5$ cells/ml.
- 650μl of medium containing 10% FBS (chemoattractant) was added to receiver wells in triplicate and 650μl of serum-free medium (no chemoattractant) to the receiver control transwell.
- The 8μm inserts were placed in each of the receiver wells and 500μl of cell suspension was added to each transwell insert.
- Following twenty-four hours of incubation, the transwells inserts were removed and washed gently with PBS and then incubated for a further hour in 350μl Cell Dissociation Solution (CDS; Sigma Aldrich, Dorset, UK)/Calcein AM (eBioscience, Hatfield, UK) at a ratio of 1.2μl Calcein AM in 1 ml CDS. This detaches the cells from the lower surface of the membrane insert and labels them fluorescently with calcein.
- The cell suspension was then aliquoted into a black 96-well plate and relative fluorescence was measured (excitation 485nm/emission 520nm) using the Glomax Multi Detection System.

- To analyse the total directed cell movement, the wells containing no chemoattractant was subtracted from the test wells.

2.21.3 Tubule formation assay

The tubule formation is one of the most widely used *in vitro* assays to study the ability of the endothelial cells to form vessels. Endothelial cells are plated with the appropriate extracellular matrix support to form capillary-like structures. This assay allows the ability of various compounds to promote or inhibit tubule formation to be determined. Despite *in vivo* assays mimicking better the physiological state, the *in vitro* assays have some advantages compared to their *in vivo* counterpart. *In vitro* assays allow measurement of the direct effect of a compound on endothelial cell function, endothelial cells being the key cell type involved in angiogenesis. Whereas *in vivo* models involve multiple cell types and cellular/molecular pathways. Moreover, angiogenesis *in vitro* is easier to quantify than an *in vivo* model (Goodwin, 2007). Overall the tubule formation assay represents the best way so far to understand the specific angiogenic and antiangiogenic activities of various compounds.

One of the most well-established assays to model the formation of three-dimensional vessels is the tube-formation assay using Matrigel (BD Biosciences, NJ USA). Matrigel is effective for the attachment and differentiation of both normal and transformed anchorage-dependent epithelioid and other cell types.

In this study, the ability of HUVECs to form new vessels in response to media from cells treated with miRNA mimics was monitored. HUVECs were suspended at $1.4x10^5$ cells/ml in EBM-2 complete medium (containing EGM-2

growth supplements) and 100 µl of cells were added to each well of a 96-well plate coated with 50 µl of 50% Matrigel prepared in serum-free medium. 100µl of 60% diluted tumour condition medium from cells treated with miRNA mimics (or matching medium only control) was added to each well and the tubule formation was monitored for 6 hours at 37 °C, 5% CO_2, in time lapse using the EVOS FL Auto Imaging System (Thermo Fisher Scientific, Waltham, MA USA). To evaluate the ability of HUVECs to form vessels, two parameters were evaluated: the tubule length and the total number of closed meshes at 5 hours after monitoring. The tubule length was quantified in pixels using ImageJ, whereas the closed meshes were counted manually (http://image.bio.methods.free.fr/ImageJ/?Angiogenesis-Analyzer-for-ImageJ).

2.21.4 Adhesion assay

Cell adhesion refers to the binding of a cell to the extracellular matrix (ECM) to other cells, or to surfaces. Cell adhesion is important to evaluate the growth and survival of the cells and their communication with other cells. The adhesion assay is often used to study the metastatic ability of cancer cells that usually enhance their adhesion ability to facilitate their movement. In addition, it can be used to investigate the effect of some treatments on cell behaviour. In this study, we focused on laminin and collagen IV, two of the main components of the ECM.

Protocol:

- Collagen IV or laminin at a concentration of 10 μg/well were added to each well of a 96-well plate and incubated at 55 °C for 2-3 hours.
- The wells were rehydrated using serum-free DMEM and incubated at room temperature for 40 minutes.
- The medium was removed and replaced with 100 μl of miRNA mimic transfected cells in 10% FBS DMEM at a concentration of $1x10^5$ cells/ml. The cells were incubated at 37 °C for 40 minutes.
- The cells were washed with PBS to remove any non-adherent cells and adherent cells were fixed using 200 μl of 4% Formalin in each well and incubated at room temperature for 10 minutes.
- The fixed cells were then stained using 100 μl of 0.5% Crystal Violet in each well and incubated again at room temperature for 10 minutes.
- The cells were washed twice using distilled water and allowed to air dry overnight.
- The absorbance was then measured using the Glomax Multi Detection System (Promega, Wisconsin, USA) .

2.22 Seahorse XF^e assays

Cellular metabolism is the process of substrate uptake (oxygen, glucose *etc*) and energy conversion through a series of enzymatically controlled oxidation/reduction reactions. These reactions occur through a series of intracellular biochemical processes (glycolysis, Kreb Cycle, electron transport chain, and oxidative phosphorylation) resulting in the production of ATP, the

release of heat, lactate and CO_2 into the extracellular microenvironment (Ferrick et al., 2008). The Seahorse XF^e analyser simultaneously measures the two major energy pathway of the cells, mitochondrial respiration and glycolysis. This is measured in live cells in real time by using the extracellular flux (XF), which is the change in oxygen and proton concentrations in the media surrounding the cells. Glycolysis is measured by using the extracellular acidification rate (ECAR) and mitochondrial respiration by using the oxygen consumption rate (OCR) of cells.

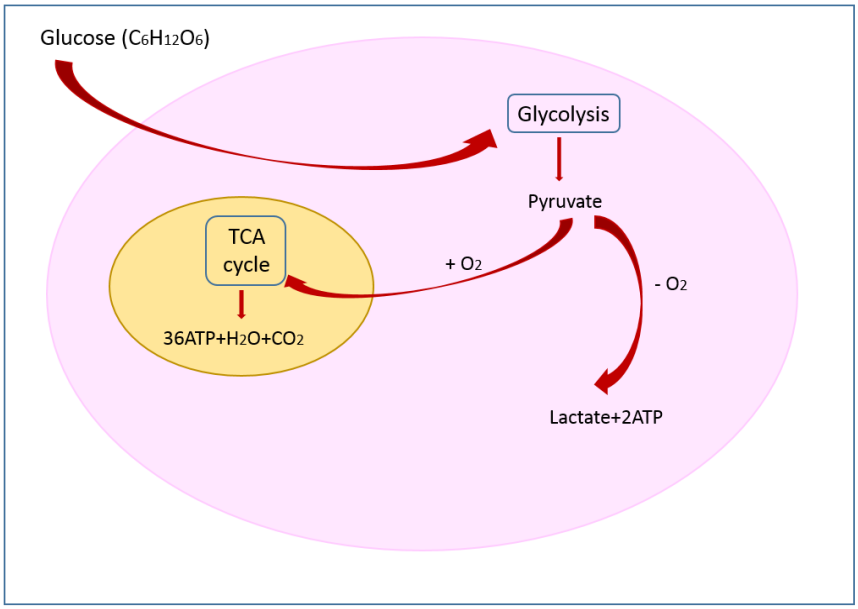

Figure 2.14. Schematic representation of the cellular respiration in animals. Glucose is transported into the cells and converted in pyruvate and other intermediates through a process named glycolysis. In the presence of oxygen, pyruvate enters into the mitochondrion and is converted in ATP, water and carbon dioxide by the citric acid cycle (TCA), also called Krebs cycle. In the absence of oxygen, pyruvate is converted into lactate and ATP

In this study, the Seahorse XFe96 Analyzer (Agilent Technologies, CA, USA) and XF96 cell culture microplates (Seahorse Bioscience, CA, USA) were used. Cells were seeded into the wells of an XF96 cell culture microplate and a bicarbonate-free medium (Seahorse Bioscience, CA, USA), was used during the assay. Up to four drugs may be added to the assay calibration cartridge for automated injection during the assay. Next, the microplate containing cells was inserted into the instrument and data collected in real time. In this study the Cell Mito Stress and Glycolysis Stress Test were used to measure the oxygen consumption rate (OCR) and extracellular acidification rate (ECAR) respectively.

The Seahorse XF Cell Mito Stress Test measures the key parameters of mitochondrial function: basal respiration, ATP production, proton leak, maximal respiration and spare respiratory capacity (Figure 2.15) by using modulators of respiration that target components of the electron transport chain (ETC) (Figure 2.15). Three types of compounds were serially injected into the wells of the XF96 cell culture microplate as follows:

- Oligomycin: It inhibits ATP synthase (complex V) and the decrease in OCR following this injection correlates with the mitochondrial respiration associated with cellular ATP production (Table 20). Before this injection cells have a basal respiration, which is the oxygen consumption used to meet cellular ATP demand and resulting from mitochondrial proton leak. The proton leak refers to the remaining basal respiration not coupled to ATP production. Proton leak may be due to mitochondrial damage or can be used as a mechanism to regulate the mitochondrial ATP production.

- Carbonyl cyanide-4 (trifluoromethoxy) phenylhydrazone (FCCP): An uncoupling agent that collapses the proton gradient and disrupts the mitochondrial membrane potential. After the injection of FCCP the electron flow through the ETC is uninhibited and oxygen is maximally used by the complex IV. The OCR measured corresponds to the spare respiratory capacity, which is the difference between the maximal and basal respiration (Table 20). The spare respiratory capacity measures the ability of the cells to respond to increased energy demand.
- Rotenone and antimycin A mixture: Inhibitors of complex I and complex III respectively. These are able to shut down the mitochondrial respiration and allow calculation of the non-mitochondrial respiration driven by processes outside the mitochondria (Table 2.15).

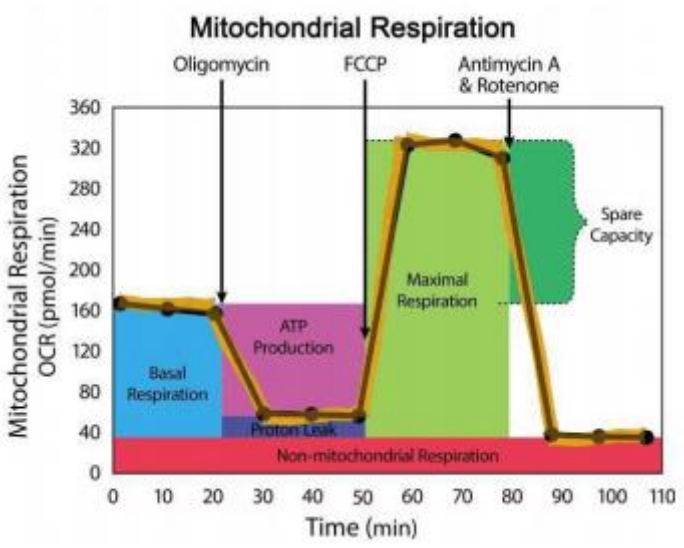

Figure 2.15. Example of a Seahorse XF Cell Mito Stress profile following the injections with oligomycin, FCCP and antimycin A/rotenone. From (http://www.agilent.com/en-us/support/cell-analysis-(seahorse)/seahorse-xf-software)

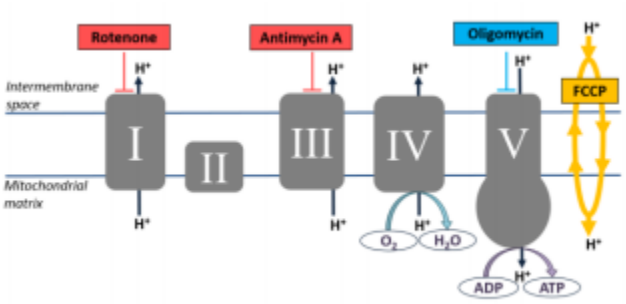

Figure 2.16. Effects of the injections on aerobic respiration. The compounds injected in the Cell Mito Stress assay inhibit different components of the electron transport chain. Oligomycin and the mix of rotenone/antimycin A decrease the OCR, whereas FCCP increases the OCR. From (http://www.agilent.com/en-us/support/cell-analysis-(seahorse)/seahorse-xf-software)

The parameter calculations performed in the XF Cell Mito Stress Test are described in Table 2.15 (http://www.agilent.com/en-us/support/cell-analysis-(seahorse)/seahorse-xf-software).

Table 2.15. Cell Mito Stress Test parameter equations.

Parameter value	Equation
Non-mitochondrial Respiration	Minimum rate measurement after Rotenone/antimycin A injection
Basal Respiration	(Last rate measurement before first injection)-(Non-mitochondrial respiration)
Maximal respiration	(Maximum rate measurement after FCCP injection)-(Non-mitochondrial respiration)
H^+ Proton Leak	(Minimum rate measurement after Oligomycin injection)-(Non-mitochondrial respiration)
ATP Production	(Last rate measurement after Oligomycin injection)-(Minimum rate measurement after Oligomycin injection)
Spare Respiratory Capacity	(Maximal Respiration)-(Basal Respiration)
Spare Respiratory Capacity as a %	(Maximal Respiration)-(Basal Respiration) x 100
Acute Response	(Last rate measurement before Oligomycin injection)-(Last rate measurement before acute injection)
Coupling efficiency	(ATP Production Rate)/(Basal Respiration Rate) x 100

The Seahorse XF Cell Glycolysis Stress Test reports three key parameters of glycolytic function: glycolysis, glycolytic capacity and glycolytic reserve (Figure 2.17). Glucose in cells is converted into pyruvate (glycolysis) and then into lactate, thus resulting in a net production of protons into the extracellular space. The extrusion of protons into the extracellular space results in the acidification of the environment. The cells in the XF96 cell culture microplate are first incubated in a medium deprived of glucose or pyruvate and ECAR is measured after injections with glucose, oligomycin and 2-deoxy-glucose (2-DG) (Figure 2.17).

- The first injection is a saturating concentration of glucose that cells catabolise through the glycolytic pathway to pyruvate, producing ATP, NADH, water and protons. This glucose-induced response is the rate of glycolysis under basal conditions (Table 2.16). ECAR prior glucose injection is referred to as non-glycolytic acidification caused by processes different from glycolysis.
- The second injection is the oligomycin, which inhibits the mitochondrial ATP production and shifts the energy production to glycolysis, revealing the cellular maximum glycolytic capacity (Table 2.16), when the maximum ECAR rate is reached because of the shutting down of the oxidative phosphorylation.
- The third injection is 2-DG, a glucose analogue, which inhibits glycolysis through a competitive binding to glucose hexokinase (Figure 2.17), the first enzyme involved in the glycolytic pathway. The difference between the Glycolytic capacity and Glycolytic rate is the Glycolytic reserve (Table 2.16).

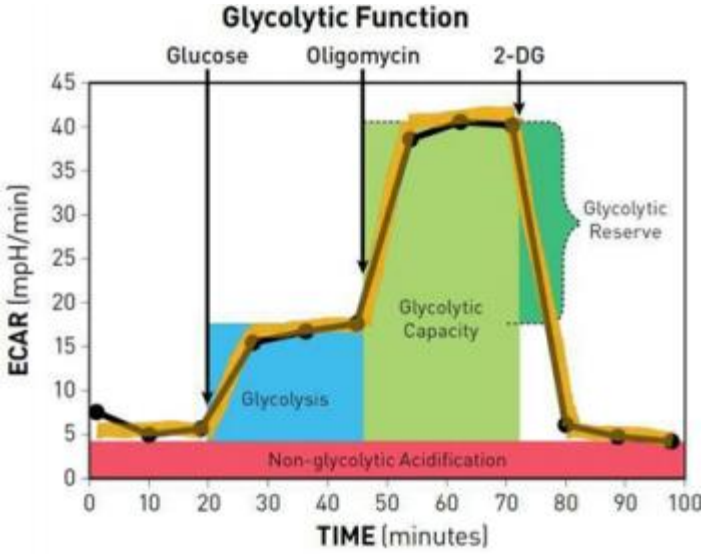

Figure 2.17. Seahorse XF Glycolysis Stress profile following the injections with glucose, oligomycin and 2-DG. From (http://www.agilent.com/en-us/support/cell-analysis-(seahorse)/seahorse-xf-software).

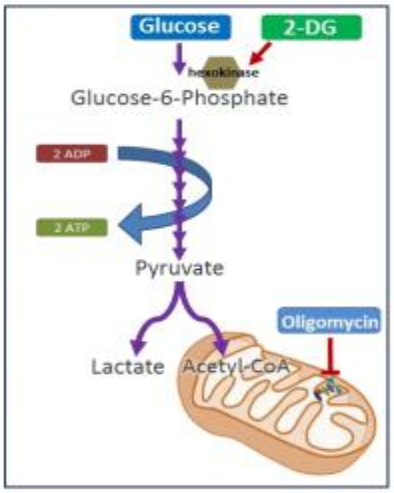

Figure 2.18. Glycolysis. The compounds injected in the Glycolysis Stress assay inhibit key components of the glycolysis as described above. Glucose and oligomycin increase the ECAR, whereas 2-DG inhibits the glycolytic process and, consequently, the glycolytic pathway (http://www.agilent.com/en-us/support/cell-analysis-(seahorse)/seahorse-xf-software).

The parameter calculations performed in the XF Glycolysis Stress Test are described in Table 2.16 (http://www.agilent.com/en-us/support/cell-analysis-(seahorse)/seahorse-xf-software).

Table 2.16. **Glycolysis Stress Test parameter equations**.

Parameter value	Equation
Glycolysis	(Maximum rate measurement before Olygomicin injection)-(Last rate measurement before Glucose injection)
Glycolytic capacity	(Maximum rate measurement after Olygomicin injection)-(Last rate measurement before Glucose injection)
Glycolytic Reserve	(Glycolytic capacity)-(Glycolysis)
Glycolytic Reserve as a %	(Glycolytic capacity)/(Glycolysis) x100
Non-glycolytic Acidification	Last rate measurement prior to Glucose injection
Acute response	(Last rate measurement before Glucose injection)-(Last rate measurement before acute injection)

Each parameter value described in Cell Mito and Glycolysis Stress assays represents the average of individual well calculations for each assay group. Error bars are calculated based on the individual calculations for each parameter.

80µl of BEAS-2B, A549 and SK-MES-1 cells were seeded into each well of the XF96 cell culture microplates at the following densities: 60,000 cells/wells for

BEAS-2B and 25,000 cells/well for A549 and SK-MES-1 and then left overnight at 37°C, 5% CO_2. The day after the cells were treated using a negative control, miR-140-3p and miR-140-5p mimics as described in Section 2.17. The Cell Mito and Glycolysis Stress assays were performed simultaneously on the same microplate for all the cell lines after 24 and 48 hours of transfection with mimics.

Cell Mito Stress assay protocol:

- Cell Mito Stress medium was made using XF Modified DMEM (Seahorse Bioscience, CA, USA). 1 mM Pyruvate (Sigma Aldrich, Dorset, UK), 2 mM Glutamine (Sigma Aldrich, Dorset, UK) and 10 mM Glucose (Sigma Aldrich, Dorset, UK) were added and pH adjusted to 7.4 using 0.1 N NaOH.
- Cells were washed twice with filtered Cell Mito Stress filtered medium and 150 µl/well was finally left and then incubated 1 hour at 37°C in a CO_2 free incubator.
- Meanwhile, the injections for the calibration plates were prepared as follows: oligomycin, FCCP and rotenone/antimycin A were diluted in Cell Mito Stress filtered medium at a final concentration of 100 µM, 100 µM and 50 µM respectively. 25 µl/well was added into the assigned wells of the calibration plate.
- The microplate was placed into the Seahorse XFe96 Analyser.

Glycolysis Stress assay protocol:

- Glycolysis Stress medium was made using XF Base Medium (Seahorse Bioscience, CA, USA). 1 mM Glutamine (Sigma Aldrich, Dorset, UK) were added and pH adjusted to 7.4 using 0.1 N NaOH.

- Cells were washed twice with filtered Glycolysis Stress medium. The cells were incubated 1 hour at 37°C in a CO2 free incubator with 150 µl/well glycolysis stress medium.
- In the meantime, the injections for the calibration plates were prepared as follows: glucose, oligomycin and 2-DG were prepared in filtered Glycolysis Stress medium at a final concentration of 5 µM. 25 µl/well was added into the assigned wells of the calibration plate.
- The microplate was placed into the Seahorse XFe96 Analyser.

There are four factors which influence the mitochondrial energetic measurements: cell number, cell mass, mitochondria mass or number and mitochondrial complex activity. In this study, the protein concentration was used to normalise XF data. After each assay, the cells were washed, lysed and proteins were quantified for normalisation. The Seahorse XF Mito Stress and Glycolysis Test Report Generator (http://www.agilent.com/en-us/support/cell-analysis-(seahorse)/seahorse-xf-software) automatically calculates the parameters for each test. Data were then exported to Excel for further analysis.

2.23 Enzyme Linked Immunosorbent Assay (ELISA)

ELISA is widely used in biomedical research for the detection and quantification of specific antigens or antibodies in a given sample. This technique uses antibodies (the most common ones are horseradish peroxidase-HRP- or alkaline phosphatase-AP- conjugated) and an enzyme-mediated colour change to detect the presence of either antigens (proteins, peptides, hormones, etc) or antibodies.

The antigen in fluid phase is usually immobilized to the surface of 96- or 384-well plates and the antigen is allowed to bind to a specific antibody, which is itself subsequently detected by a secondary, enzyme-coupled antibody. In the presence of its antigen, the chromogenic substrate for the enzyme produces a visible colour change or fluorescence. The change of colour is normally quantified using a colorimetric reading. The choice of substrate depends upon the required assay sensitivity and the instrumentation available for signal-detection (spectrophotometer, fluorometer or luminometer). Having the antigen in fluid phase immobilized to the plate surface makes it easy to separate bound from non-bound material and this ability to wash away non-specifically bound materials makes the ELISA a powerful tool for measuring specific analytes in a solution, even if their concentration is very low. The advantage of ELISA compared to other techniques, such as immunohistochemistry and Western Blot, is the quantitative measure of very low concentrated intracellular and extracellular materials.

ELISA can be performed with different modifications to the basic procedure called "indirect ELISA", "sandwich ELISA" and "competitive ELISA".

In the indirect ELISA the protein sample is bound through adsorption, directly (and non-specifically) to the well. Then a solution such as bovine serum albumin is used to block any areas of the wells not coated with the antigen. The primary antibody, specific for the antigen is added first, followed by an enzyme-conjugated secondary antibody. Finally, a substrate for the enzyme is introduced to quantify the primary antibody through a colour change which is directly proportional to the concentration of the primary antibody. The major disadvantage of indirect ELISA is that the method of antigen immobilization is

not specific because when serum is used, all proteins in the sample may adhere to the surface of the well.

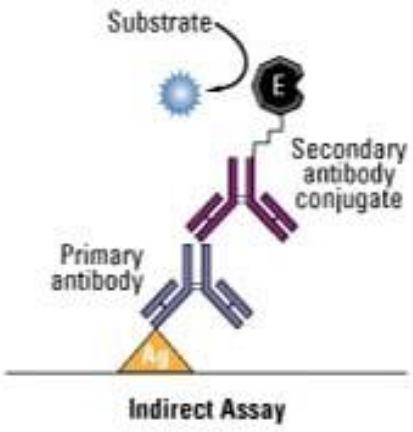

Figure 2.19. **Illustration of the indirect ELISA.** From (http://www.rajaha.com/elisa-test-what-principle-types/).

In the sandwich ELISA, a "capture" antibody is bound to the well and when the sample is added, only the proteins specifically recognised by the antibody are "captured". After a solution such as BSA is used to block any areas of the wells not coated with the antigen, a second "detection" antibody is used to detect the protein. Finally, a third enzyme-labelled antibody is added to detect the "detection" antibody. Finally, a substrate for the enzyme is introduced to quantify the primary antibody through a colour change which is directly proportional to the concentration of the primary antibody. One advantage of using a purified specific antibody to capture the antigen is that there is no need to purify the antigen from a mixture of other antigens.

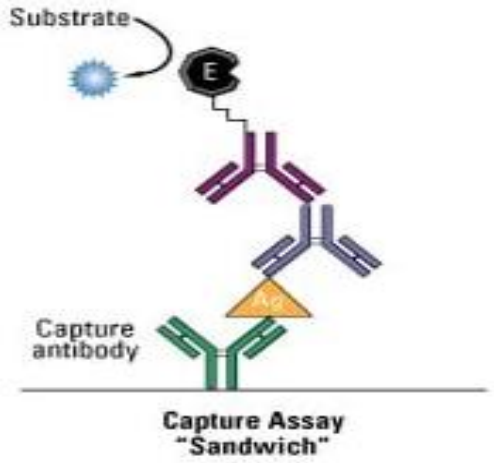

Figure 2.20. Illustration of the sandwich ELISA. From (http://www.rajaha.com/elisa-test-what-principle-types/).

In the competitive ELISA the primary antibody is incubated with the sample, thus forming a complex. The complex is then adsorbed to the wells and then a secondary antibody is added. The secondary antibody recognises the primary antibody only if it is not bound to the antigen. In this case the secondary antibody "competes" with the antigen. Finally, a substrate for the enzyme is introduced to quantify the primary antibody through a colour change. The absence of colour indicates the presence of the antigen in the sample. The main advantage of the competitive ELISA is its high sensitivity to compositional differences in complex antigen mixtures, even when the specific detecting antibody is present in relatively small amounts.

In this study, the human vascular endothelial growth factor (VEGF-A) in the conditioned medium of cells transfected with negative, miR-140-3p and miR-140-5p was quantified by using 96-well plates pre-coated with VEGF-A primary antibody (i.e. sandwich ELISA). All the reagents and plates were purchased from Aviva System Biology, San Diego, USA.

Protocol:

- The medium from cells transfected with negative, miR-140-3p and miR-140-5p mimics was centrifuged 15 minutes at 1000 xg to remove any cell debris and the supernatant was collected.
- 100 µl of the media or serial-diluted standard VEGF curve (1:2 dilution) samples were added to each well of the 96 well plate and incubated 90 minutes at 37 °C.
- The medium was aspirated and washed 4 times with the Wash Buffer provided with the kit.
- 100 µl of Biotin-Conjugate anti-human VEGF antibody solution was added into each well and incubated 60 minutes at 37 °C.
- The solution was aspirated and washed 4 times with the Wash Buffer provided with the kit.
- 100 µl of the Streptavidin-HRP solution was added into each well and incubated 30 minutes at 37 °C.
- The solution was aspirated and washed 4 times with the Wash Buffer provided with the kit.
- 100 µl of the substrate solution was added into each well and incubated 10-20 minutes at 37 °C in the dark.
- 100 µl of Stop solution was added into each well and the plate was read at 450nm within 30 minutes.

2.24 Statistical analysis

Pearson-D'Agostino test was used to verify if the data were normally distributed. For normal distributions, the parametric Student's t-test was used to compare two sets of data. Mann-Whitney for non-matched data and Wilcoxon Signed-Rank Tests for matched samples were used as non-parametric methods to compare two sets of data that do not follow a normal distribution. When more than two sets of data were compared, On-Way Analysis of Variance ANOVA was used for normal distributions and Kruskal-Wallis for non-normal distributions. Graphs plotting and statistical analysis were performed using GraphPad Prism 6.04 software (GraphPad Software, San Diego, CA, USA). Statistical significance was indicated with the following nomenclature: *$p<0.05$, **$p<0.01$, ***$p<0.001$.

CHAPTER 3

MIR-140-3p AND MIR-140-5p EXPRESSION IN NSCLC PATIENT TISSUES AND CELL LINES

3.1 Introduction

Several studies showed that miR-140-3p and 140-5p are both downregulated in different cancer cell lines and tissues compared to their normal counterparts, including lung, thus suggesting their role as tumour suppressors (Yuan et al., 2013, Dong et al., 2016, Li et al., 2014b, Li et al., 2014a). The level of miRNAs can be modified *in vitro* and *in vivo* by using miRNA mimics or inhibitors. MiRNA mimics are synthetic small double-stranded molecules that mimic the endogenous miRNA in cells, whereas miRNA inhibitors are double-stranded RNA molecules that bind and inhibit their corresponding endogenous miRNA.

In the classic model of miRNA biogenesis, the duplex of mature miRNAs is produced by Dicer processing of the hairpin precursor. Then, a following strand selection step determines which mature miRNA acts as a guide for the mature miRNA-mediated silencing complex (miRISC). The strand selection process is finely regulated and may vary among tissues and between normal and malignant cells (Griffiths-Jones et al., 2011, Ha and Kim, 2014a, Meijer et al., 2014).

Recent studies have introduced innovative concepts and revealed that both sister mature miRNAs may accumulate in some tissues and cell types. In this scenario, the strand selection might be tissue-specific but not deterministic, thus a given strand could act as a guide strand in a specific cell type and but a passenger in another one (Li et al., 2012, Hu et al., 2009). In this respect, different biological contexts most likely share complex mechanisms of strand selection regulation, leading to either alternative expression of a single mature form or to concurrent expression of both mature sister miRNA (Salvatore et al., 2016).

Therefore, in this chapter the differential expression of miR-140-3p and 140-5p was examined in two NSCLC cell lines, A549 and SK-MES-1, and in the normal lung cell line BEAS-2B. A549 cells originate from a localised carcinoma, whereas the SK-MES-1 from a lung metastasis. BEAS-2B derives from normal human bronchial epithelium transfected with the 12-SV40 adenovirus. The efficiency of transfection of miR-140-3p and 140-5p mimics into the cell lines have been compared and evaluated. The time course of miR-140-3p and 140-5p mimic treatment has also been investigated, considering that it is a transient transfection and the life time of miRNA mimics in cells is limited. Finally, the ratio of miR-140-3p / miR140-5p has been evaluated to check whether one of the forms is highly expressed in one, both or neither if the strand selection process is different between normal and cancer cells.

3.2 Materials and methods

Cell lines

BEAS-2B, A549 and SK-MES-1 NSCLC cell lines were cultured as described in Section 2.1.

Collection of human lung tissues

All the tissues from NSCLC patients were collected immediately after surgery by Beijing Friendship Hospital, Capital Medical University, Beijing, China and stored at -80°C until use, with approval from the Health Authority local research ethics committee. In Beijing, RNA was extracted from a piece of frozen tissue using the TRI-reagent protocol as described in Section 2.8. The cohort includes 19 paired normal and tumour lung tissues together with 49 unpaired normal and tumour tissues. All the specimens used in the current study were verified by a consultant pathologist. Tissues were divided in to two categories, depending on the availability. Paired tissues refer to tissues from the same patients, in which the tumour part and the adjacent normal counterpart have been resected surgically, whereas the unpaired are tissues from different patients. The patient clinic-pathological information is described in Section 2.2.

Transient miRNA transfections

For each cell line, cells were seeded at a concentration 1.2 x 10^6 cells/ml in a 6'well plate their appropriate media and allowed to adhere overnight at 37 °C. Cells were then transfected as described in Section 2.17.

RNA isolation and RT-PCR

RNA isolation, DNA isolation and RT-PCR were performed on the cell lines using the TRI-reagent protocol as previously described in Sections 2.8.

DNA sequencing

Samples were sent to the Central Biotechnology Services (CBS), Heath Park, Cardiff University, to be sequenced. The pre-miR-140 genomic sequence of the lung cancer cells used in this study was compared to the wild-type sequence on chromosome 16q22.1 by using the Basic Local Alignment Search Tool (BLAST, National Centre for Biotechnology Information) online.

Quantitative PCR (qPCR)

cDNA was produced from RNA in lung cell lines and human tissues using reverse transcription as detailed in Section 2.10. qPCR was undertaken with the primers for miR-140-3p, miR-140-5p and U6 (listed in Table 2.4). The analysis was performed using Ct values obtained from these processes were analysed using $2^{-(\Delta\Delta CT)}$ normalisation to U6 for cell lines and U48 for tissues. Each qPCR sample was analysed in triplicate, with the experiment being independently set up three times.

Statistical analysis

Statistical analysis was performed as described in Section 2.24.

3.3 Results

3.3.1 MiR-140-3p and 140-5p are downregulated in NSCLC tissues and cell lines

The expression of miR-140-3p and 140-5p were assessed in the two NSCLC cell lines A549 and SK-MES-1 and in the immortalised normal lung epithelial cell line BEAS-2B. Both miR-140-3p and 140-5p have been found to be significantly downregulated in cancer cell lines, compared to the normal one (in A549 $p=0.0134$ and $p=0.0018$ for miR-140-3p and 140-5p respectively and in SK-MES1 $p=0.004$ and $p=0.0016$ for miR-140-3p and 140-5p, respectively) (Figure 3.1a). In Figure 3.1b the expressions of the two forms of miR-140 (-3p and -5p) have been compared to try to understand whether one of the strands could be preferentially loaded into the RISC complex. To better address this, the ratio (miR-140-3p/miR-140-5p) between the two forms of miR-140 has been calculated. The comparison between the two forms of miR-140 precursor in each cell line (Figure 3.1b) shows that there is no difference in the normal cell line BEAS-2B, as the ratio between the relative expression levels of two forms (miR-140-3p/miR-140-5p) is 1.47. On the contrary, the amount of the two forms differs in cancer cells, with a ratio miR-140-3p/miR-140-5p of 4.2 and 3.2 in A549 and SK-MES-1, respectively, with the miR-140-3p form being significantly higher in both cancer cell lines.

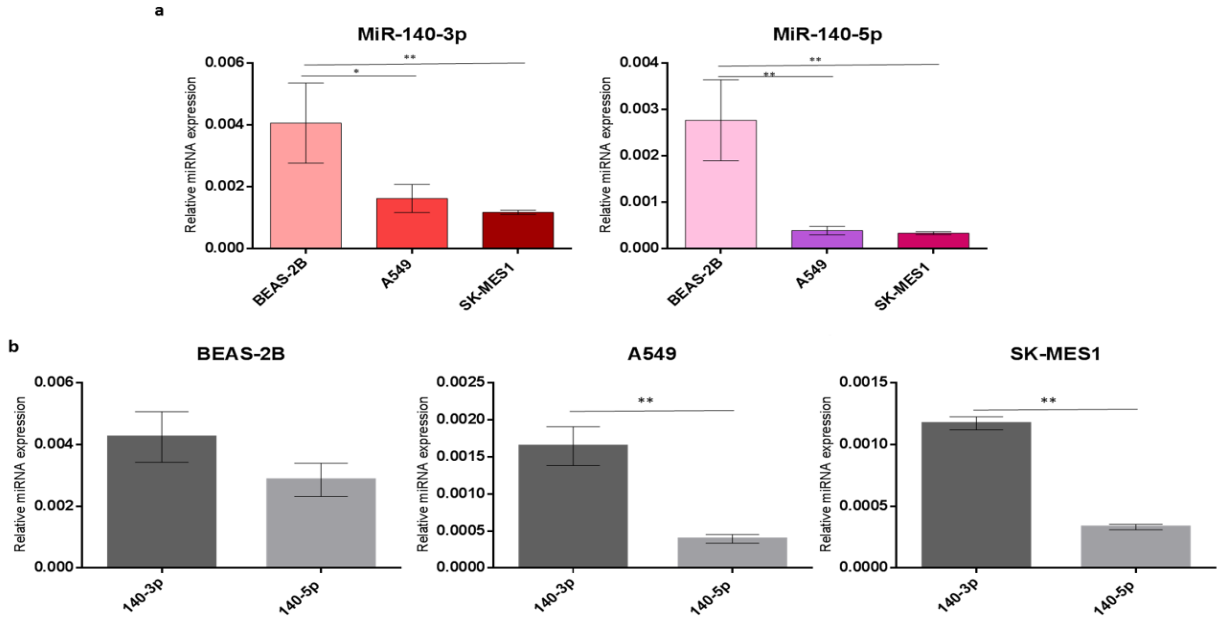

Figure 3.1 MiR-140-3p and 140-5p expression in lung cell lines. MiR-140-3p and miR-140-5p expression in BEAS-2B, A549 and SK-MES-1 lung cell lines was evaluated by q RT-PCR. a) Compared to BEAS-2B, both miR-140-3p (left) and miR-140-5p (right) are downregulated. Data are presented as mean $\pm$ SEM, three individual experiments undertaken in triplicate, ANOVA-test has been used to assess significance with*$p<0.05$, **$p<0.01$ b) The two forms of miR-140 in each cell line show no strand selection in BEAS-2B (left) and a preferential maturation of miR-140-3p in A549 (middle) and SK-MES-1 (right). Data are presented as mean $\pm$ SEM, three individual experiments undertaken in triplicate, t-test has been used to assess significance with **$p<0.01$.

The results obtained in the cell lines have also been confirmed in paired human lung cancer clinical samples, where a lower expression of both miR-140-3p ($p=0.026$) and 140-5p ($p=0.0428$) was found in the cancer cells compared to the adjacent normal counterpart tissue (Figure 3.2a).

In non-paired tissues the expression of miR-140-3p was also significantly downregulated in cancer samples, reflecting the result obtained in cell lines and paired tissues ($p=0.0014$) (Figure 3.2b). No significant difference was detected in the unpaired samples when miR-140-5p was analysed.

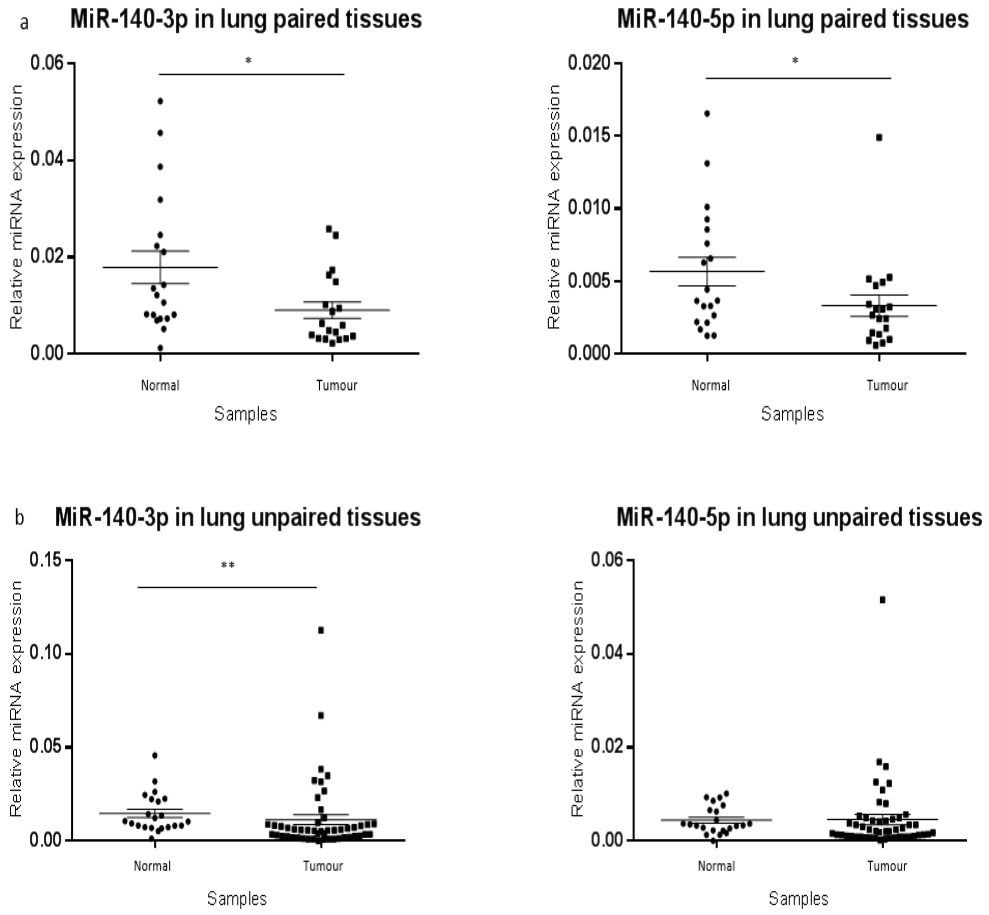

Figure 3.2 MiR-140-3p and 140-5p expression in lung tissues. MiR-140-3p and 140-5p expression in lung tissues was evaluated by miR-specific qRT-PCR. a) In paired tissues (n=19), both miR-140-3p (left) and miR-140-5p (right) was significantly downregulated in lung cancer tissues compared to their normal adjacent counterpart. Data are presented as mean ± SEM, three individual experiments undertaken in triplicate. Wilcoxon-Rank test has been used to assess significance with *$p<0.05$. b) In non-paired tissues (n=49), miR-140-3p (left) was significantly downregulated in lung cancer tissues compared to their normal non-paired counterpart. No significant difference was observed in the unpaired group when analysing miR-140-5p. Data are presented as mean ± SEM, three individual experiments undertaken in triplicate. T-test test has been used to assess significance with **$p<0.01$.

3.3.2 The analysis of the pre-miR-140 sequence shows two DNA variants in SK-MES-1 cell line

In this study, both forms of miR-140 precursor have been investigated, as other studies showed the importance of the strand selection on cancer progression. I found that the sequence of the miR-140 precursor shows variants within both the mature 3p and 5p sequences in SK-MES-1 cells. An A converted to a T in 5p and 2 changes in 3p A to C and A to T. The A to T change from the wild type was also found in the BEAS-2B and A549 cells 3p (Figure 3.3).

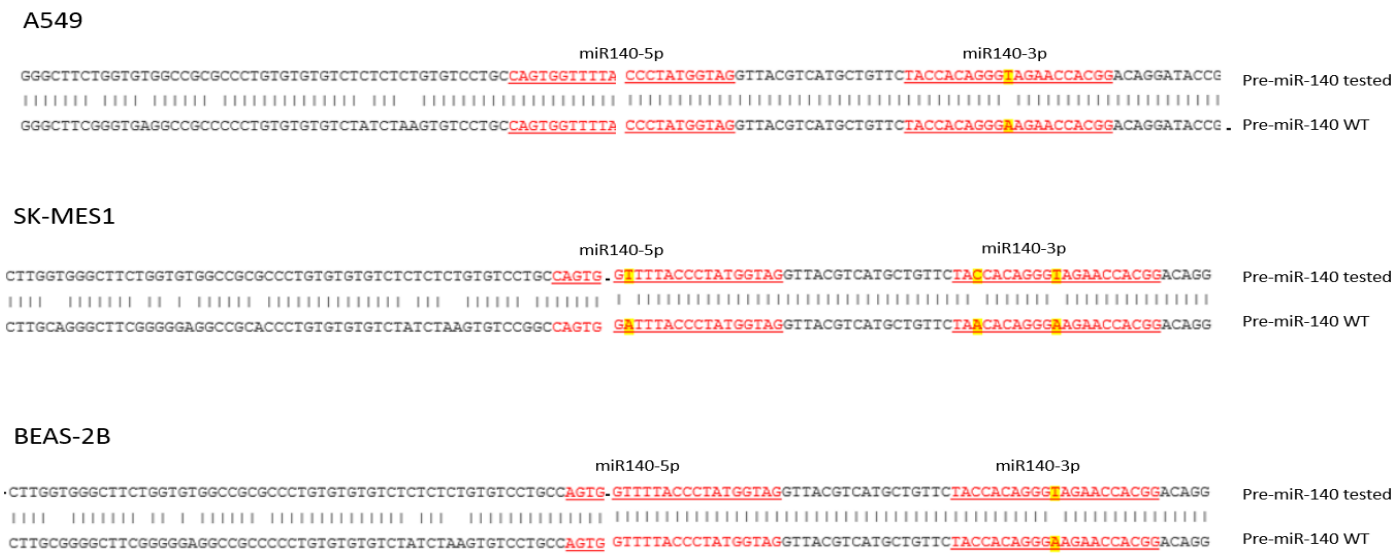

Figure 3.3 Pre-miR- 140 genomic sequencing. The sequences encoding the pre-miR-140 from BEAS-2B, A549 and SK-MES-1 cell lines were isolated, sequenced and finally compared with the wild type sequence. The first row of each alignment includes the sequencing data from the cell lines, whereas the second one represents the wild type sequence, as indicated on the miRBase website (http://www.mirbase.org/). The red letters indicate the regions encoding miR-140-3p and miR-140-5p. The variants are underlined in yellow.

3.3.3 MiR-140-3p and 140-5p mimics increase the levels of the two miRNAs in NSCLC cells

MiR-140-3p and 140-5p mimics were found to increase the levels of the respective miRNAs into NSCLC cell lines A549 and SK-MES-1 (Figures 3.4 and 3.5).

Both cell lines were transfected with miR-140-3p and 5p mimics as described in section 2.17. MiR-140-3p and 140-5p mRNA levels were measured by qPCR and were shown to significantly increase at the two time points considered (24 and 48 hours) in the mimic treatment cells compared to the negative control. However, in both SKMES and A549 cells, MiR-140-3p and 140-5p levels were significantly lower after 48h compared to 24h mimic treatment (Figure 3.4). The fold change of miR-140-3p levels in A549 cells after 24 and 48 hours is 26,508 ($p<0.0001$) and 1737 ($p<0.0001$), respectively (Figure 3.4). The expression of miR-140-3p is significantly different between the two time points considered (Figure 3.4, left), with the highest level after 24 hours of transfection. The fold change of miR-140-5p levels in A549 cells after 24 and 48 hours is 33,129 ($p<0.0001$) and 911 ($p<0.0001$), respectively (Figure 3.4, right). The expression of miR-140-5p is significantly different between the two time points considered (Figure 3.4, right), with the highest level after 24 hours of transfection.

MiR-140-3p and 140-5p levels increase significantly at the two time points considered (24 and 48 hours) in the SK-MES-1 cell line, however they both decrease with the time (Figure 3.5).

The fold change of miR-140-3p levels in SK-MES1 cells after 24 and 48 hours is 4,084 ($p<0.0001$) and 2,757 ($p<0.0001$), respectively (Figure 3.5). The

expression of miR-140-3p is significantly different between the two time points considered (Figure 3.4, left), with the highest level after 24 hours of transfection. The fold change of miR-140-5p levels in SK-MES-1 cells after 24 and 48 hours is 5,650 ($p<0.0001$) and 1,663 ($p<0.0001$), respectively (Figure 3.5, right). The expression of miR-140-5p is significantly different between the two time points considered (Figure 3.5, right), with the highest level after 24 hours of transfection.

In general, the transfection efficiency with miR-140-3p and miR-140-5p mimics is higher in A549 than in SK-MES-1.

.

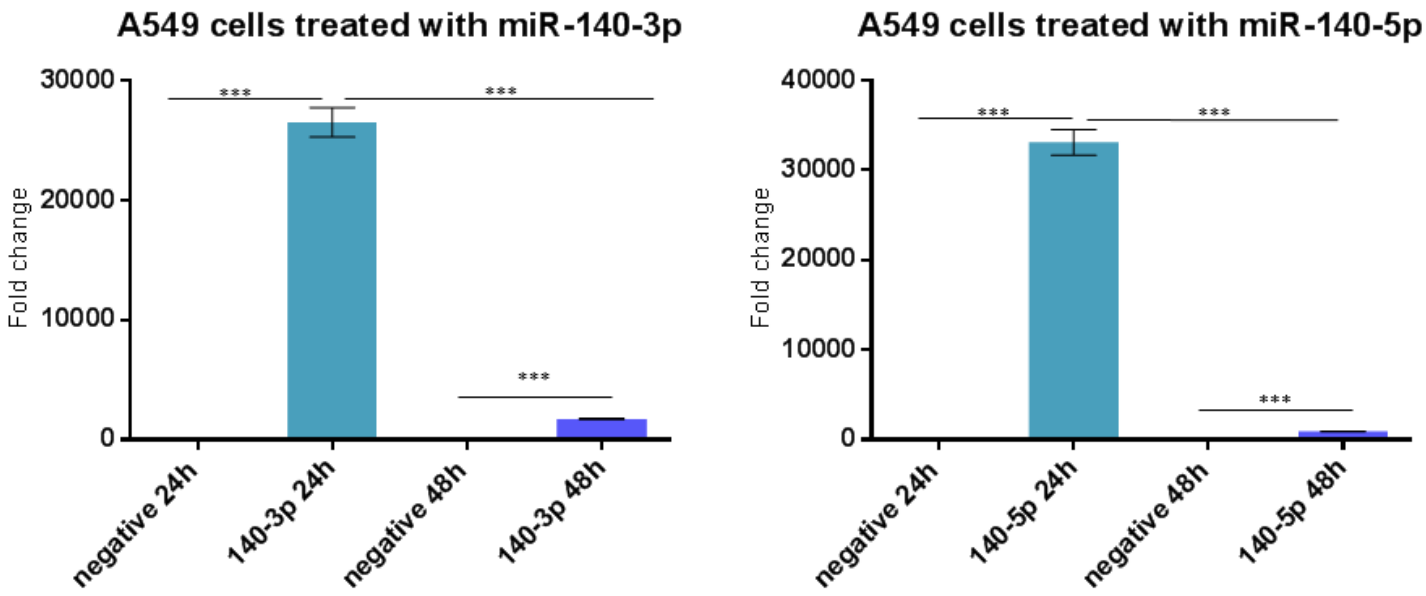

Figure 3.4 MiR-140-3p and 140-5p fold-change in expression levels A549 cells after transfection with miR-140-3p and 140-5p mimics. MiR-140-3p and 140-5p mRNA fold-change (y-axis) in A549 cells was evaluated 24 and 48 hours (x-axis) after transfection with miRNA mimics by using a miR-specific qRT-PCR. Following 24 hours transfection with miRNA mimics, the levels of both miR-140-3p (left) and miR-140-5p (right) are significantly higher than in the control. Following further 24 hours, miR-140-3p and miR-140-5p expression start to reduce but it is still higher than the control. Data are presented as mean $\pm$ SEM, three individual experiments undertaken in triplicate, ANOVA test has been used to assess significance with ***$p<0.001$.

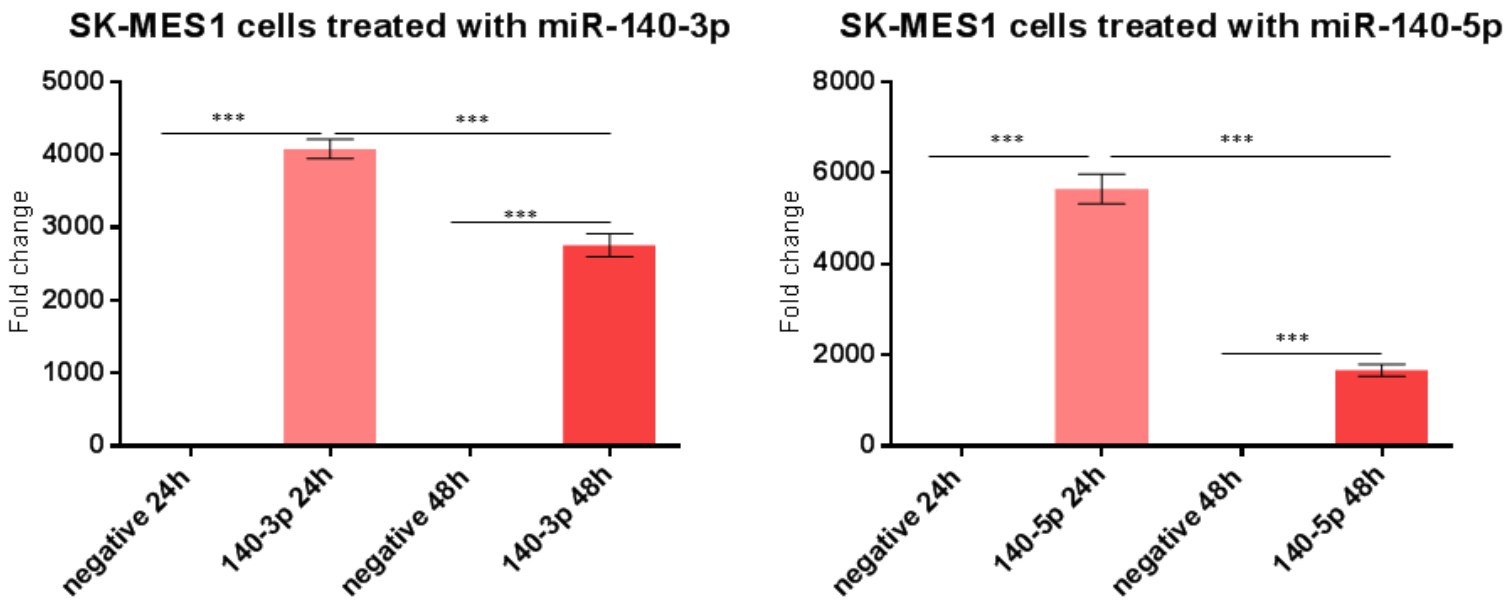

Figure 3.5 MiR-140-3p and 140-5p fold-change in expression levels in SK-MES1 cells after transfection with miR-140-3p and 140-5p mimics. MiR-140-3p and 140-5p fold-change (y-axis) in SK-MES-1 cells was evaluated 24 and 48 hours (x-axis) after transfection with miRNA mimics by using a miR-specific qRT-PCR. Following 24 hours transfection with miRNA mimics, the levels of both miR-140-3p (left) and miR-140-5p (right) are significantly higher than in the control. Following further 24 hours, miR-140-3p and miR-140-5p expression start to reduce but it is still higher than the control. Data are presented as mean $\pm$ SEM, three individual experiments undertaken in triplicate, ANOVA test has been used to assess significance with ***$p<0.001$.

The efficiency of transfection has been evaluated at 24 and 48 hours by pPCR in both A549 and SK-MES-1 cells and the fold changes of miR-140-3p and miR-140-5p have been described in Figure 3.6.

In A549, there is a significant difference in the fold-change between miR-140-3p and miR-140-5p at 24 ($p<0.0001$) but not at 48 hour time point (Figure 3.6 a). At 24hours, miR-140-5p mimics are more efficient than the miR-140-3p mimics, whereas at 48 hours the efficiency is higher in the cells treated with miR-140-3p. As previously acknowledged, the efficiency of transfection decreases over time.

In SK-MES-1, there is a significant difference in the fold-change between miR-140-3p and miR-140-5p at both 24 ($p<0.0001$) and 48 hours time points ($p=0.0034$) (Figure 3.6 b. At 24hours, miR-140-5p mimics are more efficient than the miR-140-3p mimics, whereas at 48 hours the efficiency is higher in the cells treated with miR-140-3p mimics, a similar situation occurs in the A549 cells which additionally, as reported above, shows a decrease in the efficiency of transfection over time.

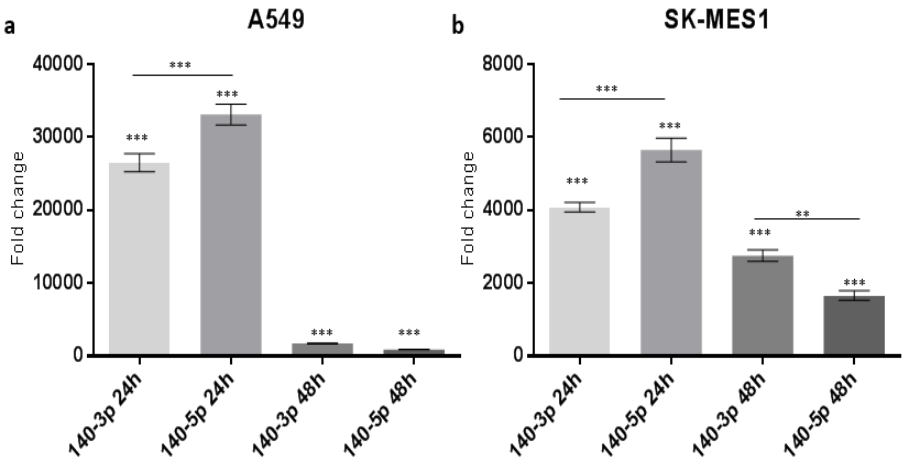

Figure3.6 Fold change of miR-140-3p and 140-5p following transfections with miRNA mimics in A549 and SK-MES-1 cell lines . MiR-140-3p and 140-5p fold-change (y-axis) was evaluated following 24 and 48 hours (x-axis) after transfection with miRNA mimics by using a miR-specific qRT-PCR. a) In A549 cells, following 24 hours transfection, the transfection with miR-140-5p mimics is significantly more efficient than the one with miR-140-3p. No differences have been recorded after a further 24 hours. b) In SK-MES-1 cells, following 24 hours transfection, the transfection with miR-140-5p mimics is significantly more efficient than the one with miR-140-3p. After a further 24 hours, there is a difference between the delivery of the two mimics, with miR-140-3p higher than miR-140-5p. Data are presented as mean $\pm$ SEM, three individual experiments undertaken in triplicate, ANOVA test has been used to assess significance with ***$p<0.001$.

3.4 Discussion

The miR-140 precursor is located on chromosome 16q22.1 and produces two different mature forms named miR-140-3p and miR-140-5p that have multiple targets and are downregulated in several tumours, including NSCLC (Yuan et al., 2013, Dong et al., 2016). Most of miRNAs are downregulated in malignancies, and therapies based on miRNA replacement have been successful in both *in vitro* and *in vivo* models. Nanoparticles have been used in cancer for systemic delivery of miRNA and siRNA without toxicity in several tumour types, including lung (Kota et al., 2009, Xue et al., 2014). In this study, I assessed the effect of the two forms of miR-140 on a NSCLC *in vitro* model .

To better address this, I firstly evaluated miR-140-3p and 140-5p expression in tissues from NSCLC patients and cell lines. I found that both miRNAs are downregulated in lung cancer cell lines, compared to the immortalised non-cancerous control BEAS-2B. I decided to use BEAS-2B as a control because, even though it has been virally transformed, it was the only normal lung epithelial cell line available and one of most widely used, according to the literature (Yang et al., 2016, Guerriero et al., 2016). To check whether my *in vitro* model reflected the *in vivo* state of cancer, I investigated the expression of miR-140-3p and 140-5p in lung cancer tissues and verified that both miRNAs have a lower expression in cancer tissues than in non-tumour adjacent sections, significantly so in paired samples.

I also studied whether the strand selection process might differ between normal and cancer cells as any modification in the miRNA strand selection process may represent one of the mechanisms used by a tumour for its survival and spread. The two forms of the same miRNA are associated with different sets of target

genes, and a difference in the expression of the two forms may result in a loss of regulation in favour of the malignant state, as hypothesised for miR-483 in hepatoblastoma and breast cancer (Salvatore et al., 2016, Tsai et al., 2016). Moreover, the strand selection of pre-miR-140 has been widely investigated in embryonic development, as an alteration of the expression of the two mature forms contributes to many congenital malformations (Li et al., 2010, Rakoczy et al., 2013). To address that, I sequenced the genomic region of the pre-miR-140 to assess the presence of Single Nucleotide Polymorphisms or variants within the regions encoding the two miR-140 sister strands. SK-MES-1 shows two variants in both miR-140-3p and miR-140-5p sister strands. Although this change does not affect the strand selection, as miR-140-3p remains the predominant form, I speculated that this might affect the biogenesis of both the strands because the expression of both miR-140-3p and miR-140-5p is lower in SK-MES-1 than in A549 and this may influence the efficiency of the transfection of miR-140-3p and miR-140-5p mimics.

I then evaluated the ratio of the intracellular miR-140-3p and 140-5p and found that it was close to 1 for BEAS-2B and higher in A549 and SK-MES-1 lung cancer cells. This evidence supports the hypothesis of no strand selection in BEAS-2B. On the contrary, a ratio higher than 1 in cancer cells, suggests that the predominant form in my NSCLC model is miR-140-3p. This evidence supports the hypothesis that the strand selection exists predominantly in lung cancer cells instead of normal cells. This implies that miR-140-3p may act as a guide strand, while as miR-140-5p is a passenger in the malignant cells.

Finally, I verified that miRNA mimics can be delivered into lung cells with high efficiency up to 48 hours after transfection using a lipid-based technique (e.g.

DharmaFECT1 Transfection). However, the delivery of miR-140-3p and miR-140-5p mimics differs between the two cell lines. In both the cell lines, following 24 hours of transfection, miR-140-5p is delivered more efficiently than miR-140-3p. The overall efficiency of transfection, however, is higher in A549 and this may be because of the variants that are present in pre-miR-140 in SK-MES-1 cells. As I expected, as this was a transient transfection, the levels of the two miRNAs decreased with time. Interestingly, miR-140-3p levels decreased more slowly than the levels of miR-140-5p, thus suggesting that miR-140-3p is more stable. This confirms the hypothesis that a strand selection probably occurs in cancer cells and that miR-140-3p is the guide strand.

At this stage, I decided to restore the levels of miR-140-3p and 140-5p by using specific miRNA mimicking wild type in both the lung cancer cell lines and evaluate this effect on cancer cell behaviour. The results will be discussed in the next chapter.

CHAPTER 4

EFFECT OF MIR-140-3P AND MIR-140-5P MIMICS ON LUNG CANCER CELL BEHAVIOUR

4.1 Introduction

Malignant cells acquire many of characteristics that enable their growth and spread, such as the ability to proliferate indefinitely, to migrate and invade new tissues, to modify their own metabolism and the tumour microenvironment (Hanahan and Weinberg, 2011). The down-regulation of either miR-140-3p or 140-5p enhances the invasion properties of cancer cells in many tumours (Zhai et al., 2015, Liu et al., 2016b, Dong et al., 2016, Li et al., 2014b) and to better evaluate their possible role as therapeutic agents, I investigated the effect of both miR-140-3p and 140-5p on different aspects of NSCLC cell behaviour *in vitro* by using both A549 and SK-MES-1 cell lines. Considering that a single miRNA targets hundreds of mRNAs, this approach also helped in focusing on the multiple pathways that can be influenced by these treatments.

Although other studies have already suggested the role of miR140-3p and 140-5p as oncosuppressors in lung cancer (Yuan et al., 2013, Dong et al., 2016), most of the researchers focus was on a single step of the malignancy process and looked for one or two targets, rather than considering the global effect of the treatment on cancer cell behaviour. For this reason, in this study, the two lung cancer cell lines A549 and SK-MES-1 were transfected with miR-140-3p and 140-5p mimics and the effect on several aspects of the cancer cell response to the treatment, such as proliferation, apoptosis, cell cycle, migration, invasion and adhesion to the components of the extracellular matrix, have been investigated.

I strongly believe that this approach is extremely important for the development of new miRNA therapeutics, specific for the treatment of NSCLC patients.

In this chapter, I investigated *in vitro* the effect of miR-140-3p and miR-140-5p replacement treatment on the following aspects of the NSCLC cell behaviour: proliferation, apoptosis, cell cycle, migration, invasion and adhesion onto collagen and laminin, two of the main components of the Extracellular matrix (ECM).

4.2 Materials and methods

Proliferation assay

A549 and SK-MES-1 (5×10^3cells/well) cells were seeded onto 96-well plates in 100µl growth medium. Following 24 and 48 hours of miRNA treatment, the cells were fixed and analysed for a proliferation assay as described in section 2.21.1.

Transwell migration and invasion assays

Cells were detached using HYQTase Cell Detachment Solution (Hyclone, Logan, UT, USA) 24 hours after being transfected and resuspended in serum-free medium, at a concentration of $1x10^5$ cells/ml and 650µl of medium containing 10% FBS (chemoattractant) was added to receiver wells in triplicate and 650µl of serum-free medium (no chemoattractant) to receiver control wells. The polycarbonate 8µm pore size ThinCert™ 24-well plate inserts (Grenier, Bio-One GmbH, Austria) were placed in each of the receiver wells and 500 µl of cell suspension added. Invasion assay chambers were coated with 100µl of Matrigel (BD Biosciences, NJ, USA) diluted in serum-free media at 500 µg/ml and allowed to dehydrate for 2 hours at 55°C. After 2 hours, the cells were seeded as described for a migration assay.

Cell migration and invasion were assessed after 24h as described in section 2.21.2.

Adhesion assay

A total of 10^4 transfected cells/well were added into a 96 well plate coated with 50μg/well of laminin or collagen, two of the three main components of the basal membrane. A549 and SK-MES-1 were allowed to attach at 37°C for 40 and 60 minutes, the attached cells were washed, fixed and analysed as described in section 2.21.4

Apoptosis and cell cycle assay

Cancer cells were treated with miRNA mimics and then the apoptosis and cell cycle assays were carried out after 24 and 48 hours of treatment using the Annexin V kit (Santa Cruz Biotechnology, Surrey, UK) as described in Section 2.15. This kit includes fluorescent conjugated annexin V (FITC annexin V) and propidium iodide (PI) solution. For cell cycle assay, cells were harvested, washed with PBS, resuspended in 75% v/v ethanol and then 150 μl of 2 μg/ml PI (Thermo Fisher Scientific, Waltham, MA USA) was added to each of the samples. Flow cytometry analysis was performed for apoptosis and cell cycle assays on a FACS Canto II (BD Biosciences, NJ USA) and data analysed using FCS Express 4 Flow Research Edition (De Novo Software, California, USA).

Statistical analysis

Statistical analysis was performed as described in Section 2.24.

4.3 Results

4.3.1 MiR-1403p and miR-140-5p do not affect the proliferation of NSCLC cells

The ability of cancer cells to proliferate in response to miR-140-3p and miR-140-5p treatment has been investigated by considering two time points (24 and 48 hours) after the transfection with the miRNA mimics (Figure 4.1). No significant differences were observed in the proliferation of all the cancer cells treated with miR-140-3p and miR-140-5p mimics and the cells treated with the control at both the time points considered. Although not statistically significant, miR-140-3p appears to mildly reduce the number of A549 cells at 24 and 48 hours (Figure 4.1 a and b), whereas the number of the cells transfected with miR-140-5p is higher than in the control after 48hours (Figure 4.1b). In the SK-MES-1 cells, the two miRNA mimics look to slightly increase the proliferation of the cancer cells compared to the control at 24 (Figure 4.1c) and 48 hours (Figure 4.1d) but this data has no any statistical significance.

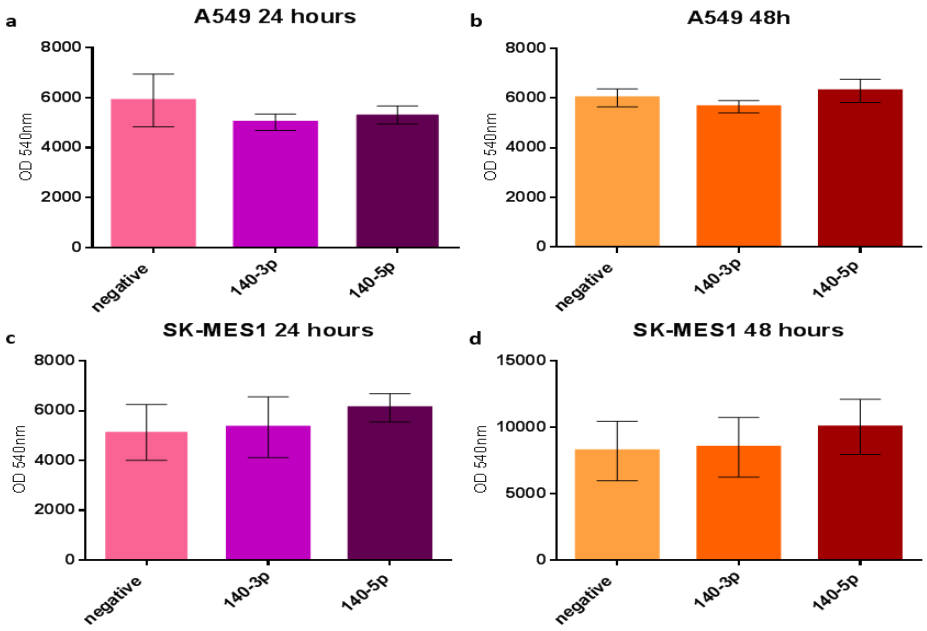

Figure 4.1 Proliferation ability of A549 and SK-MES1 lung cancer cells following 24 and 48 hours of miRNA mimics treatment. The ability of A549 and SK-MES-1 to proliferate following the treatment with miR-140-3p and miR-140-5p mimics has been evaluated by staining the cells with crystal violet 24 and 48 hours after the transfection with the mimics. No significant differences have been seen at the two time points in both A549 (a and b) and SK-MES-1 (c and d). Data are presented as mean of the optical density at 540nm (OD) ±SEM, three individual experiments undertaken in six replicates, Kruskal-Wallis -test has been used to assess significance.

4.3.2 MiR-1403p and miR-140-5p have a small effect on apoptosis of NSCLC cells

Since miR-140-3p and miR-140-5p have no significant effect on the proliferation of A549 and SK-MES-1 cells, I checked whether this might be because the cells undergo apoptosis. To address that, I performed an apoptosis analysis on our lung cancer cells by studying the cells following 48 hours treatment with mimics. I did not show the effect of mimics after 24 hours because there was no difference at all between the control and treated cells (data not shown).

My data show that A549 cells show a small increase in apoptosis following miR-140-5p mimic treatment for 48 hours (Figure 4.2 a, b), whereas in SK-MES-1, both the miR-140-3p and miR-140-5p treatments had a minimal increase in apoptosis at the early and late stage (Figure 4.3 a, b).

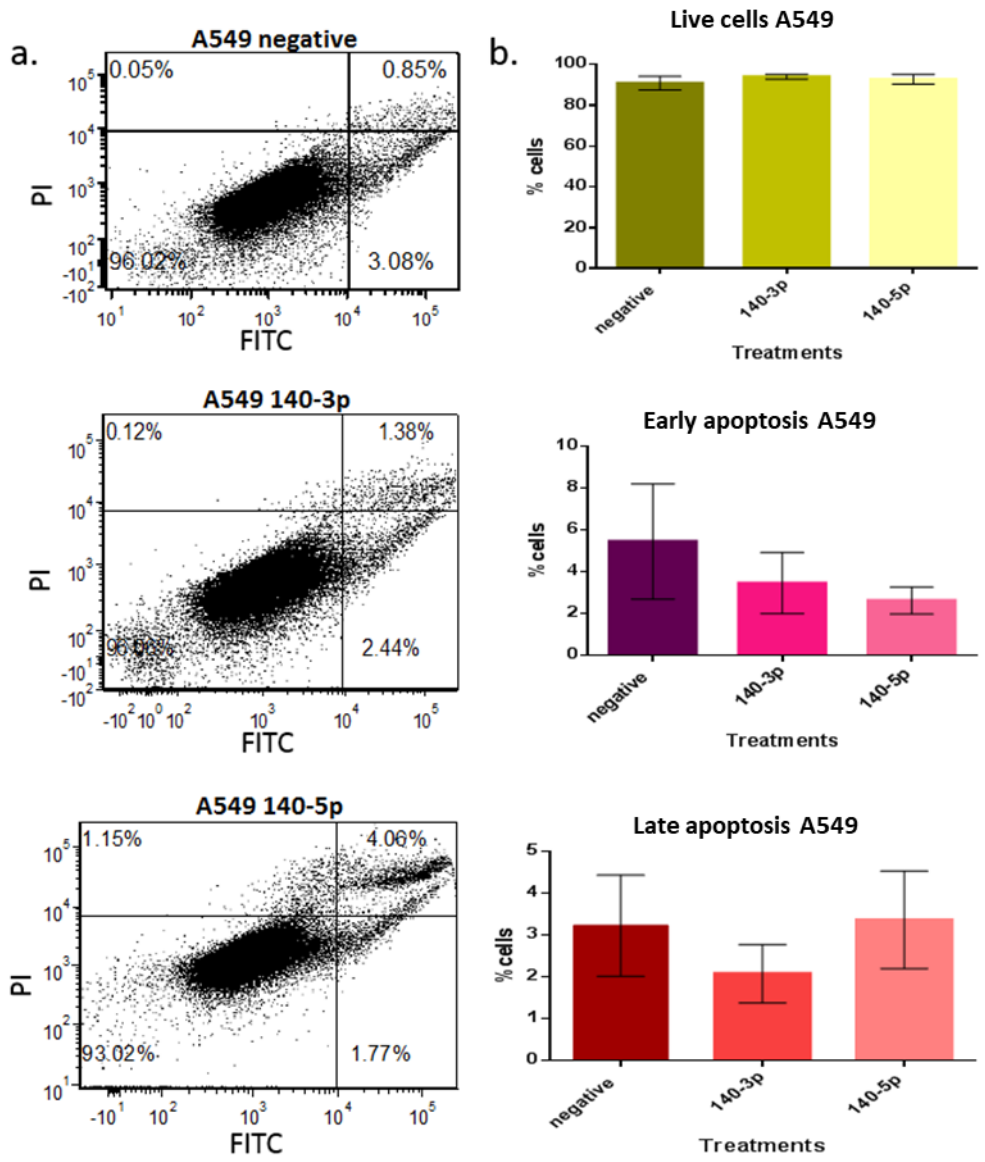

Figure 4.2. Early and late apoptosis of A549 lung cancer cells treated with miR-140-3p and miR-140-5p mimics. a) Percentage of live (bottom left), early apoptotic (bottom right) or late apoptotic (top right) A549 following 48 hours of treatment with negative, 140-3p or 140-5p miRNA mimics (representative data). b) Percentage of A549 cells in each stage (live, early and late apoptosis) at 48 hours of transfection. Graphs show % cells ± SEM, n=3)

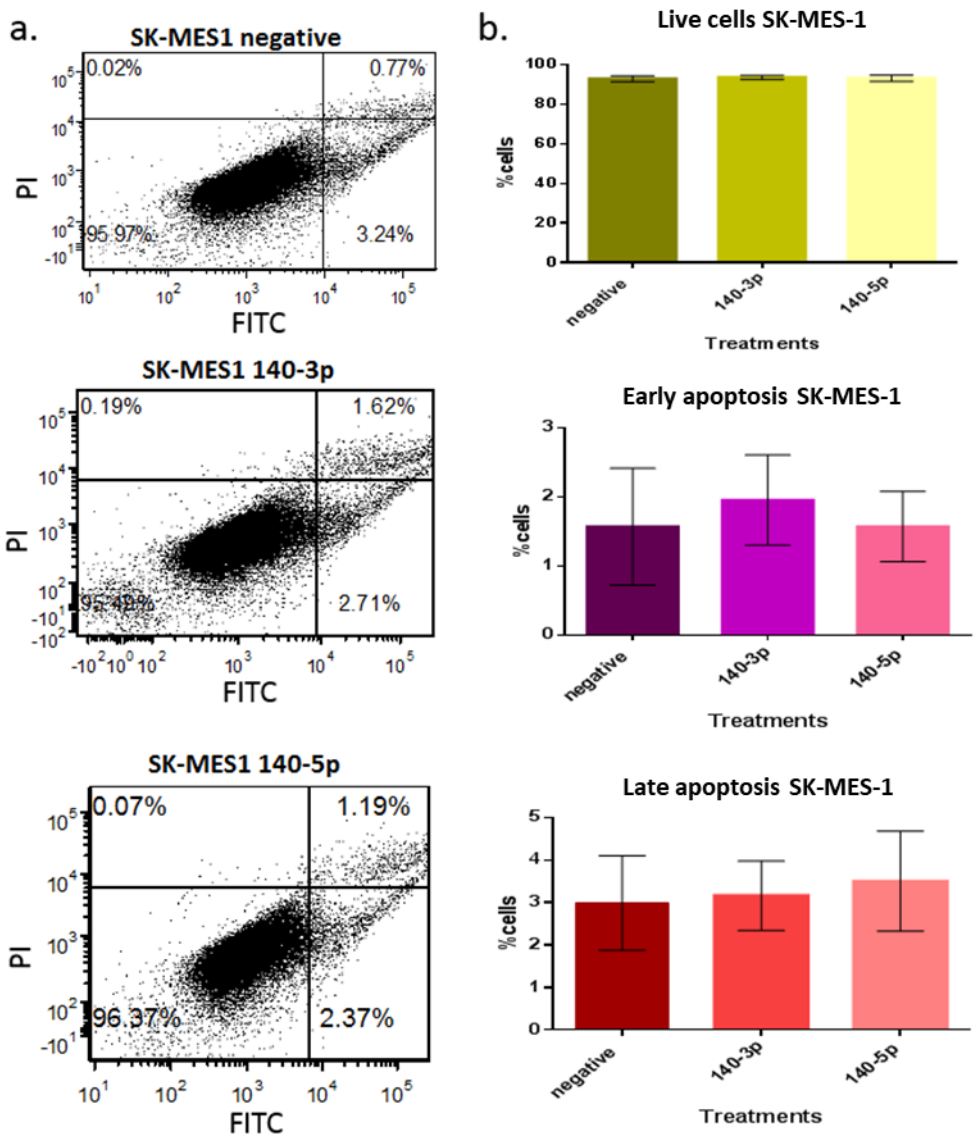

Figure 4.3. Early and late apoptosis of SK-MES-1 lung cancer cells treated with miR-140-3p and miR-140-5p mimics. a) Percentage of live (bottom left), early apoptotic (bottom right) or late apoptotic (top right) SK-MES-1 following 48 hours of treatment with negative, 140-3p or 140-5p miRNA mimics (representative data). b) Percentage of SK-MES-1 cells in each stage (live, early and late apoptosis) at 48 hours of transfection. Graphs show % cells ± SEM, n=3).

4.3.3 MiR-140-3p and miR-140-5p have no effect on NSCLC cell cycle

We then hypothesised that the treatment with miR-140-3p and miR-140-5p might have some effect on the cell cycle progression, as no significant difference in proliferation and apoptosis have been seen. To verify our hypothesis, the effect of miRNA mimic treatment in the lung cancer cell lines A549 and SK-MES-1 has been evaluated through flow cytometry analysis by investigating changes in the cell cycle 48 hours after transfections. We did not show the effect of mimics after 24 hours treatment because there was no difference at all between the control and treated cells (data not shown).

We found that, following 48 hours of transfection with miR-140-3p and miR-140-5p mimics, there are no variations in the percentage of cells in G1 S and G2-M phase in both A549 and SK-MES-1 cell lines (Figure 4.4, representative).

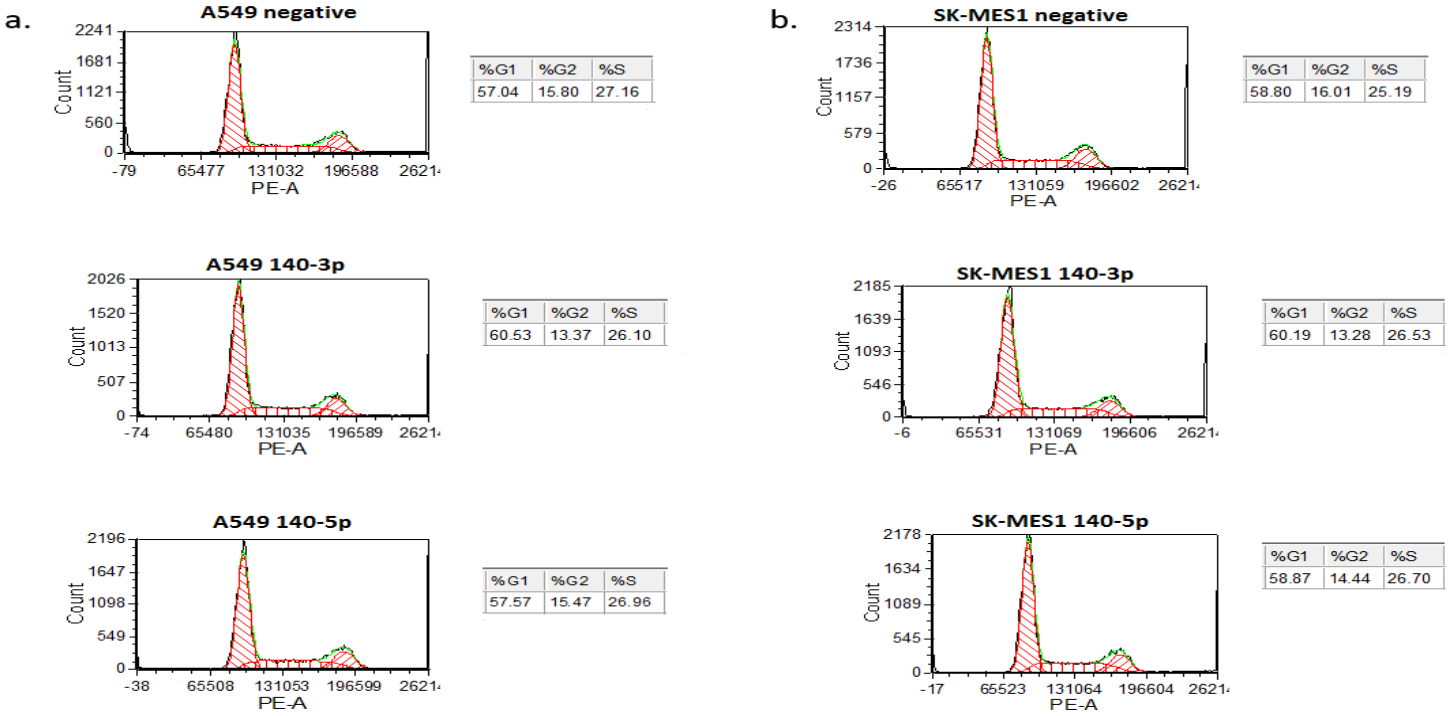

Figure 4.4. The effect of 48hours of miR-140-3p and miR-140-5p treatment on A549 and SK-MES1 cell cycle. Graphs show the percentage of cells in each stage of the cell cycle, gap1 (G1), gap2 (G2) and DNA synthesis (S) following 48 hours treatment with negative, miR-140-3p and miR-140-5p mimics. Graphs show a representative result of three independent experiments made using A549 (a) and SK-MES-1 (b) lung cancer cell lines.

4.3.4 MiR- 140-5p reduces the migration capability of SK-MES1 and both miR-140-3p and 140-5p limit invasion ability of NSCLC cells

Twenty-four hours after transfection with miRNA mimics, A549 and SK-MES-1 cells were detached and incubated for a further 24 hours on non-coated inserts (8µm pore membrane) in order to mimic the movement of cells towards a chemotactic factor, FBS. The aim was to reproduce the *in vivo* migration of cells from the primary tumour site into the bloodstream. MiR-140-5p mimic is able to decrease significantly the migration ability of SK-MES-1 after 48 hours of transfection ($p=0.0285$), whereas no significant effect was observed in A549 and in SK-MES-1 cells treated with miR-140-3p mimics (Figure 4.5)

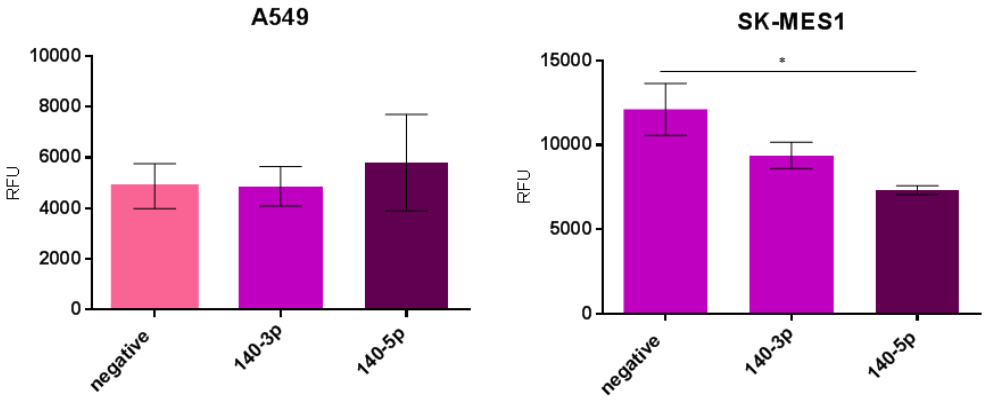

Figure 4.5 Migration ability of A549 and SK-MES1 lung cancer cells following 24 and 48 hours of miRNA mimics treatment. The migration ability of A549 and SK-MES-1 cells following the transfection with miR-140-3p and miR-140-5p mimics has been evaluated by using non-coated inserts containing the cells with FBS as a chemoattractant in the lower chamber. The treatments do not affect the migration properties of A549 (on the left), whereas miR-140-5p mimics reduce the migration of SK-MES-1 (on the right) significantly. Data are presented as mean of the relative fluorescence (RFU) $\pm$ SEM, three individual experiments were undertaken in triplicate, ANOVA-test has been used to assess significance with $*p<0.05$.

The invasive ability of NSCLC cells was reproduced in the same way as the migration assay, with the transwell inserts coated with Matrigel, to mimic the ECM. A549 invasive capability decreases significantly when the cells are treated with miR-140-3p ($p<0.001$) and 140-5p ($p=0.0036$) mimics (Figure 4.6). There is also a significant difference between the two treatments, as miR-140-3p has a greater inhibitory effect than miR-140-5p ($p=0.0067$). A similar result has been observed in SK-MES-1 cells, with a significant reduction of their invasion when treated with both the miR-140-3p ($p<0.001$) and 140-5p mimics ($p<0.001$) (Figure 4.6).

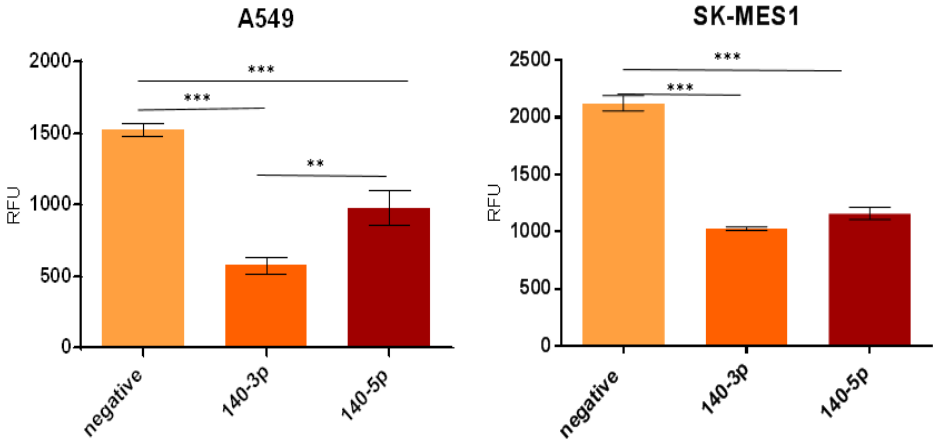

Figure 4.6 Invasive ability of A549 and SK-MES-1 lung cancer cells following 24 and 48 hours of miRNA mimics treatment. The invasion ability of A549 and SK-MES1 cells following the transfection with miR-140-3p and miR-140-5p mimics has been evaluated by using Matrigel-coated inserts containing the cells and complete medium below. Both miR-140-3p and miR-140-5p treatments reduce the invasion of A549 (on the left) and SK-MES-1 (on the right) significantly. MiR-140-3p, in particular, exerts a higher inhibition than miR-140-5p in both the cell lines. Data are presented as mean of the relative fluorescence (RFU) $\pm$ SEM, three individual experiments were undertaken in triplicate, ANOVA-test has been used to assess significance with *$p<0.05$, **$p<0.01$, ***$p<0.001$.

4.3.5. miR-140-3p and miR-140-5p enhances the adhesion ability of A549 cells

The adhesion ability of A549 and SK-MES-1 NSCLC cells was assessed by seeding the cells transfected with miRNA mimics into wells coated with laminin and collagen IV, two of the three main components of the basal membrane. Following 40 and 60 minutes of time for A549 and SK-MES-1 respectively to adhere, the number of cancer cells were assessed using a fluorescent plate reader.

The adherence of A549 to laminin and collagen increases after 24 hours of transfection with miR-140-3p and miR-140-5p mimics (Figures 4.7 and 4.8). In A549 following 24 hours of transfection, both miR-140-3p ($p=0.0006$) and 140-5p ($p=0.0137$) improve the adhesion properties of the cells on surface coated with laminin (Figure 4.7), whereas only miR-140-5p ($p=0.0084$) has a significant effect on the adhesion of cells to collagen IV (Figure 4.7). After transfection for 48 hours, miR-140-3p starts to have a significant effect on A549 cells seeded onto collagen IV ($p=0.0006$) (Figure 4.8). MiR-140-3p or miR-140-5p treatment has no effect on the adherence of SK-MES-1 at the two time points considered (Figures 4.9, 4.10).

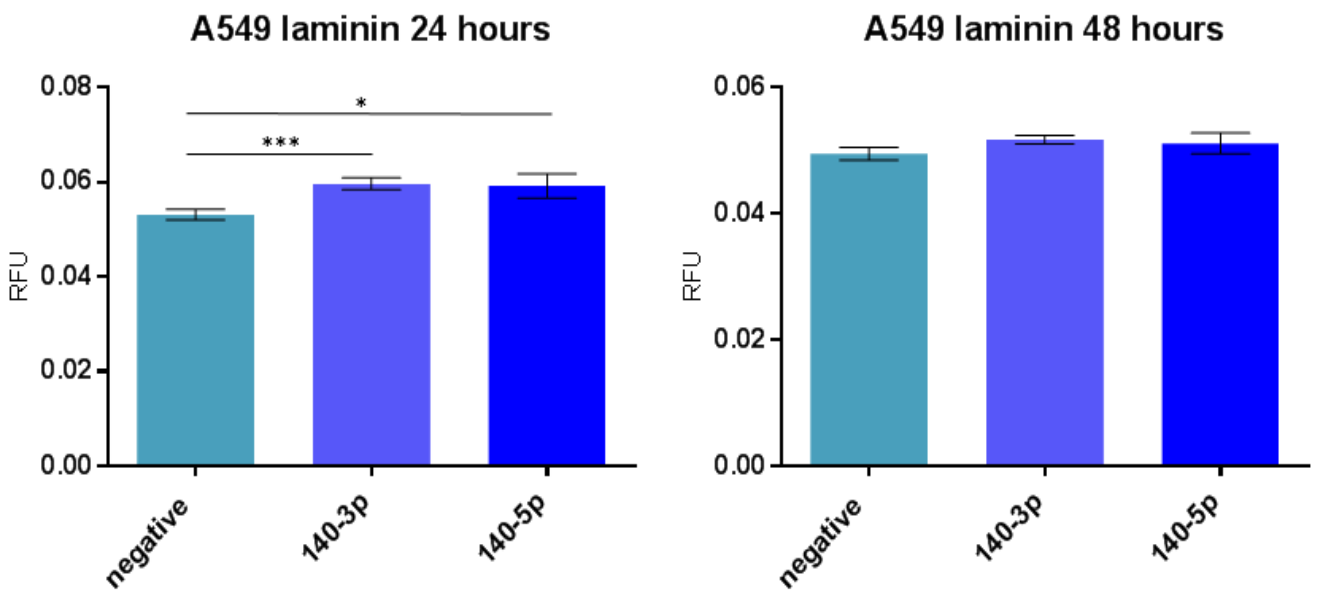

Figure 4.7 Adhesion ability of A549 cells seeded onto laminin following 24 (left) and 48 hours (right) transfection with miR-140-3p and 140-5p mimics. 24 hours after transfection, both miR-140-3p and miR-140-5p increase the ability of A549 to adhere to laminin (left), whereas no effect has been after cells were transfected for 48 hours (right). . Data are presented as mean of the relative fluorescence (RFU) $\pm$ SEM, three individual experiments were undertaken in triplicate, ANOVA-test has been used to assess significance with *$p<0.05$,***$p<0.001$.

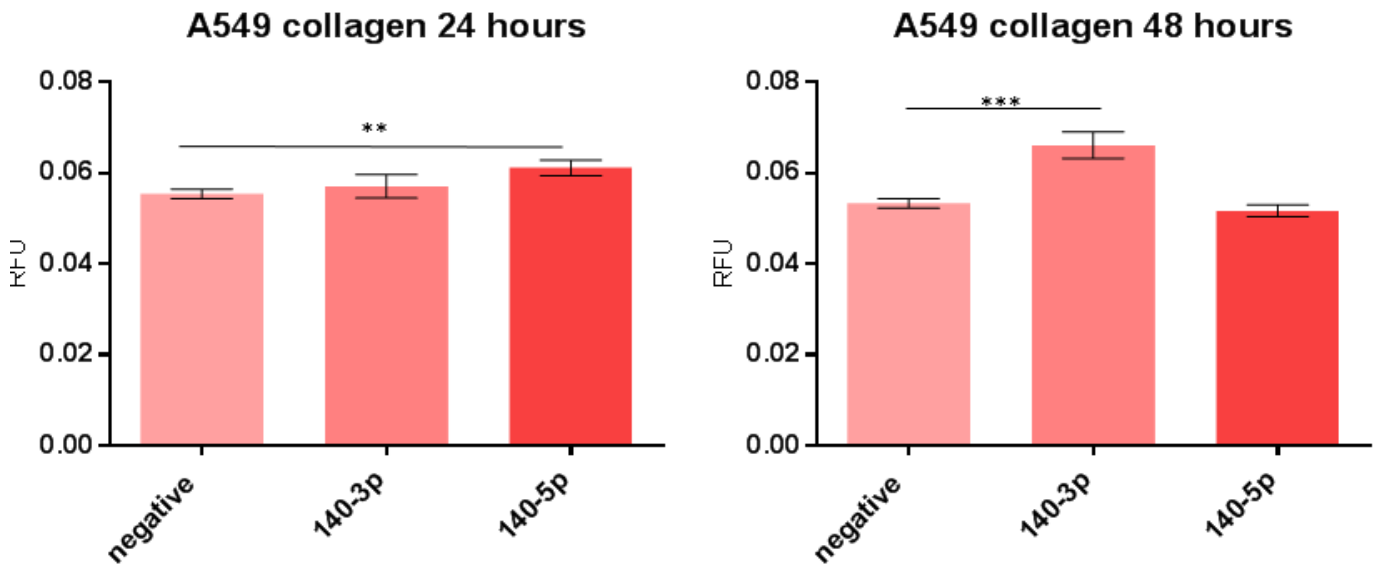

Figure 4.8 Adhesion ability of A549 cells seeded on collagen IV following 24 (left) and 48 hours (right) transfection with miR-140-3p and 140-5p mimics. 24 hours after transfection, miR-140-5p increases ability of A549 to adhere to collagen IV (left), and miR-140-3p enhances the adhesion 48 hours after trasnfection (right). Data are presented as mean of the relative fluorescence (RFU) ± SEM, three individual experiments were undertaken in triplicate, ANOVA-test has been used to assess significance with **p<0.01,***p<0.001

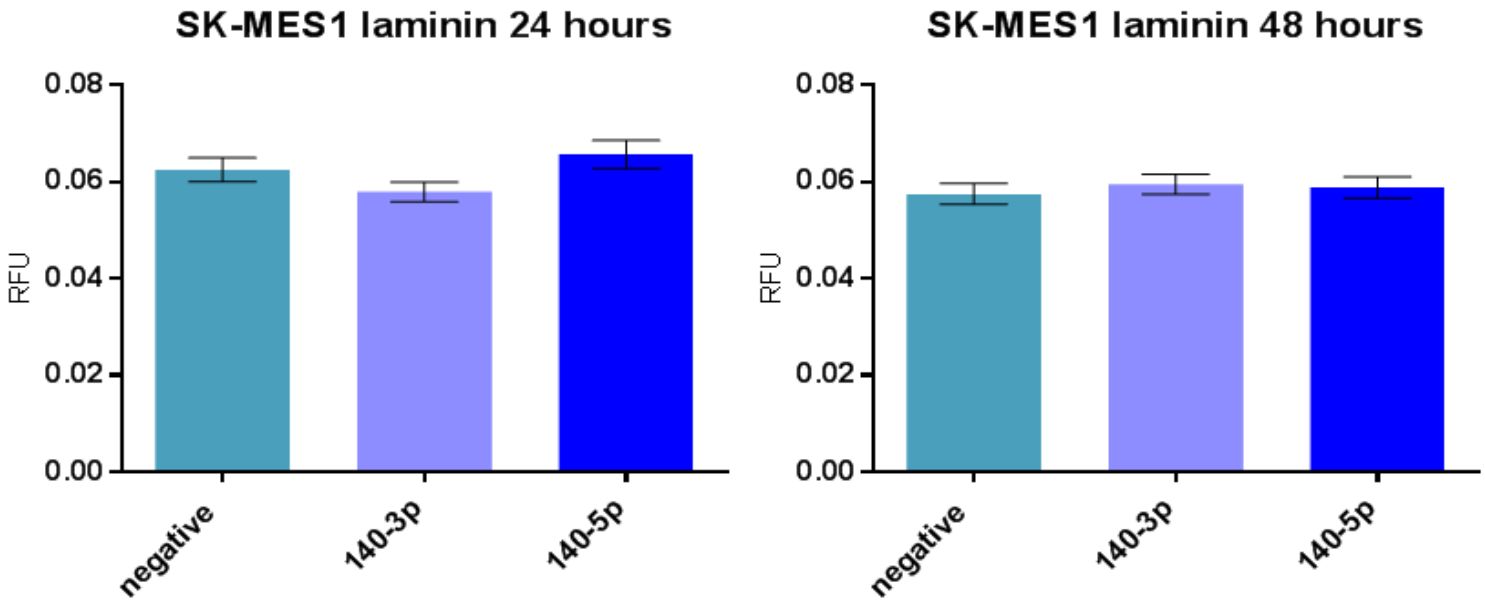

Figure 4.9 Adhesion ability of SK-MES-1 cells seeded on laminin following 24 (left) and 48 hours (right) transfection with miR-140-3p and 140-5p mimics. The treatment with miR-140-3p and miR-140-5p mimics has no effect on the adhesion properties of the cancer cells. Data are presented as mean of the relative fluorescence (RFU) ± SEM, three individual experiments were undertaken in triplicate, ANOVA-test has been used to assess significance.

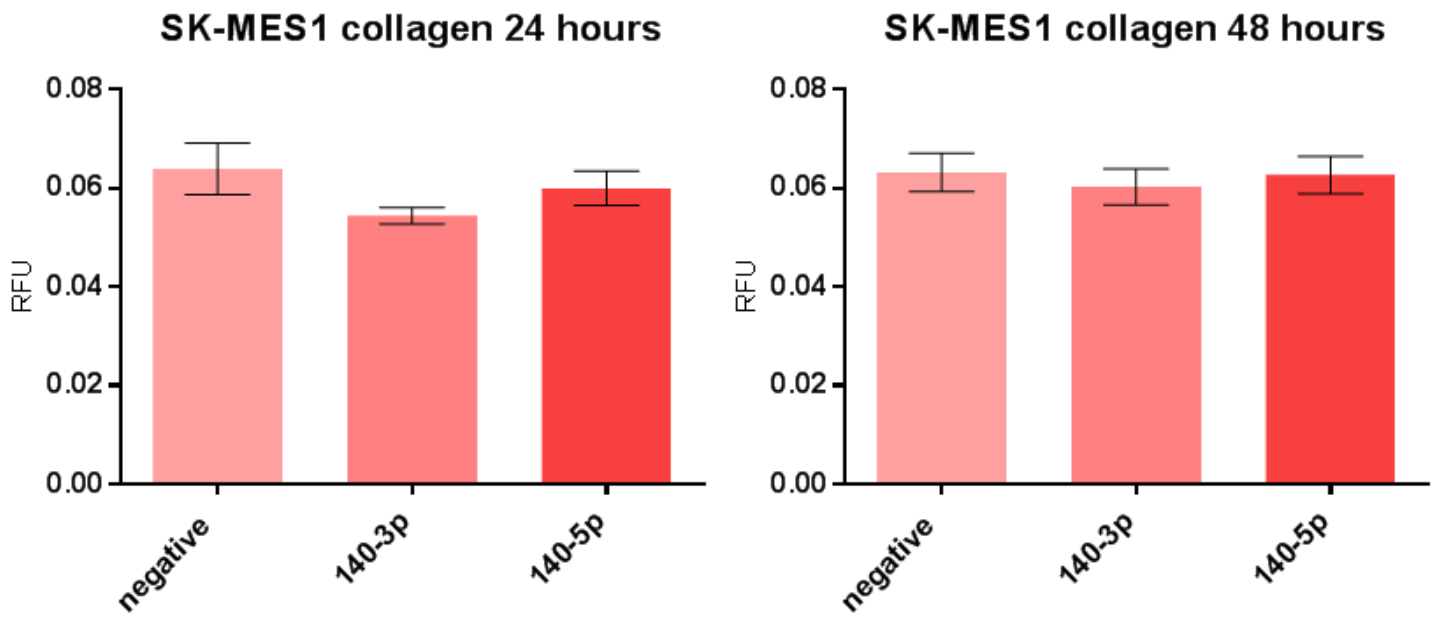

Figure 4.10 Adhesion ability of SK-MES-1 cells seeded on collagenIV following 24 (left) and 48 hours (right) transfection with miR-140-3p and 140-5p mimics. The treatment with miR-140-3p and miR-140-5p mimics has no effect on the adhesion properties of the cancer cells. Data are presented as mean of the relative fluorescence (RFU) ± SEM, three individual experiments were undertaken in triplicate, ANOVA-test has been used to assess significance.

4.4 Discussion

One miRNA can target hundreds of mRNAs and thus may influence many aspects of cell behaviour (Bartel, 2009). However, the effect of a miRNA on a specific pathway may be abolished by other upstream or downstream effectors involved in that molecular network. For this reason, in this study the overall physiological effect of the two sister strands of the miR-140 has been evaluated *in vitro*, before searching for the direct and indirect targets of the two miRNAs.

Many aspects of the cell behaviour have been investigated, such as the ability of the NSCLC cells to proliferate indefinitely, evade cell death, migrate and invade new tissues. In the next chapters, the capability of the cancer cells to modify their own cellular energetics and to influence the tumour microenvironment will be also studied.

The first step in the oncogenesis is the uncontrolled proliferation of the cancer cells. This may be controlled by the reduced expression of miR-140 often seen in cancer cells compared to "normal" cells. These abnormalities, together with the chronic activation of growth factors, make the cells able to potentially proliferate forever (Hanahan and Weinberg, 2011). My experiments aimed to increased mIR-140 expression in the cancer cells, to mimic the higher expression often seen in normal cells. In this study, I did not find any statistically significant difference in the proliferation of NSCLC cells treated with miR-140-3p and miR-140-5p mimics.

I then investigated whether the apoptosis and cell cycle were affected by the increased expression of miR-140-3p and miR-140-5p to better confirm the data from the proliferation assay. In fact, the proliferation of cancer cells may result

in the treatment having not effect on proliferation because the cells undergo apoptosis or because the cell cycle has been stopped. My results also show no significant difference either in cell cycle or apoptosis of A549 and SK-MES-1 cells, thus leading to the conclusion that the growth and proliferation of the cancer cell lines were not affected by the treatment with miR-140-3p and miR-140-5p mimics *in vitro*.

Cancer, in general, is a multi-step process and, apart from the ability to proliferate indefinitely, malignant cells acquire many other characteristics that enable them to survive, migrate and invade new tissues to form colonies at distant sites (Hanahan and Weinberg, 2011). To spread to other tissues, the cells lose their adhesion to the ECM, change their epithelial morphology and become mesenchymal-like cells. This is named epithelial-mesenchymal transition (EMT) (Heerboth et al., 2015). Through specific functional assays, I investigated whether the re-establishment of the "normal/non-cancerous" miR-140-3p and miR-140-5p levels might have any effect on the motility and the invasive capability of the NSCLC cells.

The ECM is formed by proteoglycans (heparin sulphate, ketaran sulphate, chondroitin sulphate), collagen, fibronectin and laminin. Both miR-140-3p and miR-140-5p increase significantly the adhesion properties of the A549 cells on laminin and collagen, two of the main components of the extracellular matrix. This effect is stronger following 24 hours of transfection, when the miRNA in the cells are at their highest levels, thus suggesting their possible role as regulators of the cell adhesion. No significant differences have been recorded in the adhesion properties of the SK-MES-1 cells following the treatment with miR-140-3p and miR-140-5p mimics. I speculated that this because the SK-

MES-1 has no WT sequence of the two miRNAs. Another hypothesis could be that the adhesion of NSCLC cells is affected when the levels of the two miRNAs are above an unspecified threshold, as the efficiency of transfection in A549 is higher than in SK-MES-1.

The motility of NSCLC can be significantly impaired by the miRNA replacement treatment. Both miR-140-3p and miR-140-5p mimics reduce significantly the invasion property of A549 and SK-MES1 cells. This finding supports that previously reported by different groups who have demonstrated the involvement of both miRNAs in the lung cancer (Yuan et al., 2013, Dong et al., 2016).

All these results taken together suggest that the miR-140-3p and miR-140-5p replacement treatment may be of use to reduce the invasion and spread of limit the invasion of the NSCLC.

To better understand which aspect of the cancer cell behaviour is influenced by the treatment with miR-140-3p and miR-140-5p mimics, in the following chapters I will evaluate their effect on the cancer cell metabolism and their interaction with other cells in the environment; specifically, their effect on the ability of endothelial cells to form tubules, as occurs in angiogenesis.

CHAPTER 5

EFFECT OF MIR-140-3p AND MIR-140-5p ON THE ABILITY OF ENDOTHELIAL CELLS TO FORM TUBULES

5.1 Introduction

In this study, I attempted to evaluate the effect of the miR-140-3p and miR-140-5p mimics on the tumour microenvironment. During tumour progression there is a repurposing of both the cancer cells and the surrounding stromal cells (Hanahan and Weinberg, 2011). Stromal cells include fibroblasts, immune-system cells and endothelial cells. For this purpose and considering the intrinsic limitations of my *in vitro* model, I focused just on the ability of the endothelial cells, HUVECs, to form new vessels in response to the treatment of the cancer cells with miR-140-3p and miR-140-5p mimics

Primary endothelial cells HUVECs were grown on a layer of Matrigel, a compound that mimics the ECM, in growth medium composed of 60% of EGM-2 and 40% conditioned medium from A549 and SK-MES-1 cells that had been transfected with miR-140-3p and miR-140-5p. Endothelial tubule formation was evaluated in Real-Time by using the cell imaging system EVOS. This concentration of tumour conditioned media added has been chosen because I observed that a higher amount is toxic for HUVEC growth.

It is known that the Vascular Endothelial Growth Factor-A (VEGF-A), a key factor involved in angiogenesis, is one of the direct targets of miR-140-5p, (Zhang et al., 2015, Sun et al., 2016), VEGF-A content was quantified by ELISA in the conditioned media of A549 and SK-MES-1 cells treated with miR-140-3p and miR-140-5p mimics.

5.2 Materials and Methods

Tubule formation assay

The primary endothelial cells HUVECs were diluted to $1.4x10^5$ cells/ml and the assay was performed and data analysed as described in Section 2.21.3.

ELISA

Following 24 and 48 hours of negative control, or miR-140-3p and miR-140-5p mimic treatment the conditioned medium was removed from the cells and centrifuged at 1700 xg for 10 minutes to remove cellular debris. The 5. The assays were then carried out as specified in Section 2.23.

Statistical analysis

Statistical analysis was performed as described in Section 2.24.

5.3 Results

5.3.1 The conditioned media from lung cancer cells transfected with miR-140-3p mimics inhibit the tubule formation in HUVECs

The effect of miRNA mimics treatment on the ability of the endothelial cells to form new vessels has been investigated through a specific technique, named "tubule formation assay" (Section 2.21.3) and the growth of the HUVEC cells was monitored in real-time by using the EVOS Cell Imaging System over 6 hours. The medium collected from A549 cells treated with miR-140-3p following 24 and 48 hours transfection, significantly reduces the ability of HUVECs to form vessels ($p<0.0001$ and $p<0.05$ respectively) (Figure 5.1). There was also a significant effect on the tubule length of HUVECs grown with media from A549 treated with miR-140-5p following 48hours of transfection ($p<0.05$) (Figure 5.2), whereas no effects have been observed with media from SK-MES-1 at any of the time points observed (Figures 5.3 and 5.4). Notably, although not statistically significant, conditioned medium from SK-MES-1 cells transfected for 48 hours with miR-140-3p mimics did reduce the tubule formation of HUVECs (Figure 5.3 b). The parameters used to evaluate whether the miRNA mimics treatment had any effect on HUVEC behaviour, including the tubule length of the nascent vessels and the number of meshes that formed.

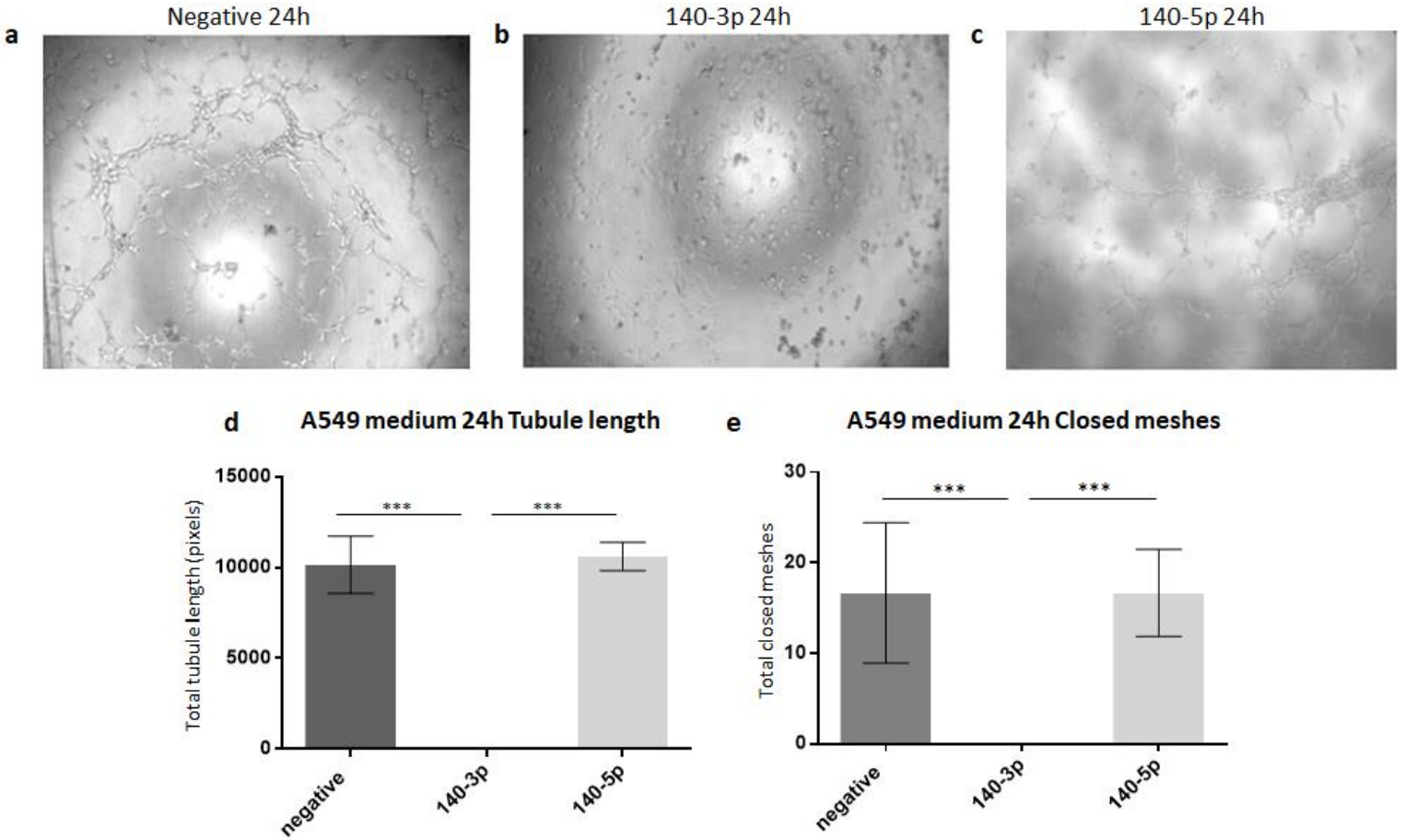
a
Negative 24h
b
140-3p 24h
c
140-5p 24h
d
A549 medium 24h Tubule length
Total tubule length (pixels)
15000
10000
5000
0
***
***
negative
140-3p
140-5p
e
A549 medium 24h Closed meshes
Total closed meshes
30
20
10
0
***
***
negative
140-3p
140-5p

Figure 5.1 Tubule formation ability of the primary endothelial cells HUVECs cultured in the conditioned media of A549 cells following 24 hours transfection with miR-140-3p and 140-5p mimics. The primary endothelial cells HUVECs were seeded onto a layer of Matrigel with their own normal growth medium plus 40% conditioned medium from A549 following 24 hours transfection with miR-140-3p and miR-140-5p. The behaviour of the endothelial cells has been monitored in real-time by using the EVOS Cell Imaging System. Pictures were taken every 30 minutes for about 6 hours. The figures show representative wells for each treatment group 5 hours after cell seeding. a) HUVECs grown with 40% conditioned media from cells transfected with negative mimics. b) HUVECs grown with 40% conditioned media from cells transfected with miR-140-3p mimics. c) HUVECs grown with 40% conditioned media from cells transfected with miR-140-5p mimics. d) Tubule length of HUVECs after 5 hours incubation with the media described in a), b) and c). e) Number of closed meshes of HUVECs after 5 hours incubation with the media described in a), b) and c). Data are presented as mean $\pm$ SEM, two individual experiments were undertaken in triplicate, Kruskal-Wallis-test was used to assess significance with ***$p<0.0001$.

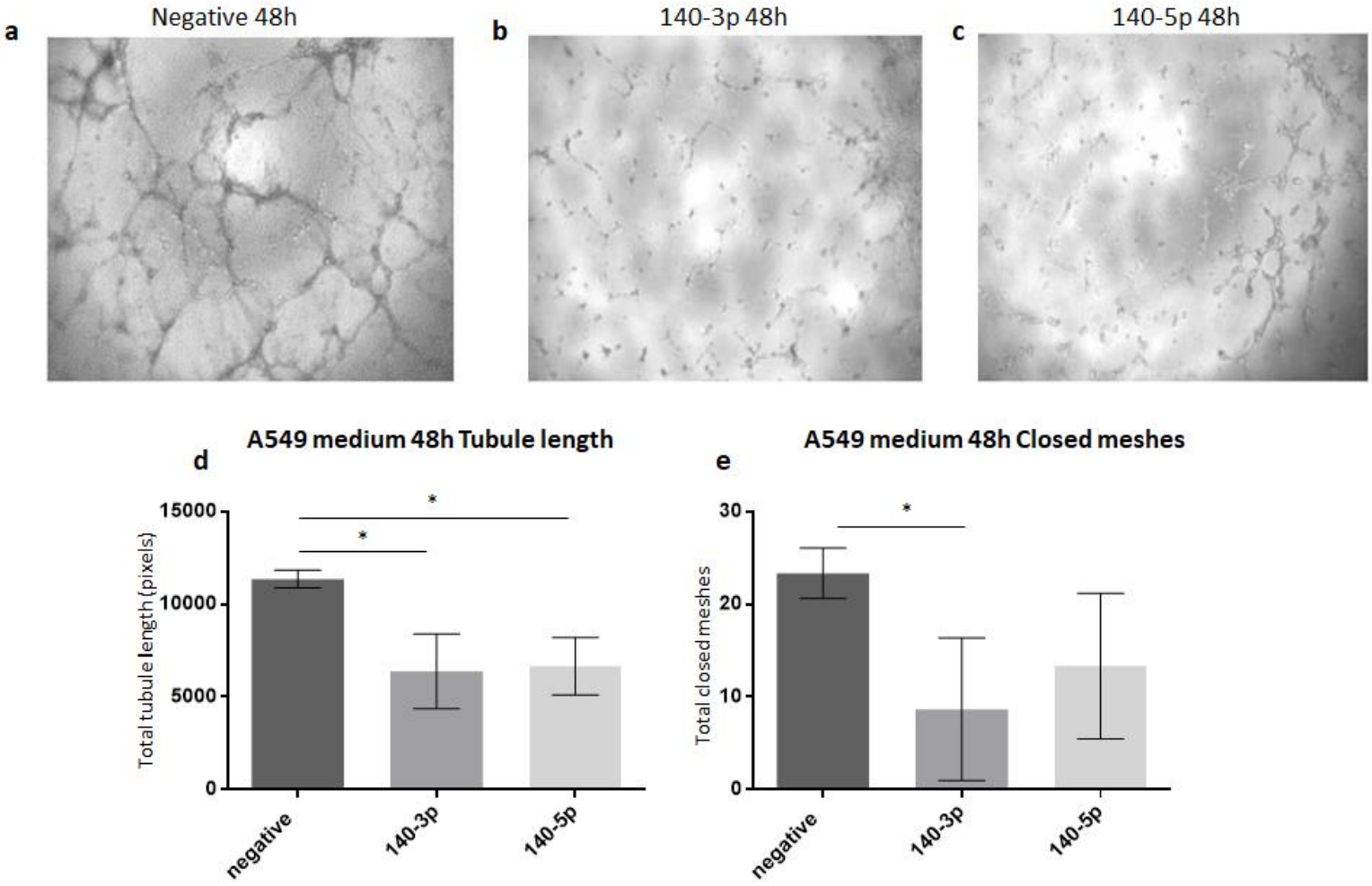
a
Negative 48h
b
140-3p 48h
c
140-5p 48h
d
A549 medium 48h Tubule length
Total tubule length (pixels)
15000
10000
5000
0
*
*
negative
140-3p
140-5p
e
A549 medium 48h Closed meshes
Total closed meshes
30
20
10
0
*
negative
140-3p
140-5p

Figure 5.2 Tubule formation ability of the primary endothelial cells HUVECs cultured in the media of A549 cells following 48 hours transfection with miR-140-3p and 140-5p mimics. The primary endothelial cells HUVECs were seeded onto a layer of Matrigel with their own normal growth medium plus 40% conditioned medium from A549 following 24 hours transfection with miR-140-3p and miR-140-5p. The behaviour of the endothelial cells has been monitored in real-time by using the EVOS Cell Imaging System. Pictures were taken every 30 minutes for about 6 hours. The figures show representative wells for each treatment group 5 hours after cell seeding. a) HUVECs grown with 40% conditioned media from cells transfected with negative mimics. b) HUVECs grown with 40% conditioned media from cells transfected with miR-140-3p mimics. c) HUVECs grown with 40% conditioned media from cells transfected with miR-140-5p mimics. d) Tubule length of HUVECs after 5 hours incubation with the media described in a), b) and c). e) Number of closed meshes of HUVECs after 5 hours incubation with the media described in a), b) and c). Data are presented as mean $\pm$ SEM, two individual experiments were undertaken in triplicate, Kruskal-Wallis-test was used to assess significance with $*p<0.05$.

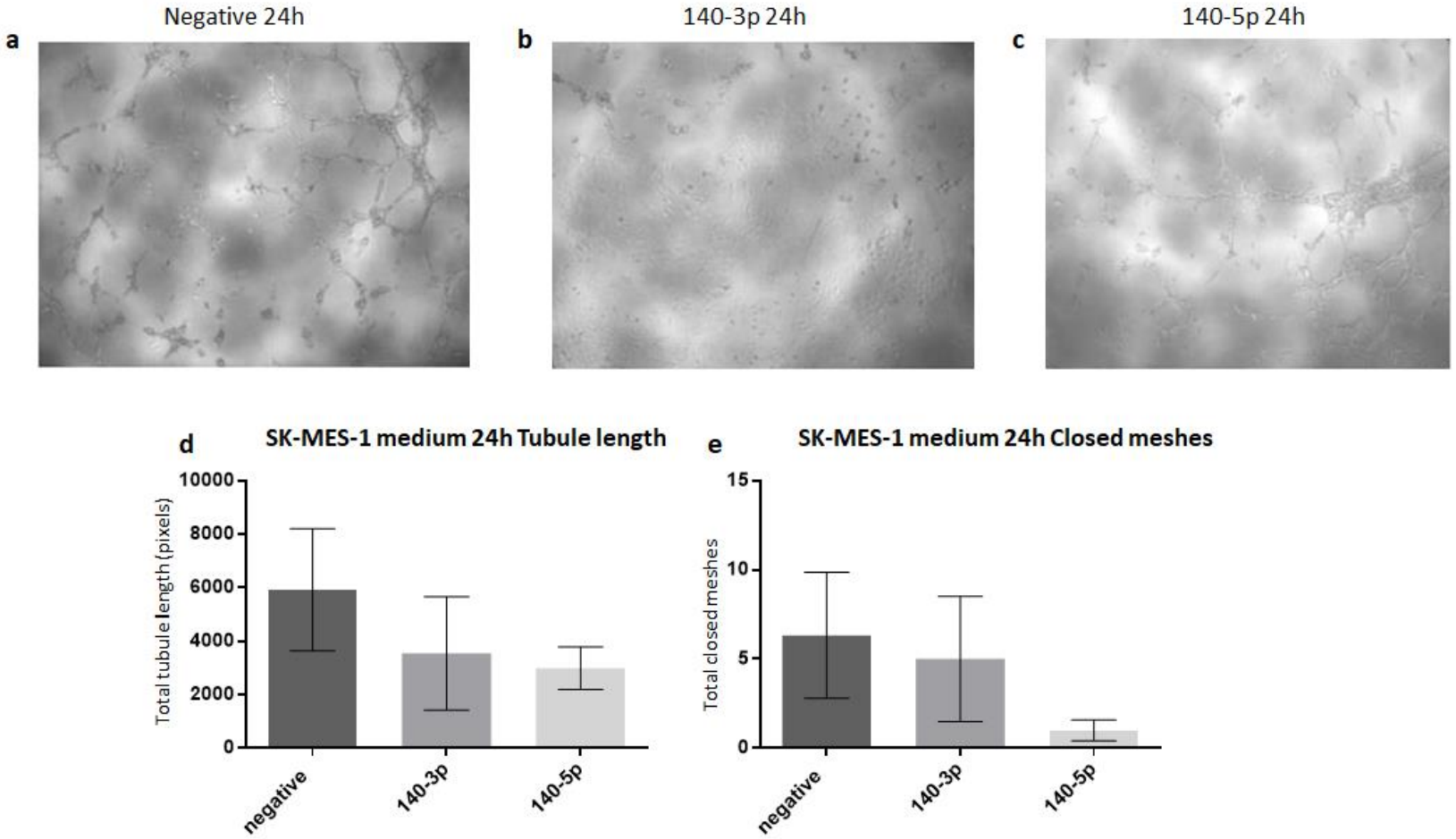
a
Negative 24h
b
140-3p 24h
c
140-5p 24h
d
SK-MES-1 medium 24h Tubule length
Total tubule length (pixels)
10000
8000
6000
4000
2000
0
negative
140-3p
140-5p
e
SK-MES-1 medium 24h Closed meshes
Total closed meshes
15
10
5
0
negative
140-3p
140-5p

Figure 5.3. Tubule formation ability of the primary endothelial cells HUVECs cultured in the media of SK-MES-1 cells following 24 hours transfection with miR-140-3p and 140-5p mimics. The primary endothelial cells HUVECs were seeded onto a layer of Matrigel with their own normal growth medium plus 40% conditioned medium from SK-MES1 following 24 hours transfection with miR-140-3p and miR-140-5p. The behaviour of the endothelial cells has been monitored in real-time by using the EVOS Cell Imaging System. Pictures were taken every 30 minutes for about 6 hours. The figures show representative wells for each treatment group 5 hours after cell seeding. a) HUVECs grown with 40% conditioned media from cells transfected with negative mimics. b) HUVECs grown with 40% conditioned media from cells transfected with miR-140-3p mimics. c) HUVECs grown with 40% conditioned media from cells transfected with miR-140-5p mimics. d) Tubule length of HUVECs after 5 hours incubation with the media described in a), b) and c). e) Number of closed meshes of HUVECs after 5 hours incubation with the media described in a), b) and c). Data are presented as mean $\pm$ SEM, two individual experiments were undertaken in triplicate, Kruskal-Wallis-test was used to assess significance.

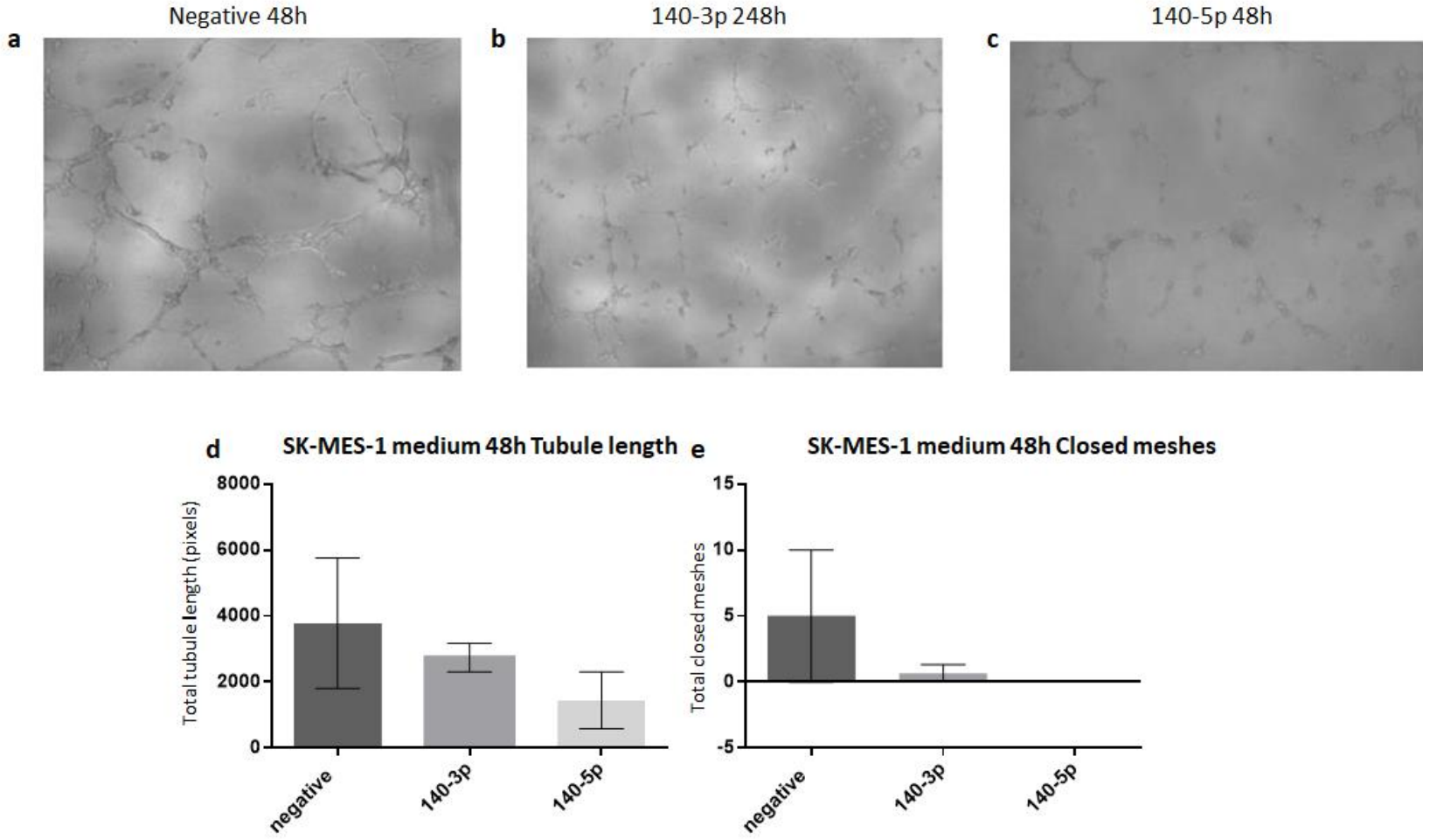
a
Negative 48h
b
140-3p 248h
c
140-5p 48h
d
SK-MES-1 medium 48h Tubule length
Total tubule length (pixels)
8000
6000
4000
2000
0
negative
140-3p
140-5p
e
SK-MES-1 medium 48h Closed meshes
Total closed meshes
15
10
5
0
-5
negative
140-3p
140-5p

Figure 5.4 Tubule formation ability of the primary endothelial cells HUVECs cultured in the media of SK-MES-1 cells following 48 hours transfection with miR-140-3p and 140-5p mimics. The primary endothelial cells HUVECs were seeded onto a layer of Matrigel with their own normal growth medium plus 40% conditioned medium from SK-MES1 following 24 hours transfection with miR-140-3p and miR-140-5p. The behaviour of the endothelial cells has been monitored in real-time by using the EVOS Cell Imaging System. Pictures were taken every 30 minutes for about 6 hours. The figures show representative wells for each treatment group 5 hours after cell seeding. a) HUVECs grown with 40% conditioned media from cells transfected with negative mimics. b) HUVECs grown with 40% conditioned media from cells transfected with miR-140-3p mimics. c) HUVECs grown with 40% conditioned media from cells transfected with miR-140-5p mimics. d) Tubule length of HUVECs after 5 hours incubation with the media described in a), b) and c). e) Number of closed meshes of HUVECs after 5 hours incubation with the media described in a), b) and c). Data are presented as mean $\pm$ SEM, two individual experiments were undertaken in triplicate, Kruskal-Wallis-test was used to assess significance.

5.3.2 The ability of miR-140-3p to inhibit the tubule formation ability of endothelial cells is VEGF-A independent

To assess whether the treatment with miR-140-5p and miR-140 mimics affects the release of VEGF-A from the NSCLC cells, conditioned media from cancer cells that have been transfected with mimics for 24 and 48 hours mimics treatments were analysed by using ELISA. In A549 cells following 24 hours treatment, the VEGF-A content in the media of cells transfected with miR-140-5p was significantly less than in the control ($p=0.0154$) (Figure 5.5a). On the contrary, VEGF-A levels were significantly higher after 48 hours treatment in A549 cells treated with miR-140-3p ($p=0.0249$) (Figure 5.5b). There was no statistically significant difference in the release of VEGF-A from SK-MES1-cells at the two time points considered, though the data suggests a general decrease of the VEGF-A levels in the conditioned medium from A549 cells treated with miR-140-3p and miR-140-5p mimics (Figures 5.5c and d).

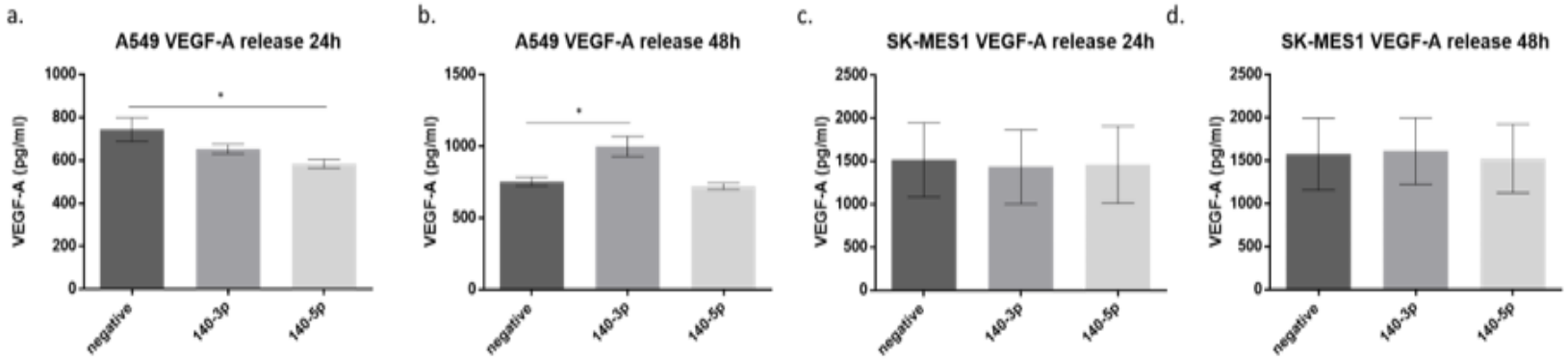

Figure 5.5. Secreted VEGF-A levels from A549 and SK-MES1 NSCLC cell lines, following 24 and 48 hours of transfection with miR-140-3p and miR-140-5p mimics. a) and b) VEGF-A secreted by A549 cells following 24 and 48 hours transfection with negative, miR-140-3p and miR-140-5p mimics. b) and c) VEGF-A secreted by SK-MES-1 cells following 24 and 48 hours transfection with negative, miR-140-3p and miR-140-5p mimics. Data are presented as mean ± SEM, representative data of two individual experiments undertaken in triplicate, Kruskal-Wallis-test was used to assess significance.

5.4 Discussion

I considered the effect of the miRNA mimics treatment on the tubule formation ability of the HUVEC cells *in vitro* to assess whether miR-140-3p and miR-140-5p might influence this facet of the tumour microenvironment. The formation of new blood vessels is crucial for a tumour because the malignant mass needs more and more nutrients and oxygen to sustain its growth (Hanahan and Weinberg, 2011). Additionally, cancer cells invade the blood or lymphatic vessels (intravasation) and enter the bloodstream, to develop metastases at distant sites (extravasation) (Hanahan and Weinberg, 2011). In the previous chapter, I have shown that both miR-140-3p and miR-140-5p act as onco-suppressors by limiting the migration of the lung cancer cells.

In this study, the tumour microenvironment has been partially reproduced by using Matrigel, a compound that mimics the ECM and supports the growth of the primary endothelial HUVECs. Although the variation amongst the experiments is high, I found that the media from A549 cells treated with miR-140-3p after 24 hours stopped the tubule formation of the endothelial cells completely. The same trend was observed using conditioned medium from SK-MES-1 transfected with miR-140-3p mimics. Following 48 hours of transfection, the formation of a vascular network seems to be slightly reduced in SK-MES-1 although there is no statistical significance.

I then evaluated whether the effect I observed was due to a VEGF-A-dependent mechanism. To do this, I analysed the VEGF-A content in the media of A549 and SK-MES-1 cells transfected with the negative, miR-140-3p and miR-140-5p mimics. The slight impairment observed by growing the HUVECs with media from cancer cells transfected with miR-140-5p may have been VEGF-A

dependent, as VEGF-A is one of the targets of miR-140-5p (Sun et al., 2016). As expected, the ELISA results show that following 24 hours of treatment with miR-140-5p, there is a significant decrease of VEGF-A levels in the media from A549 cell. Notably, this happened at the time point in which the efficiency of transfection is the highest and in the cells without any variation in pre-miR-140 sequence. On the contrary, following 48 hours treatment, miR-140-3p significantly enhanced the release of VEGF-A in A549 cells. I therefore conclude that the inhibition of the tubule formation of the endothelial cells following the treatment with miR-140-3p mimics in A549 cells is likely to be VEGF-A independent. VEGF-A does not seem to be the key molecule involved in the tubule formation ability of the endothelial cells because the decrease of VEGF-A in the cancer cells which occurs 24 hours after the treatment with miR-140-5p, does not correspond to an impairment of the tubule formation. However, these data cannot explain the inhibition of the tubule formation in A549 cells following 24 hours of treatment with miR-140-3p. Finally, after further 24 hours, there is an increase of VEGF-A production but this is not followed by an increase of the tubule formation ability of HUVECs, suggesting that the dynamics of tubule formation is mediated by multiple factors (Ferrara, 2010, Butler et al., 2017).

I speculate that the treatment with the miRNA mimics stimulates the release of something different from VEGF-A in the microenvironment and that these compounds/molecules inhibit the tubule formation ability of the HUVECs. It is known that miRNAs can be released by the cells encapsulated into either micro-vesicles or exosomes (Turchinovich et al., 2014, Arroyo et al., 2011), which may contribute to many physiological and pathological processes,

including angiogenesis (Zhou et al., 2014). The release of other miRNAs or other anti-angiogenic substances may explain the inhibition of the tubule formation induced by miR-140-3p and this hypothesis is strengthened by the fact that after 24 hours of the treatment, the concentration of each mimic in the media is quite high and it might be incorporated itself into the endothelial cells, thus inhibiting some key pathways involved in the formation of the vascular network.

CHAPTER 6

EFFECT OF MIR-140-3p AND MIR-140-5p ON LUNG CANCER CELL METABOLISM

6.1 Introduction

An emerging hallmark in cancer progression is the reprogramming of the energy metabolism in malignant cells (Hanahan and Weinberg, 2011). Otto Warburg, who won the Nobel Prize in Medicine in 1931, first observed that tumour cells metabolise glucose differently from the normal cells by a process named glycolysis (Warburg, 1956). In fact, the metabolism of normal cells depends on the oxygen consumption (aerobic respiration), whereas cancer cells can proliferate in the absence of oxygen and produce lactic acid (anaerobic respiration or fermentation).

The involvement of miRNAs in mitochondrial metabolism has been demonstrated, as has the downregulation of some miRNAs that contribute to the metabolic reprogramming in many diseases, including cancer (Duroux-Richard et al., 2016, Mazar et al., 2016). The loss of miR-114 in lung cancer, for example, contributes to the metabolic changes that lead to the spread of cancer (Liu et al., 2016a). This miRNA targets GLUT1, one of the transporters of glucose, together with GLUT4, thus leading to an increase in the glucose uptake and lactate secretion.

In this chapter, I studied the effects of miRNA mimics on the metabolism of A549 and SK-MES-1 lung cancer cell lines to investigate whether these two miRNAs contribute to the metabolic reprogramming of the metabolism of cancer cells. If miRNA mimics restore normal aerobic metabolism, this may partially explain why the medium from the treated cells impair the tubule formation ability of HUVECs, as I described in the previous chapter.

The strategy I used enabled us to quantify mitochondrial function in intact cells by measuring the Oxygen Consumption Rate (OCR) and, at the same time, the Extracellular Acidification Rate (ECAR) in response to specific compounds, as described in Section 2.22.

6.2 Materials and Methods

Seahorse XF Cell Mito Stress Assay

Seahorse stress assay was performed as described in section 2.22. The cells used were BEAS-2B (6×104cells/well), A549 and SK-MES-1 (2.5×104cells/well) which were seeded onto XF96 cell culture microplates (Seahorse Bioscience, CA, USA) in 80 µl growth medium. Following 24 or 48 hours of miRNA treatment, mitochondrial stress was measured in response to oligomycin, FCCP and rotenone/antimycin A at a final concentration of 100µM, 100µM and 50µM respectively measured over a 2-hours period

Seahorse XF Glycolysis Stress Assay

The glycolysis stress assay protocol is described in full in section 2.22. BEAS-2B (6×104cells/well), A549 and SK-MES-1 (2.5×104cells/well) cells were seeded onto XF96 cell culture microplates (Seahorse Bioscience, CA, USA) in 80 µl growth medium. Following 24 and 48 hours of miRNA treatment, glycolysis stress was measured in response to glucose, oligomycin and 2-DG at a final concentration of 5 µM.

Statistical analysis

Statistical analysis was performed as described in Section 2.24.

6.3 Results

6.3.1 MiR-140-3p limits the ATP production in A549 cells

The effect of 24 and 48 hours miR-140-3p and miR-140-5p mimic transfection on the mitochondrial respiration of A549 and SK-MES-1 cells was assessed with the Seahorse XF Cell Mito Stress Assay. The Oxygen Consumption Rate (OCR) was measured before and after the injections with Oligomycin, Carbonyl cyanide-4 (trifluoromethoxy) phenylhydrazone (FCCP) and a mix of Rotenone and Antimycin A. Oligomycin inhibits the synthesis of the ATP by targeting the complex V of the ATP synthase, thus stopping the formation of ATP from ADP. FCCP disrupts the ATP synthesis by ruining the mitochondrial membrane potential. Finally, rotenone and antimycin-A shut down the mitochondrial respiration completely by inhibiting the complex I and III of the electron transport chain, respectively. OCR was monitored for each 96 wells of the plate. For every cell line at each time point, the bioenergetics trace has been reported (Figure 6.1) and the individual parameters indicated in percentage in Figure 6.2.

a.

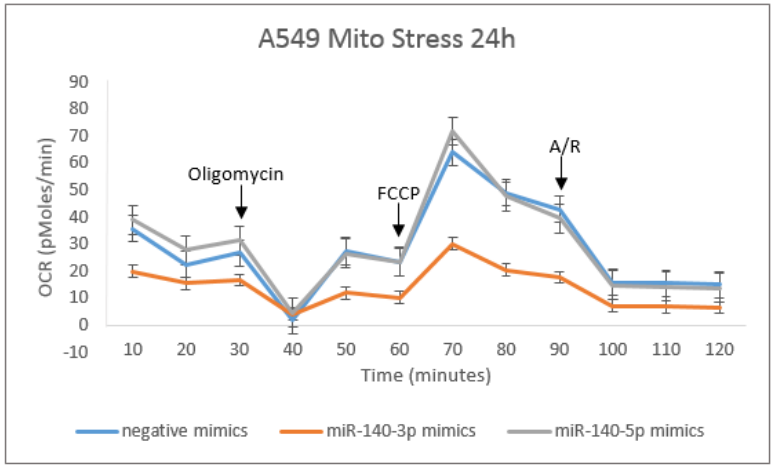
A549 Mito Stress 24h
OCR (pMoles/min)
Time (minutes)
Oligomycin
FCCP
A/R
negative mimics
miR-140-3p mimics
miR-140-5p mimics

b.

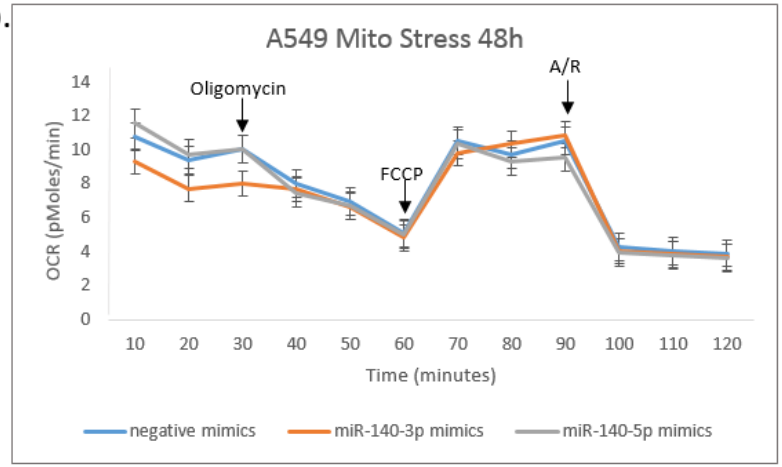
A549 Mito Stress 48h
OCR (pMoles/min)
Time (minutes)
Oligomycin
FCCP
A/R
negative mimics
miR-140-3p mimics
miR-140-5p mimics

c.

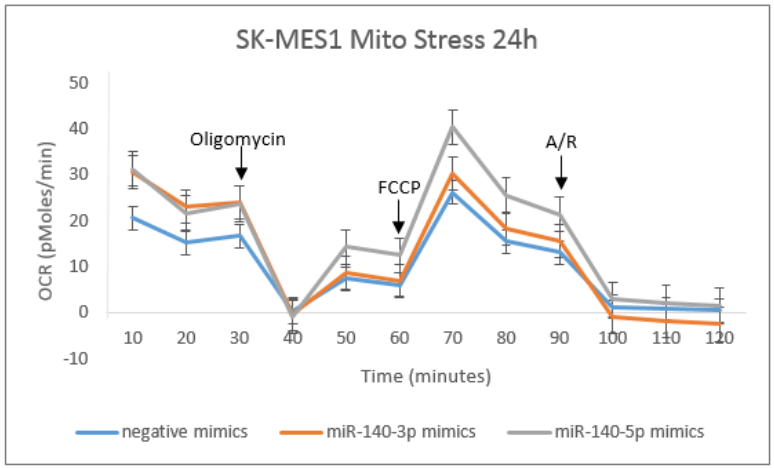
SK-MES1 Mito Stress 24h
OCR (pMoles/min)
Time (minutes)
Oligomycin
FCCP
A/R
negative mimics
miR-140-3p mimics
miR-140-5p mimics

d.

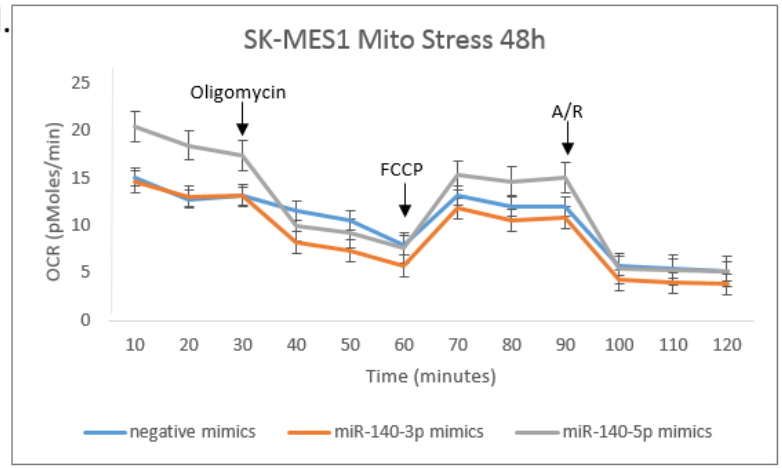
SK-MES1 Mito Stress 48h
OCR (pMoles/min)
Time (minutes)
Oligomycin
FCCP
A/R
negative mimics
miR-140-3p mimics
miR-140-5p mimics

e.

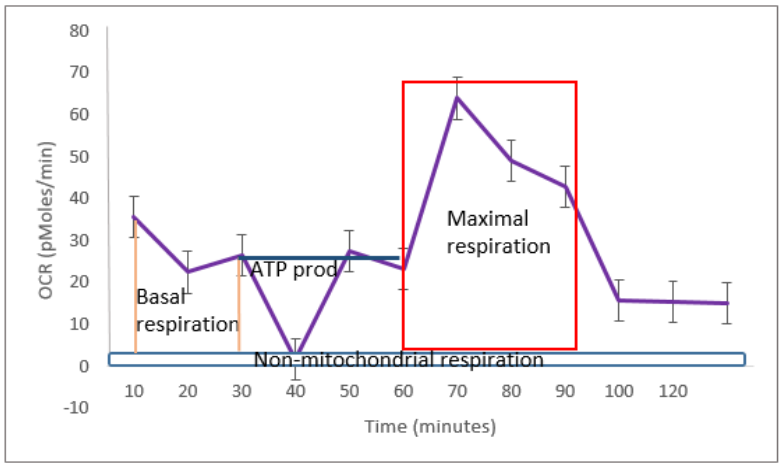

Figure 6.1. Seahorse Mito stress test profile. NSCLC cell lines were treated with miR-140-3p, miR-140-5p and negative mimics for 24 and 48 hours. At these two time points the Seahorse Mito Stress Test was performed to assess the metabolic status of the mitochondria by using three different compounds: oligomycin, carbonyl cyanide 4-phenylhydrazone (FCCP) and rotenone/antimycin A. a) and b) A549 metabolic profile and response to the injections following 24 and 48 hours treatment with miRNA mimics, respectively. c) and d) SK-MES-1 metabolic profile and response to the injections following 24 and 48 hours treatment with miRNA mimics, respectively. e) Representative trace of a Mito Stress metabolic cell profile (A549 treated with miR-140-3p at 24hours) and parameters used to evaluate the mitochondria respiration (basal respiration, ATP production and maximal respiration). Data are presented as mean $\pm$ SD, three individual experiments undertaken in triplicate

The Seahorse traces of the A549 and SK-MES-1 NSCLC cell lines following 24 hours treatment with miRNA mimics show more differences in the OCR amongst the groups within the same cell line, compared to the traces at 48 hours. In both the cell lines, the OCR consumption decreases with time. For example, in the A549 cells treated with miR-140-5p and negative control, the starting OCR is about 40 pmole/min and it slows down to 12p mole/min after a further 24 hours (Figures 6.1a and b). The representative Figure 5.1e illustrates the parameters considered to study the mitochondrial features. They have been quantified by using the method described in Section 2.22 and the results, in percentage, have been reported in Figure 5.2.

The traces of A549 cells following 24 and 48 hours treatment with the miRNA mimics, follow the same trend, with the cells transfected with miR-140-3p starting from a lower basal respiration point at the beginning of the assay, compared to control and the cells treated with miR-140-5p (Figures 6.1a and b). In particular, after 24 hours, the traces of the cells transfected with miR-140-5p and the control overlie each other (Figure 6.1a). The basal respiration, ATP production and maximal respiration were quantified as a percentage, by taking the control as 100%. Although the starting point for each trace is different, there is no significant difference between the control and the treated cells, whereas the cells treated with miR-140-3p at 24 hours, produce less ATP than the control (Figure 6.2 a). The other results are not statistically significant, however, the trend of A549 after 24 and 48 hours treatment is the same (Figures 6.2a and b): miR-140-3p decrease the basal respiration, ATP production and maximal respiration, whereas the miR-140-5p has the opposite effect (Figures 6.2a and b).

The traces of SK-MES-1 cells following 24 and 48 hours treatment with the miRNA mimics does not show any common trend. At the starting point, the basal respiration of the cells treated with miR-140-3p and miR-140-5p is higher at 24 hours than the control (Figure 6.1c), whereas at 48 hours the basal respiration is increased in the cells treated with miR-140-5p and assumes the same value in the cells treated with the miR-140-3p and negative control (Figure 5.1d). Overall, as in the case of the A549, there are greater differences amongst the groups following 24 treatments with the miRNA mimics (Figure 5.1a), than 48 hours (Figure 6.1b). The levels of the basal respiration, ATP production and maximal respiration appears higher in the cells treated with miR-140-5p and miR-140-3p at both the time points considered (Figures 6.2c and d). These data, however, are not statistically significant.

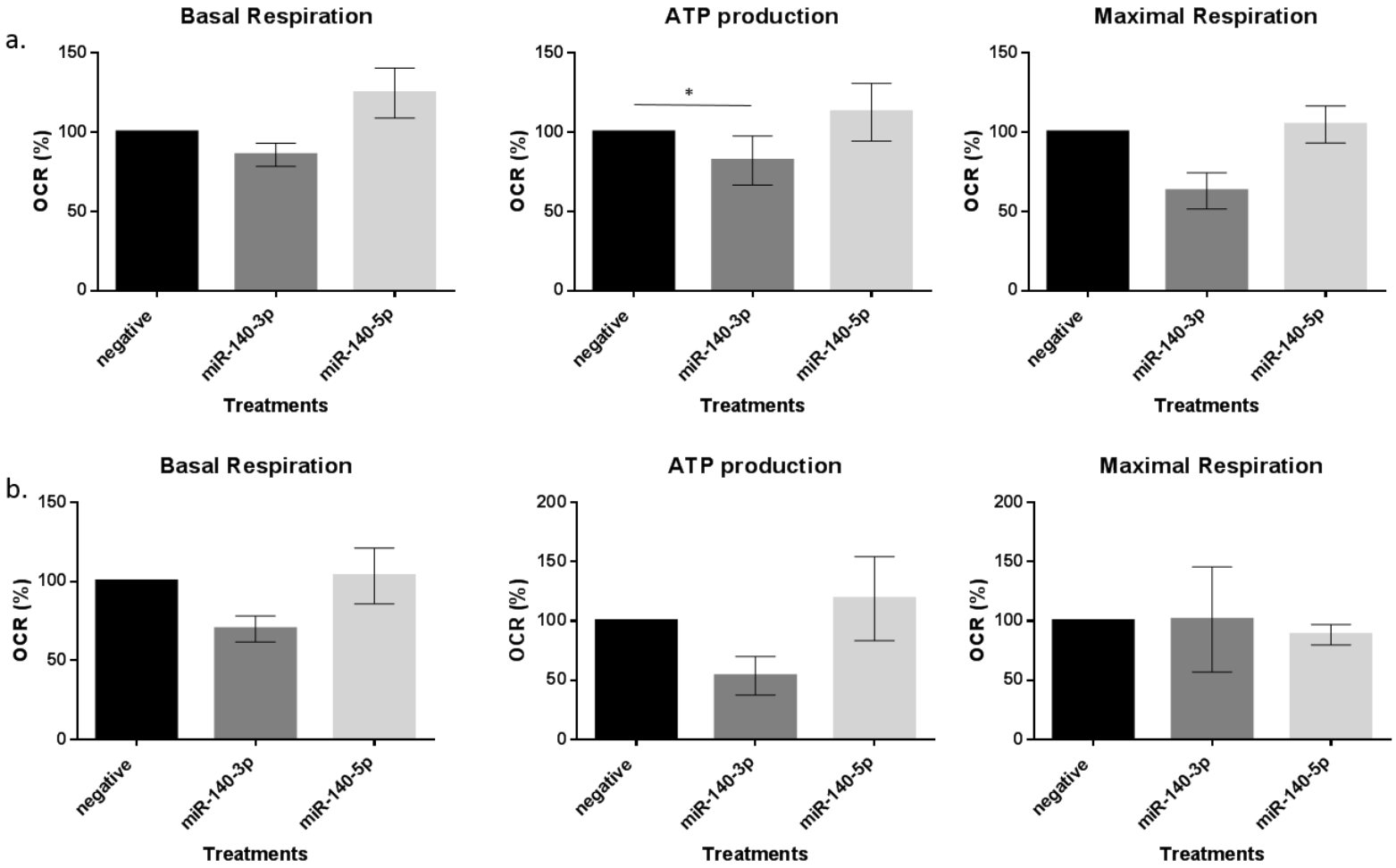
a.
Basal Respiration
ATP production
Maximal Respiration
OCR (%)
150
100
50
0
*
negative
miR-140-3p
miR-140-5p
Treatments
b.
Basal Respiration
ATP production
Maximal Respiration
OCR (%)
200
150
100
50
0
negative
miR-140-3p
miR-140-5p
Treatments

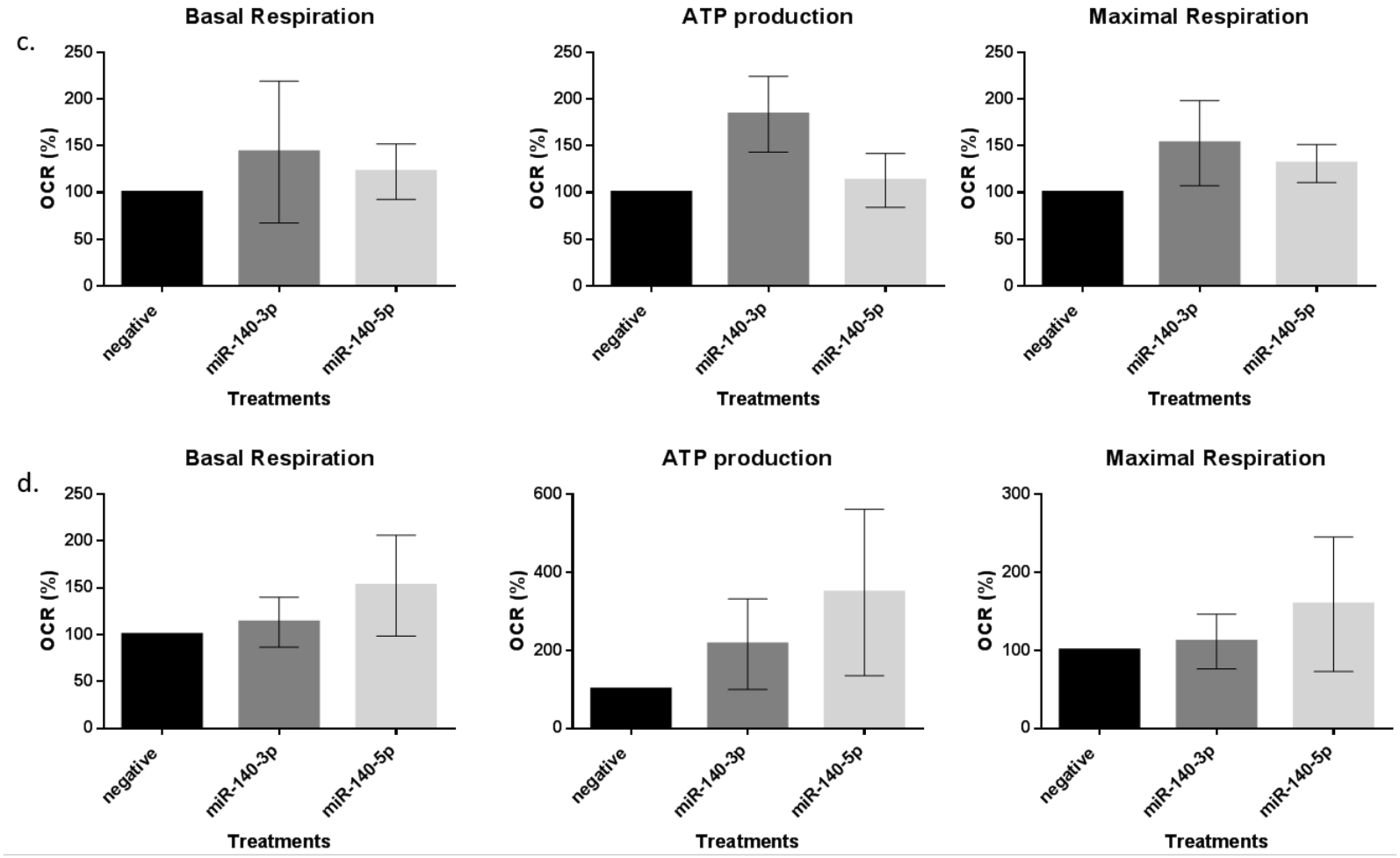
c.
Basal Respiration
ATP production
Maximal Respiration
OCR (%)
250
200
150
100
50
0
negative
miR-140-3p
miR-140-5p
Treatments
d.
Basal Respiration
ATP production
Maximal Respiration
OCR (%)
600
400
300
200
100
0
negative
miR-140-3p
miR-140-5p
Treatments

Figure 6.2. Seahorse Mito stress test parameter quantitation. The Basal respiration, ATP production and maximal respiration of the cells treated with miR-140-3p, miR-140-5p and negative mimics have been quantified and illustrate in percentage as described in the Section 2.22. A549 metabolic response to the injections following a) 24 and b) 48 hours treatment with miRNA mimics, respectively. SK-MES-1 metabolic response to the injections following c) 24 and d) 48 hours treatment with miRNA mimics, respectively. Data are presented as mean $\pm$ SEM, three individual experiments were undertaken in triplicate, ANOVA was used to assess significance with $*p<0.05$. The data represents the percentage and the statistical analysis was performed by using row data.

6.3.2 MiR-140-3p and miR-140-5p do not reduce the glycolysis in NSCLC cell lines

Glycolysis is the first step in cellular respiration. It occurs in the cytoplasm of the cells, outside of mitochondria, and produces 2 molecules of ATP per glucose and pyruvate. In the presence of oxygen, pyruvate is transported into the mitochondria for the aerobic respiration which produces ATP, CO_2 and water. Without oxygen, glycolysis is followed by a process named fermentation, which produces lactate in animals and ethanol in plants. The conversion of glucose to lactate, results in the release of protons, which reduces the pH of the extracellular environment. Glycolysis is the preferred energetic process used by cancer cells and here we assessed whether the miRNA mimics treatment has any effect on the glycolytic function of the NSCLC cells, A549 and SK-MES-1.

In the first instance, the cells were incubated with a specific media without glucose or pyruvate and then three compounds were injected into the cells: glucose, oligomycin and 2-deoxy-glucose (2-DG). Glucose initiates the respiration in the cells. Oligomycin is an ATP synthase inhibitor and, consequently, stops the aerobic respiration, in favour of glycolysis. Finally, the glucose-analog, 2-DG, inhibits the glycolysis by binding to glucose hexokinase, the first enzyme involved in the glycolytic process. The extracellular acidification rate (ECAR), which corresponds to the protons produced by the cells, was monitored for each of the 96 wells on the plate. For every cell line at each time point, the bioenergetics trace was reported (Figure 6.3) and the individual parameters indicated in percentage in Figure 6.4.

a.

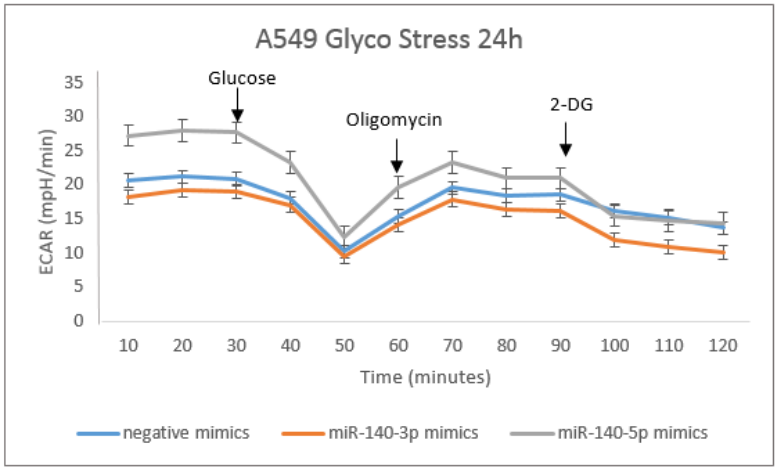
A549 Glyco Stress 24h
Glucose
Oligomycin
2-DG
ECAR (mpH/min)
Time (minutes)
negative mimics
miR-140-3p mimics
miR-140-5p mimics

b.

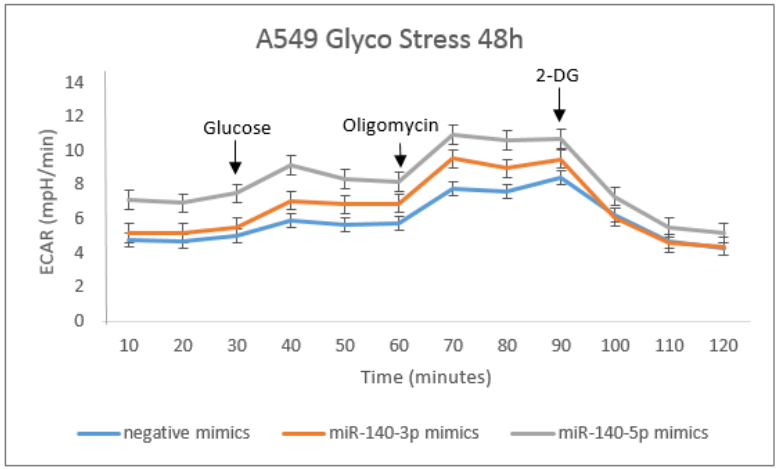
A549 Glyco Stress 48h
Glucose
Oligomycin
2-DG
ECAR (mpH/min)
Time (minutes)
negative mimics
miR-140-3p mimics
miR-140-5p mimics

c.

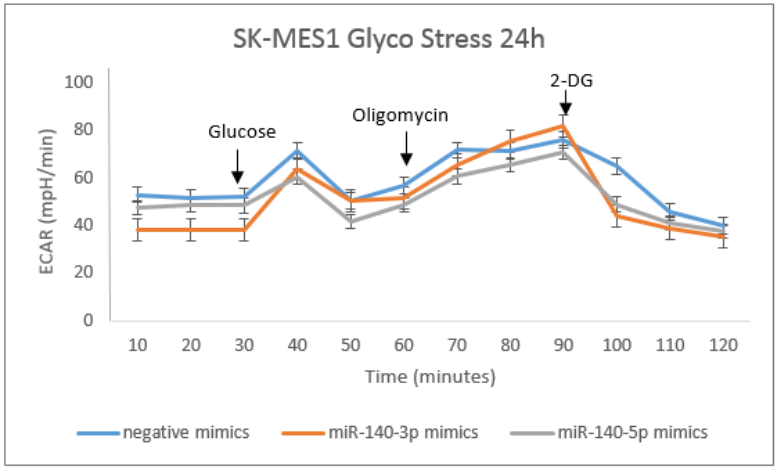
SK-MES1 Glyco Stress 24h
Glucose
Oligomycin
2-DG
ECAR (mpH/min)
Time (minutes)
negative mimics
miR-140-3p mimics
miR-140-5p mimics

d.

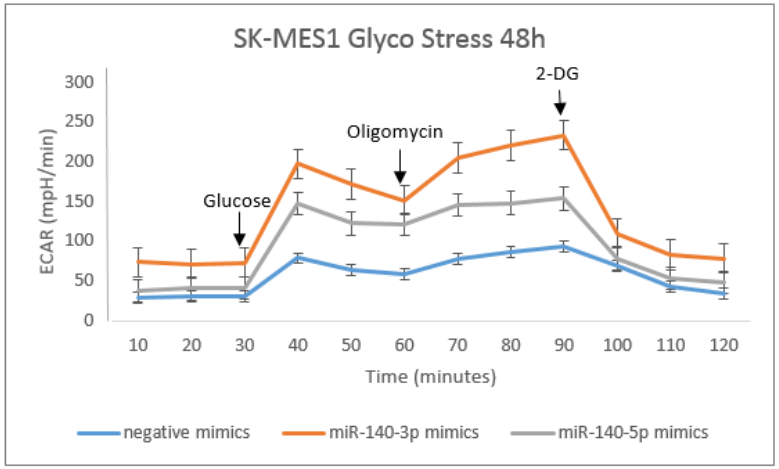
SK-MES1 Glyco Stress 48h
Glucose
Oligomycin
2-DG
ECAR (mpH/min)
Time (minutes)
negative mimics
miR-140-3p mimics
miR-140-5p mimics

e.

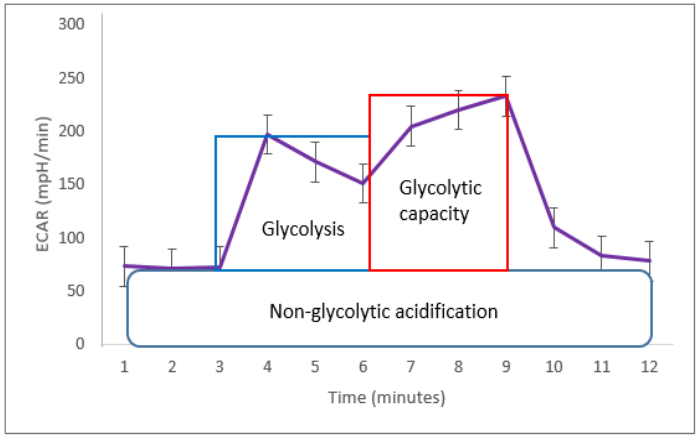

Figure 6.3. Seahorse Glycolysis stress test profile. NSCLC cell lines were treated with miR-140-3p, miR-140-5p and negative mimics for 24 and 48 hours. At these two time points, the Seahorse Glyco Stress Test has been performed to assess the respiration in the cells by using three different compounds: glucose, oligomycin and 2-deoxy-glucose. A549 metabolic profile and response to the injections following a) 24 and b) 48 hours treatment with miRNA mimics, respectively. SK-MES-1 metabolic profile and response to the injections following c) 24 and d) 48 hours treatment with miRNA mimics, respectively. e) Representative trace of a Glyco Stress metabolic cell profile (SK-MES-1 treated with miR-140-3p at 48hours) and parameters used to evaluate the cellular respiration (Glycolysis and glycolytic capacity). Data are presented as mean $\pm$ SD, three individual experiments undertaken in triplicate

The Seahorse traces show that both the A549 and SK-MES-1 cell lines have a better response at 24 hours (Figure 6.3a and c) than at 48 (Figure 6.3b and d). A representative graph, with a good response to the injections, is displayed in Figure 5.3e. The traces also show that the ECAR decreases with time, as the OCR does in the Mito Stress assay. For example, in A549 cells treated with miR-140-3p and negative control, the starting ECAR is about 20 mpH/min and then slows down to 4 mpH/min after a further 24 hours (Figures 6.3a and b).

The traces of A549 cells following 24 and 48 hours treatment with the miRNA mimics, follow the same trend, with the cells transfected with miR-140-5p starting from a higher ECAR at the beginning of the assay, compared to the control and the ones treated with miR-140-3p (Figures 6.3a and b). However, at 24 hours the graph is not reliable, as the injection of glucose should be the saturation point and the ECAR should increase afterwards. The glycolysis and glycolytic capacity of the cells have been quantified as percentage, by taking the control as 100% (Figure 5.4). At both the time points, both the treatments look to increase the glycolysis of the NSCLC cells (Figures 6.4a and c). These data, however, are not statistically significant. The data that has a statistical significance is the reduction of the glycolytic capacity of the A549 cells following 24 hours of transfection with the miR-140-5p mimics (Figure 6.4a).

The traces of SK-MES-1 cells following 24 and 48 hours treatment with miRNA mimics, do not follow any common trend, even if the cells at 48 hours (Figure 6.3d) respond better to the injections than the cells at 24 hours (Figure 6.3c). No statistically significant difference has been recorded in the glycolysis and the glycolytic capacity of the SK-MES-1 at both the time points (Figure 6.4 a and b,

respectively), even if the treatment with the mimics tends to increase the anaerobic respiration of the cancer cells.

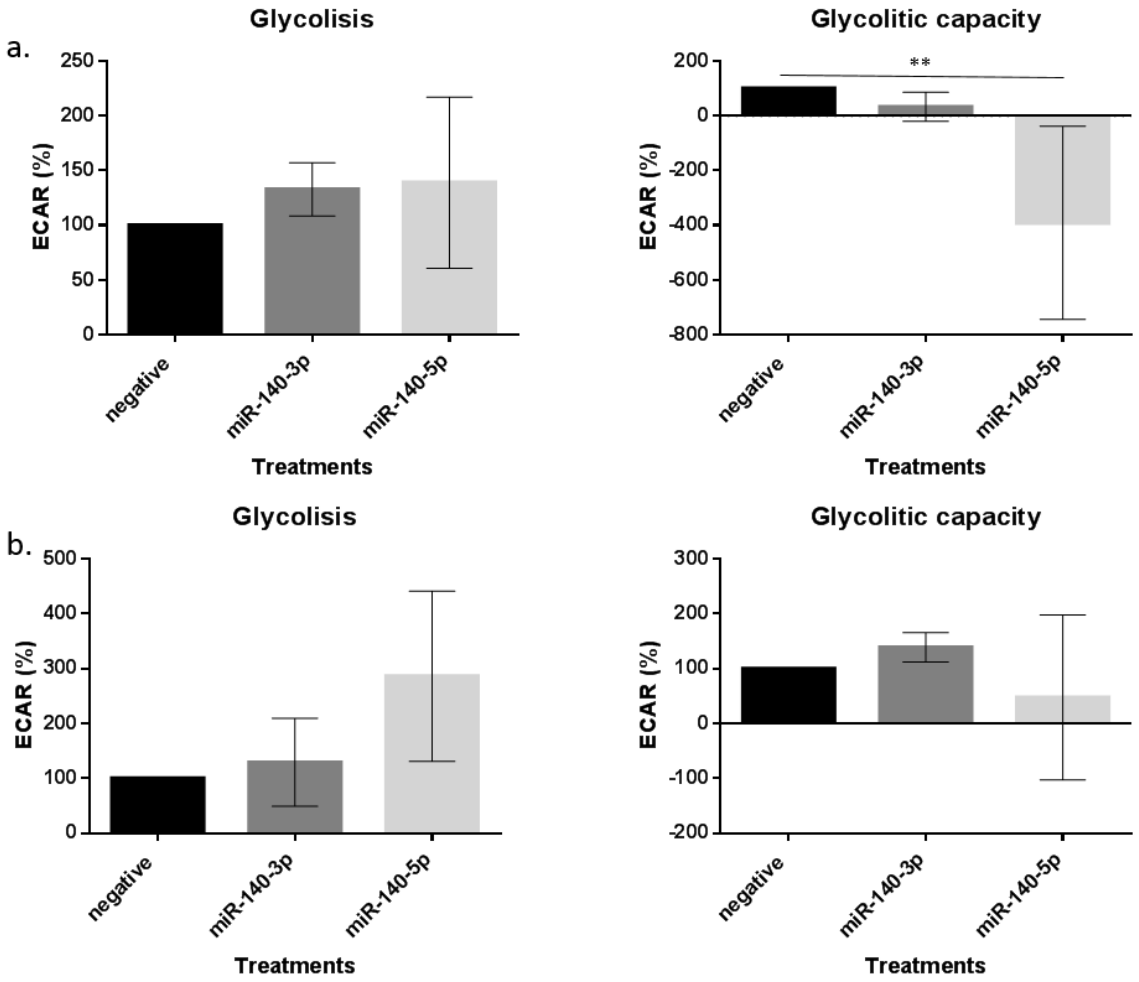
a.
Glycolisis
ECAR (%)
250
200
150
100
50
0
negative
miR-140-3p
miR-140-5p
Treatments
Glycolitic capacity
**
200
0
-200
-400
-600
-800
negative
miR-140-3p
miR-140-5p
Treatments
b.
Glycolisis
ECAR (%)
500
400
300
200
100
0
negative
miR-140-3p
miR-140-5p
Treatments
Glycolitic capacity
ECAR (%)
300
200
100
0
-100
-200
negative
miR-140-3p
miR-140-5p
Treatments

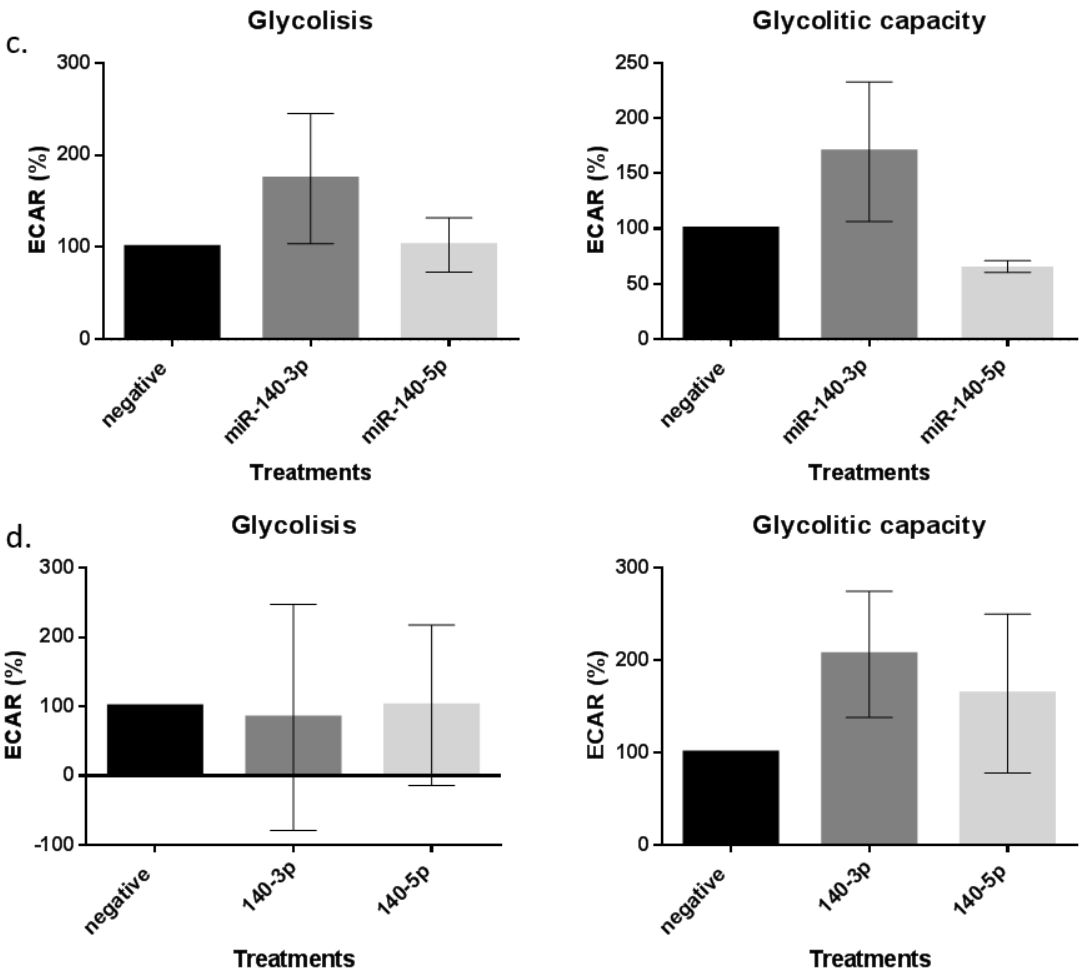
c.
Glycolisis
ECAR (%)
300
200
100
0
negative
miR-140-3p
miR-140-5p
Treatments
Glycolitic capacity
ECAR (%)
250
200
150
100
50
0
negative
miR-140-3p
miR-140-5p
Treatments
d.
Glycolisis
ECAR (%)
300
200
100
0
-100
negative
140-3p
140-5p
Treatments
Glycolitic capacity
ECAR (%)
300
200
100
0
negative
140-3p
140-5p
Treatments

Figure 6.4. Seahorse Glycolysis stress test parameter quantitation. The Basal respiration, ATP production and maximal respiration of the cells treated with miR-140-3p, miR-140-5p and negative mimics have been quantified and illustrate in percentage as described in the Section 2.22 a) and b) A549 respiration response to the injections following 24 and 48 hours treatment with miRNA mimics, respectively. c and d) SK-MES-1 respiration response to the injections following 24 and 48 hours treatment with miRNA mimics, respectively. Data are presented as percentage mean ± SEM, three individual experiments were undertaken in triplicate, ANOVA was used to assess significance with **$p<0.01$. Data represents the percentage and the statistical analysis was performed by using row data.

.

6.4 Discussion

Cancer cells switch from an aerobic to an anaerobic respiration, regardless of the presence of oxygen. Many factors may contribute to this change, including mutations in key genes and epigenetic modifications that regulate cell metabolism.

In presence of oxygen, the normal cells in our body use glucose to produce pyruvate first and then energy, water and carbon oxide in mitochondria. When the levels of oxygen are low, the pyruvate does not enter the mitochondrion, but is converted into lactate and energy in the cytoplasm through a process named glycolysis. This normally happens in the working muscles, where there is a high demand for oxygen and thus the levels become lower and lower.

In this study, the mitochondrial respiration and the glycolytic function of NSCLC cells treated with miR-140-3p and miR-140-5p have been investigated to see whether the mimics treatment can revert any metabolic changes which have occurred in malignant cells.

The Cell Mito Stress assay allows study of the mitochondrial respiration by using compounds that inhibit aerobic respiration. Both A549 and SK-MES-1 cells respond well to these injections, as the metabolic traces show that the oligomycin and rotenone/antimycin A decrease the OCR by impeding the synthesis of the ATP, whereas the FCCP stimulates the oxygen consumption by disrupting the electron flow through the Krebs cycle. However, the best response is following 24 hours mimic transfection in both the cell lines. The OCR decreases with time, as the OCR in both the cell lines decreases proportionally to the time of transfection. This may be due to the availability of oxygen in each well. The cells

may be proliferating and, over time, need more and more oxygen, thus making the environment potentially hypoxic.

In A549 cells, the important statistically significant data obtained through this assay is the ATP production. Twenty-four hours following transfection with miR-140-3p, A549 cells produced less ATP than the control cells. This suggests that miR-140-3p may target some key factors involved in the aerobic respiration. Low ATP levels and a high glycolysis are associated with chemoresistance and proteasome impairment in cancer (Zhou et al., 2012, Huang et al., 2010) and this may confer an advantage to the cancer cells. In contrast, miR-140-5p appears to restore the anaerobic respiration and ATP production. These data, however, are not significant. As expected, glycolysis in the A549 cells was shown to increase following the treatment with miR-140-3p and this strengthens the hypothesis that miR-140-3p may enhance the metabolic switch in the cancer cell. It should be noted that we cannot rely completely on the study of the glycolytic functions of the NSCLC cells treated with the miRNA mimics, because by looking at the metabolic trace at 24 hours, I see that the cells did not respond well to the injections for the study of glycolysis. The first injection with glucose should increase the ECAR of the cells, as the saturating concentration of glucose stimulates glycolysis and, consequently, the release of protons in the extracellular space. In my experiment, the ECAR decreased after the first injection. The trace indicates that the ECAR rises again before the injection with the oligomycin that inhibits the synthesis of the ATP. The glucose analogue 2-DG, did reduce the ECAR as expected, by limiting the glycolytic process.

The data obtained on SK-MES-1 cells were very variable and no statistically significant differences have been found between the cells treated with the

control and the negative mimics, even though the cells responded well to the stimuli given by the injections in both the Cell Mito and Glycolysis assays. The trend they follow is controversial, as miR-140-3p and miR-140-5p seem to increase the basal respiration and ATP production but, at the same time, they also increase the glycolysis of cancer cells.

Taken together, I conclude from these experiments that there is no significant evidence that shows that miR-140-3p and miR-140-5p mimics treatments affect the metabolism of the NSCLC cells.

The main limitation of this *in vitro* study, is the contribution of the microenvironment (Anastasiou, 2017). During the progression of the malignancy, many cell types are involved, such as immune and endothelial cells and we do not know how the NSCLC cells treated with miR-140-3p and miR-140-5p would respond to the external stimuli.

In view of the above findings that in A549 and SK-MES-1 cells, miR-140-3p and miR-140-5p do not appear to target genes involved in metabolism; in the next chapters, I will focus on the investigation of other potential candidate targets of both miR-140-3p and miR-140-5p.

CHAPTER 7

TARGET PREDICTION AND PATHWAY INVESTIGATION OF MIR-140-3p AND MIR-140-5p IN LUNG CANCER CELLS

7.1 Introduction

In the previous chapters I assessed the impact of the miR-140-3p and miR-140-5p mimic treatments on NSCLC and endothelial cell behaviour using a variety of *in vitro* functional assays. The results suggest that the treatment with these miRNA mimics significantly decreased the invasive properties of malignant NSCLC cells and limited the tubule formation ability of endothelial cells *in vitro*.

In order to understand the possible mechanisms that are involved in the alteration of the malignant properties of lung cancer cells after miRNA treatments, in this chapter the EMT markers were assessed for their expression in NSCLC cells in response to transfection with miR-140-3p and miR-140-5p mimics. This included the epithelial cell marker E-cadherin, the mesenchymal marker N-cadherin, the cytoskeletal marker Vimentin and the transcription factors Snail and Slug.

The targets of both miR-140-3p and miR-140-5p were investigated by using two different approaches. Apart from the bioinformatic approach with *in silico* tools, I merged the data obtained from the RNA-sequencing technique using biotinylated-mimic RNA pulldown with the data from a Kinexus protein array. The targets predicted by the bioinformatics tools were validated by western blotting.

By using the bioinformatics approach, I focused on integrin-β3 (ITGB3) as a potential target of miR-140-3p. It is known that integrins mediate the migration of tumour cells by cooperating with specific growth factor receptors, including EGFR (Desgrosellier and Cheresh, 2010). Specifically, ITGB3 has been associated with lung cancer progression (Hong et al., 2016) . Their expression,

in fact, is not just altered in malignant cells, but also in tumour-associated cells, including endothelial cells (Desgrosellier and Cheresh, 2010). Thus, integrins may regulate and affect many pathways, especially when considering the vast array of stimuli within the tumour microenvironment (Desgrosellier and Cheresh, 2010). For example, when ITGB3 is associated with the αV subunit (α5β3), they regulate angiogenesis with growth factor specific receptors, such as the Fibroblast Growth Factor Receptor (FGFR) (Hood et al., 2003). As my results suggest that the effect of miR-140-3p on the formation of new vessels in HUVECs appears to be VEGF-A independent, I hypothesise that ITGB3 may influence tumour progression in NSCLC by affecting both cancer and endothelial cell behaviour.

Data from RNA-Seq suggests that the cyclin-dependent kinase 3 (CDK3) and the sulfatase 2 (SULF2) may be two targets of miR-140-5p. The involvement of these molecules in cancer progression has been demonstrated (Xiao et al., 2017, Wang et al., 2014, Zhu et al., 2016, Lui et al., 2016, Lemjabbar-Alaoui et al., 2010) and to better validate this hypothesis, I studied the effect of miR-140-5p on the levels of EGFR and β-catenin, two critical factors involved in the cellular transformation mediated by CDK3 and SULF2, respectively.

7.2 Materials and methods

Western blotting

Following 48 hours of treatment of A549 with negative control or miR-140-3p and miR-140-5p mimics, cells were washed with PBS and lysed with RIPA buffer with proteinase inhibitors, placed on a rotating wheel for 30 minutes at 4˚C, centrifuged at 16,000 xg for 20 minutes then the proteins in the supernatant were quantified as described in Section 2.12. Following this, an equal amount of 2 x Llaemelli buffer was added and western blotting was performed using 80 ng of proteins for each sample and the respective antibodies, as listed in Tables 11-12.

MiRNA Target Validation by using the Luciferase Assay

The pmirGLO Dual-Luciferase miRNA Target Expression Vector (Promega, Wisconsin, USA) was used to evaluate the miRNA activity by inserting the putative miRNA target sites at the 3´ of the firefly luciferase gene (luc2). The target sites were cloned into the pmirGLO Vector, propagated in competent *E. coli* cells and purified as indicated in Section 2.18. Plasmids were partially sequenced to verify the integrity of the cloned inserts. Cells were transfected with plasmids containing the pmirGlo vector and wild-type and mutated target sequences of miR-140-3p. After 24 hours cells were analysed for luciferase activity.

MiRNA Target Identification by using mRNA-sequencing (mRNA-Seq)

Following 24 hours of transfection with negative control, miR-140-3p or miR-140-5p biotinylated mimics, A549 cells were lysed with a hypotonic buffer and the mRNA-miRNA complexes were isolated with magnetic beads, as indicated in Section 2.19. The captured mRNAs were amplified and labelled to obtain a

library. The RNA was sequenced as described in Section 2.20 and the analysis of the RNA-Seq data were performed with Partek Genomics Suite software (http://www.partek.com/pgs). The potential targets were expressed in reads per million (RPM) and the differences between the control and testing samples calculated as log2 (RPM sample-RPM control) on an Excel spreadsheet.

EMT markers validation qRT-PCR

QRT-PCR was undertaken using cDNA produced in reverse transcription detailed above, using primers for SLUG, SNAIL, ARAF and EGFR (listed in Table 2.4), following the procedure outlined in Section 2.11. The analysis was performed using Ct values obtained from these processes were analysed using $2^{-(\Delta\Delta CT)}$ normalisation to GAPDH. Each qPCR sample was analysed in triplicate, with the experiment being independently set up three times.

Protein microarray (Kinexus)

Following 48 hours transfection with a negative control or miR-140-3p and miR-140-5p miRNA mimics, A549 cells were lysed as indicated in Section 2.14 and sent to the Kinexus Bioinformatics Corporation (Vancouver, British Columbia, Canada) for protein array analysis. Results were sorted in Excel by the lowest % CFC (percentage change from control) in response to each miRNA treatment.

Statistical Analysis

Statistical analysis was performed as described in Section 2.24.

7.3 Results

7.3.1 Treatment with miR-140-3p and miR-140-5p mimics decreases the EMT markers in A549 cells

Due to the reduced invasive potential of A549 NSCLC cells following miR-140-3p and miR-140-5p mimic treatments (Chapter 4, Figure 4.6), I assessed whether the markers of EMT were affected. We screened the A549 cells for E-cadherin, N-cadherin, Vimentin, Snail and Slug following transfection with miR-140-3p and miR-140-5p (Figure 7.1).

In A549 cells, both miR-140-3p and miR-140-5p mimics were shown to increase E-cadherin protein levels and decrease N-cadherin (Figure 7.1a). Vimentin, a cytoskeletal marker overexpressed in cancer, was downregulated by the treatment with both miR-140-3p and miR-140-5p mimics (Figure 7.1a). The transcription factors Snail and Slug, usually overexpressed in tumours, were downregulated after the transfections with the two forms of miR-140 (Figure 7.1 b and c). Compared to the negative mimic, miR-140-3p significantly decreases the levels of both Snail ($p=0.0423$) and Slug ($p<0.0001$). Similarly, miR-140-5p reduced the expression of Snail ($p=0.0211$) and Slug ($p<0.0001$) in the same manner

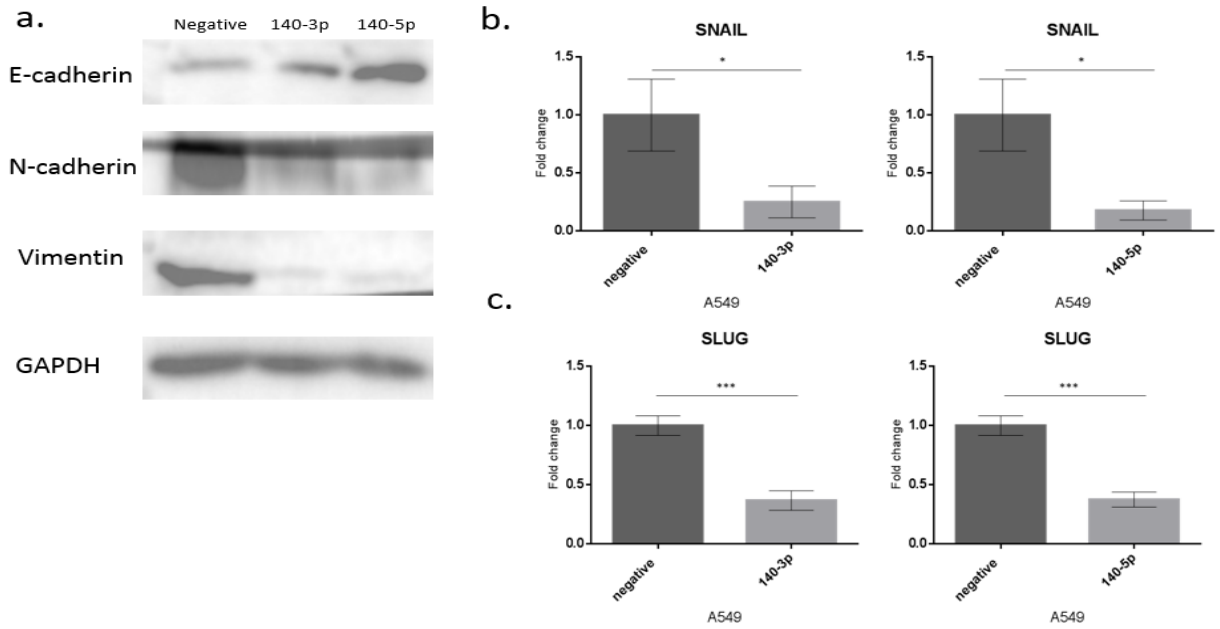

Figure 7.1. Expression of EMT markers in A549 cells following the treatment with miR-140-3p and miR-140-5p mimics. a) Western blotting of the cell surface markers E-cadherin, N-cadherin and the cytoskeletal marker Vimentin after transfection with miRNA mimics for 48 hours b) qPCR of the transcription factor Snail after transfection with the miRNA mimics for 24 hours. c) qPCR of the transcription factor Slug after transfection with the miRNA mimics for 24 hours. Data are presented as change fold of the mean $\pm$ SEM, three individual experiments were undertaken in triplicate, t-test has been used to assess significance with *$p<0.005$***$p<0.001$.

7.3.2 Integrin beta-3 (ITGB3) is the direct target of miR-140-3p

In order to further investigate the phenotypical changes of adhesive, migratory and invasive capabilities that were detected following the transfection with miR-140-3p and miR-140-5p mimics (Chapter 4), I also explored the potential direct targets of miR-140-3p and miR-140-5p by using *in silico* tools. The criteria I have used were the following:

- Conservation of the miRNA sequence among the species
- Consider the genes involved in invasion and angiogenesis

By combining the data from the main bioinformatic algorithms, especially TargetScan and MiRWalk, I identified ITGB3 as potential direct target, which is usually up-regulated in both tumour and tumour-associated endothelial cells.

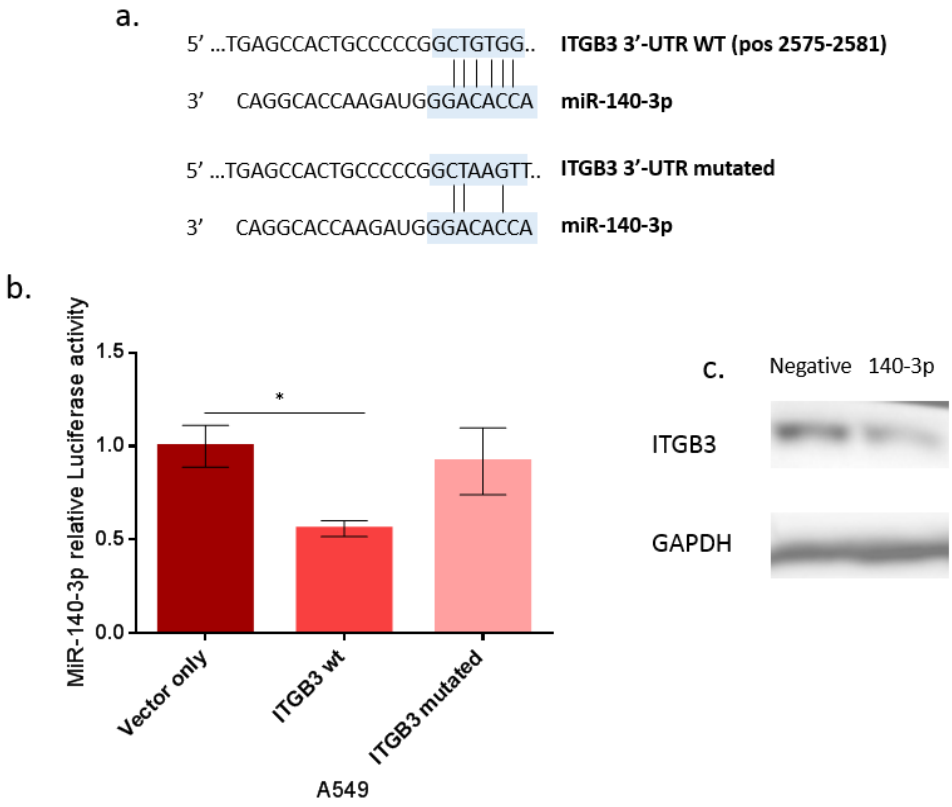

Figure 7.2. Identification of ITGB3 as a direct target of miR-140-3p. a) Predicted binding sites of ITGB3 3'-UTR and miR-140-3p from TargetScan (top). The base pairing between the ITGB3 3'UTR binding site and the seed region of miR-140-3p is underlined. The binding site of miR-140-3p on ITGB3 includes 7 nucleotides (top). The binding site of miR-140-3p and the mutated form of ITGB3 3'-UTR includes 3 nucleotides (bottom). b) Relative luciferase activity levels following 24 hours transfection of A549 cells with the Luciferase reporter vector containing the backbone vector only, ITGB3 3'-UTR (ITGB3 WT) and the mutated form of the 3'-UTR (ITGB3 mutated), respectively. Data are presented as fold change of the mean $\pm$ SEM, three individual experiments were undertaken in triplicate, ANOVA-test was used to assess significance with *$p<0.05$. c) ITGB3 protein is downregulated in A549 cells after 48 hours of transfection with miR-140-3p mimics as shown by western blotting.

The presence of the reporter construct containing the binding site of the wild-type ITGB3 3'-UTR to miR-140-3p in A549 cells led to a significant decrease in luciferase activity ($p=0.0438$) (Figure 7.2b). As a control, in the experiment using the mutated ITGB3 3'-UTR which disrupted miRNA-3'UTR binding (Figure 6.2 a, bottom), the activity of the luciferase in A549 cells was similar to the negative control containing the vector only and, as expected, was not repressed (Figure 7.2 b).

We further validated the result obtained from the luciferase assay through western blotting. Following 48 hours of transfection with negative and miR-140-3p mimics, we verified that the levels of ITGB3 were lower in the cells treated with miR-140-3p than in the control (Figure 7.2 c).

7.3.3 MiR-140-3p suppresses the invasive capability of NSCLC and the ability of the endothelial cells to form new vessels by targeting Integrin-beta3 (ITGB3)

To confirm the ability of miR-140-3p to decrease the invasive properties of A549 cells *in vitro*, I assessed the effect of miR-140-3p mimics treatment on some of the molecular pathways linked to ITGB3 activation. I considered data from western blotting and the Kinexus protein array following 48 hours transfection with negative control or miR-140-3p mimics.

Data from western blotting showed that p-Src (Y 530) levels do not change (Figure 7.3), whereas the oncosuppressor PTEN was slightly up-regulated (Figure 7.3). AKT1 and ERK, two of the downstream effectors of EGFR, were downregulated (Fgure7.3), as was EGFR itself (Figure 7.4). This suggests that miR-140-3p exerts an inhibitory effect on cancer progression, as it may disrupt the crosstalk between integrins and EGFR.

Data from the protein array contradict the western blot results because was shown that EGFR is up-regulated following transfection with miR-140-3p. Despite this, phosphorylated EGFR proteins at tyrosine 998, 1172, 1069, 869, and 1197 were downregulated by miR-140-3p (Table 7.2). Other EGFR downstream molecules, such as ARAF, MEK1 and PI3K were also found to be lower in cells treated with miR-140-3p than in the cells treated with the negative mimics (Table 7.2). The protein array data reported that both the Platelet-derived growth factor receptor PDGFR-A and PDGFR-B, involved in angiogenesis, were regulated by the treatment with miR-140-3p (Table 7.2). In Figure 7.4, the proposed mechanism of action of ITGB3 in lung cancer invasion is shown.

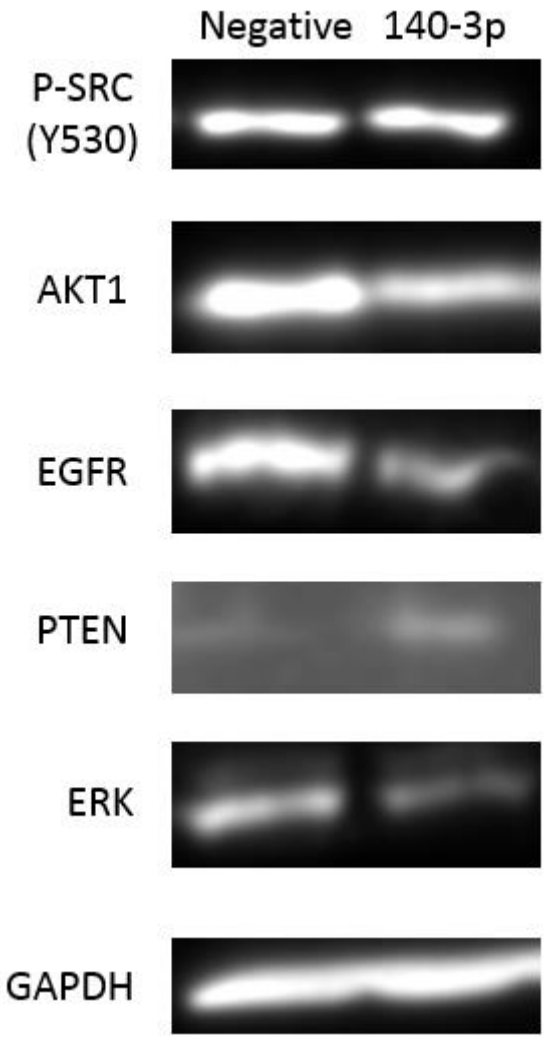

Figure 7.3. Western blotting of key downstream effectors of ITGB3 in A549 cells following 48 hours of transfection with negative control or miR-140-3p mimics. P-Src^{Y530} levels are not affected by the treatment, whereas there is an increase of PTEN levels and a decrease of AKT1, EGFR and ERK.

Table 7.1. Protein expression in A549 cells following a 48 hours transfection with a negative control or a miR-140-3p mimic.

Protein name	Phosphorylation site (Humans)	%CFC (140-3p-negative)
EGFR	Pan-specific	11
EGFR	Y998	-2
EGFR	Y1172	-56
EGFR	Y1069	-4
EGFR	Y869	-12
EGFR	Y1197	-52
ARAF	Pan-specific	-6
MEK1	Pan-specific	-7
PDGFRA	Pan-specific	-11
PDGFRB	Pan-specific	-2

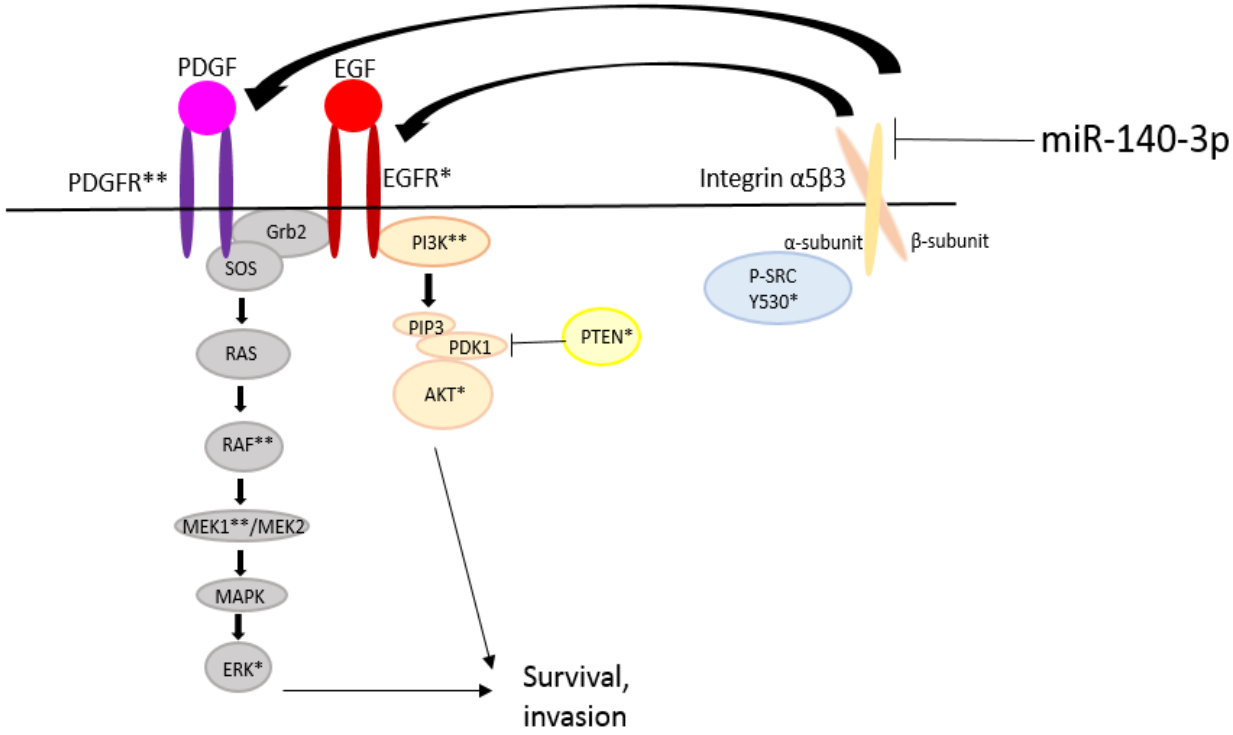

Figure 7.4. Proposed mechanism of action of miR-140-3p in NSCLC. MiR-140-3p reduces the invasive ability of A549 cells and the ability of HUVECs to form vessels by disrupting the interaction between integrins and EGFR and PDGFR respectively. The proteins validated by western blotting were indicated with * and the proteins validated by Kinexus protein array with **.

7.3.4 Global study of the targets of the two forms of miR-140 in A549 cells

Most of the studies seek to identify new direct targets of miRNAs by using bioinformatics algorithms of prediction. However, this approach restricts the discovery of new potential targets to a small group of mRNAs because the *in silico* tools investigate new molecules one by one. As described in Section 2.16, once a potential target is identified, the validation requires the use of cloning techniques and the use of a Luciferase assay and this make the procedure slow. Moreover, when a target is found, the last validation step is by western blotting which requires optimisation, as other pathways may be involved and may compensate for the effect caused by that specific miRNA. Finally, the prediction algorithms consider just the canonical binding of the mRNA to the 3'UTR of the mRNA target, thus omitting any other interaction that may happen in other regions.

All these issues may be overcome by global approaches that allow the study of multiple targets at the same time. In this study, we attempted to identify the potential targets of both forms of miR-140 by mRNA-Seq. The results showed that on a total of 20,816 genes in the Ampliseq, 5,847 were pulled down in A549 cells transfected with either miR-140-3p or 140-5p (Figure 7.5). There were 1141 unique 140-3p enriched genes and 1333 unique miR-140-5p enriched genes (Figure 7.5). The top ten enriched genes were selected for each miR-140 strand and it was found that the binding between the miRNA and the potential target gene was stronger in the samples transfected with miR-140-3p (Tables 7.2 and 7.3). Also, I found that cysteine rich hydrophobic domain 2 (CHIC2) was one of the predicted targets of miR-140-3p and sulfatase 2 (SULF2) was one of the predicted targets of miR-140-5p (Tables 7.2 and 7.3).

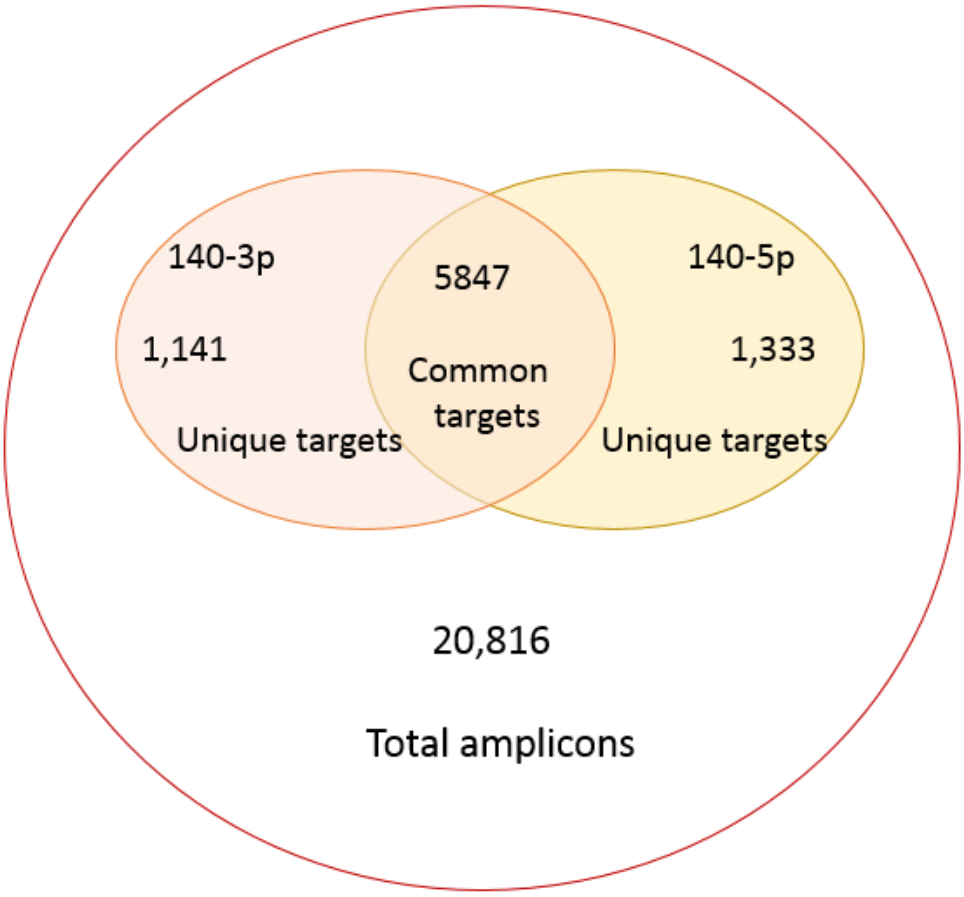

Figure 7.5. Relationship of the gene targets identified by the RNA-sequencing data after biotin-miRNA pulldown. The mRNA gene targets enriched by the biotinylated miR-140-3p and miR-140-5p are indicated in two different groups and the common targets are included in the merged section of the two diagrams.

Table 7.2. Top 10 miR-140-3p enriched genes in A549 cells transfected with biotinylated miR-140-3p mimics.

Target	Log_2 (RPM 140-3p-RPM control)	Role in human cancer	Predicted
SSBP3	1.113	Oncogene (Simonik et al., 2016)	No
TEKT4P2	1.105	Unknown	No
DCLRE1A	1.062	Unknown	No
ZXDA	0.963	Unknown	No
CDC25C	0.948	Oncogene (Yin et al., 2016, Sur and Agrawal, 2016)	No
CD302	0.91	Unknown	No
FBXO46	0.892	Unknown	No
SNX16	0.882	Tumour suppressor (Zhang et al., 2013)	No
HELQ	0.856	Tumour suppressor (Liu et al., 2017)	No
CHIC2	0.856	Unknown	Yes (TargetScan)

Table 7.3. Top 10 miR-140-5p enriched genes in A549 cells transfected with biotinylated miR-140-5p mimics.

Target	Log2 (RPM 140-5p-RPM control)	Role in human cancer	Predicted
CSRNP2	0.837	Unknown	No
CDK3	0.783	Oncogene (Xiao et al., 2017, Wang et al., 2014)	No
DFFB	0.726	Tumour suppressor (Hsieh et al., 2003)	No
COA6	0.606	Unknown	No
MAGI1	0.606	Tumour suppressor (Zhang and Wang, 2011)	No
SULF2	0.606	Oncogene (Zhu et al., 2016, Lui et al., 2016, Lemjabbar-Alaoui et al., 2010)	Yes (TargetScan)
ZNF101	0.606	Unknown	No
CCDC144B	0.542	Unknown	No
PCOLCE	0.542	Oncogene (Anastassiou et al., 2011)	No
SNORA70F	0.542	Unknown	No

7.3.5 MiR-140-5p may limit NSCLC progression by targeting the cyclin-dependent kinase 3 (CDK3) and the sulfatase 2 (SULF2)

Data from RNA-sequencing suggests that CDK3 and SULF2 might be two potential targets of miR-140-3p. SULF2 was also predicted by TargetScan. To better investigate this finding, I verified the protein levels of two downstream molecules influenced by CDK3 and SULF2, which are EGFR and β-catenin, respectively. By western blotting, both EGFR and β-catenin were found to be downregulated in A549 cells treated with miR-140-5p mimics (Figure 7.6). Notably, the levels of β-catenin were not affected by miR-140-3p, thus suggesting that the two forms of miR-140 may suppress the invasion properties of NSCLC cells by acting on different molecular pathways.

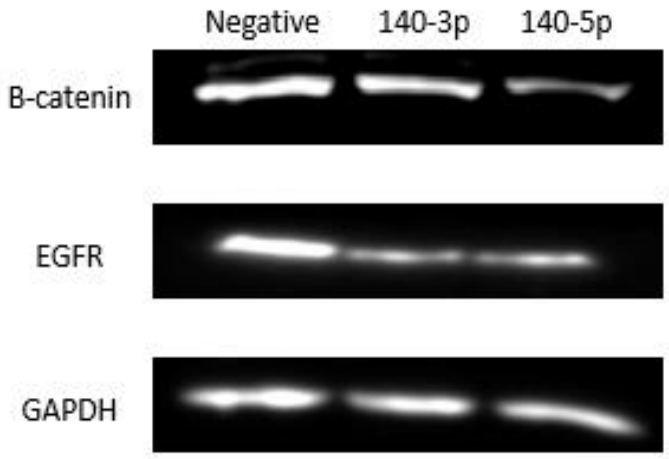

Figure 7.6. Western blotting of β-catenin and EGFR in A549 cells following 48 hours of transfection with negative, miR-140-3p and miR-140-5p mimics. B-catenin levels are lower in cells treated with miR-140-5p mimics. EGFR levels decrease in cells treated with miR-140-3p and miR-140-5p.

7.4 Discussion

In this chapter, I investigated the molecular mechanisms involved in the inhibition of the invasive properties of NSCLC cells following treatment with miR-140-3p and miR-140-5p mimics respectively.

In EMT, the tumour cells lose their epithelial morphology and characteristics and acquire some mesenchymal-like properties that enable them to survive and form metastasis in distant sites (Zeisberg and Neilson, 2009). I focused on some EMT markers specifically involved in lung cancer progression, such as E-cadherin, N-cadherin, Snail, Slug and Vimentin (Heerboth et al., 2015). Both miR-140-3p and miR-140-5p were found to restore the normal levels of E-cadherin and reduce N-cadherin, Vimentin, Slug and Snail expression. These finding strengthen my previous data from the migration and invasion assays and guided my research on the discovery of some novel direct targets of miR-140-3p and miR-140-5p.

The challenge in the study of miRNAs is the identification of the directly targeted mRNAs. Although most of the miRNA-mRNA interactions occur between the seed region of the miRNA and the 3'UTR of the mRNA, more-non canonical bindings have been discovered (Martin et al., 2014), thus making the search for novel targets more complicated. Bioinformatics tools are widely used to predict the potential targets of a miRNA. However, the biological validation of the predicted molecules often fails. This may be due to the low or lack of expression of the miRNA in a specific tissue or in a specific phase of the cell cycle. Moreover, as previously stated, the computational methods consider only the canonical seed region-3'UTR interactions, thus excluding other types of binding, outside the 3'-UTR (Barbato et al., 2009, Hausser and Zavolan, 2014).

Finally, different algorithms often produce different results with no overlap at all and this may discourage the researcher from undertaking any further validation.

Many techniques have been recently developed to integrate bioinformatics techniques as the identification of a single target may not reflect the global physiological effect of a specific miRNA. In one of these methods biotinylated miRNAs at the 3'UTR are delivered into cells, purified together with bound mRNAs through a streptavidin-base technique after which the mRNA profile can be identified using microarray or sequencing. The biotinylated mimics are incorporated into the miRNA-induced silencing complex (RISC) and bind their mRNA targets. This technique leads to the discovery of many *bona fide* targets at the same time, thus allowing a more effective and reliable study of a single miRNA and its direct targets (Tan et al., 2014).

My RNA-Seq data showed that the two forms of miR-140 have different targets. MiR-140-5p appears to be able to target more mRNAs than its sister strand but miR-140-3p binds its targets more specifically. The main limitation of this experiment is the lack of replicate data. For a matter of time, the RNA sequencing after biotin-miRNA pulldown was only carried out once. These experiments should be repeated two more times at least to make these observations more reliable. However, the first result is very encouraging because I found two targets already predicted by *in silico* tools.

Although both miR-140-3p and miR-140-5p reduced the invasive properties of the lung cancer cells by inhibiting the EMT process, I have mainly focused on the potential direct targets of miR-140-3p for two main reasons: Firstly, although there is no a proper strand selection in normal lung cells, miR-140-3p is the

predominant strand in both normal and lung cancer cell lines. Secondly, miR-140-3p has an inhibitory effect on both cancer invasion and the tubule formation ability of the endothelial cells, thus making its role as therapeutic agent more attractive.

Thanks to the "classical" bioinformatics approach, I have discovered that miR-140-3p targets ITGB3 by binding its 3'UTR. The lower expression of ITGB3 following the treatment with miR-140-3p mimics may explain the decrease in invasion observed in the A549 cells as well as the inhibition of HUVEC tubule formation. In fact, it has been demonstrated that epigenetic modifications may occur far from the primary tumour and that the stromal cells themselves change their epigenome during EMT (Heerboth et al., 2015). There is a crosstalk between the stromal and cancer cells in a paracrine manner, as some miRNAs released in the tumour microenvironment by the malignant cells can modify the cell transcriptome of other cells, including endothelial cells, thus stimulating tumour growth, angiogenesis and metastasis. For example, miR-105 from metastatic breast cancer cells is packed into exosomes and delivered to the endothelial cells, thus facilitating the vascular permeability and the metastatic process by targeting the tight junction protein ZO-1 (Zhou et al., 2014).

It is likely that miR-140-3p limits the invasion of A549 cells by targeting ITGB3 on A549 and endothelial cells for three main reasons. First of all, ITGB3 has been found to be up-regulated in both cancer and endothelial cells (Desgrosellier and Cheresh, 2010). Secondly, the media from cells transfected with miR-140-3p mimics is taken from the cells after 24 hours of treatment at which time point there is the highest concentration of the miRNA and thus may be incorporated in the endothelial cells. Finally, the inhibition of the HUVEC tubule formation

ability by conditioned medium from miR-140-3p transfected NSCLC cells is VEGF-A independent (Chapter 5) and other studies have shown the involvement of ITGB3 in angiogenesis (Hood et al., 2003). It is known that integrins partially activate the EGFR signalling pathway (Bill et al., 2004). My data demonstrated that miR-140-3p can disrupt EGFR regulation by targeting ITGB3 in a Src-independent manner. Src has two phosphorylation sites important for its activation, Tyr530 and Tyr419. In this study the carboxy-terminal Tyr530 has been considered, as it is the crucial site for Src activation (Bjorge et al., 2000). Dephosphorylation of Tyr530 opens up the molecule to an active state. Although the Kinexus data showed a decrease in p-Src^{Tyr530}, the western blotting seemed to show that this p-Src^{Tyr530} protein is not significantly affected by the treatment with miR-140-3p.

Integrins also interact with other growth factor receptors involved in angiogenesis, including PDGFR-A and PDGFR-B (Bill et al., 2004, Somanath et al., 2009). My data shows that the inhibition of the tubule formation ability of HUVECs may be due to the lack of activation of PDGF receptors by ITGB3.

I investigated the RNA-Seq data to identify any potential targets of miR-140-5p. I focused on CDK3 and SULF2 because their role as oncogenes has been previously demonstrated (Xiao et al., 2017, Wang et al., 2014, Zhu et al., 2016, Lui et al., 2016, Lemjabbar-Alaoui et al., 2010). I performed a preliminary validation by western blotting and considered EGFR and β-catenin, as their expression is influenced by CDK3 and SULF2, respectively (Xiao et al., 2017, Lemjabbar-Alaoui et al., 2010). I found that the treatment with miR-140-5p mimics reduced the protein levels of both of these molecules. This finding reinforced the RNA-Seq data and may confirm the repressive activity of miR-

140-5p on the invasion properties of NSCLC cells that I demonstrated through specific functional assays.

CHAPTER 8

GENERAL DISCUSSION AND FUTURE WORK

Lung cancer is the most frequently diagnosed cancer worldwide, in both men and women, with 46,403 new cases diagnosed in the UK in 2014 . Historically, lung cancers from the cells of the respiratory epithelium have been broadly classified into two types based on the microscopic appearance of the tumour, NSCLC and SCLC. In this study, I focused on NSCLC, as it is the most common type accounting for about 85-90% of all cases .

The diagnosis based on the histological characteristics is not the only feature that should be considered for the treatment of NSCLC patients, therefore a histological and molecular diagnostic is desirable (Reck et al., 2013). For many years, the standard chemotherapeutics for NSCLC were based exclusively on the use of cytotoxic compounds. However, by using drugs able to target specific molecular pathways, such as the EGFR inhibitors, as a second or third line therapy in eligible patients, it is now possible to improve the overall survival of the patients and shows additional clinical benefits, such as a lower cytotoxicity. However, not all patients affected by NSCLC show the same genetic mutations. (Reck et al., 2013). In addition, although these oncogene-specific treatments have some beneficial effects, some patients acquire resistance after the treatment which may be due to two main mechanisms (Reck et al., 2013): the target gene may undergo to a second mutation, thus making the binding between the inhibitor and the target less efficient, or there could be some downstream signals that bypass the inhibitory effect of a particular drug (Reck et al., 2013). Moreover, it has been demonstrated that the tumour microenvironment plays a crucial role in tumour development and may influence the efficacy of the anti-cancer treatments (Hanahan and Weinberg, 2011, Swartz et al., 2012). In this context, some anti-cancer treatments specific for the stromal cells have been

developed. Avastin, for example, is an anti-angiogenic drug, used as a second-line therapy for many cancers, including NSCLC (Reck et al., 2013). Although the use of Avastin improved the overall survival of some eligible patients, its high toxicity together with a limited efficacy restricts its administration to a small cohort of patients (Reck et al., 2013, Swartz et al., 2012). This is because cancer is a multi-step process, involves many molecules (Hanahan and Weinberg, 2011) and for this reason targeting just one aspect may not be enough to halt the spread of the malignancy.

In the last few years, specific epigenetic signatures, such as histone modifications, DNA methylation and miRNA regulation, have been associated with many tumours, including NSCLC (Ansari et al., 2016). Some drugs that act on the epigenome of NSCLC patients have been tested but failed at the clinical trial stages (Ansari et al., 2016, Mehta et al., 2015).

In the current study, a miRNA based approach for the treatment of NSCLC has been investigated *in vitro*. I propose that miRNAs represent a new opportunity for cancer treatment because of their intrinsic characteristics, such as their low molecular weight and small size, together with their ability to target multiple molecules with lower toxicity. So far, some miRNA mimics and inhibitors have been tested and included in clinical trials (Rupaimoole and Slack, 2017). MRX34, for example, is a compound that mimics miR-34a and has just completed a phase 1 clinical trial in humans for the treatment of multiple solid tumours (Rupaimoole and Slack, 2017). MiR-34a is normally lost in cancer and this leads to the activation of some oncogenic pathways, because miR-34a usually targets key mRNAs involved in tumour progression, such as MET, MEK1, MYC,

PDGFR-A, Cyclin-dependent kinases 4/6 (CDK4/6), BCL2, WNT 1/3, Notch1, CD44 and the Programmed death-ligand 1 (PD-L1) (Beg et al., 2017).

I focused on both of the mature strands of miR-140, named miR-140-3p and miR-140-5p respectively. In the classic model of miRNA biogenesis, the duplex of mature miRNAs is produced by Dicer processing of the hairpin precursor. Then, a following strand selection step determines which mature miRNA acts as a guide for the mature miRISC. The strand selection process is tightly regulated and may vary among tissues and between normal and malignant cells (Tsai et al., 2016).

Recent studies introduced innovative concepts and unravelled that both sister mature miRNAs may be accumulated in some tissues and cell types. In this scenario, the strand selection might be tissue-specific but not deterministic, and a given strand could act as a guide strand in a specific cell type and a passenger in another one (Li et al., 2012, Hu et al., 2009).

In this respect, different biological contexts most likely share complex mechanisms of strand selection regulation, leading either to the alternative expression of a single mature form or to the concurrent expression of both mature sister miRNAs (Salvatore et al., 2016).

It has previously been demonstrated that both miR-140-3p and miR-140-5p are downregulated in NSCLC and this is associated with the progression of the malignancy (Yuan et al., 2013, Dong et al., 2016, Li and He, 2014). Also, a different maturation of the sister strands due to a SNP (rs7205289: C>A) on pre-miR-140 sequence, leads to an increase of miR-140-3p and a decrease of miR-140-5p levels and this contributes to the cleft palate syndrome, as the

regulation of PDGFR-A by miR-140-5p is lost (Li et al., 2010). Considering this, I decided to investigate the role of both of the forms of miR-140 in NSCLC and see whether a different strand selection plays a role in the progression of the disease. Moreover, I attempted to identify novel targets of the two forms of miR-140 not only by considering the potential targets one by one but also by using a global approach that combined the analysis of the transcriptome and the proteome of cancer cells treated with either miR-140-3p or miR-140-5p.

In the current study I have confirmed that both miR-140-3p and miR-140-5p are downregulated in A549 and SK-MES-1 lung cancer cell lines compared to a "normal" lung cell BEAS-2B. Most importantly these results were also confirmed in the clinical context, as samples from human lung cancer tumours expressed significantly less miR-140-3p and miR-140-5p than specimens taken from a non-cancerous lung region.

In A549 and SK-MES-1 lung cancer cells miR-140-3p is the predominant and the most stable strand compared to miR-140-5p. After transfection with miRNA mimics, the levels of miR-140-3p remain much higher over time than miR-140-5p in both A549 and SK-MES-1 cells. Also, in SK-MES-1 cells, the levels of both miR-140-3p and miR-140-5p are lower than in A549. In contrast, there is no strand selection in the normal control cell line, BEAS-2B, suggesting the miR-140-3p strand may have a more important role to play in cancer cells.

By sequencing, I found that the pre-miR-140 of SK-MES-1 has two DNA variants, one in the regions encoding for miR-140-3p and another one in the region encoding for miR-140-5p. I then speculated that these may affect the miRNA biogenesis process and the progression of the malignancy, as in the case

of the congenital malformations (Li et al., 2010). However, these results would benefit from further validation.

Increasing the expression level of either miR-140-3p or miR-140-5p was found to reduce the ability of the A549 NSCLC cells to invade and increased their ability to adhere. Increasing the level of miR-140-3p in these cells also inhibited the tubule formation ability of endothelial cells. Although this was only an *in vitro* study; in a broader context it is suggesting that treatments aimed to increase miR-140-3p expression could potentially be considered to play a role in preventing primary tumours from dissociating, metastasising and stimulating angiogenesis.

I have attempted to identify whether the inhibitory effect on the tubule formation ability of the endothelial cells was due to factors released by the miRNA-transfected cancer cells themselves or by the miR-140-3p itself. It has previously been demonstrated that miRNAs in the tumour microenvironment can be internalised into the endothelial cells and halt angiogenesis (Zhou et al., 2014) and reports show that VEGF-A and PDGFR-A are deeply involved in tumour angiogenesis and are targeted by miR-140-5p (Zhang et al., 2015, Eberhart et al., 2008). In contrast to these previous studies, I found that medium from NSCLC cells transfected with miR-140-5p had no significant effect on HUVEC tubule formation. It is probable that many of the previous findings are cell-type specific, because, although I found that the factors produced by A549 cells treated with miR-140-3p did impair tubule forming ability of HUVECs; my studies have also shown that this occurred in a VEGF-A independent manner. The important "angiogenesis" inhibitory factor used here remains unknown, but my studies have identified a list of possible mechanisms.

First I did consider whether changes in the metabolism of the cancer cells might have any effect on the endothelial cells in the tumour microenvironment. It is known that cancer cells undergo to a "metabolic switch" and use the glycolysis instead of the aerobic respiration to produce energy, with the release of lactic acid in the extracellular space (Liberti and Locasale, 2016, Cairns et al., 2011). This process is regulated by miRNAs in many tumours, including lung (Liu et al., 2016a). However, my data demonstrated that the metabolism of the cancer cells does not appear to be significantly affected by the treatment with miR-140-3p and miR-140-5p mimics. Therefore, I conclude that the inhibitory effect of miR-140-3p on endothelial cells may be due to the miR-140-3p itself, that may be included in the receiver cells and inhibits the formation of the tubules. Incidentally, the metabolic "switch" to glycolysis is actually something that is quite difficult to investigate in vitro where cancer cells are grown as monolayers where gaseous exchange easily occurs. *In vivo* the cells at the centre of a tumour mass are more likely to be starved of oxygen and hence may switch to glycolysis. In the future, the miRNA effect on cancer metabolism may be more easily studied in vitro using 3D models.

When considering potential targets of miR-140-3p, that might reduce both the invasion properties of the NSCLC cells and the tubule formation ability of the endothelial cells, a number of signalling molecules were investigated.

Firstly, I found that some key molecules involved in the EMT were downregulated following the transfection of NSCLC with miR-140-3p. Using bioinformatics tools, I demonstrated that ITGB3 is one of the direct targets of miR-130-3p. ITGB3 together with its partner, integrin-α5, forms a complex named αvβ3. This complex binds component of the ECM and interacts with

growth factors, such as EGFR and VEGFR2, to promote the invasion of cancer cells and tumour-associated angiogenesis (Desgrosellier and Cheresh, 2010). ITGB3 normally has low expression levels in normal epithelial cells but its levels increase in many tumours, including lung, and targeting integrins as a strategy to reduce the cancer progression has been successful in both *in vitro* and *in vivo* models (Desgrosellier and Cheresh, 2010, Weis and Cheresh, 2011). It has also been suggested by a previous study that integrins sometimes promote the metastasis formation through the Src family kinase signalling (Desgrosellier and Cheresh, 2010). In other cases, Src is not required, such as in the VEGF-A independent angiogenesis (Hood et al., 2003). Using a bioinformatics approach, I have identified that A549 cells express ITGB3 and by western blotting have shown that this protein is downregulated in cells transfected with miR-140-3p. Western blotting has shown that EGFR and Akt signalling proteins are also down regulated by miR-140-3p, but p-src levels are unchanged. This has led to the proposal that miR-140-3p may inhibit the invasive properties of the tumour cells by targeting ITGB3 with a Src-independent mechanism.

I have also demonstrated that the downregulation of ITGB3 leads to a decrease of EGFR signalling pathway, thus confirming the link between miR-140-3p and this key growth factor receptor in lung cancer (Desgrosellier and Cheresh, 2010). I have hypothesised that miR-140-3p potentially inhibits the lung cancer progression by disrupting the tyrosine kinase activity of EGFR and inhibits the tubule formation of HUVECs by blocking the cascade of the Platelet-Derived Growth Factor Receptors, PDGFR-A and PDGFR-B. According to my data, miR-140-3p induced inhibition of tubule formation by the endothelial cells appears to be independent of VEGF-A. This conforms to previous findings, in

which it has been demonstrated that integrin antagonists may not require Src in the VEGF-A independent angiogenesis (Hood et al., 2003).

The mRNA sequencing study demonstrated that the two forms of miR-140 have different targets, some of them predicted by the bioinformatics tools. Although this experiment needs to be repeated to integrate and overcome all the limits of the investigation made using mathematical algorithms, I verified that CDK3 and SULF2 may be two targets of miR-140-5p. In addition to its role in the cell cycle regulation, CDK3 indirectly enhances the EGFR-dependent transformation, as previously demonstrated (Xiao et al., 2017). On the other hand, a reduction of SULF2 levels, may reduce Wnt signalling pathway (Lemjabbar-Alaoui et al., 2010), thus leasing to a reduction of the invasive properties of lung cancer cells.

The main limitation of this study is the lack of investigation into the contribution of the microenvironment to the molecular pathways involved in ITGB3 downregulation by miR-140-3p. ITGB3 expression is frequently induced by the Transforming growth factor beta (TGFβ) secreted by the stromal cells. It acts as an inducer of the EMT (Hong et al., 2016) and is deeply involved in the regulation of both NSCLC and miR-140-5p (Ischenko et al., 2014, Tardif et al., 2013). This extracellular signalling may explain why I did not see any significant changes in some key cancer aspects, such as proliferation and apoptosis, following the treatment with miR-140-3p and miR-140-5p mimics in A549 and SK-MES-1 cells.

Integrin antagonists, such as the anti-αvβ3, Cilengitide, have shown positive results in Phase II clinical trials in prostate and lung cancer (Desgrosellier and Cheresh, 2010). The prolonged use of integrin antagonists, however, stimulated angiogenesis in mice (Desgrosellier and Cheresh, 2010). In this scenario, the use

of miRNA mimics, which have the ability to target multiple pathways simultaneously, may be a better strategy to prevent the tumour growth.

Future work

This work demonstrates the potential impact of the two forms of miR-140 on the invasive properties of NSCLC. However, there are some limitations that need to be solved before I translate this study to an *in vivo* model. It is essential to understand whether miR-140-3p and miR-140-5p are still able to reduce the progression of the malignancy in the presence of some external stimuli from the tumour microenvironment. For instance, the exposure of lung cancer cells to TGF-β may be useful to address this aspect. I also speculate that miR-140-3p is encapsulated in the endothelial cells and may inhibit the tubule formation ability of the endothelial cells by targeting ITGB3. This finding may require an extensive validation on endothelial cells and in the presence of other tumour-associated cells (*eg* stromal and fibroblast cells *etc*). A repetition of the RNA-Sequencing not only in lung cancer cell lines but also in NSCLC primary cells treated with biotinylated miR-140-3p and miR-140-5p mimics, would be valuable to evaluate the reproducibility and clinical impact of my work. The delivery of both the strands of the miR-140 mimics into an appropriate *in vivo* model using a clinical-feasible strategy would be desirable for translational research.

REFERENCES

http://www.cancer.org/cancer/non-small-cell-lung-cancer/about/key-statistics.html [Online].

http://www.cancerresearchuk.org/health-professional/cancer-statistics/statistics-by-cancer-type/lung-cancer/incidence [Online].

ALBINI, A. & SPORN, M. B. 2007. The tumour microenvironment as a target for chemoprevention. *Nat Rev Cancer,* 7**,** 139-147.

ALTOMARE, D. A. & TESTA, J. R. 2005. Perturbations of the AKT signaling pathway in human cancer. *Oncogene,* 24**,** 7455-64.

AMBROS, V. & HORVITZ, H. 1984. Heterochronic mutants of the nematode. *Science,* 226**,** 409-416.

AMBROS, V. & HORVITZ, H. R. 1987. The lin-14 locus of Caenorhabditis elegans controls the time of expression of specific postembryonic developmental events. *Genes & development,* 1**,** 398-414.

AMBROS, V., LEE, R. C., LAVANWAY, A., WILLIAMS, P. T. & JEWELL, D. 2003. MicroRNAs and other tiny endogenous RNAs in C. elegans. *Current Biology,* 13**,** 807-818.

ANASTASIOU, D. 2017. Tumour microenvironment factors shaping the cancer metabolism landscape. *Br J Cancer,* 116**,** 277-286.

ANASTASSIOU, D., RUMJANTSEVA, V., CHENG, W., HUANG, J., CANOLL, P. D., YAMASHIRO, D. J. & KANDEL, J. J. 2011. Human cancer cells express Slug-based epithelial-mesenchymal transition gene expression signature obtained in vivo. *BMC Cancer,* 11**,** 529.

ANDO, Y., MAIDA, Y., MORINAGA, A., BURROUGHS, A. M., KIMURA, R., CHIBA, J., SUZUKI, H., MASUTOMI, K. & HAYASHIZAKI, Y. 2011. Two-step cleavage of hairpin RNA with 5'overhangs by human DICER. *BMC molecular biology,* 12**,** 6.

ANSARI, J., SHACKELFORD, R. E. & EL-OSTA, H. 2016. Epigenetics in non-small cell lung cancer: from basics to therapeutics. *Transl Lung Cancer Res,* 5**,** 155-71.

ARROYO, J. D., CHEVILLET, J. R., KROH, E. M., RUF, I. K., PRITCHARD, C. C., GIBSON, D. F., MITCHELL, P. S., BENNETT, C. F., POGOSOVA-AGADJANYAN, E. L. & STIREWALT, D. L. 2011. Argonaute2 complexes carry a population of circulating microRNAs independent of vesicles in human plasma. *Proceedings of the National Academy of Sciences,* 108**,** 5003-5008.

ATTOUB, S., RIVAT, C., RODRIGUES, S., VAN BOCXLAER, S., BEDIN, M., BRUYNEEL, E., LOUVET, C., KORNPROBST, M., ANDRE, T., MAREEL, M., MESTER, J. & GESPACH, C. 2002. The c-kit tyrosine kinase inhibitor STI571 for colorectal cancer therapy. *Cancer Res,* 62**,** 4879-83.

AZIZ, N. & MUNRO, H. N. 1987. Iron regulates ferritin mRNA translation through a segment of its 5'untranslated region. *Proceedings of the National Academy of Sciences,* 84**,** 8478-8482.

BARBATO, C., ARISI, I., FRIZZO, M. E., BRANDI, R., DA SACCO, L. & MASOTTI, A. 2009. Computational challenges in miRNA target predictions: to be or not to be a true target? *J Biomed Biotechnol,* 2009**,** 803069.

BARTEL, D. P. 2009. MicroRNAs: target recognition and regulatory functions. *Cell,* 136**,** 215-233.

BEG, M. S., BRENNER, A. J., SACHDEV, J., BORAD, M., KANG, Y. K., STOUDEMIRE, J., SMITH, S., BADER, A. G., KIM, S. & HONG, D. S. 2017. Phase I study of

MRX34, a liposomal miR-34a mimic, administered twice weekly in patients with advanced solid tumors. *Invest New Drugs,* 35**,** 180-188.
BENES, V. & CASTOLDI, M. 2010. Expression profiling of microRNA using real-time quantitative PCR, how to use it and what is available. *Methods,* 50**,** 244-249.
BERNSTEIN, E., CAUDY, A. A., HAMMOND, S. M. & HANNON, G. J. 2001. Role for a bidentate ribonuclease in the initiation step of RNA interference. *nature,* 409**,** 363-366.
BILL, H. M., KNUDSEN, B., MOORES, S. L., MUTHUSWAMY, S. K., RAO, V. R., BRUGGE, J. S. & MIRANTI, C. K. 2004. Epidermal growth factor receptor-dependent regulation of integrin-mediated signaling and cell cycle entry in epithelial cells. *Mol Cell Biol,* 24**,** 8586-99.
BJORGE, J. D., JAKYMIW, A. & FUJITA, D. J. 2000. Selected glimpses into the activation and function of Src kinase. *Oncogene,* 19**,** 5620-35.
BOYDEN, S. 1962. The chemotactic effect of mixtures of antibody and antigen on polymorphonuclear leucocytes. *J Exp Med,* 115**,** 453-66.
BURKE, J. M., KELENIS, D. P., KINCAID, R. P. & SULLIVAN, C. S. 2014. A central role for the primary microRNA stem in guiding the position and efficiency of Drosha processing of a viral pri-miRNA. *rna*.
BUSTIN, S. A. 2000. Absolute quantification of mRNA using real-time reverse transcription polymerase chain reaction assays. *Journal of molecular endocrinology,* 25**,** 169-193.
BUTLER, C. T., REYNOLDS, A. L., TOSETTO, M., DILLON, E. T., GUIRY, P. J., CAGNEY, G., O'SULLIVAN, J. & KENNEDY, B. N. 2017. A Quininib Analogue and Cysteinyl Leukotriene Receptor Antagonist Inhibits Vascular Endothelial Growth Factor (VEGF)-independent Angiogenesis and Exerts an Additive Antiangiogenic Response with Bevacizumab. *J Biol Chem,* 292**,** 3552-3567.
CAIRNS, R. A., HARRIS, I. S. & MAK, T. W. 2011. Regulation of cancer cell metabolism. *Nature Reviews Cancer,* 11**,** 85-95.
CALIN, G. A. 2007. Ultraconserved regions encoding ncRNAs are altered in human leukemias and carcinomas. *Cancer Cell,* 12**,** 215-229.
CALIN, G. A. & CROCE, C. M. 2006. MicroRNA signatures in human cancers. *Nat Rev Cancer,* 6**,** 857-66.
CALIN, G. A., DUMITRU, C. D., SHIMIZU, M., BICHI, R., ZUPO, S., NOCH, E., ALDLER, H., RATTAN, S., KEATING, M., RAI, K., RASSENTI, L., KIPPS, T., NEGRINI, M., BULLRICH, F. & CROCE, C. M. 2002. Frequent deletions and down-regulation of micro- RNA genes miR15 and miR16 at 13q14 in chronic lymphocytic leukemia. *Proc Natl Acad Sci U S A,* 99**,** 15524-9.
CALIN, G. A., SEVIGNANI, C., DUMITRU, C. D., HYSLOP, T., NOCH, E., YENDAMURI, S., SHIMIZU, M., RATTAN, S., BULLRICH, F., NEGRINI, M. & CROCE, C. M. 2004. Human microRNA genes are frequently located at fragile sites and genomic regions involved in cancers. *Proc Natl Acad Sci U S A,* 101**,** 2999-3004.
CHATTERJEE, S., FASLER, M., BUSSING, I. & GROSSHANS, H. 2011. Target-mediated protection of endogenous microRNAs in C. elegans. *Dev Cell,* 20**,** 388-96.
CHEN, C., TAN, R., WONG, L., FEKETE, R. & HALSEY, J. 2011a. Quantitation of microRNAs by real-time RT-qPCR. *Methods Mol Biol,* 687**,** 113-34.
CHEN, C., TAN, R., WONG, L., FEKETE, R. & HALSEY, J. 2011b. Quantitation of MicroRNAs by Real-Time RT-qPCR. *In:* PARK, D. J. (ed.) *PCR Protocols.* Humana Press.

CHEN, Y., ZHU, X., ZHANG, X., LIU, B. & HUANG, L. 2010. Nanoparticles modified with tumor-targeting scFv deliver siRNA and miRNA for cancer therapy. *Mol Ther,* 18**,** 1650-6.

CHENDRIMADA, T. P., GREGORY, R. I., KUMARASWAMY, E., NORMAN, J., COOCH, N., NISHIKURA, K. & SHIEKHATTAR, R. 2005. TRBP recruits the Dicer complex to Ago2 for microRNA processing and gene silencing. *Nature,* 436**,** 740-744.

CHIN, L. J., RATNER, E., LENG, S., ZHAI, R., NALLUR, S., BABAR, I., MULLER, R. U., STRAKA, E., SU, L., BURKI, E. A., CROWELL, R. E., PATEL, R., KULKARNI, T., HOMER, R., ZELTERMAN, D., KIDD, K. K., ZHU, Y., CHRISTIANI, D. C., BELINSKY, S. A., SLACK, F. J. & WEIDHAAS, J. B. 2008. A SNP in a let-7 microRNA complementary site in the KRAS 3' untranslated region increases non-small cell lung cancer risk. *Cancer Res,* 68**,** 8535-40.

CHOI, K. Y., SILVESTRE, O. F., HUANG, X., HIDA, N., LIU, G., HO, D. N., LEE, S., LEE, S. W., HONG, J. I. & CHEN, X. 2014. A nanoparticle formula for delivering siRNA or miRNAs to tumor cells in cell culture and in vivo. *Nat Protoc,* 9**,** 1900-15.

CONRAD, T., MARSICO, A., GEHRE, M. & ØROM, U. A. 2014. Microprocessor activity controls differential miRNA biogenesis in vivo. *Cell reports,* 9**,** 542-554.

DANGWAL, S., STRATMANN, B., BANG, C., LORENZEN, J. M., KUMARSWAMY, R., FIEDLER, J., FALK, C. S., SCHOLZ, C. J., THUM, T. & TSCHOEPE, D. 2015. Impairment of Wound Healing in Patients With Type 2 Diabetes Mellitus Influences Circulating MicroRNA Patterns via Inflammatory Cytokines. *Arterioscler Thromb Vasc Biol,* 35**,** 1480-8.

DE BOER, H. C., VAN SOLINGEN, C., PRINS, J., DUIJS, J. M., HUISMAN, M. V., RABELINK, T. J. & VAN ZONNEVELD, A. J. 2013. Aspirin treatment hampers the use of plasma microRNA-126 as a biomarker for the progression of vascular disease. *Eur Heart J,* 34**,** 3451-7.

DESGROSELLIER, J. S. & CHERESH, D. A. 2010. Integrins in cancer: biological implications and therapeutic opportunities. *Nat Rev Cancer,* 10**,** 9-22.

DETTERBECK, F. C., BOFFA, D. J. & TANOUE, L. T. 2009. The new lung cancer staging system. *Chest,* 136**,** 260-71.

DI LEVA, G. & CROCE, C. M. 2013. miRNA profiling of cancer. *Curr Opin Genet Dev,* 23**,** 3-11.

DIAZ-GARCIA, C. V., AGUDO-LOPEZ, A., PEREZ, C., LOPEZ-MARTIN, J. A., RODRIGUEZ-PERALTO, J. L., DE CASTRO, J., CORTIJO, A., MARTINEZ-VILLANUEVA, M., IGLESIAS, L., GARCIA-CARBONERO, R., FRESNO VARA, J. A., GAMEZ-POZO, A., PALACIOS, J., CORTES-FUNES, H., PAZ-ARES, L. & AGULLO-ORTUNO, M. T. 2013. DICER1, DROSHA and miRNAs in patients with non-small cell lung cancer: implications for outcomes and histologic classification. *Carcinogenesis,* 34**,** 1031-8.

DÍAZ, M., HERRERO, M., GARCÍA, L. A. & QUIRÓS, C. 2010. Application of flow cytometry to industrial microbial bioprocesses. *Biochemical engineering journal,* 48**,** 385-407.

DICTIONARY.COM. 2014.

DONG, W., YAO, C., TENG, X., CHAI, J., YANG, X. & LI, B. 2016. MiR-140-3p suppressed cell growth and invasion by downregulating the expression of ATP8A1 in non-small cell lung cancer. *Tumour Biol,* 37**,** 2973-85.

DUROUX-RICHARD, I., ROUBERT, C., AMMARI, M., PRESUMEY, J., GRUN, J. R., HAUPL, T., GRUTZKAU, A., LECELLIER, C. H., BOITEZ, V., CODOGNO, P.,

ESCOUBET, J., PERS, Y. M., JORGENSEN, C. & APPARAILLY, F. 2016. miR-125b controls monocyte adaptation to inflammation through mitochondrial metabolism and dynamics. *Blood,* 128**,** 3125-3136.
DWEEP, H., STICHT, C., PANDEY, P. & GRETZ, N. 2011. miRWalk–database: prediction of possible miRNA binding sites by "walking" the genes of three genomes. *Journal of biomedical informatics,* 44**,** 839-847.
EBERHART, J. K., HE, X., SWARTZ, M. E., YAN, Y. L., SONG, H., BOLING, T. C., KUNERTH, A. K., WALKER, M. B., KIMMEL, C. B. & POSTLETHWAIT, J. H. 2008. MicroRNA Mirn140 modulates Pdgf signaling during palatogenesis. *Nat Genet,* 40**,** 290-8.
EBERT, M. S., NEILSON, J. R. & SHARP, P. A. 2007. MicroRNA sponges: competitive inhibitors of small RNAs in mammalian cells. *Nat Methods,* 4**,** 721-6.
ECKERT, K. A. & KUNKEL, T. A. 1991. DNA polymerase fidelity and the polymerase chain reaction. *Genome Research,* 1**,** 17-24.
ESQUELA-KERSCHER, A., TRANG, P., WIGGINS, J. F., PATRAWALA, L., CHENG, A., FORD, L., WEIDHAAS, J. B., BROWN, D., BADER, A. G. & SLACK, F. J. 2008. The let-7 microRNA reduces tumor growth in mouse models of lung cancer. *Cell Cycle,* 7**,** 759-64.
ESTELLER, M. 2011. Non-coding RNAs in human disease. *Nat Rev Genet,* 12**,** 861-874.
FERLAY J, S. I., ERVIK M, ET AL. 2013. Cancer Incidence and Mortality Worldwide: IARC CancerBase No. 11 [Internet]. *In:* CANCER, I. A. F. R. O. (ed.). Lyon, France.
FERLAY, J., SOERJOMATARAM, I., DIKSHIT, R., ESER, S., MATHERS, C., REBELO, M., PARKIN, D. M., FORMAN, D. & BRAY, F. 2015a. Cancer incidence and mortality worldwide: sources, methods and major patterns in GLOBOCAN 2012. *Int J Cancer,* 136**,** E359-86.
FERLAY, J., SOERJOMATARAM, I., DIKSHIT, R., ESER, S., MATHERS, C., REBELO, M., PARKIN, D. M., FORMAN, D. & BRAY, F. 2015b. Cancer incidence and mortality worldwide: sources, methods and major patterns in GLOBOCAN 2012. *International journal of cancer,* 136.
FERRARA, N. 2010. Pathways mediating VEGF-independent tumor angiogenesis. *Cytokine Growth Factor Rev,* 21**,** 21-6.
FERRICK, D. A., NEILSON, A. & BEESON, C. 2008. Advances in measuring cellular bioenergetics using extracellular flux. *Drug Discov Today,* 13**,** 268-74.
FILIPOWICZ, W., JASKIEWICZ, L., KOLB, F. A. & PILLAI, R. S. 2005. Post-transcriptional gene silencing by siRNAs and miRNAs. *Current opinion in structural biology,* 15**,** 331-341.
FIRE, A., XU, S., MONTGOMERY, M. K., KOSTAS, S. A., DRIVER, S. E. & MELLO, C. C. 1998. Potent and specific genetic interference by double-stranded RNA in Caenorhabditis elegans. *nature,* 391**,** 806-811.
FRANK, F., SONENBERG, N. & NAGAR, B. 2010. Structural basis for 5 [prime]-nucleotide base-specific recognition of guide RNA by human AGO2. *Nature,* 465**,** 818-822.
FS, B. 1986. Palaeo-Oncology. The Antiquity of Cancer. *In:* E.S. RETSAS, E. (ed.).
GAROFALO, M., ROMANO, G., DI LEVA, G., NUOVO, G., JEON, Y. J., NGANKEU, A., SUN, J., LOVAT, F., ALDER, H., CONDORELLI, G., ENGELMAN, J. A., ONO, M., RHO, J. K., CASCIONE, L., VOLINIA, S., NEPHEW, K. P. & CROCE, C. M. 2011. EGFR and MET receptor tyrosine kinase-altered microRNA expression induces tumorigenesis and gefitinib resistance in lung cancers. *Nat Med,* 18**,** 74-82.

GERNAPUDI, R., WOLFSON, B., ZHANG, Y., YAO, Y., YANG, P., ASAHARA, H. & ZHOU, Q. 2016. MicroRNA 140 Promotes Expression of Long Noncoding RNA NEAT1 in Adipogenesis. *Mol Cell Biol,* 36**,** 30-8.

GIZA, D. E., VASILESCU, C. & CALIN, G. A. 2014. Key principles of miRNA involvement in human diseases. *Discoveries (Craiova),* 2**,** e34.

GOODWIN, A. M. 2007. In vitro assays of angiogenesis for assessment of angiogenic and anti-angiogenic agents. *Microvascular research,* 74**,** 172-183.

GORETTI, E., WAGNER, D. R. & DEVAUX, Y. 2014. miRNAs as biomarkers of myocardial infarction: a step forward towards personalized medicine? *Trends Mol Med,* 20**,** 716-25.

GOTTWEIN, E., CAI, X. & CULLEN, B. R. 2006. Expression and function of microRNAs encoded by Kaposi's sarcoma-associated herpesvirus. *Cold Spring Harb Symp Quant Biol,* 71**,** 357-64.

GRIDELLI, C., ROSSI, A., CARBONE, D. P., GUARIZE, J., KARACHALIOU, N., MOK, T., PETRELLA, F., SPAGGIARI, L. & ROSELL, R. 2015. Non-small-cell lung cancer. *Nat Rev Dis Primers,* 1**,** 15009.

GRIFFITHS-JONES, S., HUI, J. H., MARCO, A. & RONSHAUGEN, M. 2011. MicroRNA evolution by arm switching. *EMBO reports,* 12**,** 172-177.

GUERRIERO, I., D'ANGELO, D., PALLANTE, P., SANTOS, M., SCRIMA, M., MALANGA, D., DE MARCO, C., RAVO, M., WEISZ, A., LAUDANNA, C., CECCARELLI, M., FALCO, G., RIZZUTO, A. & VIGLIETTO, G. 2016. Analysis of miRNA profiles identified miR-196a as a crucial mediator of aberrant PI3K/AKT signaling in lung cancer cells. *Oncotarget*.

GUPTA, R. A., SHAH, N., WANG, K. C., KIM, J., HORLINGS, H. M., WONG, D. J., TSAI, M.-C., HUNG, T., ARGANI, P., RINN, J. L., WANG, Y., BRZOSKA, P., KONG, B., LI, R., WEST, R. B., VAN DE VIJVER, M. J., SUKUMAR, S. & CHANG, H. Y. 2010. Long non-coding RNA HOTAIR reprograms chromatin state to promote cancer metastasis. *Nature,* 464**,** 1071-1076.

HA, M. & KIM, V. N. 2014a. Regulation of microRNA biogenesis. *Nat Rev Mol Cell Biol,* 15**,** 509-524.

HA, M. & KIM, V. N. 2014b. Regulation of microRNA biogenesis. *Nature Reviews Molecular Cell Biology,* 15**,** 509-524.

HAFTMANN, C., RIEDEL, R., PORSTNER, M., WITTMANN, J., CHANG, H. D., RADBRUCH, A. & MASHREGHI, M. F. 2015. Direct uptake of Antagomirs and efficient knockdown of miRNA in primary B and T lymphocytes. *J Immunol Methods,* 426**,** 128-33.

HAN, J., LEE, Y., YEOM, K.-H., KIM, Y.-K., JIN, H. & KIM, V. N. 2004. The Drosha-DGCR8 complex in primary microRNA processing. *Genes & development,* 18**,** 3016-3027.

HAN, J., LEE, Y., YEOM, K.-H., NAM, J.-W., HEO, I., RHEE, J.-K., SOHN, S. Y., CHO, Y., ZHANG, B.-T. & KIM, V. N. 2006. Molecular basis for the recognition of primary microRNAs by the Drosha-DGCR8 complex. *cell,* 125**,** 887-901.

HAN, J., PEDERSEN, J. S., KWON, S. C., BELAIR, C. D., KIM, Y.-K., YEOM, K.-H., YANG, W.-Y., HAUSSLER, D., BLELLOCH, R. & KIM, V. N. 2009. Posttranscriptional crossregulation between Drosha and DGCR8. *Cell,* 136**,** 75-84.

HANAHAN, D. & WEINBERG, R. A. 2000. The hallmarks of cancer. *cell,* 100**,** 57-70.

HANAHAN, D. & WEINBERG, R. A. 2011. Hallmarks of cancer: the next generation. *Cell,* 144**,** 646-74.

HAUSSER, J. & ZAVOLAN, M. 2014. Identification and consequences of miRNA-target interactions--beyond repression of gene expression. *Nat Rev Genet,* 15**,** 599-612.

HAYASHITA, Y., OSADA, H., TATEMATSU, Y., YAMADA, H., YANAGISAWA, K., TOMIDA, S., YATABE, Y., KAWAHARA, K., SEKIDO, Y. & TAKAHASHI, T. 2005. A polycistronic microRNA cluster, miR-17-92, is overexpressed in human lung cancers and enhances cell proliferation. *Cancer Res,* 65**,** 9628-32.

HAYES, J., PERUZZI, P. P. & LAWLER, S. 2014. MicroRNAs in cancer: biomarkers, functions and therapy. *Trends Mol Med,* 20**,** 460-9.

HEERBOTH, S., HOUSMAN, G., LEARY, M., LONGACRE, M., BYLER, S., LAPINSKA, K., WILLBANKS, A. & SARKAR, S. 2015. EMT and tumor metastasis. *Clin Transl Med,* 4**,** 6.

HERBST, R. S., HEYMACH, J. V. & LIPPMAN, S. M. 2008. Lung Cancer. *New England Journal of Medicine,* 359**,** 1367-1380.

HOCKEL, M. & VAUPEL, P. 2001. Tumor hypoxia: definitions and current clinical, biologic, and molecular aspects. *J Natl Cancer Inst,* 93**,** 266-76.

HOEKSTRA, M., VAN DER LANS, C. A., HALVORSEN, B., GULLESTAD, L., KUIPER, J., AUKRUST, P., VAN BERKEL, T. J. & BIESSEN, E. A. 2010. The peripheral blood mononuclear cell microRNA signature of coronary artery disease. *Biochem Biophys Res Commun,* 394**,** 792-7.

HONG, S. K., PARK, J. R., KWON, O. S., KIM, K. T., BAE, G. Y. & CHA, H. J. 2016. Induction of integrin beta3 by sustained ERK activity promotes the invasiveness of TGFbeta-induced mesenchymal tumor cells. *Cancer Lett,* 376**,** 339-46.

HOOD, J. D., FRAUSTO, R., KIOSSES, W. B., SCHWARTZ, M. A. & CHERESH, D. A. 2003. Differential alphav integrin-mediated Ras-ERK signaling during two pathways of angiogenesis. *J Cell Biol,* 162**,** 933-43.

HSIEH, S. Y., LIAW, S. F., LEE, S. N., HSIEH, P. S., LIN, K. H., CHU, C. M. & LIAW, Y. F. 2003. Aberrant caspase-activated DNase (CAD) transcripts in human hepatoma cells. *Br J Cancer,* 88**,** 210-6.

HSU, S. H., YU, B., WANG, X., LU, Y., SCHMIDT, C. R., LEE, R. J., LEE, L. J., JACOB, S. T. & GHOSHAL, K. 2013. Cationic lipid nanoparticles for therapeutic delivery of siRNA and miRNA to murine liver tumor. *Nanomedicine,* 9**,** 1169-80.

HTTP://ABOUT-CANCER.CANCERRESEARCHUK.ORG/ABOUT-CANCER/LUNG-CANCER/ADVANCED/ABOUT.

HTTP://IMAGE.BIO.METHODS.FREE.FR/IMAGEJ/?ANGIOGENESIS-ANALYZER-FOR-IMAGEJ.

HTTP://PATHWAYS.NICE.ORG.UK/PATHWAYS/LUNG-CANCER#PATH=VIEW%3A/PATHWAYS/LUNG-CANCER/TREATING-NON-SMALL-CELL-LUNG-CANCER.XML&CONTENT=VIEW-INDEX. 2017.

HTTP://WWW.AGILENT.COM/EN-US/SUPPORT/CELL-ANALYSIS-(SEAHORSE)/SEAHORSE-XF-SOFTWARE.

HTTP://WWW.BIO-RAD.COM/EN-UK/APPLICATIONS-TECHNOLOGIES/INTRODUCTION-PCR-PRIMER-PROBE-CHEMISTRIES.

HTTP://WWW.IARC.FR/.

HTTP://WWW.INCHEM.ORG/DOCUMENTS/EHC/EHC/EHC222.HTM.

HTTP://WWW.MIRBASE.ORG.

HTTP://WWW.NATURE.COM/SCITABLE/DEFINITION/TRANSCRIPTION-UNIT-260.

HTTP://WWW.NCBI.NLM.NIH.GOV/GENOME/PROBE/DOC/TECHQPCR.SHTML.

HTTP://WWW.PARTEK.COM/PGS.
HTTP://WWW.RAJAHA.COM/ELISA-TEST-WHAT-PRINCIPLE-TYPES/.
HTTPS://PERSONALWEBS.COLORADOCOLLEGE.EDU/~DKILLIAN/HOME/SDS_PAGE_AND_WESTERN_BLOTTING.HTML.
HTTPS://WWW.BDBIOSCIENCES.COM/DOCUMENTS/BD_FACSVERSE_APOPTOSIS_DETECTION_APPNOTE.PDF.
HTTPS://WWW.CORNING.COM/MEDIA/WORLDWIDE/CLS/DOCUMENTS/CLS-DL-CC-026%20DL.PDF.
HTTPS://WWW.MYCANCERGENOME.ORG/CONTENT/DISEASE/LUNG-CANCER/.
HU, H. Y., YAN, Z., XU, Y., HU, H., MENZEL, C., ZHOU, Y. H., CHEN, W. & KHAITOVICH, P. 2009. Sequence features associated with microRNA strand selection in humans and flies. *BMC genomics,* 10**,** 413.
HUANG, H., ZHANG, X., LI, S., LIU, N., LIAN, W., MCDOWELL, E., ZHOU, P., ZHAO, C., GUO, H., ZHANG, C., YANG, C., WEN, G., DONG, X., LU, L., MA, N., DONG, W., DOU, Q. P., WANG, X. & LIU, J. 2010. Physiological levels of ATP negatively regulate proteasome function. *Cell Res,* 20**,** 1372-85.
HUARTE, M., GUTTMAN, M., FELDSER, D., GARBER, M., KOZIOL, M. J., KENZELMANN-BROZ, D., KHALIL, A. M., ZUK, O., AMIT, I., RABANI, M., ATTARDI, L. D., REGEV, A., LANDER, E. S., JACKS, T. & RINN, J. L. 2010. A large intergenic noncoding RNA induced by p53 mediates global gene repression in the p53 response. *Cell,* 142**,** 409-19.
INAMURA, K. & ISHIKAWA, Y. 2016. MicroRNA In Lung Cancer: Novel Biomarkers and Potential Tools for Treatment. *J Clin Med,* 5.
ISCHENKO, I., LIU, J., PETRENKO, O. & HAYMAN, M. J. 2014. Transforming growth factor-beta signaling network regulates plasticity and lineage commitment of lung cancer cells. *Cell Death Differ,* 21**,** 1218-28.
JANIC, A., MENDIZABAL, L., LLAMAZARES, S., ROSSELL, D. & GONZALEZ, C. 2010. Ectopic expression of germline genes drives malignant brain tumor growth in Drosophila. *Science,* 330**,** 1824-1827.
JAZDZEWSKI, K., LIYANARACHCHI, S., SWIERNIAK, M., PACHUCKI, J., RINGEL, M. D., JARZAB, B. & DE LA CHAPELLE, A. 2009. Polymorphic mature microRNAs from passenger strand of pre-miR-146a contribute to thyroid cancer. *Proc Natl Acad Sci U S A,* 106**,** 1502-5.
JOHNSON, S. M., GROSSHANS, H., SHINGARA, J., BYROM, M., JARVIS, R., CHENG, A., LABOURIER, E., REINERT, K. L., BROWN, D. & SLACK, F. J. 2005. RAS is regulated by the let-7 microRNA family. *Cell,* 120**,** 635-47.
KARAYIORGOU, M., MORRIS, M. A., MORROW, B., SHPRINTZEN, R. J., GOLDBERG, R., BORROW, J., GOS, A., NESTADT, G., WOLYNIEC, P. S., LASSETER, V. K. & ET AL. 1995. Schizophrenia susceptibility associated with interstitial deletions of chromosome 22q11. *Proc Natl Acad Sci U S A,* 92**,** 7612-6.
KARGE III, W. H., SCHAEFER, E. J. & ORDOVAS, J. M. 1998. Quantification of mRNA by polymerase chain reaction (PCR) using an internal standard and a nonradioactive detection method. *Lipoprotein Protocols.* Springer.
KARUBE, Y., TANAKA, H., OSADA, H., TOMIDA, S., TATEMATSU, Y., YANAGISAWA, K., YATABE, Y., TAKAMIZAWA, J., MIYOSHI, S., MITSUDOMI, T. & TAKAHASHI, T. 2005. Reduced expression of Dicer associated with poor prognosis in lung cancer patients. *Cancer Sci,* 96**,** 111-5.
KHVOROVA, A., REYNOLDS, A. & JAYASENA, S. D. 2003. Functional siRNAs and miRNAs exhibit strand bias. *Cell,* 115**,** 209-216.
KIM, V. N. 2004. MicroRNA precursors in motion: exportin-5 mediates their nuclear export. *Trends in cell biology,* 14**,** 156-159.

KIM, V. N. 2005a. MicroRNA biogenesis: coordinated cropping and dicing. *Nat Rev Mol Cell Biol,* 6**,** 376-85.
KIM, V. N. 2005b. MicroRNA biogenesis: coordinated cropping and dicing. *Nature reviews Molecular cell biology,* 6**,** 376-385.
KIM, V. N., HAN, J. & SIOMI, M. C. 2009. Biogenesis of small RNAs in animals. *Nature reviews Molecular cell biology,* 10**,** 126-139.
KIM, V. N. & NAM, J. W. 2006. Genomics of microRNA. *Trends Genet,* 22**,** 165-73.
KISHORE, S. & STAMM, S. 2006. The snoRNA HBII-52 regulates alternative splicing of the serotonin receptor 2C. *Science,* 311**,** 230-232.
KISS-LÁSZLÓ, Z., HENRY, Y., BACHELLERIE, J.-P., CAIZERGUES-FERRER, M. & KISS, T. 1996. Site-specific ribose methylation of preribosomal RNA: a novel function for small nucleolar RNAs. *Cell,* 85**,** 1077-1088.
KOTA, J., CHIVUKULA, R. R., O'DONNELL, K. A., WENTZEL, E. A., MONTGOMERY, C. L., HWANG, H. W., CHANG, T. C., VIVEKANANDAN, P., TORBENSON, M., CLARK, K. R., MENDELL, J. R. & MENDELL, J. T. 2009. Therapeutic microRNA delivery suppresses tumorigenesis in a murine liver cancer model. *Cell,* 137**,** 1005-17.
KRAMER, N., WALZL, A., UNGER, C., ROSNER, M., KRUPITZA, G., HENGSTSCHLAGER, M. & DOLZNIG, H. 2013. In vitro cell migration and invasion assays. *Mutat Res,* 752**,** 10-24.
KREK, A., GRÜN, D., POY, M. N., WOLF, R., ROSENBERG, L., EPSTEIN, E. J., MACMENAMIN, P., DA PIEDADE, I., GUNSALUS, K. C. & STOFFEL, M. 2005. Combinatorial microRNA target predictions. *Nature genetics,* 37**,** 495-500.
KROL, J., LOEDIGE, I. & FILIPOWICZ, W. 2010. The widespread regulation of microRNA biogenesis, function and decay. *Nature Reviews Genetics,* 11**,** 597.
KRUTZFELDT, J., RAJEWSKY, N., BRAICH, R., RAJEEV, K. G., TUSCHL, T., MANOHARAN, M. & STOFFEL, M. 2005. Silencing of microRNAs in vivo with 'antagomirs'. *Nature,* 438**,** 685-9.
KUMAR, M. S., ERKELAND, S. J., PESTER, R. E., CHEN, C. Y., EBERT, M. S., SHARP, P. A. & JACKS, T. 2008. Suppression of non-small cell lung tumor development by the let-7 microRNA family. *Proc Natl Acad Sci U S A,* 105**,** 3903-8.
KUMAR, M. S., LU, J., MERCER, K. L., GOLUB, T. R. & JACKS, T. 2007. Impaired microRNA processing enhances cellular transformation and tumorigenesis. *Nat Genet,* 39**,** 673-7.
KUROZUMI, S., YAMAGUCHI, Y., KUROSUMI, M., OHIRA, M., MATSUMOTO, H. & HORIGUCHI, J. 2017. Recent trends in microRNA research into breast cancer with particular focus on the associations between microRNAs and intrinsic subtypes. *J Hum Genet,* 62**,** 15-24.
LAGOS-QUINTANA, M., RAUHUT, R., YALCIN, A., MEYER, J., LENDECKEL, W. & TUSCHL, T. 2002. Identification of tissue-specific microRNAs from mouse. *Current biology,* 12**,** 735-739.
LAL, A., NAVARRO, F., MAHER, C. A., MALISZEWSKI, L. E., YAN, N., O'DAY, E., CHOWDHURY, D., DYKXHOORN, D. M., TSAI, P., HOFMANN, O., BECKER, K. G., GOROSPE, M., HIDE, W. & LIEBERMAN, J. 2009. miR-24 Inhibits cell proliferation by targeting E2F2, MYC, and other cell-cycle genes via binding to "seedless" 3'UTR microRNA recognition elements. *Mol Cell,* 35**,** 610-25.
LANDGRAF, P., RUSU, M., SHERIDAN, R., SEWER, A., IOVINO, N., ARAVIN, A., PFEFFER, S., RICE, A., KAMPHORST, A. O. & LANDTHALER, M. 2007. A

mammalian microRNA expression atlas based on small RNA library sequencing. *Cell,* 129**,** 1401-1414.
LEARY, A. 2012. *Lung Cancer-A multidisciplinary approach*.
LEE, R. C., FEINBAUM, R. L. & AMBROS, V. 1993. The C. elegans heterochronic gene lin-4 encodes small RNAs with antisense complementarity to lin-14. *cell,* 75**,** 843-854.
LEE, Y., HUR, I., PARK, S. Y., KIM, Y. K., SUH, M. R. & KIM, V. N. 2006. The role of PACT in the RNA silencing pathway. *The EMBO journal,* 25**,** 522-532.
LEMJABBAR-ALAOUI, H., VAN ZANTE, A., SINGER, M. S., XUE, Q., WANG, Y. Q., TSAY, D., HE, B., JABLONS, D. M. & ROSEN, S. D. 2010. Sulf-2, a heparan sulfate endosulfatase, promotes human lung carcinogenesis. *Oncogene,* 29**,** 635-46.
LI, L., MENG, T., JIA, Z., ZHU, G. & SHI, B. 2010. Single nucleotide polymorphism associated with nonsyndromic cleft palate influences the processing of miR-140. *Am J Med Genet A,* 152a**,** 856-62.
LI, Q., YAO, Y., EADES, G., LIU, Z., ZHANG, Y. & ZHOU, Q. 2014a. Downregulation of miR-140 promotes cancer stem cell formation in basal-like early stage breast cancer. *Oncogene,* 33**,** 2589-2600.
LI, Q. J., CHAU, J., EBERT, P. J., SYLVESTER, G., MIN, H., LIU, G., BRAICH, R., MANOHARAN, M., SOUTSCHEK, J., SKARE, P., KLEIN, L. O., DAVIS, M. M. & CHEN, C. Z. 2007. miR-181a is an intrinsic modulator of T cell sensitivity and selection. *Cell,* 129**,** 147-61.
LI, S.-C., TSAI, K.-W., PAN, H.-W., JENG, Y.-M., HO, M.-R. & LI, W.-H. 2012. MicroRNA 3'end nucleotide modification patterns and arm selection preference in liver tissues. *BMC systems biology,* 6**,** S14.
LI, W. & HE, F. 2014. Monocyte to macrophage differentiation-associated (MMD) targeted by miR-140-5p regulates tumor growth in non-small cell lung cancer. *Biochemical and biophysical research communications,* 450**,** 844-850.
LI, W., JIANG, G., ZHOU, J., WANG, H., GONG, Z., ZHANG, Z., MIN, K., ZHU, H. & TAN, Y. 2014b. Down-Regulation of miR-140 Induces EMT and Promotes Invasion by Targeting Slug in Esophageal Cancer. *Cellular Physiology and Biochemistry,* 34**,** 1466-1476.
LIBERTI, M. V. & LOCASALE, J. W. 2016. The Warburg Effect: How Does it Benefit Cancer Cells? *Trends Biochem Sci,* 41**,** 211-8.
LIU, D. N., ZHOU, Y. F., PENG, A. F., LONG, X. H., CHEN, X. Y., LIU, Z. L. & XIA, H. 2017. HELQ reverses the malignant phenotype of osteosarcoma cells via CHK1-RAD51 signaling pathway. *Oncol Rep,* 37**,** 1107-1113.
LIU, M., GAO, J., HUANG, Q., JIN, Y. & WEI, Z. 2016a. Downregulating microRNA-144 mediates a metabolic shift in lung cancer cells by regulating GLUT1 expression. *Oncol Lett,* 11**,** 3772-3776.
LIU, X., WANG, S., YUAN, A., YUAN, X. & LIU, B. 2016b. MicroRNA-140 represses glioma growth and metastasis by directly targeting ADAM9. *Oncol Rep*.
LOBO, N. A., SHIMONO, Y., QIAN, D. & CLARKE, M. F. 2007. The biology of cancer stem cells. *Annu Rev Cell Dev Biol,* 23**,** 675-99.
LOHER, P. & RIGOUTSOS, I. 2012. Interactive exploration of RNA22 microRNA target predictions. *Bioinformatics,* 28**,** 3322-3323.
LONVIK, K., SORBYE, S. W., NILSEN, M. N. & PAULSSEN, R. H. 2014. Prognostic value of the MicroRNA regulators Dicer and Drosha in non-small-cell lung cancer: co-expression of Drosha and miR-126 predicts poor survival. *BMC Clin Pathol,* 14**,** 45.

LORTET-TIEULENT, J., SOERJOMATARAM, I., FERLAY, J., RUTHERFORD, M., WEIDERPASS, E. & BRAY, F. 2014. International trends in lung cancer incidence by histological subtype: Adenocarcinoma stabilizing in men but still increasing in women. *Lung Cancer,* 84**,** 13-22.

LU, J., GETZ, G., MISKA, E. A., ALVAREZ-SAAVEDRA, E., LAMB, J., PECK, D., SWEET-CORDERO, A., EBERT, B. L., MAK, R. H., FERRANDO, A. A., DOWNING, J. R., JACKS, T., HORVITZ, H. R. & GOLUB, T. R. 2005. MicroRNA expression profiles classify human cancers. *Nature,* 435**,** 834-8.

LUI, N. S., YANG, Y. W., VAN ZANTE, A., BUCHANAN, P., JABLONS, D. M. & LEMJABBAR-ALAOUI, H. 2016. SULF2 Expression Is a Potential Diagnostic and Prognostic Marker in Lung Cancer. *PLoS One,* 11**,** e0148911.

MA, J., WANG, P., YAO, Y., LIU, Y., LI, Z., LIU, X., LI, Z., ZHAO, X., XI, Z., TENG, H., LIU, J. & XUE, Y. 2016. Knockdown of long non-coding RNA MALAT1 increases the blood-tumor barrier permeability by up-regulating miR-140. *Biochim Biophys Acta,* 1859**,** 324-38.

MANNOOR, K., LIAO, J. & JIANG, F. 2012. Small nucleolar RNAs in cancer. *Biochimica et Biophysica Acta (BBA)-Reviews on Cancer,* 1826**,** 121-128.

MARAGKAKIS, M., RECZKO, M., SIMOSSIS, V. A., ALEXIOU, P., PAPADOPOULOS, G. L., DALAMAGAS, T., GIANNOPOULOS, G., GOUMAS, G., KOUKIS, E. & KOURTIS, K. 2009. DIANA-microT web server: elucidating microRNA functions through target prediction. *Nucleic acids research***,** gkp292.

MARTIN, H. C., WANI, S., STEPTOE, A. L., KRISHNAN, K., NONES, K., NOURBAKHSH, E., VLASSOV, A., GRIMMOND, S. M. & CLOONAN, N. 2014. Imperfect centered miRNA binding sites are common and can mediate repression of target mRNAs. *Genome Biol,* 15**,** R51.

MAZAR, J., QI, F., LEE, B., MARCHICA, J., GOVINDARAJAN, S., SHELLEY, J., LI, J. L., RAY, A. & PERERA, R. J. 2016. MicroRNA 211 Functions as a Metabolic Switch in Human Melanoma Cells. *Mol Cell Biol,* 36**,** 1090-108.

MEHTA, A., DOBERSCH, S., ROMERO-OLMEDO, A. J. & BARRETO, G. 2015. Epigenetics in lung cancer diagnosis and therapy. *Cancer Metastasis Rev,* 34**,** 229-41.

MEIJER, H. A., SMITH, E. M. & BUSHELL, M. 2014. Regulation of miRNA strand selection: follow the leader? *Biochem Soc Trans,* 42**,** 1135-40.

MEYERSON, M. 2007. Cancer: broken genes in solid tumours. *Nature,* 448**,** 545-6.

MORTAZAVI, A., WILLIAMS, B. A., MCCUE, K., SCHAEFFER, L. & WOLD, B. 2008. Mapping and quantifying mammalian transcriptomes by RNA-Seq. *Nat Methods,* 5**,** 621-8.

NAKIELNY, S. & DREYFUSS, G. 1999. Transport of proteins and RNAs in and out of the nucleus. *Cell,* 99**,** 677-690.

NAM, S., KIM, D., CHENG, J. Q., ZHANG, S., LEE, J. H., BUETTNER, R., MIROSEVICH, J., LEE, F. Y. & JOVE, R. 2005. Action of the Src family kinase inhibitor, dasatinib (BMS-354825), on human prostate cancer cells. *Cancer Res,* 65**,** 9185-9.

NAVARRO, P., PAGE, D. R., AVNER, P. & ROUGEULLE, C. 2006. Tsix-mediated epigenetic switch of a CTCF-flanked region of the Xist promoter determines the Xist transcription program. *Genes Dev,* 20**,** 2787-92.

NI, J., TIEN, A. L. & FOURNIER, M. J. 1997. Small nucleolar RNAs direct site-specific synthesis of pseudouridine in ribosomal RNA. *Cell,* 89**,** 565-573.

NOLAND, C. L. & DOUDNA, J. A. 2013. Multiple sensors ensure guide strand selection in human RNAi pathways. *Rna,* 19**,** 639-648.

OKAMURA, K., PHILLIPS, M. D., TYLER, D. M., DUAN, H., CHOU, Y. T. & LAI, E. C. 2008. The regulatory activity of microRNA* species has substantial influence on microRNA and 3' UTR evolution. *Nat Struct Mol Biol,* 15**,** 354-63.

ORGANIZATION, W. H. 2014. http://www.who.int/mediacentre/factsheets/fs164/en/.

OSADA, H. & TAKAHASHI, T. 2011. let-7 and miR-17-92: small-sized major players in lung cancer development. *Cancer Sci,* 102**,** 9-17.

PAN, L. J., ZHONG, T. F., TANG, R. X., LI, P., DANG, Y. W., HUANG, S. N. & CHEN, G. 2015. Upregulation and clinicopathological significance of long non-coding NEAT1 RNA in NSCLC tissues. *Asian Pac J Cancer Prev,* 16**,** 2851-5.

PAO, W. & CHMIELECKI, J. 2010. Rational, biologically based treatment of EGFR-mutant non-small-cell lung cancer. *Nat Rev Cancer,* 10**,** 760-74.

PEARL, R. 1938. Tobacco smoking and longevity. *Science***,** 216-217.

PETERSON, S. M., THOMPSON, J. A., UFKIN, M. L., SATHYANARAYANA, P., LIAW, L. & CONGDON, C. B. 2014. Common features of microRNA target prediction tools. *Frontiers in genetics,* 5.

PRESKILL, C. & WEIDHAAS, J. B. 2013. SNPs in microRNA binding sites as prognostic and predictive cancer biomarkers. *Crit Rev Oncog,* 18**,** 327-40.

PU, X., ROTH, J. A., HILDEBRANDT, M. A., YE, Y., WEI, H., MINNA, J. D., LIPPMAN, S. M. & WU, X. 2013. MicroRNA-related genetic variants associated with clinical outcomes in early-stage non-small cell lung cancer patients. *Cancer Res,* 73**,** 1867-75.

RAKOCZY, J., FERNANDEZ-VALVERDE, S. L., GLAZOV, E. A., WAINWRIGHT, E. N., SATO, T., TAKADA, S., COMBES, A. N., KORBIE, D. J., MILLER, D., GRIMMOND, S. M., LITTLE, M. H., ASAHARA, H., MATTICK, J. S., TAFT, R. J. & WILHELM, D. 2013. MicroRNAs-140-5p/140-3p modulate Leydig cell numbers in the developing mouse testis. *Biol Reprod,* 88**,** 143.

RAMALINGAM, P., PALANICHAMY, J. K., SINGH, A., DAS, P., BHAGAT, M., KASSAB, M. A., SINHA, S. & CHATTOPADHYAY, P. 2014. Biogenesis of intronic miRNAs located in clusters by independent transcription and alternative splicing. *Rna,* 20**,** 76-87.

RATTANASOPHA, S., TONGKOBPETCH, S., SRICHOMTHONG, C., SIRIWAN, P., SUPHAPEETIPORN, K. & SHOTELERSUK, V. 2012. PDGFRa mutations in humans with isolated cleft palate. *Eur J Hum Genet,* 20**,** 1058-62.

RECK, M., HEIGENER, D. F., MOK, T., SORIA, J. C. & RABE, K. F. 2013. Management of non-small-cell lung cancer: recent developments. *Lancet,* 382**,** 709-19.

RINN, J. L., KERTESZ, M., WANG, J. K., SQUAZZO, S. L., XU, X., BRUGMANN, S. A., GOODNOUGH, L. H., HELMS, J. A., FARNHAM, P. J. & SEGAL, E. 2007. Functional demarcation of active and silent chromatin domains in human HOX loci by noncoding RNAs. *Cell,* 129**,** 1311-1323.

RISCH, A. & PLASS, C. 2008. Lung cancer epigenetics and genetics. *Int J Cancer,* 123**,** 1-7.

RODRIGUEZ, A., GRIFFITHS-JONES, S., ASHURST, J. L. & BRADLEY, A. 2004. Identification of mammalian microRNA host genes and transcription units. *Genome research,* 14**,** 1902-1910.

RUPAIMOOLE, R. & SLACK, F. J. 2017. MicroRNA therapeutics: towards a new era for the management of cancer and other diseases. *Nat Rev Drug Discov,* 16**,** 203-222.

RUSEK, A. M., ABBA, M., ELJASZEWICZ, A., MONIUSZKO, M., NIKLINSKI, J. & ALLGAYER, H. 2015. MicroRNA modulators of epigenetic regulation, the

tumor microenvironment and the immune system in lung cancer. *Mol Cancer,* 14**,** 34.
SAITO, K., IWASHITA, J., MURATA, J. & ABE, T. 2006. The tyrosine kinase inhibitor AG490 inhibits growth of cancer cells and activates ERK in LS174T and HT-29 cells. *Anticancer Res,* 26**,** 1085-90.
SALVATORE, M., MAGRELLI, A., FLAMINI, V., BRUNATI, A., BASSO, E., ROMAGNOLI, R., DAVID, E. & TARUSCIO, D. 2016. Hepatoblastoma and microRNA-483 Two Forms and One Outcome. *Journal of Genetic Syndromes & Gene Therapy,* 2016.
SCHOEN, C., ASCHRAFI, A., THONISSEN, M., POELMANS, G., VON DEN HOFF, J. W. & CARELS, C. E. L. 2017. MicroRNAs in Palatogenesis and Cleft Palate. *Front Physiol,* 8**,** 165.
SCHWARZ, D. S., HUTVÁGNER, G., DU, T., XU, Z., ARONIN, N. & ZAMORE, P. D. 2003. Asymmetry in the assembly of the RNAi enzyme complex. *Cell,* 115**,** 199-208.
SHI, X. B., TEPPER, C. G. & DEVERE WHITE, R. W. 2008. Cancerous miRNAs and their regulation. *Cell Cycle,* 7**,** 1529-38.
SHTIVELMAN, E., HENSING, T., SIMON, G. R., DENNIS, P. A., OTTERSON, G. A., BUENO, R. & SALGIA, R. 2014. Molecular pathways and therapeutic targets in lung cancer. *Oncotarget,* 5**,** 1392-433.
SIMONIK, E. A., CAI, Y., KIMMELSHUE, K. N., BRANTLEY-SIEDERS, D. M., LOOMANS, H. A., ANDL, C. D., WESTLAKE, G. M., YOUNGBLOOD, V. M., CHEN, J., YARBROUGH, W. G., BROWN, B. T., NAGARAJAN, L. & BRANDT, S. J. 2016. LIM-Only Protein 4 (LMO4) and LIM Domain Binding Protein 1 (LDB1) Promote Growth and Metastasis of Human Head and Neck Cancer (LMO4 and LDB1 in Head and Neck Cancer). *PLoS One,* 11**,** e0164804.
SOMANATH, P. R., CIOCEA, A. & BYZOVA, T. V. 2009. Integrin and growth factor receptor alliance in angiogenesis. *Cell Biochem Biophys,* 53**,** 53-64.
SONG, J.-J., SMITH, S. K., HANNON, G. J. & JOSHUA-TOR, L. 2004. Crystal structure of Argonaute and its implications for RISC slicer activity. *science,* 305**,** 1434-1437.
STAHEL, R. 2007. Adenocarcinoma, a molecular perspective. *Annals of oncology,* 18**,** ix147-ix149.
STARK, K. L., XU, B., BAGCHI, A., LAI, W. S., LIU, H., HSU, R., WAN, X., PAVLIDIS, P., MILLS, A. A., KARAYIORGOU, M. & GOGOS, J. A. 2008. Altered brain microRNA biogenesis contributes to phenotypic deficits in a 22q11-deletion mouse model. *Nat Genet,* 40**,** 751-60.
SU, H., XU, T., GANAPATHY, S., SHADFAN, M., LONG, M., HUANG, T. H., THOMPSON, I. & YUAN, Z. 2014. Elevated snoRNA biogenesis is essential in breast cancer. *Oncogene,* 33**,** 1348-1358.
SULLIVAN, C. S., GRUNDHOFF, A. T., TEVETHIA, S., PIPAS, J. M. & GANEM, D. 2005. SV40-encoded microRNAs regulate viral gene expression and reduce susceptibility to cytotoxic T cells. *Nature,* 435**,** 682-6.
SUN, G., YAN, J., NOLTNER, K., FENG, J., LI, H., SARKIS, D. A., SOMMER, S. S. & ROSSI, J. J. 2009. SNPs in human miRNA genes affect biogenesis and function. *Rna,* 15**,** 1640-51.
SUN, J., TAO, S., LIU, L., GUO, D., XIA, Z. & HUANG, M. 2016. miR1405p regulates angiogenesis following ischemic stroke by targeting VEGFA. *Mol Med Rep,* 13**,** 4499-505.

SUR, S. & AGRAWAL, D. K. 2016. Phosphatases and kinases regulating CDC25 activity in the cell cycle: clinical implications of CDC25 overexpression and potential treatment strategies. *Mol Cell Biochem,* 416**,** 33-46.

SWARTZ, M. A., IIDA, N., ROBERTS, E. W., SANGALETTI, S., WONG, M. H., YULL, F. E., COUSSENS, L. M. & DECLERCK, Y. A. 2012. Tumor microenvironment complexity: emerging roles in cancer therapy. *Cancer research,* 72**,** 2473-2480.

TAKAMIZAWA, J., KONISHI, H., YANAGISAWA, K., TOMIDA, S., OSADA, H., ENDOH, H., HARANO, T., YATABE, Y., NAGINO, M., NIMURA, Y., MITSUDOMI, T. & TAKAHASHI, T. 2004. Reduced expression of the let-7 microRNAs in human lung cancers in association with shortened postoperative survival. *Cancer Res,* 64**,** 3753-6.

TAN, S. M., KIRCHNER, R., JIN, J., HOFMANN, O., MCREYNOLDS, L., HIDE, W. & LIEBERMAN, J. 2014. Sequencing of captive target transcripts identifies the network of regulated genes and functions of primate-specific miR-522. *Cell Rep,* 8**,** 1225-39.

TARDIF, G., PELLETIER, J. P., FAHMI, H., HUM, D., ZHANG, Y., KAPOOR, M. & MARTEL-PELLETIER, J. 2013. NFAT3 and TGF-beta/SMAD3 regulate the expression of miR-140 in osteoarthritis. *Arthritis Res Ther,* 15**,** R197.

THE CANCER GENOME ATLAS RESEARCH, N. 2014. Comprehensive molecular profiling of lung adenocarcinoma. *Nature,* 511**,** 543-550.

THOMAS, C. E., EHRHARDT, A. & KAY, M. A. 2003. Progress and problems with the use of viral vectors for gene therapy. *Nat Rev Genet,* 4**,** 346-58.

THOMSON, T. & LIN, H. 2009. The biogenesis and function PIWI proteins and piRNAs: progress and prospect. *Annual review of cell and developmental biology,* 25**,** 355.

TIBERIO, P., CALLARI, M., ANGELONI, V., DAIDONE, M. G. & APPIERTO, V. 2015. Challenges in using circulating miRNAs as cancer biomarkers. *Biomed Res Int,* 2015**,** 731479.

TREIBER, T., TREIBER, N. & MEISTER, G. 2012. Regulation of microRNA biogenesis and function. *Thrombosis and haemostasis,* 107**,** 605.

TSAI, K. W., LEUNG, C. M., LO, Y. H., CHEN, T. W., CHAN, W. C., YU, S. Y., TU, Y. T., LAM, H. C., LI, S. C., GER, L. P., LIU, W. S. & CHANG, H. T. 2016. Arm Selection Preference of MicroRNA-193a Varies in Breast Cancer. *Sci Rep,* 6**,** 28176.

TURCHINOVICH, A., SAMATOV, T., TONEVITSKY, A. & BURWINKEL, B. 2014. Circulating miRNAs: cell–cell communication function? *The origin, function and diagnostic potential of extracellular microRNA in human body fluids***,** 27.

UMEZU, T., TADOKORO, H., AZUMA, K., YOSHIZAWA, S., OHYASHIKI, K. & OHYASHIKI, J. H. 2014. Exosomal miR-135b shed from hypoxic multiple myeloma cells enhances angiogenesis by targeting factor-inhibiting HIF-1. *Blood,* 124**,** 3748-57.

VAN ROOIJ, E. & OLSON, E. N. 2012. MicroRNA therapeutics for cardiovascular disease: opportunities and obstacles. *Nat Rev Drug Discov,* 11**,** 860-72.

VAN ZANDWIJK, N., PAVLAKIS, N., KAO, S. C., LINTON, A., BOYER, M. J., CLARKE, S., HUYNH, Y., CHRZANOWSKA, A., FULHAM, M. J. & BAILEY, D. L. 2017. Safety and activity of microRNA-loaded minicells in patients with recurrent malignant pleural mesothelioma: a first-in-man, phase 1, open-label, dose-escalation study. *The Lancet Oncology,* 18**,** 1386-1396.

VERDEL, A., JIA, S., GERBER, S., SUGIYAMA, T., GYGI, S., GREWAL, S. I. & MOAZED, D. 2004. RNAi-mediated targeting of heterochromatin by the RITS complex. *Science,* 303**,** 672-676.

WALBOOMERS, J. M., JACOBS, M. V., MANOS, M. M., BOSCH, F. X., KUMMER, J. A., SHAH, K. V., SNIJDERS, P. J., PETO, J., MEIJER, C. J. & MUNOZ, N. 1999. Human papillomavirus is a necessary cause of invasive cervical cancer worldwide. *J Pathol,* 189**,** 12-9.

WAN, P. T., GARNETT, M. J., ROE, S. M., LEE, S., NICULESCU-DUVAZ, D., GOOD, V. M., JONES, C. M., MARSHALL, C. J., SPRINGER, C. J., BARFORD, D. & MARAIS, R. 2004. Mechanism of activation of the RAF-ERK signaling pathway by oncogenic mutations of B-RAF. *Cell,* 116**,** 855-67.

WANG, C., WAN, S., YANG, T., NIU, D., ZHANG, A., YANG, C., CAI, J., WU, J., SONG, J., ZHANG, C. Y., ZHANG, C. & WANG, J. 2016a. Increased serum microRNAs are closely associated with the presence of microvascular complications in type 2 diabetes mellitus. *Sci Rep,* 6**,** 20032.

WANG, L., HU, H. Y., LIN, Y. L., ZHAO, Z. X., TAN, L., YU, P., WAN, H. J., JIN, Z. & ZHENG, D. 2014. CDK3 expression and its clinical significance in human nasopharyngeal carcinoma. *Mol Med Rep,* 9**,** 2582-6.

WANG, Q. Z., XU, W., HABIB, N. & XU, R. 2009. Potential uses of microRNA in lung cancer diagnosis, prognosis, and therapy. *Curr Cancer Drug Targets,* 9**,** 572-94.

WANG, S., WAN, X. & RUAN, Q. 2016b. The MicroRNA-21 in Autoimmune Diseases. *Int J Mol Sci,* 17.

WANG, Y., HOU, J., HE, D., SUN, M., ZHANG, P., YU, Y. & CHEN, Y. 2016c. The Emerging Function and Mechanism of ceRNAs in Cancer. *Trends Genet,* 32**,** 211-24.

WANG, Z., YAO, H., LIN, S., ZHU, X., SHEN, Z., LU, G., POON, W. S., XIE, D., LIN, M. C.-M. & KUNG, H.-F. 2013. Transcriptional and epigenetic regulation of human microRNAs. *Cancer letters,* 331**,** 1-10.

WARBURG, O. 1956. On the origin of cancer cells. *Science,* 123**,** 309-14.

WATANABE, T., TOMIZAWA, S.-I., MITSUYA, K., TOTOKI, Y., YAMAMOTO, Y., KURAMOCHI-MIYAGAWA, S., IIDA, N., HOKI, Y., MURPHY, P. J. & TOYODA, A. 2011. Role for piRNAs and noncoding RNA in de novo DNA methylation of the imprinted mouse Rasgrf1 locus. *Science,* 332**,** 848-852.

WEBER, J. A., BAXTER, D. H., ZHANG, S., HUANG, D. Y., HUANG, K. H., LEE, M. J., GALAS, D. J. & WANG, K. 2010. The microRNA spectrum in 12 body fluids. *Clinical chemistry,* 56**,** 1733-1741.

WEIS, S. M. & CHERESH, D. A. 2011. Tumor angiogenesis: molecular pathways and therapeutic targets. *Nat Med,* 17**,** 1359-70.

WEISS, L. 2000. Early concepts of cancer. *Cancer and Metastasis Reviews,* 19**,** 205-217.

WONG, M. L. & MEDRANO, J. F. 2005. Real-time PCR for mRNA quantitation. *Biotechniques,* 39**,** 75.

XIANG, J. & WU, J. 2010. Feud or Friend? The Role of the miR-17-92 Cluster in Tumorigenesis. *Curr Genomics,* 11**,** 129-35.

XIAO, T., ZHU, J. J., HUANG, S., PENG, C., HE, S., DU, J., HONG, R., CHEN, X., BODE, A. M., JIANG, W., DONG, Z. & ZHENG, D. 2017. Phosphorylation of NFAT3 by CDK3 induces cell transformation and promotes tumor growth in skin cancer. *Oncogene,* 36**,** 2835-2845.

XUE, W., DAHLMAN, J. E., TAMMELA, T., KHAN, O. F., SOOD, S., DAVE, A., CAI, W., CHIRINO, L. M., YANG, G. R., BRONSON, R., CROWLEY, D. G., SAHAY, G.,

SCHROEDER, A., LANGER, R., ANDERSON, D. G. & JACKS, T. 2014. Small RNA combination therapy for lung cancer. *Proc Natl Acad Sci U S A,* 111**,** E3553-61.

YAMASHITA, R., SATO, M., KAKUMU, T., HASE, T., YOGO, N., MARUYAMA, E., SEKIDO, Y., KONDO, M. & HASEGAWA, Y. 2015. Growth inhibitory effects of miR-221 and miR-222 in non-small cell lung cancer cells. *Cancer Med,* 4**,** 551-64.

YANAIHARA, N., CAPLEN, N., BOWMAN, E., SEIKE, M., KUMAMOTO, K., YI, M., STEPHENS, R. M., OKAMOTO, A., YOKOTA, J., TANAKA, T., CALIN, G. A., LIU, C. G., CROCE, C. M. & HARRIS, C. C. 2006. Unique microRNA molecular profiles in lung cancer diagnosis and prognosis. *Cancer Cell,* 9**,** 189-98.

YANG, X., LEI, P., HUANG, Y., ZHANG, Z. & ZHANG, Y. 2016. MicroRNA-133b inhibits the migration and invasion of non small cell lung cancer cells via targeting FSCN1. *Oncol Lett,* 12**,** 3619-3625.

YEOM, K.-H., LEE, Y., HAN, J., SUH, M. R. & KIM, V. N. 2006. Characterization of DGCR8/Pasha, the essential cofactor for Drosha in primary miRNA processing. *Nucleic acids research,* 34**,** 4622-4629.

YIN, Y., DOU, X., DUAN, S., ZHANG, L., XU, Q., LI, H. & LI, D. 2016. Downregulation of cell division cycle 25 homolog C reduces the radiosensitivity and proliferation activity of esophageal squamous cell carcinoma. *Gene,* 590**,** 244-9.

YING, S.-Y. & LIN, S.-L. 2005. Intronic microRNAs. *Biochemical and biophysical research communications,* 326**,** 515-520.

YU, S. L., CHEN, H. Y., CHANG, G. C., CHEN, C. Y., CHEN, H. W., SINGH, S., CHENG, C. L., YU, C. J., LEE, Y. C., CHEN, H. S., SU, T. J., CHIANG, C. C., LI, H. N., HONG, Q. S., SU, H. Y., CHEN, C. C., CHEN, W. J., LIU, C. C., CHAN, W. K., CHEN, W. J., LI, K. C., CHEN, J. J. & YANG, P. C. 2008. MicroRNA signature predicts survival and relapse in lung cancer. *Cancer Cell,* 13**,** 48-57.

YUAN, T. L. & CANTLEY, L. C. 2008. PI3K pathway alterations in cancer: variations on a theme. *Oncogene,* 27**,** 5497-510.

YUAN, Y., SHEN, Y., XUE, L. & FAN, H. 2013. miR-140 suppresses tumor growth and metastasis of non-small cell lung cancer by targeting insulin-like growth factor 1 receptor. *PloS one,* 8**,** e73604.

YUE, D., LIU, H. & HUANG, Y. 2009. Survey of computational algorithms for MicroRNA target prediction. *Current genomics,* 10**,** 478.

ZEISBERG, M. & NEILSON, E. G. 2009. Biomarkers for epithelial-mesenchymal transitions. *J Clin Invest,* 119**,** 1429-37.

ZHAI, H., FESLER, A., BA, Y., WU, S. & JU, J. 2015. Inhibition of colorectal cancer stem cell survival and invasive potential by hsa-miR-140-5p mediated suppression of Smad2 and autophagy. *Oncotarget,* 6**,** 19735-46.

ZHANG, G. & WANG, Z. 2011. MAGI1 inhibits cancer cell migration and invasion of hepatocellular carcinoma via regulating PTEN. *Zhong Nan Da Xue Xue Bao Yi Xue Ban,* 36**,** 381-5.

ZHANG, H., KOLB, F. A., BRONDANI, V., BILLY, E. & FILIPOWICZ, W. 2002. Human Dicer preferentially cleaves dsRNAs at their termini without a requirement for ATP. *The EMBO journal,* 21**,** 5875-5885.

ZHANG, H., KOLB, F. A., JASKIEWICZ, L., WESTHOF, E. & FILIPOWICZ, W. 2004. Single processing center models for human Dicer and bacterial RNase III. *Cell,* 118**,** 57-68.

ZHANG, L., QIN, D., HAO, C., SHU, X. & PEI, D. 2013. SNX16 negatively regulates the migration and tumorigenesis of MCF-7 cells. *Cell Regen (Lond),* 2**,** 3.

ZHANG, W., ZOU, C., PAN, L., XU, Y., QI, W., MA, G., HOU, Y. & JIANG, P. 2015. MicroRNA-140-5p inhibits the progression of colorectal cancer by targeting VEGFA. *Cell Physiol Biochem,* 37**,** 1123-33.

ZHOU, W., FONG, M. Y., MIN, Y., SOMLO, G., LIU, L., PALOMARES, M. R., YU, Y., CHOW, A., O'CONNOR, S. T., CHIN, A. R., YEN, Y., WANG, Y., MARCUSSON, E. G., CHU, P., WU, J., WU, X., LI, A. X., LI, Z., GAO, H., REN, X., BOLDIN, M. P., LIN, P. C. & WANG, S. E. 2014. Cancer-secreted miR-105 destroys vascular endothelial barriers to promote metastasis. *Cancer Cell,* 25**,** 501-15.

ZHOU, Y., TOZZI, F., CHEN, J., FAN, F., XIA, L., WANG, J., GAO, G., ZHANG, A., XIA, X., BRASHER, H., WIDGER, W., ELLIS, L. M. & WEIHUA, Z. 2012. Intracellular ATP levels are a pivotal determinant of chemoresistance in colon cancer cells. *Cancer Res,* 72**,** 304-14.

ZHU, C., HE, L., ZHOU, X., NIE, X. & GU, Y. 2016. Sulfatase 2 promotes breast cancer progression through regulating some tumor-related factors. *Oncol Rep,* 35**,** 1318-28.